THE UNIVERSITY
of EDINBURGH

High resolution modelling of particulate matter air quality in the UK with a focus on carbonaceous aerosol

Riinu Ots

A thesis submitted in fulfilment of the requirements
for the degree of Doctor of Philosophy
The University of Edinburgh

2016

Lay summary

The Earth's atmosphere consists of both gaseous and condensed-phase components, the condensed-phase material is called particulate matter (PM). The effects of atmospheric PM include adverse health impacts, as well as climate forcing. A major component of atmospheric PM is carbonaceous aerosol (i.e. carbon containing compounds), and in this work, some of the different sources of atmospheric carbonaceous aerosol are investigated. This is done using a model that simulates the dispersion and evolution of atmospheric pollutants based on emissions, meteorology, and chemical reactions.

Firstly, recent studies have identified emissions from diesel cars that are heavier than most gases, but lighter than the condensed-phase material (i.e. they are of intermediate volatility). These compounds are currently not included in official emissions inventories. In this work, the missing diesel emissions are quantified and added to the model. According to the model simulations these compounds can have a notable effect on particulate matter air quality.

Secondly, emissions from meat charbroiling, or frying and deep-frying are currently neglected in European emissions inventories. By combining recent measurements with population density maps, cooking organic aerosol emissions are developed for the UK. The importance of these emissions on the air quality in major cities was found to be significant, but the concentrations are negligible for rural areas.

Thirdly, coal and wood burning is a major source of carbonaceous aerosol. Motivated by the Great Smog of 1952 in London, highly populated areas in the UK have been subject to smoke control legislations whereby only smokeless fuels and approved appliances are allowed. This is, however, no longer actively reinforced and the simulation experiments undertaken here suggest that substantial illegal wood burning takes place in urban areas.

Abstract

The Earth's atmosphere consists of both gaseous and condensed-phase components, the condensed-phase material is called particulate matter (PM). The effects of atmospheric PM include adverse health impacts, as well as climate forcing. Both qualitative and quantitative knowledge about PM is necessary to assess these effects, and to devise best mitigation strategies. Understanding the distribution of atmospheric particulate matter is complex because much of it is of secondary origin rather than from primary emissions. Furthermore, there are multiple anthropogenic and natural sources of the contributing precursors, and all these processes are influenced by atmospheric conditions and transport. In this work, one of the major constituents of atmospheric PM - carbonaceous aerosol - is studied.

A regional application of the EMEP MSC-W atmospheric chemical transport model - EMEP4UK - was used to model air pollution over the British Isles with a horizontal resolution of 5 km $\times$ 5 km. One-way nesting was used from the European computational domain of 50 km $\times$ 50 km to the finer spatial grid of EMEP4UK. Several model experiments were devised in order to investigate the well-known deficiency that models currently underestimate organic aerosol (OA) concentrations compared with observations. The model experiments were evaluated with comprehensive year-long novel measurements from the Clear Air for London (ClearfLo) campaign in 2012. Several sources of organic aerosol that are either missing, greatly underestimated, or may be spatially misplaced in official emissions inventories were re-evaluated.

Firstly, missing diesel-related intermediate volatility organic compound (IVOC) emissions from diesel vehicles derived directly from field measurements at the urban background site during the 2012 ClearfLo campaign were added into the model. According to the model simulations, these diesel-IVOCs can explain on average ~30% of the annual secondary organic aerosol (SOA) in and around London. Furthermore, the 90-th percentile of modelled daily SOA concentrations for the whole year was 3.8 $\mu g\,m^{-3}$, constituting a notable addition to total particulate matter. More measurements of these

precursors (currently not included in official emissions inventories) is recommended.

Secondly, spatially and temporally resolved emissions of cooking OA (COA; emissions from meat charbroiling, or frying and deep-frying) were developed. These emissions are currently neglected in European emissions inventories, yet measurements point to significant COA contribution to ambient PM concentrations (up to 2.0 $\mu g\,m^{-3}$ on annual average for central London). The final COA emission source strength derived here (320 $mg\,person^{-1}\,day^{-1}$) was spatially distributed to workday population density (as opposed to residential population density). The impact of COA on surface concentrations is spatially very limited, however, as the modelled concentrations dropped markedly outside of urban areas. For example, annual average modelled concentration for the Harwell location was just 0.1 $\mu g\,m^{-3}$.

Thirdly, redistributing 50% of non-industrial wood and coal burning emissions to residential population density (thus over-writing, in part, the assumption made by the national emissions inventory that only smokeless fuels are burned in smoke control areas) increased the modelled solid fuel OA (SFOA) concentration at the London North Kensington site to 0.8 $\mu g\,m^{-3}$, from the Base run value (using the emissions' spatial distribution and total as officially reported) of just 0.3 $\mu g\,m^{-3}$. For comparison, the measured annual mean concentration of SFOA at this site was 1.0 $\mu g\,m^{-3}$. Based on the model evaluation presented, redistribution of SFOA emissions into smoke control areas is justified, but further refinement of the amount, as well as the temporal emission profile of this component is necessary.

The total effect of the three refinements undertaken in this work increased the model estimate of the annual mean OA concentration at the London North Kensington site from 1.8 $\mu g\,m^{-3}$ to 3.8 $\mu g\,m^{-3}$, which is much closer to the observed value of 4.2 $\mu g\,m^{-3}$. Thus, this work has provided relevant insight into the nature and magnitude of missing, under-represented, and spatially inappropriately-distributed emissions of primary OA and OA precursors.

Although the study area was focused on pollutant concentrations over the British Isles, all of the components examined here are of great relevance to the air quality in other countries as well — in Europe and globally. Therefore, the inclusion of these improvements into other air quality models and official emissions' inventories is advised.

Declaration

I declare that this thesis was composed by myself, that the work contained herein is my own except where explicitly stated otherwise in the text, and that this work has not been submitted for any other degree or professional qualification except as specified.

Parts of this work have been published in

Ots, R., et al. (2016). Simulating secondary organic aerosol from missing diesel-related intermediate-volatility organic compound emissions during the Clean Air for London (ClearfLo) campaign, 16, 6453-6473, *Atmos. Chem. Phys.*, doi: 10.5194/acp-2015-920.

and

Ots, R., et al. (2016). Model simulations of cooking organic aerosol (COA) over the UK using estimates of emissions based on measurements at two sites in London, *Atmos. Chem. Phys. Discuss.*, 1–28, doi: 10.5194/acp-2016-342, accepted for publication in *Atmos. Chem. Phys.*.

(*Riinu Ots, 2016*)

Acknowledgements

I owe my deepest gratitude to my supervisor, Mat Heal, for his ceaseless and unfailing help throughout this PhD. His guidance has enabled me to become the scientist I am today. I could not be happier with the time spent in his research group.

I am grateful for my supervisors Massimo Vieno and Stefan Reis from the Centre for Ecology&Hydrology for providing a basis for this research project, as well as for interesting and stimulating discussions throughout.

I thank my past supervisors, Marko Kaasik and Tony Dore, for introducing me to the field of air pollution modelling.

Weekly meetings of the EMEP4UK users' support group with Ian and Ksenia have been crucial for getting the model to run whilst maintaining one's sanity.

I appreciate my co-authors and collaborators for constructive discussions, as well as for providing me with the measurements on which parts of this work are based. I am also grateful to all members of the MACAQUE (Modelling and measuring atmospheric chemistry and air quality at Edinburgh) group for their valuable questions and suggestions during our biweekly presentations.

Finally, I am very grateful for my partner Einar who not only has helped me with technical issues and proofreading, but first and foremost believes in me so much that I want to prove him right. His reassurance has made me more capable than I ever thought I could be.

Contents

List of Figures

List of Tables

Chapter 1

Introduction

Particulate matter (PM) is the term used to describe condensed-phase material (solid or liquid) suspended in the atmosphere. Atmospheric particulate matter is often also referred to as atmospheric aerosol, and the two terms are used interchangeably[1].

1.1 Importance and impact of PM

The impacts of atmospheric PM include adverse health effects, climate forcing, chemical processing, deposition, and effects on visibility (Pöschl, 2005).

The health effects of atmospheric PM are often assessed for two categories: short-term exposure (usually focusing on changes in daily-average PM concentration in a single population), and long-term exposure (focusing on populations living in areas with different annual-average or long term PM concentrations). The use of human challenge studies with controlled exposures in the laboratory is limited by ethical constraints (Heal et al., 2012), but for the quantification of adverse cardiovascular effects of diesel exhaust, for example, experiments on mice have been conducted (Miller et al., 2013).

The daily mortality risk estimate per 10 $\mu g\,m^{-3}$ of PM is around 1% (between 0.2% and 1.3% for different causes of death), whereas the long-term mortality risk estimate per 10 $\mu g\,m^{-3}$ from all causes as about 4%, as in a review by the Word Health Organization (WHO, 2006). An update of the WHO Air Quality Guidelines (WHO, 2013) concluded

[1]Conceptually, the two terms are different: aerosols are two-phase systems, consisting of the particles and the gas in which they are suspended, whereas PM only refers to the condensed (and dispersed) phase. In this research field, however, the terms are used interchangeably.

that the estimates of the previous review are sound, but that new evidence of specific causes, as well research into the health impact of different components of PM, is available. For instance, PM from combustion sources are thought to be more harmful to human health than PM from non-combustion sources.

The effects of aerosol on climate are twofold: direct and indirect. Direct effects include the absorption of light (dark particles, such as soot), or the scattering and reflection of light (pale particles, such as secondary inorganic aerosol). Indirect effects of PM comprise acting as nuclei for cloud formation, as well as affecting the chemical formation, evaporation, or deposition of other components of the atmosphere. Overall, these effects include both positive and negative feedback mechanisms, are dependent on atmospheric composition and meteorology, and whose quantitative impacts continue to be subject to much uncertainty (Pöschl, 2005). The overall effect of aerosol radiative forcing relative to pre-industrial times has been estimated to be around -1 to -2 W m^{-2} (compared to +2.4 W m^{-2} of greenhouse gas forcing; Pöschl (2005)). However, there are several uncertainties in the understanding of the interactions, and the positive and negative feedbacks of the physiochemical effects of aerosol (Pöschl, 2005).

For qualitative and quantitative analyses of any of these effects, one needs to know as much as possible about the chemical composition, size, and spatio-temporal variability of PM. Furthermore, in order to reduce the adverse impact of these effects it is important to understand the source contributions of PM.

1.2 Size of PM

Particle size is an important parameter for characterising the behaviour and impact of an aerosol. Atmospheric PM covers a wide size range from a few nanometres (10^{-9} m) up to a hundred micrometres (10^{-4} m). The lower limit comes from the size of molecules and molecular clusters, the upper limit is set by rapid gravitational sedimentation (Pöschl, 2005; Andreae and Rosenfeld, 2008). When plotted as a function of size, the distributions of particle number, surface area, or volume concentrations give a very different picture (Figure 1.1). The latter approximates to PM mass concentration, if it is assumed that the variability in particle density is small. Table 1.1 gives an overview of the size ranges introduced in this section.

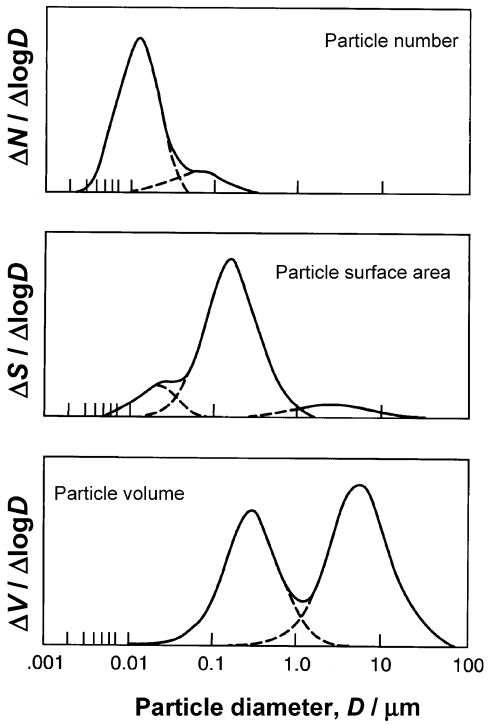

Figure 1.1 *A typical ambient particle distribution as a function of particle size expressed by particle number, surface area, and volume. The latter is equivalent to a mass distribution when variation in particle density is small. Vertical scaling is individual to each panel. Source: Heal et al. (2012).*

The smallest particles, called the *nuclei mode* (particles with diameter $<$ 50 nm; also called the *Aitken mode*), are high in number concentration, but they rarely count for more than a few per cent of total PM mass concentration (Seinfeld and Pandis, 2006). This mode consists of combustion particles emitted directly into the atmosphere (primary PM) and particles formed in the atmosphere by gas-to-particle conversion (secondary PM). Because of their high number concentration, nuclei particles coagulate rapidly with each other and are also adsorbed onto the accumulation mode particles. Nuclei particles are short-lived with lifetimes from minutes to hours (Hinds, 1999). Particles with a diameter smaller than 100 nm (0.1 μm) are also called ultrafine particles.

The *accumulation mode* includes primary combustion particles and coagulated nuclei mode particles. Further growth of accumulation mode particles by coagulation is inefficient, so they do not grow to coarse mode. Their main removal is through rainout (in-cloud scavenging) and washout (below-cloud scavenging by falling rain), gravitational sedimentation does not play a big role. This is why the mode is called "accumulation" - particles tend to accumulate in this size range because of their

Table 1.1 *Overview of the terms introduced in Chapter 1.2. Diameter refers to 'aerodynamic diameter', which for an irregular particle is defined as the diameter of a spherical particle with unit density (1 g cm^{-3}) and the same settling velocity. The term size is equivalent to diameter.*

$PM_{2.5}$	Particulate matter with diameter < 2.5 μm
PM_{10}	PM with diameter between 2.5 μm and 10 μm (the sum of fine and coarse PM)
Fine [PM]	Same as $PM_{2.5}$
Coarse [PM]	A size range of 2.5 μm to 10 μm
Large [PM]	Particulate matter with diameter > 10 μm
Nuclei mode	Particulate matter with diameter < 50 nm
Submicrometer	Particulate matter with diameter < 1 μm
Ultrafine [PM]	Particulate matter with diameter < 0.1 μm

relatively long lifetimes (from days to weeks). Particulate matter with a diameter smaller than 2.5 μm (sum of nuclei and accumulation mode) is also called *fine PM*.

The *coarse mode* (PM with diameter > 2.5 μm) is formed by mechanical processes such as mining, crushing, grinding or the effect of wind blowing on different natural and man-made surfaces. As coarse particles are relatively big in size, their atmospheric lifetime is from a few hours to days because of gravitational sedimentation. Fine and coarse PM generally have different chemical compositions, sources and lifetimes, and there is comparatively little mass exchange between the two modes (Hinds, 1999).

1.2.1 The log-normal size distribution function

Keeping track of the size of each particle is not feasible. Even if it were possible to measure or model the size of every single particle in a sample or air mass, the amount of information obtained would be too vast to handle. Therefore, in practice, distributions are used to handle the sizes of aerosols.

A simple way to do this is by dividing the size range into bins and keeping track of the number of particles in each bin (i.e. a frequency distribution). This solution does not however include information about the distribution structure within each bin and might therefore lose information necessary for some applications.

The log-normal distribution (the distribution of a variable whose logarithm is normally distributed) is often used in atmospheric applications, and for particle diameters D_p is defined as (Seinfeld and Pandis, 2006):

$$n(D_p) = \frac{N_t}{2\ln^2 \sigma_g} \exp\left(-\frac{(\ln D_p - \ln \overline{D}_{pg})^2}{2\ln^2 \sigma_g}\right), \tag{1.1}$$

where N_t is the total aerosol number concentration, $\overline{D}_{pg}$ is the geometric mean of D_p (the geometric mean of a log-normal variable is equal to its median: $\overline{D}_{pg} = D_{med}$), and σ_g is the geometric standard deviation.

1.3 Composition and sources of PM

This section gives an overview of the composition and sources of primary particulate matter; secondary formation and atmospheric ageing are discussed in the next sections. Table 1.2 gives an overview of the terms used in this section.

1.3.1 Anthropogenic sources

A major source of anthropogenic airborne primary PM is *fossil fuel combustion*. Fossil fuels are burned in industry, power plants, vehicles, and residential heating. Fossil fuel burning in stationary and mobile sources yields a mixture of PM, depending on the fuel burned and combustion technology used (Andreae and Rosenfeld, 2008). Although coal burning produces a large amount of coarse fly ash, most of it is removed by filters before its atmospheric emission (at least in developed countries; Andreae and Rosenfeld (2008)). Incomplete combustion of fossil fuels produces sub-micrometre PM, whereas mechanical processes (e.g. quarrying, tyre wear, etc.) produce coarse PM. For more detailed information about vehicular emissions see Section 3, for emissions from cooking see Chapter 4, and for residential heating Chapter 5.

Carbonaceous aerosol covers a continuum from graphitic soot through non-refractory organic material to more volatile colourless organic compounds. The range is conventionally divided into elemental and organic carbon. EC (also called soot, or, depending on context, black carbon) has a chemical structure similar to impure graphite and it is a primary pollutant. Organic carbon consists of a variety of

organic compounds and is either emitted directly from combustion processes (primary organic aerosol - POA) or it can be formed in situ by gas-to-particle conversions of hydrocarbons. The secondary formation is explained in more detail in the next section. The term OC only refers to the carbon fraction of organic material as that is what is usually measured, but the total organic material (OM, term equivalent to OA) also consists of hydrogen, oxygen, nitrogen, etc. (Seinfeld and Pandis, 2006).

Figure 1.2 gives the total OC and EC emissions from European countries for 2005 apportioned by different source sectors. The relatively large contribution (60%) of OC emissions from residential wood combustion is based on new estimates of emissions as presented in Denier van der Gon et al. (2015), whereby the OC emissions factors from wood burning were updated to be almost three times that used before. Fig. 1.2 gives and overview of the relative contributions of different sources of carbonaceous PM in Europe. Section 2.3 gives this speciation of the UK National Atmospheric Emissions Inventory (NAEI), where it can be seen that the relative contributions of different source sectors in the UK are very similar to Fig. 1.2.

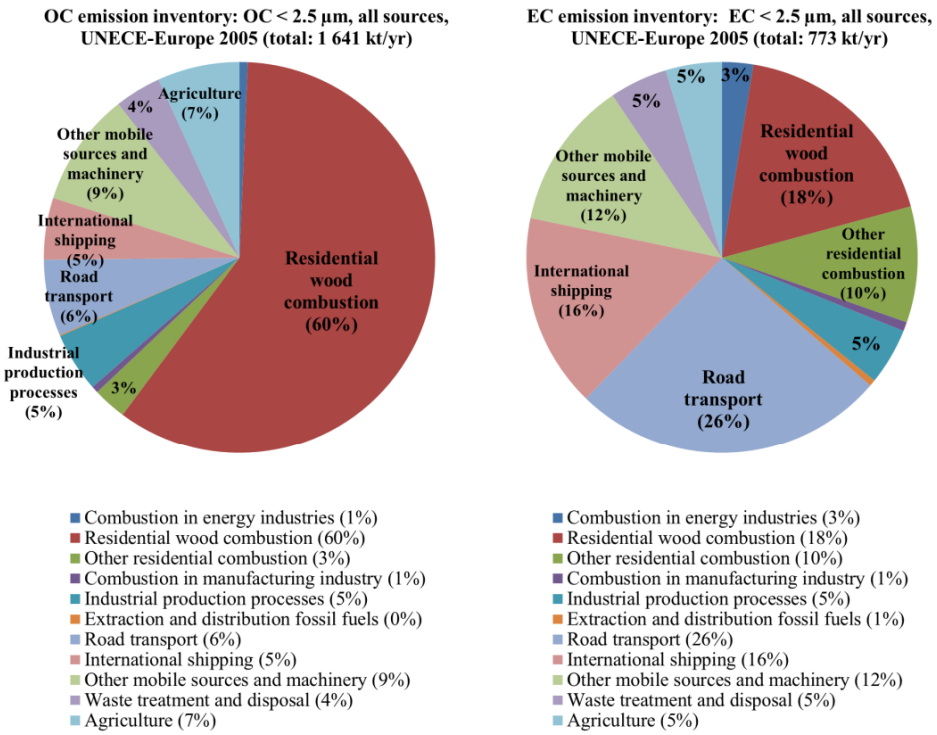

Figure 1.2 *Total OC (left) and EC (right) emissions from European countries for the year 2005. A kt is equal to a Gg which, is the unit used in this study. Source: (Bergström, 2015).*

1.3.2 Natural sources

Airborne *sea salt* is a major component of natural PM in maritime areas. The main driver of sea salt emissions is wind, but water salinity, water temperature and atmospheric stability (or turbulence) are also important characteristics. Two different mechanisms have been established for seawater droplet generation. The first is through bubbles: wind stress on the surface leads to formation of waves, then waves break and bubbles are produced (i.e. white-capping), and bursting of a bubble injects seawater jet droplets into the atmosphere. The sizes of these droplets are in the range of $0.01-10$ $\mu\mathrm{m}$ (Blanchard and Woodcock, 1957; Sofiev et al., 2011). The second mechanism takes place during strong winds (10-m wind > 11 m s^{-1}) - "spume" droplets are torn off the wave crests (Andreas, 1998). As the diameter of spume droplets is more than 10 $\mu\mathrm{m}$, their atmospheric lifetime is short (due to quick gravitational sedimentation) and they do not play a big role in regional air quality. The main dry-mass components of sea salt are Cl^- (55%), Na^+ (30%), SO_4^{2-} (8%), Mg^{2+} (4%), Ca^{2+} (1%), K^+ (1%) (Lide and Weast, 1993).

Another source of natural PM is *windblown dust* erosion from soil. Although driven by wind speed, the emission strength also depends on the size distribution of the erodible loose particles, surface roughness (which determines the friction velocity of wind) and soil moisture content (Marticorena and Bergametti, 1995; Fecan et al., 1999). The size range of wind-lifted particles is wide, but most of the windblown dust that is subject to interregional atmospheric dispersion is in the coarse fraction. As for sea salt particles, anything bigger than 10 $\mu\mathrm{m}$ will settle quickly. The main species found in soil dust are quartz, clays, calcite, gypsum and iron oxides; their relative abundances vary (Seinfeld and Pandis, 2006). Globally, major natural dust sources are deserts and semiarid regions, but meteorological conditions can govern long-range transport of, for example, Saharan dust to central and northern Europe (Begue et al., 2012; Varga et al., 2013).

In some cases, a source of atmospheric PM cannot be easily categorised as either anthropogenic or natural. For instance, anthropogenic land-use (farmlands, roads) changes surface conditions and soil moisture and can therefore increase the emission of natural windblown dust. Furthermore, wildfires can be a substantial source of PM (Toll et al., 2015).

Table 1.2 *Overview of the terms introduced in Section 1.3: Composition and sources of PM.*

Dust	Suspensions of solid particles formed by mechanical disintegration of a material (result of crushing, grinding);
Elemental carbon	Carbon in elemental form, also known as soot or black carbon;
Organic carbon	The carbon component in a variety of (condensed) organic compounds;
Organic material	OM includes all components of atmospheric organic compounds (OM = OC + hydrogen, oxygen, nitrogen etc.);
POA	Primary organic aerosol;
Smog	A general term for visible atmospheric pollution; the term was originally derived from the words smoke and fog;
Smoke	A visible aerosol resulting from incomplete combustion, consisting predominantly of carbon and other combustion products;
Spray	A droplet aerosol formed by the mechanical breakup of a liquid; usually sea spray in atmospheric context;
Primary aerosol	Particles that are introduced directly to the atmosphere;
Secondary aerosol	1. Particles that are formed in the atmosphere by chemical reactions of gaseous components (gas-to-particle conversion) and/or 2. Particles that have undergone atmospheric ageing (changed mass, size, functionality);

1.4 Secondary formation of atmospheric PM

The previous section introduced the main sources of primary PM, but atmospheric PM can also be formed by oxidation of gaseous precursors, yielding lower volatility products that might condense/be sorbed into liquid or particulate phase. There are two types of secondary PM: *secondary inorganic aerosol* (SIA) and *secondary organic aerosol* (SOA).

Although the pathways and properties of SIA and SOA are different, the key molecule of tropospheric gas-phase chemistry is the hydroxyl (OH) radical as it is the main oxidizing species in the troposphere (Seinfeld and Pandis, 2006). The principal route of OH production in the atmosphere is from the photolysis of $\mathrm{O_3}$ (the lower pathway occurs if $\lambda < 310$ nm):

$$\begin{aligned} \mathrm{O_3} + h\nu &\longrightarrow \mathrm{O_2} + \mathrm{O} \\ &\longrightarrow \mathrm{O_2}(^1\Delta_\mathrm{g}) + \mathrm{O}(^1\mathrm{D}) \end{aligned} \qquad \text{(R 1.1)}$$

The electronically-excited O(^{1}D) may be quenched back to ground-state by collision with $\mathrm{N_2}$ or $\mathrm{O_2}$:

$$\mathrm{O}(^1\mathrm{D}) + \mathrm{M} \longrightarrow \mathrm{O} + \mathrm{M} \qquad \text{(R 1.2)}$$

or react with $\mathrm{H_2O}$ to yield two OH radicals:

$$\mathrm{O}(^1\mathrm{D}) + \mathrm{H_2O} \longrightarrow 2\mathrm{OH} \qquad \text{(R 1.3)}$$

Whilst Reaction R 1.3 is the primary source of OH, its concentration is mainly determined by OH-$\mathrm{HO_2}$ interconversions (recycling; Lelieveld et al. (2016)).

1.4.1 Secondary inorganic aerosol (SIA)

The main condensed-phase inorganic components of airborne PM are nitrate aerosols $\mathrm{NaNO_3}$, $\mathrm{NH_4NO_3}$ and sulphate aerosols $\mathrm{NH_4HSO_4}$, $\mathrm{(NH_4)_2SO_4}$. The precursor gases of these secondary inorganic aerosols are NO, $\mathrm{NO_2}$, $\mathrm{SO_2}$ and $\mathrm{NH_3}$.

Atmospheric reactions of sulphur dioxide take place both in the gaseous or aqueous phases. Its dominant reaction in the gas phase is with the OH radical (Stockwell and

Calvert, 1983; Seinfeld and Pandis, 2006):

$$SO_2 + OH + M \longrightarrow HOSO_2 + M \quad \text{(R 1.4)}$$

followed by:

$$HOSO_2 + O_2 \longrightarrow HO_2 + SO_3 \quad \text{(R 1.5)}$$

and in the presence of water vapour, sulphur trioxide is rapidly converted to sulphuric acid:

$$SO_3 + H_2O + M \longrightarrow H_2SO_4 + M \quad \text{(R 1.6)}$$

Absorption of SO_2 in water results in:

$$SO_{2(g)} + H_2O \rightleftharpoons SO_2 \cdot H_2O \quad \text{(R 1.7)}$$

$$SO_2 \cdot H_2O \rightleftharpoons H^+ + HSO_3{}^- \quad \text{(R 1.8)}$$

$$HSO_3{}^- \rightleftharpoons H^+ + SO_3{}^{2-} \quad \text{(R 1.9)}$$

The results of dissolution of SO_2 in water (Reactions R 1.7, R 1.8 and R 1.9) are hydrated SO_2 ($SO_2 \cdot H_2O$), the bisulphite ion ($HSO_3{}^-$), and the sulphite ion ($SO_3{}^{2-}$). The proportions of these dissociation products of SO_2 depend on the pH of the aqueous solution. These products are oxidised in the solution by ozone (O_3), hydrogen peroxide (H_2O_2), organic peroxides or oxygen (O_2) that is catalysed by iron (Fe^{3+}) and manganese (Mn^{2+}) (Seinfeld and Pandis, 2006). The equilibrium reactions of sulphate then become:

$$H_2SO_{4(aq)} \rightleftharpoons H^+ + HSO_4{}^- \quad \text{(R 1.10)}$$

$$HSO_4{}^- \rightleftharpoons H^+ + SO_4{}^{2-} \quad \text{(R 1.11)}$$

The second major precursor of SIA is the nitrogen oxides family, denoted as $NO_x = NO + NO_2$. During daytime, NO and NO_2 rapidly interconvert by the photochemical NO_x cycle (Figure 1.3).

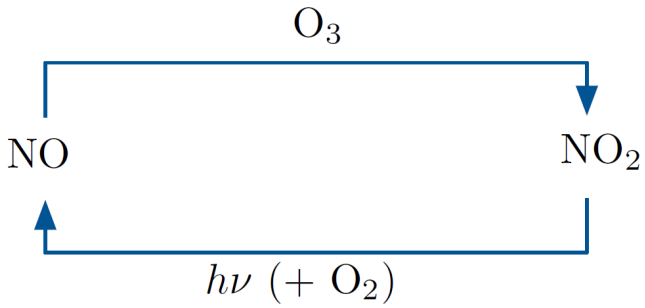

Figure 1.3 *Daytime NO and NO_2 cycle.*

NO_2 is further oxidised by the OH radical:

$$OH + NO_2 + M \longrightarrow HNO_3 + M \qquad \text{(R 1.12)}$$

During night-time, the photolysis of NO_2 to NO does not take place, so almost all of NO_x is converted to NO_2. That NO_2 will react with ozone to produce the nitrate radical:

$$NO_2 + O_3 \longrightarrow NO_3 + O_2 \qquad \text{(R 1.13)}$$

which, during daytime, will photolyse rapidly back to NO and NO_2. At night, the nitrate radical has time to react with NO_2 to produce N_2O_5:

$$NO_2 + NO_3 + M \longrightarrow N_2O_5 + M \qquad \text{(R 1.14)}$$

N_2O_5 itself can thermally decompose back to NO_2 and NO_3:

$$N_2O_5 + M \longrightarrow NO_2 + NO_3 + M \qquad \text{(R 1.15)}$$

These reactions (R 1.14 and R 1.15) establish equilibrium in a few minutes:

$$NO_2 + NO_3 + M \rightleftharpoons N_2O_5 + M \qquad \text{(R 1.16)}$$

where the equilibrium constant is equal to $[N_2O_5]/([NO_2][NO_3])$. The hydrolysis of N_2O_5 (reaction on deliquescent aerosols) produces aqueous nitric acid (Seinfeld and Pandis, 2006):

$$N_2O_{5(g)} + H_2O \longrightarrow 2\,HNO_{3(aq)} \qquad \text{(R 1.17)}$$

The third main precursor of SIA, ammonia (NH_3), which is emitted mainly from agricultural sources, dissolves to:

$$NH_3 + H_2O \rightleftharpoons NH_3 \cdot H_2O \quad \text{(R 1.18)}$$

$$NH_3 \cdot H_2O \rightleftharpoons {NH_4}^+ + OH \quad \text{(R 1.19)}$$

The concentrations of the ions in the aqueous phase will adjust to satisfy the electroneutrality of this equation (Seinfeld and Pandis, 2006):

$$[H^+] + [{NH_4}^+] = [OH^-] + [{HSO_3}^-] + 2\,[{SO_3}^{2-}] + 2\,[{SO_4}^{2-}] + [{HSO_4}^-] + [{NO_3}^-] \quad \text{(R 1.20)}$$

1.4.2 Secondary organic aerosol (SOA)

Secondary organic aerosol (SOA) is formed from volatile organic compounds (VOCs) in the air that have become more functionalized with oxygenated and nitrated functional groups (making them more polar and less volatile). The gas-phase oxidation reactions of VOCs are usually initiated by the OH radical, NO_3 radical, O_3, Cl atoms or the process of photolysis (Ziemann and Atkinson, 2012). Figure 1.4 shows a generalised scheme of atmospheric degradation reactions of VOCs.

There is a myriad of these airborne organic compounds, in gaseous and condensed phases, ranging from simple hydrocarbons to highly oxidized compounds. Out of the different properties of these compounds (e.g. molecular weight, reactivity, saturation concentration, photolability, aqueous solubility), it is the volatility, i.e., saturation vapour concentration, which is of most relevance when considering gas-particle transfer.

The absorptive partitioning of different organic compounds C_i (i denotes different compounds), with saturation concentrations C_i^* (temperature dependent) can be calculated as (Pankow, 1994; Donahue et al., 2006):

$$\xi_i = \frac{1}{1 + \frac{C_i^*}{C_{OA}}}, \quad (1.2)$$

where ξ_i is the partitioning coefficient (fraction of C_i in particulate phase) and C_{OA} is

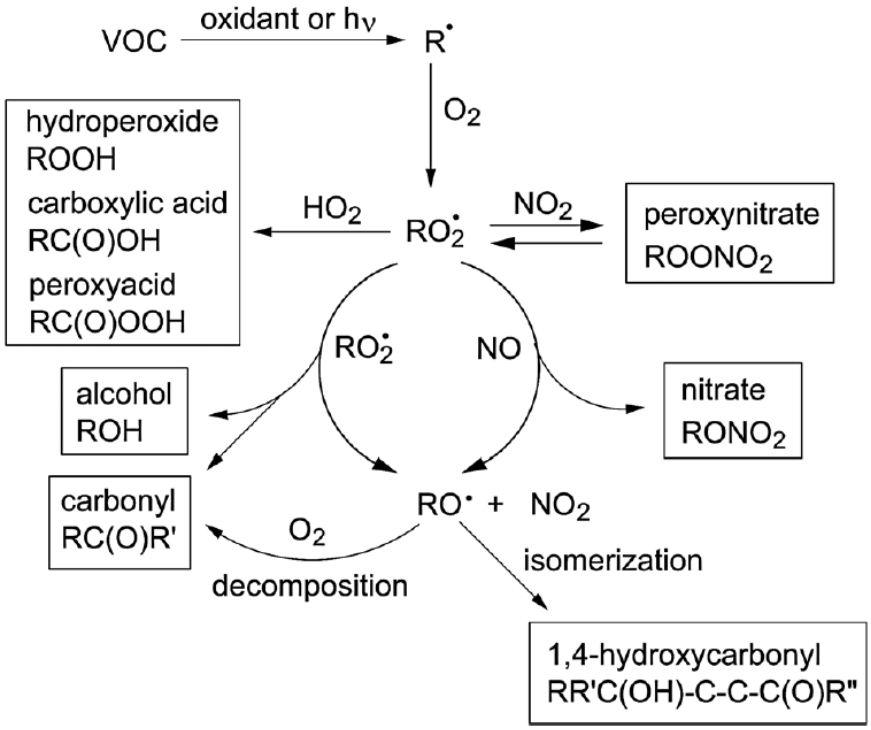

Figure 1.4 *Atmospheric degradation reactions of VOCs. Source: Ziemann and Atkinson (2012).*

the total mass concentration of organic particulate matter:

$$C_{OA} = \sum_i \xi_i C_i, \tag{1.3}$$

Therefore, the amount of gaseous organic compounds that will condense into particulate phase (and become SOA) depends both on its volatility, as well as the total organic aerosol mass loading (C_{OA}). This means the solution of Equation (1.2) needs a few iterations.

The three main processes that determine the volatility, and hence the SOA-forming potential of organic compounds in the atmosphere, are (Kroll and Seinfeld, 2008):

- oxidation reactions in the gas phase, which lower volatility by addition of functional groups, but can also increase volatility by cleavage of carbon-carbon bonds;
- reactions in the particle (condensed) phase, which can change volatility either by oxidation or formation of high-molecular-weight species;

- continuing chemistry (in either phase) over several generations.

It was shown by Robinson et al. (2007) that primary organic aerosol (POA) is also not non-volatile, meaning it can evaporate with atmospheric dilution becoming a mix of semivolatile organic compounds (SVOCs). These SVOCs may condense back to the particulate phase after photo-oxidation, forming SOA. This partitioning of POA leads to a more regionally distributed (widespread) organic PM, than it would be if it remained only in the particulate phase during its atmospheric lifetime. More information, and examples of the volatility distribution, evaporation, and atmospheric ageing of POA (denoted 'semivolatile treatment of POA') is given in Section 2.5, and Chapter 3.

1.4.3 Example iterations of gas-aerosol partitioning with two species

Consider two organic compounds with atmospheric concentrations of C_1 = 3.0 $\mu\mathrm{g\,m^{-3}}$ and C_2 = 3.0 $\mu\mathrm{g\,m^{-3}}$ and saturation concentrations (i.e. volatility) of C_1^* = 0.1 $\mu\mathrm{g\,m^{-3}}$ and C_2^* = 1.0 $\mu\mathrm{g\,m^{-3}}$. The sum of the condensed partitions of these two compounds is $\mathrm{C_{OA}}$ (total mass concentration of organic particulate matter). The calculation of the condensed vs gaseous partitions of C_1 and C_2 is as follows:

- Step 0: Choose an initial value, e.g. $\mathrm{C_{OA}}$ = 1.0 $\mu\mathrm{g\,m^{-3}}$;
- Step 1: Calculate ξ_1 and ξ_2 (i.e. proportion of C_1 and C_2 to condense into particulate phase)

$$\xi_1 = \frac{1}{1 + \frac{0.1\ \mu g\ m^{-3}}{1\ \mu g\ m^{-3}}} = 0.91, \tag{1.4}$$

$$\xi_2 = \frac{1}{1 + \frac{1.0\ \mu g\ m^{-3}}{1\ \mu g\ m^{-3}}} = 0.50; \tag{1.5}$$

- Step 2: Update total organic particulate matter

  $C_{OA} = \xi_1 C_1 + \xi_2 C_2 = 0.91 \times 3.0\ \mu\mathrm{g\,m^{-3}} + 0.50 \times 3.0\ \mu\mathrm{g\,m^{-3}} = 4.2\ \mu\mathrm{g\,m^{-3}}$;

- Iteration 2: Repeat Steps 1 and 2 using $\mathrm{C_{OA}}$ = 4.2 $\mu\mathrm{g\,m^{-3}}$;

- Iteration 3: Repeat steps 1 and 2 using updated C_{OA} from Iteration 2. The results of these calculations are illustrated in Fig.1.5.

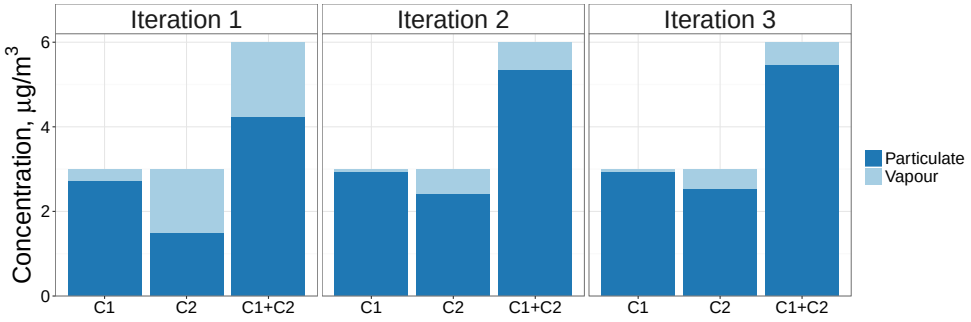

Figure 1.5 *Example iterations of gas-aerosol partitioning with two species.*

1.5 Removal and atmospheric lifetime of PM

Particulate matter is ultimately removed from the atmosphere by dry and wet deposition onto surfaces. Factors that govern the removal of a particle, as well as the relative importance of dry deposition compared with wet deposition are as follows (Seinfeld and Pandis, 2006):

- size, density, and the shape of the particle;
- the solubility of the particle in water;
- terrain or surface type (e.g. a smooth surface may lead to particle bounce-off, whereas vegetation generally promotes dry deposition);
- meteorological factors, such as level of turbulence in the atmosphere, or the amount of precipitation in the region.

1.5.1 Dry deposition

In the practical formulation of dry deposition, it is assumed that the dry deposition flux is proportional to the concentration of the depositing species (C):

$$F = -v_d C, \tag{1.6}$$

where F is the vertical dry deposition flux, and v_d is the *deposition velocity*. As C is a function of height z above the ground, v_d is also a function of z. By convention, a downward flux is negative, therefore, v_d is positive for a depositing substance (Seinfeld and Pandis, 2006).

There are three atmospheric steps that contribute to the value of deposition velocity v_d (Seinfeld and Pandis, 2006):

- aerodynamic transport down through the atmospheric surface layer to a very thin layer of stagnant air just adjacent to the surface;
- molecular (gases) or Brownian (particles) transport across this thin stagnant layer of air, called the *quasi-laminar sublayer*, to the surface itself;
- uptake at the surface or canopy.

Transport across the quasi-laminar sublayer occurs by diffusion and sedimentation. Following the three steps, atmospheric deposition processes are often described in terms of an electrical resistance analogy (Seinfeld and Pandis, 2006):

$$v_d^{-1} = r_t = r_a + r_b + r_c, \tag{1.7}$$

where r_a is the aerodynamic resistance, r_b is the quasi-laminar resistance, and r_c the surface/canopy resistance. The total resistance to deposition (r_t) is by definition the inverse of the deposition velocity v_d. For particles, the overall resistance also includes sedimentation (represented by particle settling velocity v_s), and the canopy resistance r_c is usually zero (assuming none or very little bounce-off). The formulation of v_d for particles them becomes (Seinfeld and Pandis, 2006):

$$v_d = \frac{1}{r_a + r_b + r_a r_b v_s} + v_s. \tag{1.8}$$

The aerodynamic and quasi-laminar resistances (r_a and r_b) are affected by windspeed, vegetation height, and atmospheric stability. They decrease with increasing windspeed and vegetation height. This means less deposition during high wind speeds, and higher deposition rates are expected over tall forests than over short grass. For example, typical aerodynamic layer resistance (at windspeed $4\ \mathrm{m\,s^{-1}}$) for grass is $r_a = 60\ \mathrm{sm^{-1}}$, whereas for a conifer forest it is $r_a = 10\ \mathrm{sm^{-1}}$ (Seinfeld and Pandis, 2006). The particle settling velocity is proportional to its density (ρ_p), and its diameter squared (D_p^2), and inversely proportional to viscosity of air which is a function of temperature.

1.5.2 Wet deposition

The wet deposition of PM is by rainout or washout. Rainout refers to in-cloud scavenging, i.e. particles being absorbed into water droplets inside a cloud, subsequently falling to the ground. Washout refers to below-cloud scavenging whereby falling rain or snow collides with PM and collects it (bringing it to the ground). In-cloud scavenging is a result of two processes: nucleation scavenging, and the collection of some of the remaining aerosols by the cloud droplets. From these two, nucleation scavenging is an efficient process, dominating strongly over the subsequent collection (Seinfeld and Pandis, 2006). In-cloud scavenging depends on the solubility of the particle, whereas below-cloud scavenging is determined by the size of the particle. Both depend on the amount of water in the atmosphere.

1.5.3 Atmospheric lifetime of PM

The lifetime of a pollutant is also known as their *residence time* in the atmosphere. For a primary inert pollutants, this is the time between emission and deposition. For secondary pollutants, residence time starts from their chemical production (for secondary aerosol, this includes condensation into the particulate phase). Furthermore, chemical conversion can also be considered the end of residence for a substance in the atmosphere (although the ultimate removal of pollution is by deposition). Overall, the concentrations of pollutants is a balance between emission sources and chemical production, and deposition processes (i.e. sources vs sinks).

In general, the atmospheric lifetime of fine particles is from days to weeks, whereas the lifetime of coarse particles is from minutes to days (Seinfeld and Pandis, 2006). The AeroCom framework, consisting of 31 global models, estimated that for organic

aerosol (OA), dry deposition is only responsible to 15% of the total deposition (Tsigaridis et al., 2014). This is due to small dry deposition velocities of the accumulation mode aerosols (i.e. < 2.5 μm), but dry deposition is very important for larger particles (Seinfeld and Pandis, 2006; Hodzic et al., 2016). Tsigaridis et al. (2014) also showed that the average lifetime of OA lies in the range of 3.8–9.6 days (from the 24 models that provided sufficient information to calculate this value). The main driver of this variability in OA lifetime across the models is the use of very different wet removal coefficients (Tsigaridis et al., 2014). Furthermore, Hodzic et al. (2016) suggested that these global models likely underestimate SOA production rates and underestimate SOA removal. To some extent, these shortcoming make up for each other, but more information is needed on both sources and sinks to improve the accuracy of the estimation of OA lifetime.

1.6 Measuring PM and its components

Broadly speaking, atmospheric composition can be measured in two ways: offline or online (Laj et al., 2009). Offline means collecting the sample on a filter, inertial impaction or precipitation plates, or other container, and transporting and preparing it before chemical analysis. Offline methods are prone to analytical artefacts such as evaporation of particle components, sorption (either adsorption, absorption, or both) of additional material, and chemical reactions on the sample before analysis. Offline methods are, however, generally much cheaper than online ones. Online methods measure ambient composition automatically and in real time, providing a much better temporal variability than offline measurements.

1.6.1 Measuring total PM

The UK's largest automatic air pollution monitoring network is AURN (Automatic Urban and Rural Network), which measures hourly-average concentrations of NO, NO_2, SO_2, O_3, CO, $PM_{2.5}$ and PM_{10} (but not all sites measure all of these). For measuring PM, the AURN network uses TEOM-FDMS (Tampered Element Oscillating Microbalance-Filter Dynamics Measurement System) monitors, which operate at 30 °C internal temperature. The TEOM-FDMS alternates between two 6-minute cycles. The first (called the Base measurement) measures the mass change of the microbalance filter after a 6-minute sampled airflow through it. During the

second cycle, the sampled air is directed through a cool (4 °C) filter to capture semi-volatile material, as well as PM. The purged air is then reheated and redirected through the same filter that collected PM during the Base measurement. During this 'purge' cycle, volatile components of particles on the first filter evaporate into the particle-free and SVOC-free air. This should give an indication of the volatile component of PM that might have evaporated during the Base measurement cycle. The purge cycle reading is added to the Base measurement, to try to account for material lost during the measurement. This means that the TEOM-FDMS outputs 12-minute average concentrations which are then averaged to hourly values.

1.6.2 Measuring OC and EC (BC)

As seen from above, even measuring the total PM is not straightforward, but measuring chemical speciation of PM is much more complex. Carbonaceous particulate matter (or just total carbon - TC) is a continuum from graphitic soot to non-refractory and colourless organic compounds: the first is called elemental carbon (EC) or black carbon (BC), and the end of the range is called organic carbon (OC). Although assigning a divide between the carbonaceous matter range contains ambiguity, it is necessary for the assessment of its effects (atmospheric visibility, health effects — connection to sizes, etc.). TC is usually measured by thermochemical oxidation and evolved gas analysis (CO_2 detection), EC is measured by its refractoriness (as the material that does not vaporize even at 800°C), and BC is measured by optical absorption (graphitic carbon is black, organic carbon is colourless). OC is operationally defined as the difference between TC and EC (OC = TC - EC; Quincey et al. (2009)).

Furthermore, the measured TC values only represent the carbon, and not the total organic matter (OM = OC + hydrogen, oxygen, nitrogen etc.), therefore a post-measurement scaling factor has to be applied to give an OM value for the corresponding mass contribution to PM. The scaling factor varies depending on the extent of oxidation (i.e. non-carbon mass) assumed for the organic material (usually about 1.2–1.8; Pöschl (2005)).

1.6.3 Aerosol Mass Spectrometer (AMS) and Positive Matrix Factorization (PMF) of OA components

Measurement of OA by online mass spectrometry, such as with the Aerodyne Aerosol Mass Spectrometer (AMS; Canagaratna et al. (2007)), and consideration of individual organic marker ions coupled with multivariate statistical techniques such as positive matrix factorization (PMF; Paatero and Tapper (1994); Paatero (1997)), have facilitated the subdivision of the OA component into empirical categories. These include hydrocarbon-like organic aerosol (HOA), oxygenated organic aerosol (OOA, which can be further split into low-volatility and semi-volatile oxygenated organic aerosol: LV-OOA and SV-OOA), solid-fuel organic aerosol (SFOA), biomass burning organic aerosol (BBOA), cooking organic aerosol (COA), and a number of other categories (Ulbrich et al., 2009; Ng et al., 2010; Lanz et al., 2010; Ng et al., 2011; Young et al., 2015a). The SFOA factor is a more general version of BBOA as it includes in addition to biomass other sources such as coal and charcoal (Allan et al., 2010). Figure 1.6 gives a hierarchical overview of the most commonly apportioned AMS-PMF factors. Not all analyses can identify all these different aerosol types, and in some cases although a distinct species is found, it is not always identifiable as a specific type of aerosol (e.g. OOA1 and OOA2, or sometimes unidentifiable factors are reported as Unknown: e.g. Tab. 1.3).

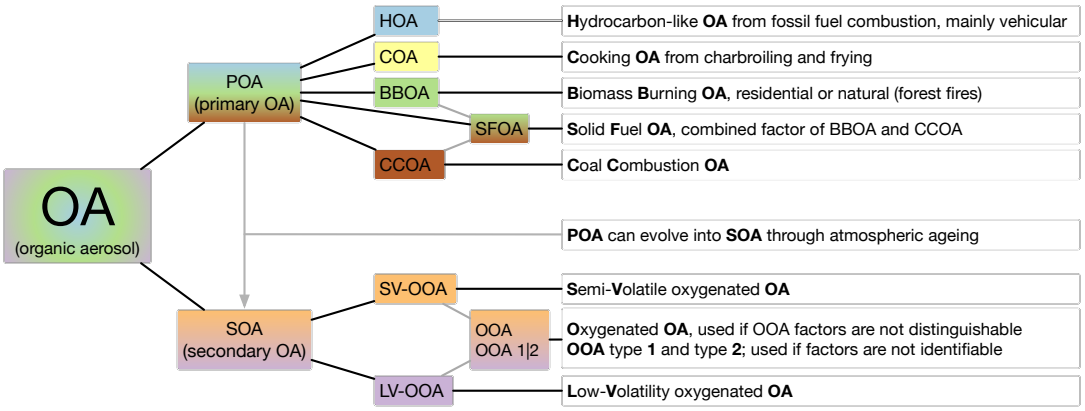

Figure 1.6 *Summary diagram of the most commonly apportioned AMS-PMF factors for organic aerosol.*

1.6.4 AMS-PMF measurements used in this study

Most of the comparison and evaluation with measurements presented in this thesis is done for measurements from the Clean Air for London (ClearfLo) campaign in 2012 (Bohnenstengel et al., 2014). Measurement site locations are shown in Fig. 1.7. Different types of AMS were deployed in this campaign. At the London North Kensington site a compact time-of-flight AMS (cToF-AMS) was deployed for a full calendar year (January 2012 January 2013), and a high-resolution time-of-flight AMS (HR-ToF-AMS) was also deployed for the IOPs at the same site. At Marylebone Road, a Quadrupole AMS (Q-AMS) was deployed for the whole calendar year. A HR-ToF-AMS was deployed in Detling during the winter IOP, and in Harwell during the summer IOP.

The first three sites (London North Kensington, London Marylebone, and Harwell) are also part of several ongoing monitoring networks, for example, the UK Automated Urban and Rural Network (AURN), TODO add more from uk-air. London Marylebone Road is classified as a roadside site capturing very high concentrations of mostly traffic-related pollutants from a major road in central London. London North Kensington is classified as an urban background site, and it is situated in a schoolyard about 5 km from the Marylebone Road location. Harwell is a rural background site ~80 km west of Central London that is also an EMEP (European Monitoring and Evaluation Programme) supersite. Detling was a rural background site ~70 km east of Central London.

PMF analysis was applied to each of the datasets to apportion measured OA into different components (Ulbrich et al., 2009). A detailed description of the derivation and optimization of the factors retrieved from the AMS data at Detling can be found in Xu et al. (2016), at London North Kensington in Young et al. (2015a) and Young et al. (2015b) (all three of these analyses were performed with the PMF2 solver), and at Harwell in Di Marco et al. (2015) (using the ME-2 solver). The OM/OC ratios for each of the PMF datasets presented in this study were calculated with the Improved-Ambient method from Canagaratna et al. (2015). A summary of the instruments, measurement periods and resolved PMF factors is given in Table 1.3.

When AMS measurements and their PMF apportionments are compared, some disagreement is observed, as shown for the two instruments measuring at the same time at the same location at London North Kensington. This is in part due to the differences in the types of AMS used, where more chemical information is retrieved from the

Figure 1.7 *Locations of measurement sites used in this work. London North Kensington is an Urban Background site, London Marylebon Road is a roadside site, Harwell and Detling are Rural Background sites. Underlying map from © OpenStreetMap contributors.*

HR-ToF-AMS, which can subsequently lead to differences in the derived PMF factors from the individual datasets. It should also be kept in mind that PMF was run on each of the full datasets, covering a full year for the cToF-AMS and only four weeks for each of the HR-ToF-AMS IOPs, thus it is not necessarily expected that the same PMF factors would be derived from the different datasets. Nevertheless, strong correlations between daily averaged primary OA components from the two instruments deployed at the London North Kensington site during the winter IOP are observed (0.95, 0.92, and 0.88 for HOA, SFOA, and COA, respectively), with less strong correlations for SOA (0.77). Scatterplots of these PMF derived OA component concentrations resolved for the cToF-AMS data and HR-ToF-AMS are shown in Fig. 1.8. This inherent uncertainty in the measurements constrains the expected correlation with the model.

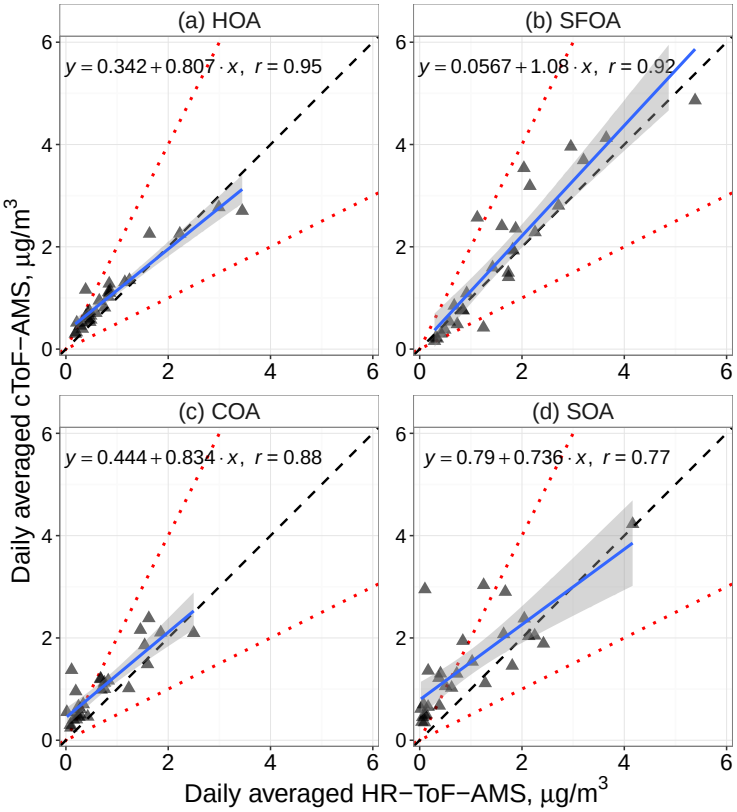

Figure 1.8 *Scatterplots of PMF-derived OA component concentrations ((a) HOA, (b) SFOA, (c) COA, (d) SOA) based on different AMS instruments at the London North Kensington site during the winter IOP. The dashed lines are the 2:1, 1:1, and 1:2 lines.*

Table 1.3 *AMS measurements and resolved PMF factors during the ClearfLo campaign and the allocation of the PMF factors to SOA for comparison with model simulations. Site locations are shown in Fig. 1.7. Site names are abbreviated as follows: NK - London North Kensington, DET - Detling, HAR - Harwell, MB - Marylebone Road.*

Period	Site	Dates (year 2012)	Instrument	POA factors	SOA factors
winter IOP	NK	13-Jan–8-Feb	HR-ToF-AMS	HOA, SFOA1, SFOA2, COA	OOA
	DET	20-Jan–14-Feb	HR-ToF-AMS	HOA, SFOA	OOA
summer IOP	NK	21-Jul–19-Aug	HR-ToF-AMS	HOA, COA, Unknown	SV-OOA, LV-OOA
	HAR	3-Aug–20-Aug	HR-ToF-AMS	HOA	SV-OOA, LV-OOA, N-OOA
annual	NK	11-Jan–24-Jan (2013)*	cToF-AMS	HOA, SFOA**, COA	OOA1, OO2**
	MB	11-Jan–1-Feb (2013)	Q-AMS	HOA, SFOA, COA	LV-OOA, SV-OOA

* As the cToF-AMS was retuned before the summer IOP and retuned to the previous tuning at the end of the IOP, the subsequent data could not be used in the PMF analysis (see Young et al. (2015a) for details). However, for the purpose of the comparison in this study, data from the HR-ToF-AMS, deployed at the same site during the summer IOP, was used to fill in this period.

** PMF analysis revealed the SFOA and OOA2 factors were convolved due to their similar, strong diurnal cycles. Daily averages have been used to estimate their concentrations (Young et al., 2015a).

1.7 Atmospheric chemical transport modelling

The concept of an atmospheric chemical transport model[2] (ACTM) is as follows: the model starts from estimates of emissions (see Chapter 1.3), then the pollutants are advected and diffused, during which they also undergo chemical reactions, and are removed from the atmosphere by deposition (Figure 1.9). ACTMs are not to be confused with statistical models that interpolate or do statistical analysis of measured concentrations of atmospheric constituents.

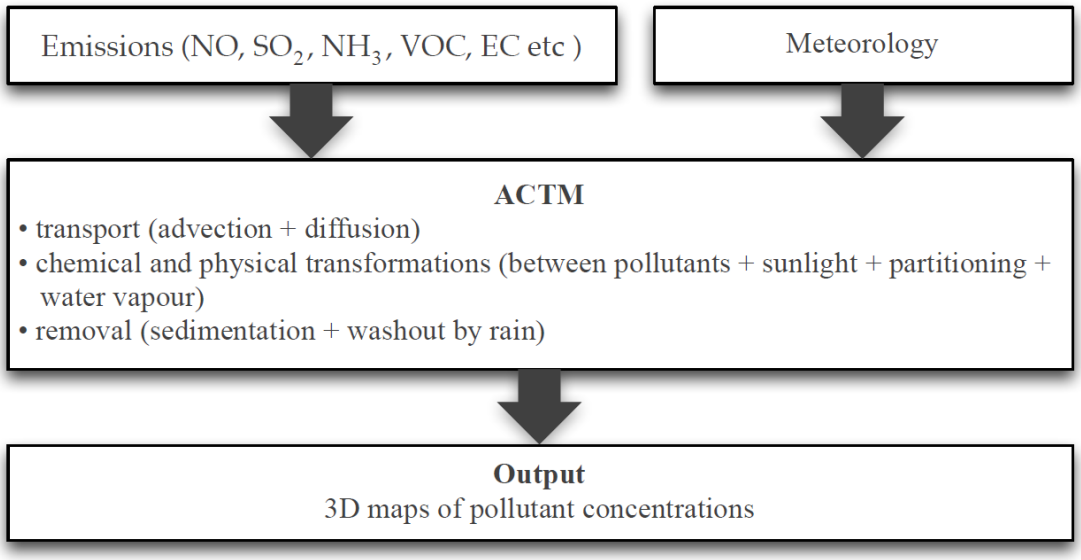

Figure 1.9 *Simplified schematic of atmospheric chemical transport models (ACTMs).*

Atmospheric advection of pollutants is driven by meteorological fields (e.g., 3 components of the wind) that are calculated with a numerical weather prediction model (NWPM). In the state-of-the-art modelling systems, NWPMs and ACTMs are coupled online, i.e. they are run together exchanging information. Offline ACTMs use meteorological fields that have been pre-calculated with a NWP model. The photochemistry and deposition of pollutants depend on atmospheric conditions such as light, temperature, relative humidity, atmospheric stability, etc., which are also available in the output of a NWP model. The calculations are performed for a 3-D grid corresponding to the area of interest. In addition to emissions and meteorological fields, various metadata can be input to ACTMs (e.g., land type: water, grassland,

[2]The terms "chemical transport model", "chemistry transport model", and "chemistry and transport model" are interchangeable. A Google Scholar search on 21-April 2016 for these three terms gave 14,000 results for "chemical transport model", 8,100 results for "chemistry transport model" (equivalent result for "chemistry-transport model"), and 1,550 results for "chemistry and transport model". The one used in this work was chosen following Simpson et al. (2012).

forest, urban, etc.; elevation; surface roughness; information about vegetation, and other).

During development, ACTMs are constantly validated against measured concentrations, but stable model versions are usually meant to be working independently from the measurements. ACTMs can provide information about atmospheric composition anywhere (that means places that do not have measurement stations) and anytime (past, present and future simulations). In addition to increased spatial and temporal abilities, models can be used to answer the following questions (Seinfeld and Pandis, 2006):

- Where could the measured pollutants have come from?
- What is the contribution of a particular emission source (e.g., a power plant) to nearby towns? Or to towns that are far away, or to neighbouring countries etc.?
- What is the best strategy for reducing pollutant levels at a certain area?
- Where should we plan a future source to minimise its environmental and health impacts?

1.7.1 Model and measurement intercomparison statistics

A variety of statistical measures are used in this study:

Mean bias (MB) is defined as the difference between the modelled and observed average values:

$$MB = \overline{M} - \overline{O}, \tag{1.9}$$

where $\overline{M}$ is the modelled mean and $\overline{O}$ the measured mean. A negative MB means that the model underestimates measured concentrations, a positive MB means that the model overestimates measured concentrations.

Normalised mean bias (NMB) is the mean bias relative to the observed mean:

$$NMB = \frac{MB}{\overline{O}}. \tag{1.10}$$

Mean gross error (MGE) is an average of the absolute differences between modelled

and observed values:

$$MGE = \frac{1}{n}\sum_{i=1}^{n}|M_i - O_i|, \tag{1.11}$$

where n is the number of values.

Normalised mean gross error (NMGE) is the mean gross error relative to the observed mean:

$$NMGE = \frac{MGE}{\overline{O}}. \tag{1.12}$$

Factor of 2 (FAC2) is the proportion of modelled concentrations that are within a factor of two of the measured concentrations.

The *Pearson's correlation coefficient* (*r*-value; *r*) is a measure of the linear relationship between the modelled and observed values:

$$r = \frac{1}{n-1}\sum_{i=1}^{n}\left(\frac{M_i - \overline{M}}{\sigma_M}\right)\left(\frac{O_i - \overline{O}}{\sigma_O}\right), \tag{1.13}$$

where σ_M is the standard deviation of the modelled values, and σ_O is the standard deviation of the observed values.

The coefficient of efficiency (COE, Legates and McCabe (2013)) is defined as:

$$COE = 1.0 - \frac{\sum_{i=1}^{n}|M_i - O_i|}{\sum_{i=1}^{n}|O_i - \overline{O}|}, \tag{1.14}$$

where M_i is the modelled value, O_i is the corresponding measured value and $\overline{O}$ is the mean measured value. A COE of 1 indicates perfect agreement between model and measurements. Although the COE does not have a lower bound, a zero or negative COE implies that the model cannot explain any of the variation in the observations (Legates and McCabe, 2013).

1.7.2 Previous modelling studies and the aim of this study

Notwithstanding the uncertainties in defining and measuring OA components, there is a general tendency for models to underestimate observed amounts of OA. The studies that have demonstrated this tendency include a range of areas from global, regional (i.e. Europe, North America), to local (i.e. one country, or city). Furthermore, current assumptions about the precursor emissions, yields, and ageing rates of secondary OA are a major source of uncertainty in these modelling studies.

Global modelling studies

For example, from global modelling studies, the AeroCom (Aerosol Comparisons between Observations and Models) project, which includes ~30 global ACTMs and global circulation models (GCMs), has concluded that the amount of OA present in the atmosphere remains largely underestimated (Tsigaridis et al., 2014). Similarly, in an evaluation of seven global models, Pan et al. (2015) reported a systematic underestimation of OA over South Asia. Lin et al. (2014) tested different mechanisms for aqueous-phase formation of SOA with a global model. For SOA, most of their experiments exhibited a NMB between -30% and -50% (compared with AMS-PMF apportionment measurements at urban background, urban downwind, and rural sites in the Northern Hemisphere in 2000-2007 from Zhang et al. (2007)). Several global modelling studies have demonstrated huge differences (up to tenfold) in total simulated SOA budgets (Pye and Seinfeld, 2010; Spracklen et al., 2011; Jathar et al., 2011).

European modelling studies

There have been a few European-wide studies with different models. For example, in Bergström et al. (2012), the measurements of OC of 1358 daily filter samples from several European measurement campaigns between 2002 and 2007 were used in the evaluation of different EMEP model experiments with different assumptions for the volatility of POA emissions, and subsequent atmospheric ageing and SOA formation. The average measured OC concentration was 3.0 $\mu g\,m^{-3}$, and the average modelled concentrations were 1.3–1.8 $\mu g\,m^{-3}$ (from four different model experiments), a NMB of -40% (for the highest experiment). The OC underestimation was smaller during summer (measured: 2.6 $\mu g\,m^{-3}$, modelled: 1.2–2.1 $\mu g\,m^{-3}$) and bigger during winter (measured: 3.3 $\mu g\,m^{-3}$, modelled: 1.4–1.5 $\mu g\,m^{-3}$). Bergström et al. (2012) also

included comparisons with AMS-PMF apportionment measurements. With the volatile treatment of POA, they underestimated secondary fossil OC (anthropogenic SOA: ASOA) concentrations. On the other hand, with the non-volatile treatment of POA, the model produced more SOA, but lost most of the POA due to evaporation. In a later study using the same model and a revised (mostly increased) residential woodburning inventory, Denier van der Gon et al. (2015) reduced the NMB of OC from -44% to -25%. Their wintertime improvement was from -54% to -29%. These tests included IVOCs added proportionally to POA emissions (+1.5x).

In another European-wide study, Fountoukis et al. (2014) used the semivolatile treatment of POA and the addition of IVOCs = 1.5xPOA. Their POA therefore evaporated, showing huge underestimations compared to measured HOA. For SOA, their site-wise NMB ranged from $+125\%$ (Mace Head) to -67% (Vavhill). Most of the sites for which SOA was underestimated were in central Europe, whereas their model was likely to overestimate concentrations at relatively remote sites (in Finland for example). Overall, there were more sites where their model underestimated SOA than overestimated.

Aksoyoglu et al. (2011) compared CAMx (Comprehensive Air Quality Model with Extensions) simulations of PM_1 components to AMS measurements in Switzerland. Both the model and the measurements suggested that particle nitrate and OA are the main components during winter and that during summer, over half of PM_1 is made up of OA. Their model did, however, underestimate the measured mean OA concentration by about -25%, as well as the relative contribution of SOA to OA.

In a study over the UK, following sensitivity tests given in their supplementary information, Redington and Derwent (2013) ended up multiplying all anthropogenic NMVOC emissions by a factor of 5 to get the modelled OC to compare with measured OC, thus all the agreement presented in their paper was with the increased NMVOC emissions.

Northern American modelling studies

Similarly to the European-wide (EMEP programme) measurement networks and campaigns, modelling studies in the US often compare with measurements from their two national networks: IMPROVE (rural sites) and STN (urban sites). Murphy and Pandis (2009) overestimated OC at rural sites (the IMPROVE network) and underestimated OC at urban sites (the STN network) by -28%. Jathar et al. (2011)

presented mainly negative biases of OA, compared with ~200 sites in the US (including the +1.5xIVOCs). Koo et al. (2014) presented a 1.5-dimensional volatility basis set approach with both CMAQ and CAMx. Their Base and Mono-POA tests with CMAQ underestimated OC by -30 to -50%, whereas their CAMx simulations were in the range of measured concentrations (NMB from -30% to $+30\%$).

Mexico City modelling studies

As a megacity with air quality challenges, Mexico City has been the subject of several studies. Simulations by Hodzic et al. (2010) underestimated total OA by about -40%. SOA was underestimated with the non-volatile assumption as well as with the semivolatile treatment of POA (including the +1.5xIVOCs). They also did an experiment with much lower enthalpy of vaporisation (ΔH_{VAP}) from Grieshop et al. (2009) which yielded overestimations in modelled SOA compared with measurements, but the underestimation of total OA remained.

Even after multiplying semivolatile POA and associated IVOCs by a factor of 3 (3x semivolatile POA emissions + 3x1.5xIVOCs = 7.5xPOA), simulations by Shrivastava et al. (2011) with WRF-Chem in Mexico city underestimated SOA concentrations at urban sites, but overestimated SOA at downwind suburban sites. For some tests they even doubled the 7.5x.

Aim of this study

To summarise, many different models applied over different countries, regions, continents, or globally have systematically underestimated modelled OA or OC concentrations in comparison with measurements. Several of these studies have achieved better agreement by increasing the estimates of the underlying emissions inventories. Thus, the work presented in this thesis focuses on three different sources of OA that have been either underestimated or misrepresented (Chapter 3: Diesel SOA), or are not included in emissions inventories (Chapter 4: Cooking OA), or are spatially misrepresented (Chapter 5: Coal and wood burning OA).

Chapter 2

Model description - EMEP4UK

The EMEP4UK modelling system is a regional application of the EMEP MSC-W (European Monitoring and Evaluation Programme Meteorological Sythesizing Centre-West) model. The EMEP MSC-W model (henceforward referred to as the EMEP model) is a 3-D Eulerian model that has been used for both scientific studies and policy making in Europe. A detailed description of the EMEP MSC-W model, including references to evaluation and application studies is available in Simpson et al. (2012), Schulz et al. (2013), and at www.emep.int. The EMEP4UK model is described in Vieno et al. (2010, 2014, 2016), and the model used here was based on version v4.5.

2.1 Grid definition

2.1.1 Horizontal resolution

The horizontal resolution of the EMEP model's official grid is 50 km $\times$ 50 km over Europe, and it uses a polar-stereographic projection (50 km $\times$ 50 km is true at 60°N). The EMEP4UK modelling framework has been using this grid for the European domain run, which is then used as a boundary condition for the finer, 5 km $\times$ 5 km horizontal resolution grid over the British Isles (Vieno et al., 2010). The domains are shown in Fig. 2.1.

The European modelling domain effectively provides the chemical boundary for the inner domain. The boundary conditions for the outer domain are prescribed using simple time and latitude dependent boundary concentration values based on

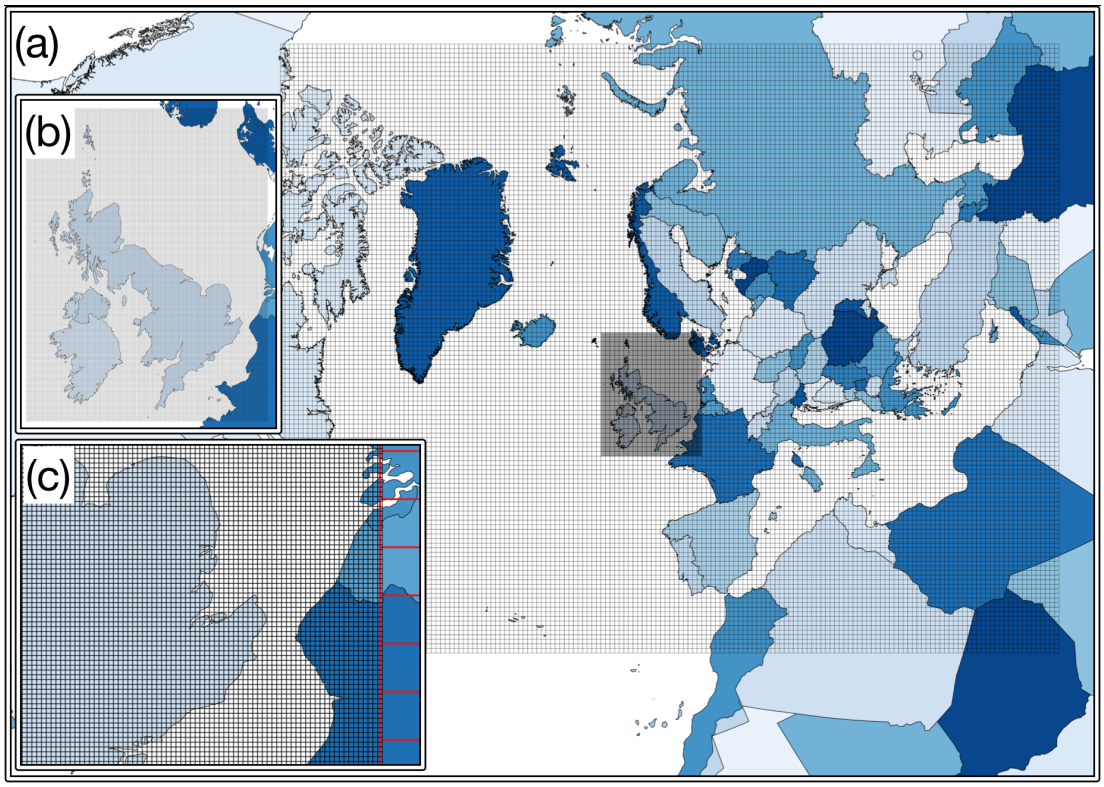

Figure 2.1 *Grids of the EMEP4UK modelling system: (a) the European domain of 50 km × 50 km with the British Isles domain shaded, (b) the 5 km × 5 km British Isles inner domain, (c) example of a nesting boundary.*

climatological measurements (as given in the Supplementary material to Simpson et al. (2012)). For most species, the seasonal changes in these boundary concentrations are prescribed with monthly variation, with the exception of methane, hydrogen, and background organic aerosol (see Sect. 2.5 for more information on this) that are prescribed as constant values. The provision of higher resolution boundary fields (e.g. daily, or simulated vertical distribution) from global chemical transport models might be scientifically advantageous for simulating European air quality, but this simplified approach is considered sufficient.

2.1.2 Vertical resolution

The vertical levels are defined with sigma coordnates:

$$\sigma = \frac{p - p_T}{p_S - p_T} \tag{2.1}$$

where σ is the vertical coordinate, and p, p_S and p_T are pressure at level σ, at the surface, and at the top of the model domain, respectively. By default, the EMEP model

uses 20 vertical levels, ranging from the ground (first level is about 90 m thick) to 100 hPa (about 16 km) (Simpson et al., 2012). In this work, the lowest level was further divided to 40 m and 50 m, thus having 21 vertical levels (levels from 90 m upwards are identical to the EMEP model default levels).

To demonstrate the impact of the change in vertical resolution, Tables 2.1 and 2.2 give model-measurement evaluation statistics for daily-average concentrations of O_3, NO_x, SO_2, CO, $PM_{2.5}$, and PM_{10} at all AURN Rural Background and Urban Background sites measuring the given species for the year 2012 using the 90 m and 40 m lowest vertical levels.

For ozone, using the 40 m layer results in marked improvements at urban sites, while reducing performance at the rural background sites. The improvement at the urban sites is, however, greater than the additional discrepancy introduced at the rural sites. Ozone concentrations at the urban sites were initially overestimated by 21% (NMB, 90 m layer). The reduction of 5 $\mu g\,m^{-3}$ (to a NMB of +9%) with the 40 m level is likely driven by ozone being titrated by the increased NO present in the thinner surface layer due to the smaller dilution of primary traffic emissions.

For NO_x, NMB is reduced for both the rural and the urban sites. For urban sites, the COE is also improved, whereas for rural locations, COE is reduced (a small negative change for the rural sites is also seen in the *r*-value). For the urban sites, FAC2 improves to 65% from 48%.

Reducing the height of the lowest level does not make a substantial difference to SO_2 concentrations modelled at rural sites, but there is a notable adverse effect at the urban sites, compared to measurements. Chiefly, the NMB is increased from +16% to +41%, and the COE reduces from -0.46 to -0.75. SO_2 is a primary pollutant, so higher modelled concentrations at urban locations within the lower surface layer of 40 m imply that the emission height might now be underestimated for some sources.

There are no measurements of CO concentrations at rural sites within the AURN, but for the urban sites using a 40 m layer results in an improvement compared to the measured daily-average concentrations. Specifically, the negative NMB is reduced from -26% to -16%.

Table 2.1 *Model-measurement evaluation statistics for the daily-average concentrations of O_3, NO_x, and SO_2 (see Table 2.2 for CO, $PM_{2.5}$, and PM_{10}) for two different model configurations (90 m surface layer and 40 m surface layer) at AURN sites in 2012. Number of data points (n) is equal to the number of sites measuring each pollutant times the number of days with measurements at that site. Notable differences between the two configurations are highlighted with green (improvement) or red (worse). MB, MGE, and RMSE are in $\mu g\ m^{-3}$.*

	Rural Background		Urban Background	
	90 m	40 m	90 m	40 m
O_3	*n* = 8131		n = 15373	
FAC2	96%	93%	90%	90%
MB	-0.38	-3.51	8.47	3.67
MGE	10.88	11.93	12.27	11.06
NMB	-1%	-6%	21%	9%
NMGE	20%	22%	30%	27%
RMSE	14.05	15.38	15.85	14.47
r	0.69	0.67	0.75	0.74
COE	0.22	0.14	0.19	0.27
NO_x	*n* = 4971		n = 17748	
FAC2	67%	68%	48%	65%
MB	-3.15	0.32	-22.73	-17.02
MGE	6.18	7.31	23.96	20.71
NMB	-23%	2%	-53%	-40%
NMGE	46%	54%	56%	49%
RMSE	11.68	13.26	39.51	36.36
r	0.74	0.67	0.68	0.66
COE	0.40	0.29	0.13	0.25
SO_2	*n* = 2082		n = 8357	
FAC2	33%	33%	39%	40%
MB	-0.18	-0.11	0.43	1.09
MGE	1.80	1.86	2.53	3.03
NMB	-9%	-5%	16%	41%
NMGE	87%	90%	95%	113%
RMSE	2.86	2.95	4.75	6.14
r	0.19	0.17	0.20	0.15
COE	-0.27	-0.31	-0.46	-0.75

Table 2.2 *Model-measurement evaluation statistics for the daily-average concentrations of CO, $PM_{2.5}$, and PM_{10} (see Table 2.2 for O_3, NO_x, and SO_2) for two different model configurations (90 m surface layer and 40 m surface layer) at AURN sites in 2012. Number of data points (n) is equal to the number of sites measuring each pollutant times the number of days with measurements at that site. Notable differences between the two configurations are highlighted with green (improvement). MB, MGE, and RMSE are in $\mu g\ m^{-3}$.*

	Rural Background		Urban Background	
	90 m	40 m	90 m	40 m
CO	n = 0		n = 4083	
FAC2			84%	88%
MB			-73	-46
MGE			100	95
NMB			-26%	-16%
NMGE			35%	33%
RMSE			144	138
r			0.42	0.42
COE			-0.07	-0.01
$PM_{2.5}$	*n* = 1071		n = 13067	
FAC2	66%	66%	75%	77%
MB	-1.56	-1.64	-3.12	-3.03
MGE	4.43	4.50	4.85	4.83
NMB	-15%	-16%	-26%	-25%
NMGE	43%	44%	40%	40%
RMSE	6.40	6.59	7.49	7.53
r	0.75	0.73	0.70	0.69
COE	0.30	0.29	0.25	0.26
PM_{10}	*n* = 1714		n = 10052	
FAC2	70%	70%	83%	83%
MB	5.66	5.22	1.79	1.59
MGE	7.63	7.30	7.11	6.95
NMB	48%	44%	11%	9%
NMGE	64%	62%	42%	41%
RMSE	11.11	10.52	10.39	10.13
r	0.55	0.55	0.54	0.53
COE	-0.31	-0.25	0.03	0.06

Neither $PM_{2.5}$ or PM_{10} exhibit notable differences in surface concentrations modelled with the 90 m or 40 m surface layers. This can be explained by the fact that over the UK much of PM is of secondary nature, and its concentrations are often driven by long range transport (Vieno et al., 2014).

Overall, the improvements in ozone (urban sites), nitrogen oxides, and carbon monoxide gained from using the 40 m lowest layer outweigh the additional disagreement introduced for ozone at the rural sites and sulphur dioxide at the urban sites.

2.1.3 Time step

The advection time-step varies with resolution: 20 minutes for the 50 km $\times$ 50 km grid, and 5 minutes for the 5 km $\times$ 5 km grid. The model checks that the time-step satisfies the Courant-Friedrichs-Lewy condition and automatically reduces the time-step when necessary (Simpson et al., 2012). In the context of atmospheric modelling, the Courant-Friedrichs-Lewy condition means the advection time-step has to be shorter than the time taken for advection from one grid cell to another.

The chemical equations are solved for much smaller time-steps than the advection. The TWOSTEP algorithm used in the EMEP model (Verwer and Simpson, 1995; Verwer et al., 1996) starts with five successive time-steps of 20 s, followed by seven time-steps of 157 s (adding up to 20 minutes, which is the advection time-step for the European domain). In the 4 layers near the ground, this is iterated 3 times, above these layers, twice, and for the 6 uppermost layers, a single iteration is used (Simpson et al., 2012).

2.2 Meteorology

The model was driven by output from the Weather Research and Forecasting (WRF) model (`www.wrf-model.org`, version 3.1.1) including data assimilation of 6-hourly model meteorological reanalysis from the US National Center for Environmental Prediction (NCEP)/National Center for Atmospheric Research (NCAR) Global Forecast System (GFS) at 1° resolution (NCEP, 2000). The WRF configuration was as follows: *Lin Purdue* for microphysics; *Grell-3* for cumulus parametrization; *Goddart Shortwave* for radiation physics; and Yonsey University (*YSU*) for planetary boundary layer (PBL) height (see NCAR (2008) for further information). The meteorological set-up of the simulations used in this study is from Vieno et al. (2010) where it is shown

to perform very well in comparison with measurements. No further meteorological evaluation is presented here.

2.3 Emissions

Gridded anthropogenic emissions of NO_x (95% NO + 5% NO_2), SO_2, NH_3, CO, NMVOCs (non-methane VOCs), $PM_{2.5}$ and PM_{10} were obtained from NAEI (National Atmospheric Emissions Inventory, NAEI (2013)) for the UK, and from CEIP (EMEP Centre on Emission Inventories and Projections; CEIP (2015)) for the rest of the model domain. All emissions are apportioned across a standard set of emission source sectors, following the sector structure defined in the Selected Nomenclature for Air Pollutant (SNAP; EEA (2013); Table 2.3), consistently applied across the whole domain.

Primary PM emissions reported as $PM_{2.5}$ and PM_{10} in the NAEI and CEIP are speciated into EC, OA from fossil fuel combustion (from here on denoted HOA - hydrocarbon-like OA), OA from domestic combustion (from here on denoted SFOA - solid fuel OA), and remaining primary PM by source sectors (using splits developed by Kuenen et al. (2014); as in Fig. 2.2). Default speciation of NMVOC emissions into 14 surrogate groups is used (Simpson et al., 2012). International shipping emissions from Entec UK Limited (now Amec Foster Wheeler) are used (Entec, 2010). Daily emissions of all the aforementioned trace gases and particles from natural fires were taken from the Fire INventory from NCAR version 1.0 (FINNv1, Wiedinmyer et al. (2011)). Monthly NO_x emissions from in-flight aircraft, soil and lightning, as well as biogenic emissions of dimethyl sulphide (DMS), are included as described in Simpson et al. (2012). Biogenic emissions of isoprene and monoterpenes are calculated by the model for every grid cell and time-step. Estimated emissions of wind-blown dust and sea salt are also included but these have no impact on the model simulations of OA (Simpson et al., 2012).

2.3.1 Temporal profiles of emissions

Annual total emissions are temporally split using monthly, day-of-week, and hourly emission profiles for each SNAP sector and pollutant. Monthly and day-of-week profiles are different for different countries (as in Simpson et al. (2012) based on Reis et al. (2004)), whereas unified profiles for all countries are used for the hourly variation

in emissions (as in Simpson et al. (2012) based on Menut et al. (2012)). Different hourly diurnal profiles are used for weekdays, Saturdays, and Sundays. Temporal emission profiles for $\mathrm{PM}_{2.5}$ are shown in Figs. 2.3 (monthly), 2.4 (day-of-week), and 2.5 (hourly).

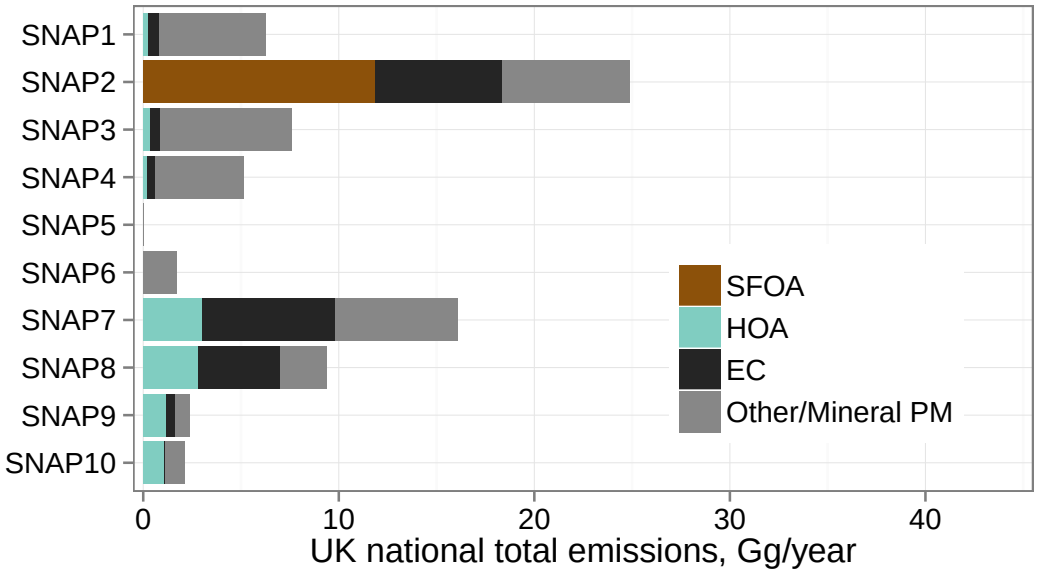

Figure 2.2 *Annual UK $PM_{2.5}$ emissions by SNAP sector (Table 2.3) as specified in the NAEI (for year 2012), with each sector split into POA (HOA or SFOA), EC, and remaining PM following Kuenen et al. (2014).*

Table 2.3 *SNAP source sectors as specified in the emissions input to the model.*

SNAP1	Combustion in energy and transformation industries
SNAP2	Residential and non-industrial combustion
SNAP3	Combustion in manufacturing industry
SNAP4	Production processes
SNAP5	Extraction and distribution of fossil fuels
SNAP6	Solvent and other product use
SNAP7	Road transport
SNAP8	Other mobile sources and machinery
SNAP9	Waste treatment and disposal
SNAP10	Agriculture
SNAP11	Natural and other sources

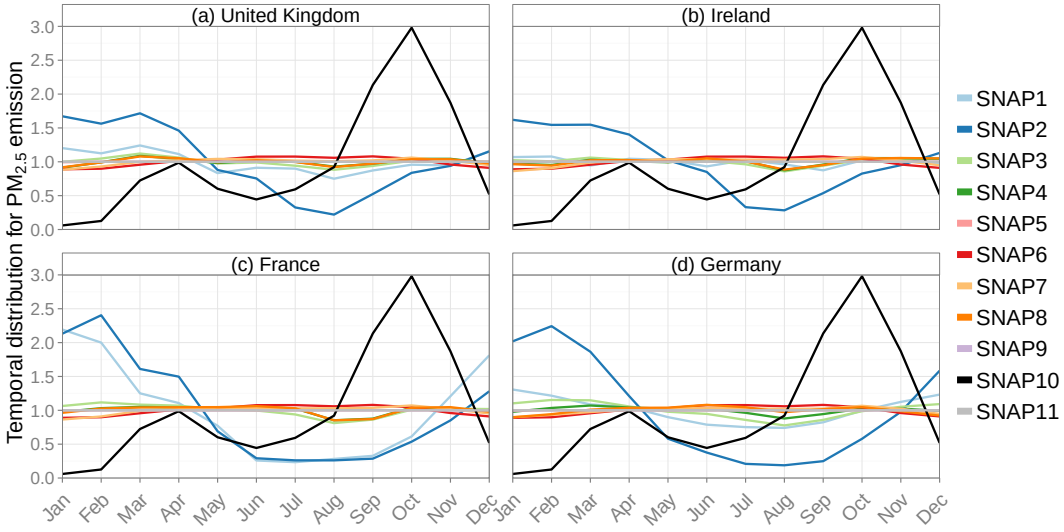

Figure 2.3 *Normalised monthly emission profiles for $PM_{2.5}$ from different SNAP sectors for select countries: (a) UK, (b) Ireland, (c) France, and (d) Germany.*

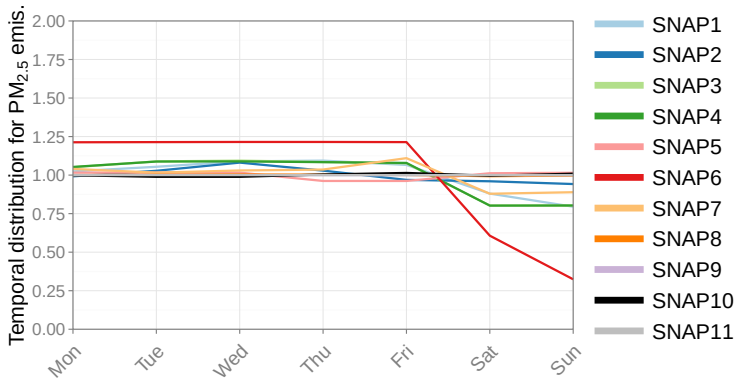

Figure 2.4 *Normalised daily emission profiles for $PM_{2.5}$ from different SNAP sectors for UK emissions.*

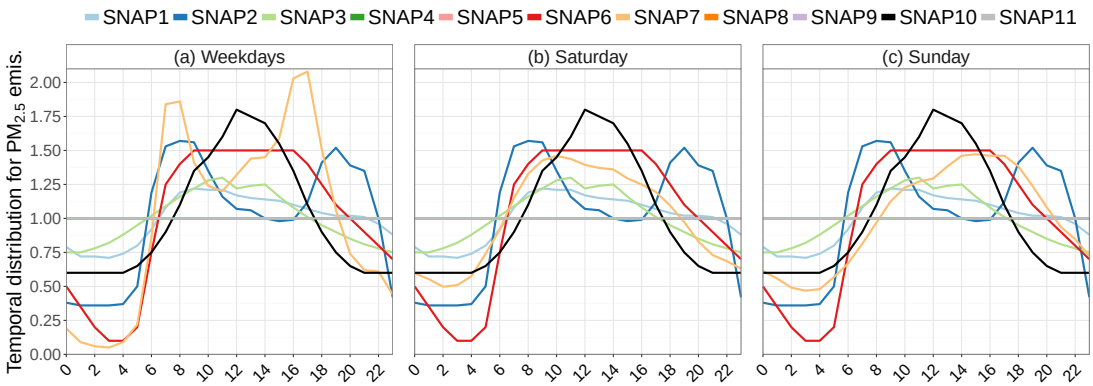

Figure 2.5 *Normalised hourly emission profiles for $PM_{2.5}$ from different SNAP sectors (same used for all countries) for different days of the week: (a) weekdays, (b) Saturdays, and (c) Sundays.*

2.4 Dry and wet deposition in the model

The mass-conservative implementation of the dry deposition resistance calculation in the model uses the following equation (Simpson et al., 2012):

$$v_d(z) = \frac{v_s}{1 - e^{-r(z)v_s}}, \tag{2.2}$$

where v_s is the settling velocity, $v_d(z)$ is the deposition velocity at height z, and $r(z)$ is the sum of the aerodynamic resistances. The overall dry deposition rate of larger particles is affected by v_s, which is strongly size-dependent. To account for this, the v_s calculations are integrated over the aerosol sizes, assuming a log-normal particle size distribution. The calculation of the aerodynamic resistance in the model makes use of 16 land use categories, and where applicable leaf area indexes (LAIs; i.e. relevant for canopy, but not for water, ice, urban) and growing seasons. However, the formulation of the latter on dry deposition of aerosols is intentionally simplistic due to the uncertainty of a reliable choice for a more detailed scheme (Simpson et al., 2012). Five characteristic aerosol classes are used in the model for the calculation of the dry deposition fluxes (Table 2.4).

Table 2.4 *Physical characteristics of different aerosol classes in the EMEP model (Simpson et al., 2012) used in the dry deposition calculation: median diameter ($\mathrm{D_p}$), geometric standard deviation (σ_g), density (ρ_p), and enhancement factor ($\mathrm{F_N}$)*.*

D_p µm	σ_g	ρ_p kg m^{-3}	F_N	Species
0.33	1.8	1600	3	fine nitrate, ammonium
0.33	1.8	1600	1	all other fine PM, e.g., sulphate, EC, OA
3.0	2.0	2200	1	coarse nitrate
4.0	2.0	2200	1	coarse sea-salt
4.5	2.2	2600	1	all other coarse PM

* The enhancement factor is an empirical modification for the dry deposition of nitrogen containing aerosol in low vegetation and forests, see Simpson et al. (2012) for more information.

The in-cloud scavenging (S_{in}; rainout) of a component with a mixing ratio χ is calculated as follows (Simpson et al., 2012):

$$S_{in} = -\chi \frac{W_{in} P}{h_s \rho_w}, \tag{2.3}$$

where where W_{in} is the in-cloud scavenging ratio of a component (given in Table 2.5), P ($\mathrm{kg\,m^{-2}\,s^{-1}}$) is the precipitation rate, h_s is the characteristic scavenging depth (assumed to be 1000 m), and ρ_w is the water density (1000 $\mathrm{kg\,m^{-3}}$). Differentiation is made between fresh EC which is hydrophobic, and EC aged by the OH radical which then becomes as hygroscopic as all other particles.

The below-cloud wet scavenging (S_{sub}; washout) is calculated as follows (Simpson et al., 2012):

$$S_{sub} = -\chi \frac{AP}{V_{dr}} \bar{E}, \tag{2.4}$$

where V_{dr} is the the raindrop fall speed (5 $\mathrm{m\,s^{-1}}$), $A = 5.2\ \mathrm{m^3\,kg^{-1}\,s^{-1}}$ is an empirical coefficient, and $\bar{E}$ is the size-dependent collection efficiency of aerosols by the raindrops (given in Table 2.5).

Table 2.5 *Wet scavenging ratios and collection efficiencies of aerosols in the EMEP MSC-W model (Simpson et al., 2012).*

$W_{in}(\times 10^6)$	$\bar{E}$	Species
0.2	0.02	Fresh (hydrophobic) EC
1.6	0.02	Fine sea-salt
1.0	0.02	All other fine particles
1.6	0.4	Coarse sea-salt
1.0	0.4	All other coarse particles

2.5 Chemistry and secondary organic aerosol formation in the model

The chemical scheme used in this study is EMEP-EmChem09soa with the MARS equilibrium module for gas-aerosol partitioning of secondary inorganic aerosol. Detailed information about these can be found in Simpson et al. (2012). The treatment of secondary organic aerosol in the EMEP model includes various options for the volatility distributions and ageing reactions (described in Bergström et al. (2012)) and the Base set-up of this study is described below.

The EMEP model uses the volatility basis set (VBS) approach for SOA formation (Donahue et al., 2006, 2009; Bergström et al., 2012; Simpson et al., 2012). The VBS approach is a computationally efficient framework to describe changes in the volatility of atmospheric compounds. The volatility (in this case the saturation concentration at 298 K, C^*) of gas-phase organic compounds is sorted into bins (illustrated in Fig. 2.6): low volatility organic compounds (LVOCs, $C^* \leq 0.1$ $\mu g\,m^{-3}$), semi-volatile organic compounds (SVOCs, C^* = 1–10^3 $\mu g\,m^{-3}$), intermediate volatility organic compounds (IVOCs, C^* = 10^4–10^6 $\mu g\,m^{-3}$) and volatile organic compounds (VOCs, $C^* \geq 10^7$). Thus, organic compounds are distributed across a continuum from particles to gases. Under typical ambient conditions, all LVOCs, some of the SVOCs, and essentially none of the IVOCs or VOCs are in the condensed phase (Donahue et al., 2006).

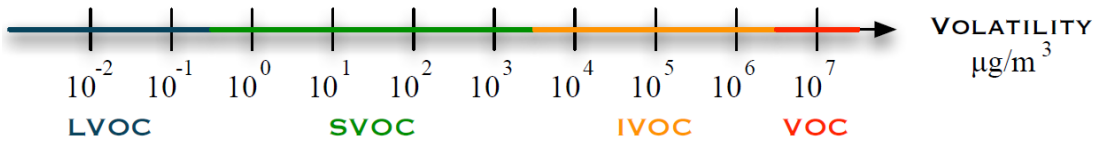

Figure 2.6 *Terminology of the different ranges of volatility (i.e. saturation concentration) at standard conditions.*

In the VBS approach, instead of keeping track of all oxidised VOCs, the lower volatility products of atmospheric degradation reactions are lumped together into the volatility bins, losing the information about their exact chemical composition. The information that the VBS method holds is the saturation concentration of each volatility bin (bins are separated by one order of magnitude each, same as in Fig. 2.6) and the total amount of organic compounds assigned to a bin. The model then iterates Equation 1.2 twice, to calculate the amount of organic compounds that condense into

the particulate phase.

In the model set-up used here, POA is treated as non-volatile and inert, as is currently assumed by emissions inventories. Having POA be non-volatile allows for better identification and isolation of the SOA formed from the study investigating additional diesel IVOCs (Chapter 3). Furthermore, it has been demonstrated by Shrivastava et al. (2011) that a 2-species VBS simulates an evolution of oxygen:carbon ratios (O:C) similar to the 9-species VBS approach. Shrivastava et al.'s two bins were of volatility 0.01 and 10^5 which, because material with the lower volatility is always completely in the particle phase under ambient conditions, is similar to the non-volatile treatment of POA used here.

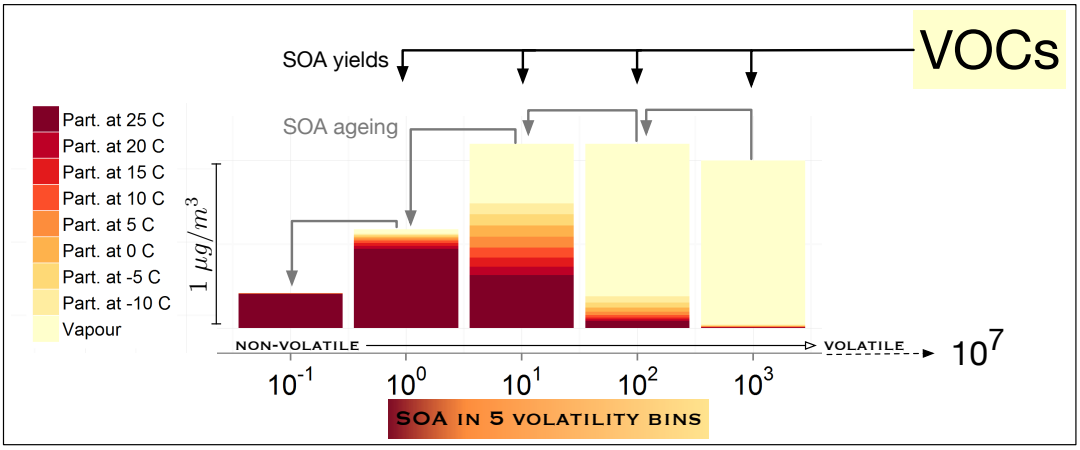

Figure 2.7 *Schematic of the 5-bin VBS used in this study. Black arrows represent different VOC degradation reactions (e.g. see Fig. 1.4), grey arrows represent atmospheric ageing of SOA products by the OH radical. Heights of the bins are concentrations for an arbitrary time-step and location (the partitioning calculations on this Figure include a non-volatile POA component with a concentration of 3 $\mu g\,m^{-3}$). Also shown is the influence of ambient temperature on gas-aerosol partitioning.*

Five volatility bins (C^* = 0.1, 1, 10, 100, 1000 $\mu g\,m^{-3}$) are used for SOA production and ageing. The SOA yields for alkanes, alkenes, aromatics, isoprene and terpenes under high and low NO_x conditions were taken from Tsimpidi et al. (2010). Note that Tsimpidi et al. (2010) reported yields for the four VBS bins between 1 and 1000 $\mu g\,m^{-3}$. In this work, the lowest VBS bin (0.1 $\mu g\,m^{-3}$) is used for the ageing reactions, as well as for SOA from the additional diesel IVOCs (explained in the next chapter). SOA from alkanes, alkenes and terpenes is assumed to have an initial organic matter to organic carbon ratio (OM/OC) ratio of 1.7; SOA from isoprene 2.0; and SOA from aromatics 2.1 (Bergström et al., 2012; Chhabra et al., 2010). For comparison, HOA and SFOA were assumed to have OM/OC ratios of 1.25 and 1.70, respectively (as

in Bergström et al. (2012), based on Aiken et al. (2008)). Both anthropogenic SOA (ASOA; from alkanes, alkenes and aromatics) and BSOA (from isoprene and terpenes) undergo atmospheric ageing by the hydroxyl (OH) radical in the model (with rate coefficient of $4.0 \times 10^{-12}\ \mathrm{cm^3\,molecule^{-1}\,s^{-1}}$; Lane et al. (2008)), resulting in a shift into the next lower volatility bin and a mass increase of 7.5%. A schematic of the 5-bin VBS used in this study is given in Fig. 2.7. Figure 2.7 also illustrates how atmospheric ageing by the OH radical results in shifts to less volatile compounds (the grey arrows).

A constant background OA of $0.4\ \mu\mathrm{g\,m^{-3}}$ is used to represent the contribution of OA sources not explicitly included in the model (e.g., oceanic sources or spores; Bergström et al. (2014)). This background OA is assumed to be highly oxygenated and is therefore included under modelled SOA when comparing with observations (with an OM/OC ratio of 2.0 it is also assumed to be non-volatile).

Chapter 3

Simulating secondary organic aerosol from missing diesel-related intermediate-volatility organic compound emissions

This chapter is based on a research paper published in 'Atmospheric Chemistry and Physics' (Ots, R., Young, D. E., Vieno, M., Xu, L., Dunmore, R. E., Allan, J. D., Coe, H., Williams, L. R., Herndon, S. C., Ng, N. L., Hamilton, J. F., Bergstrm, R., Di Marco, C., Nemitz, E., Mackenzie, I. A., Kuenen, J. J. P., Green, D. C., Reis, S., and Heal, M. R. (2016). Simulating secondary organic aerosol from missing diesel-related intermediate-volatility organic compound emissions during the Clean Air for London (ClearfLo) campaign, Atmos. Chem. Phys., 16, 6453-6473, doi: 10.5194/acp-2015-920; see Appendix D). I implemented changes to the model code, ran the model simulations and undertook all data analysis, but the co-authors, namely Dr Mathew Heal, made valuable contributions to the methodology, and the presentation of results through discussions and manuscript editing. In addition, several of the co-authors were involved in the collection and processing the measurements, on which my addition of IVOCs, and the model-measurement comparisons are based.

3.1 Introduction

Current emissions inventories only report estimates for VOCs ($C^* \geq 10^7$ $\mu g\,m^{-3}$) and for the particle fraction of the emissions of species with lower volatilities. The main reason for this is that compounds with intermediate volatility (SVOCs and IVOCs) are difficult to quantify and this is currently not routinely undertaken alongside the techniques that have been developed to measure the more volatile gases (e.g., gas chromatography) or organic-containing particles (e.g., aerosol mass spectrometry).

Robinson et al. (2007) and Shrivastava et al. (2008) estimated the mass of emitted IVOCs to be 1.5 times that of POA emissions. In their study, this addition of IVOCs = 1.5×POA was applied to all sources of POA from diesel to biomass burning. They based this estimation on chassis dynamometer tailpipe measurements by Schauer et al. (1999). Since then, several regional and global ACTM applications have adopted this factor of 1.5 (e.g., Murphy and Pandis (2009); Tsimpidi et al. (2010); Hodzic et al. (2010); Jathar et al. (2011); Fountoukis et al. (2011); Genberg et al. (2011); Bergström et al. (2012); Zhang et al. (2013); Koo et al. (2014); Tsimpidi et al. (2016)). A number of studies, including many of those cited above reporting model underestimation of OA, have highlighted the need for improved measurement and speciation of SVOCs and IVOCs and for these species to be reported in inventories.

Jathar et al. (2014) performed emissions and smog chamber experiments on SOA production from gasoline and diesel vehicles. Diesel contains hydrocarbons with a higher carbon number (C_8–C_{20}) than gasoline (mainly C_4–C_{10}). The typical method used for hydrocarbon analysis is gas chromatography (GC); however as the carbon number increases, the number of potential structural isomers increases exponentially, meaning GC is unable to distinguish individual species in the intermediate volatility range (Goldstein and Galbally, 2007). The total carbon of this unresolved complex mixture was estimated and Jathar et al. concluded that these unspeciated organic gases dominate SOA production compared with SOA from the speciated precursors commonly included in emissions inventories (single-ring aromatics, isoprene, terpenes and large alkenes). Jathar et al. (2014) also performed box-model simulations of the SOA budget for the US, with the addition of unspeciated emissions based on measurements by Schauer et al. (1999), and concluded that gasoline contributes much more to SOA than does diesel. This result is similar to that of Bahreini et al. (2012) who, based on measurements in the Los Angeles Basin, California (CA), concluded that the contribution of diesel emissions to SOA was zero within measurement uncertainty. Conversely, Gentner et al. (2012) reported that diesel was responsible

for 65-90% of vehicular-derived SOA based on measurements of gas-phase organic carbon in the Caldecoff Tunnel, CA, and in Bakersfield, CA, and on estimations of SOA yields. The huge dissimilarity in these conclusions, even in the same state in the US, emphasizes the need for continued research into gasoline- and diesel-related SOA formation. Furthermore, the US and Europe have very different diesel vehicle profiles: in the US, a negligible proportion of passenger cars are diesel (3%), whilst on average across Europe 33% of passenger cars are diesel and this proportion is increasing (Cames and Helmers, 2013). Globally, the demand for diesel fuel is increasing and by 2020 it is expected to overtake gasoline as the principal transport fuel used worldwide (Exxon Mobil, 2014).

In this chapter, simulations of SOA formation with additional diesel-related IVOC emissions derived directly from comprehensive field measurements of IVOCS and VOCs at an urban background site in central London (Dunmore et al., 2015) during the Clean Air for London (ClearfLo) campaign in 2012 (Bohnenstengel et al., 2014) are presented. Modelled concentrations are compared with OA components derived by PMF analysis of AMS measurements during the same campaign, including comparisons with the long-term measurements (full year) as well as the two month-long Intensive Observation Periods (IOPs) in winter and summer.

3.2 Methods

3.2.1 Additional IVOCs from diesel

Current emissions inventories report highly-volatile anthropogenic VOCs of C* $\geq 10^7$ $\mu g\,m^{-3}$ (Passant, 2002). However, diesel vehicles also produce substantial emissions of species with intermediate volatility in the range $10^5 \leq C* \leq 10^6$ $\mu g\,m^{-3}$ (IVOCs), as has been shown by Dunmore et al. (2015) from measurements made at an urban background site in central London during the ClearfLo project.

In this study, aliphatic IVOC emissions from diesel vehicles were introduced into the model proportionally to on-road transport VOC emissions, using *n*-pentadecane ($C_{15}H_{32}$) as a surrogate for the following reasons. First, the amount of alkenes in diesel fuel is low (< 5 %; Gentner et al. (2012)), so an alkane is the most appropriate surrogate. Second, all *n*-alkanes up to *n*-dodecane were individually speciated and quantified during two month-long Intensive Observation Periods (IOPs) during the ClearfLo project and there were strong correlations between all *n*-alkanes that have

a predominately diesel source (Dunmore et al., 2015). Third, the rate constant for the linear alkane is a reasonable representation of the rate constant for all the (unmeasured) branched and cyclic isomers, as demonstrated by Dunmore et al. (2015) for the C_{12} *n*-alkane, dodecane. The bulk of diesel emissions, however, are likely to have higher carbon numbers than were measured by a comprehensive two dimensional gas chromatography (GC×GC) system (Dunmore et al., 2015). The rate coefficient for the reaction between *n*-pentadecane and OH has been measured in a number of studies ($k = 2.07 \times 10^{-11}$ $\mathrm{cm^3\,molecule^{-1}\,s^{-1}}$; Atkinson and Arey (2003)) unlike for the majority of branched isomers in this range. Furthermore, measurements of diesel fuel composition have shown that the average carbon number on a percentage weight basis was 14.94 (Gentner et al., 2012), so *n*-pentadecane was considered to be an appropriate surrogate for diesel emissions in general.

In the NAEI, emissions from gasoline vehicles dominate the NMVOC emissions from road traffic (SNAP7), but measurements during the ClearfLo winter Intensive Observation Period showed that NMVOCs assigned to diesel vehicles dominated traffic-related NMVOC concentrations (Tab. 3.1). Table 3.1 shows that, for 2012, NAEI reported 8 Gg of diesel-VOCs and 31 Gg of gasoline-VOCs. The measurements, however, showed that the concentration of diesel-(I)VOCs (IVOCs + VOCs) is 3.2 times the concentration of gasoline-VOCs. Based on this, diesel-(I)VOCs emission should be $31\ \mathrm{Gg} \times 3.2 = 99\ \mathrm{Gg}$, and the updated total NMVOCs from SNAP7 therefore become $31\ \mathrm{Gg} + 99\ \mathrm{Gg} = 130\ \mathrm{Gg}$. The new total (130 Gg) is 3.3 times higher than what is officially reported (39 Gg), thus the missing diesel emission is a 230% (2.3× the original, reported, amount) addition to this sector.

The amount of pentadecane emitted in the model was therefore set to match the measured diesel-(I)VOCs to gasoline-VOCs concentration ratio (Fig. 3.1). This pentadecane addition was then applied to every country in the model domain using the same factor as for the UK. This first approximation is justified because the fleet share of diesel vehicles in the UK is similar to the European average (~30%; EEA (2010)), but it can introduce errors for specific countries.

For the oxidation products of $C_{15}H_{32}$, SOA mass yields were taken from Presto et al. (2010): 0.044, 0.071, 0.41, 0.30 for the 0.1, 1, 10, 100 $\mu\mathrm{g\,m^{-3}}$ bins, respectively (Presto et al. (2010) did not report a yield for the 1000 $\mu\mathrm{g\,m^{-3}}$ bin). These yields are reported for SOA with unit density (1 $\mathrm{g\,cm^{-3}}$). In this work, SOA density was assumed to be 1.5 $\mathrm{g\,cm^{-3}}$ (Tsimpidi et al., 2010; Bergström et al., 2012) and the yields were increased accordingly. The technical description of adding the new species and its reactions into the EMEP model is given in Appendix A.

Table 3.1 *Comparison of diesel and gasoline NMVOCs in the UK National Atmospheric Emissions Inventory (NAEI) with the urban background ambient concentrations measured during the ClearfLo winter Intensive Observation Period in London.*

	NAEI 2012	Measurements [a]
Diesel-(I)VOCs	8 $\mathrm{Gg\,yr^{-1}}$	107 $\mu\mathrm{g\,m^{-3}}$
Gasoline-VOCs	31 $\mathrm{Gg\,yr^{-1}}$	33 $\mu\mathrm{g\,m^{-3}}$
Diesel/Gasoline	0.26	3.2

[a] Dunmore et al. (2015)

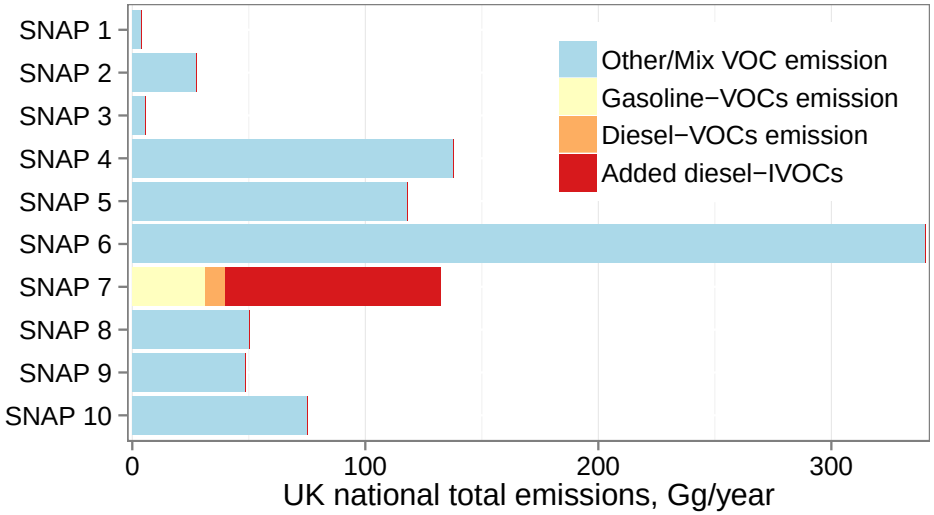

Figure 3.1 *Annual UK NMVOC emissions by SNAP sector (Table 2.3) as specified in the NAEI (for the year 2012), with the SNAP7 emissions sub-divided into gasoline and diesel vehicles, and with the additional diesel-associated IVOC emissions input to the model in this study shown in red.*

For the UK, the approach derived in this study adds 90 Gg of diesel-IVOCs emission for the year 2012 (Fig. 3.1). The 1.5xPOA approach (Shrivastava et al. (2008) based on measurements by Schauer et al. (1999)) would only add 31 Gg (Fig. 3.2). Part of this discrepancy could be attributable to the different methods and circumstances used to derive the additions (this work: five weeks of ambient measurements in a megacity; previous estimate: tailpipe laboratory measurements using different instruments). Another possible reason for the difference is an underestimate in POA emissions in the inventory; more POA would increase the amount of proportionally added IVOCs. However, Dunmore et al. (2015) show that lower carbon number (and higher volatility) NMVOCs measured during the ClearfLo campaign were consistent with emissions estimates. This lends confidence to adding IVOCs proportionally to reported NMVOC

emissions, rather than proportionally to POA emissions. Nevertheless, a model run using the POA-based IVOC estimate, and including the semivolatile treatment of POA, was also performed. The emitted semivolatile POA (SVOCs) and 1.5xPOA IVOCs are assigned to 9 VBS bins: 0.03×POA, 0.06×POA, 0.09×POA, 0.14×POA, 0.18×POA, 0.30×POA, 0.40×POA, 0.50×POA, 0.80×POA to the bins 0.01–10^6, respectively; totalling 2.5×POA (Shrivastava et al., 2008). Both SVOCs and IVOCs then go through atmospheric ageing with OH ($k = 4.0 \times 10^{-11}$ cm^3 molecule^{-1} s^{-1}; Shrivastava et al. (2008)). In this case, the additional IVOCs were calculated from POA from all sources, not just traffic-related. Note that in the UK, most of the additional IVOCs of the POA-based approach would come from SNAP2 (Residential and non-industrial combustion emissions; (Fig. 3.2)): 18 Gg, whereas only 5 Gg would be added to SNAP7 (Road transport; and 8 Gg to remaining sectors). SVOCs and IVOCs that have undergone at least one ageing shift and are in the particulate phase are included under SOA (in addition to ASOA and BSOA from VOCs as in the Base case). Due to the very different absolute amounts and source categories (the latter of which also leads to differences in the spatial pattern and temporal variation of the additional emissions), detailed comparison of the two different additions is not justified, and only annual total OA component budgets of the different addition methodologies are presented.

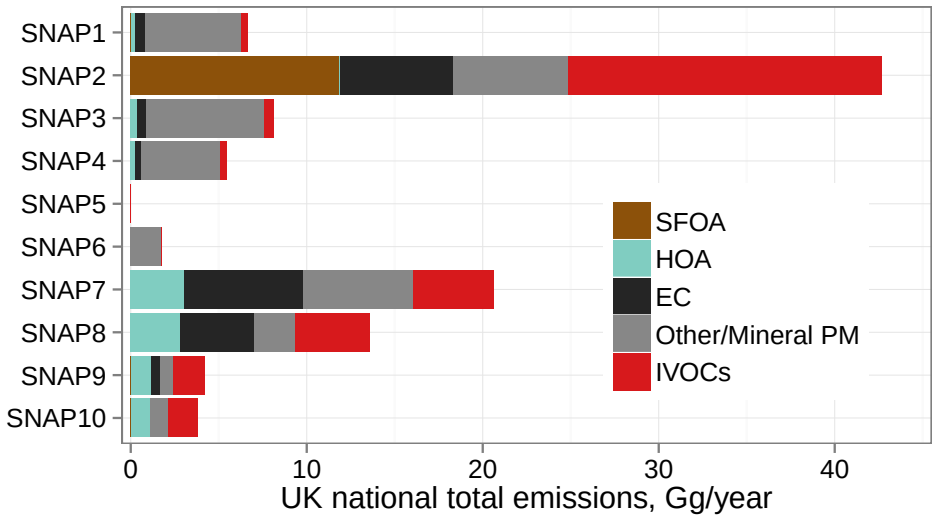

Figure 3.2 *Annual UK* $PM_{2.5}$ *emissions by SNAP sector (Table 2.3) as specified in the NAEI (for year 2012), with each sector split into POA (HOA or SFOA), EC, and remaining PM following Kuenen et al. (2014). The red bars are additional IVOCs (not included in official emission totals) that can be estimated as 1.5x the POA mass in that sector. They are included in this plot to give an indication of the relative mass of IVOC additions that has been used in other studies.*

3.2.2 Summary of model experiments

Three runs of the EMEP4UK modelling system were performed for 2012:

- Base: all anthropogenic emissions as in officially reported inventories; biogenic emissions calculated by the model for each advection time step.
- addDiesel: Base + additional diesel IVOCs added proportionally to NMVOC emissions from traffic (2.3xSNAP7; Fig. 3.1). The additional IVOCs were treated using *n*-pentadecane as the surrogate species. The semivolatile VBS-species formed after oxidation of *n*-pentadecane were treated in the same way as the ASOA-species from VOC-oxidation (the same ageing rate and mass increase due to oxygen addition; see Sect. 2.5).
- 1.5volPOA: Base + additional IVOCs added proportionally to all POA emissions (1.5xPOA; as in Shrivastava et al. (2008) based on measurements by Schauer et al. (1999); Fig.3.2).

3.2.3 Comparison with measurements

Modelled $\mathrm{OA}_{2.5}$ (OA with diameter $< 2.5\ \mu\mathrm{m}$) is compared with non-refractory submicron (NR-PM_1) OA measured by Aerodyne AMS instruments at an urban background site in central London and at two rural sites (Xu et al. (2016); Young et al. (2015a,b); Bohnenstengel et al. (2014), site locations were shown in Fig. 1.7). The error introduced to the comparison by the different size fractions is believed to be small, as measurements at an urban background site in Birmingham, England have shown that 90% of organic carbon in $\mathrm{PM}_{2.5}$ is in the submicron fraction (Harrison and Yin, 2008).

3.3 Results

The comparisons between the model results and measurements are presented in the following order. First, comparisons are presented for primary OA, $\mathrm{NO_x}$, $\mathrm{O_3}$, and for secondary inorganic aerosol (SIA) to give an overview of the overall performance of the modelling system. Second, the hourly concentrations of SOA during the two IOPs are evaluated, demonstrating the agreement between the model and measurements at high temporal resolution. Third the year-long daily SOA concentrations are compared and the relative impact of these missing diesel-IVOCs on SOA production in London is shown. Fourth, modelled and measured OM/OC ratios are presented, and finally, annual total ASOA from the addDiesel method and the previous 1.5xPOA approach are compared.

3.3.1 POA, $\mathrm{NO_x}$, $\mathrm{O_3}$, SIA: annual dataset

Figure 3.3 shows the year-long comparison between the daily-averaged model results and the cToF-AMS measurements at the London North Kensington site. The model underestimates primary OA (HOA and SFOA) concentrations (NMB of -54% and -71%, respectively), but shows good daily correlations (r-values of 0.53 and 0.72, respectively). The underestimation of HOA may be caused by a combination of lack of model resolution (e.g., the minor road close to the measurement site can not be resolved with the 5 km grid), and underestimation of PM emissions. Modelled $\mathrm{NO_x}$ concentrations are relatively less underestimated in comparison to measurements (NMB of -32%, Fig. 3.4a), suggesting that HOA emissions may be more underestimated than the emissions of $\mathrm{NO_x}$. Concentrations of secondary inorganic pollutants are simulated well by the model in the gas-phase (Fig. 3.4b, with a NMB of -1% for ozone), and for inorganic PM constituents (Fig. 3.4c–e), with NMBs of 6% for $\mathrm{SO_4^{2-}}$, -12% for $\mathrm{NH_4^+}$, and -23% for $\mathrm{NO_3^-}$.

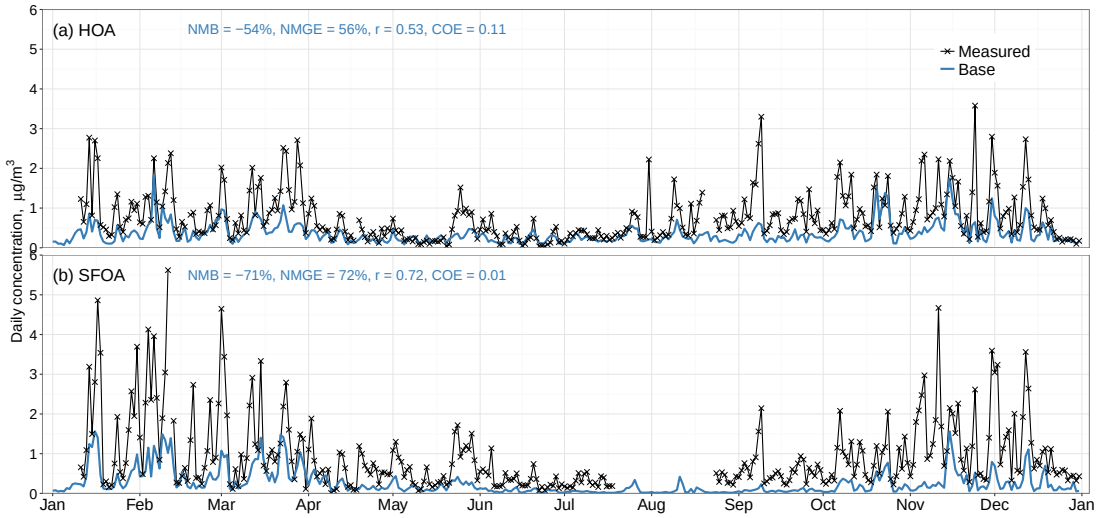

Figure 3.3 *Time-series of measured and modelled daily-average concentrations of (a) HOA, and (b) SFOA at the London North Kensington Urban Background site, 2012, measured with the cToF-AMS (Table 1.3).*

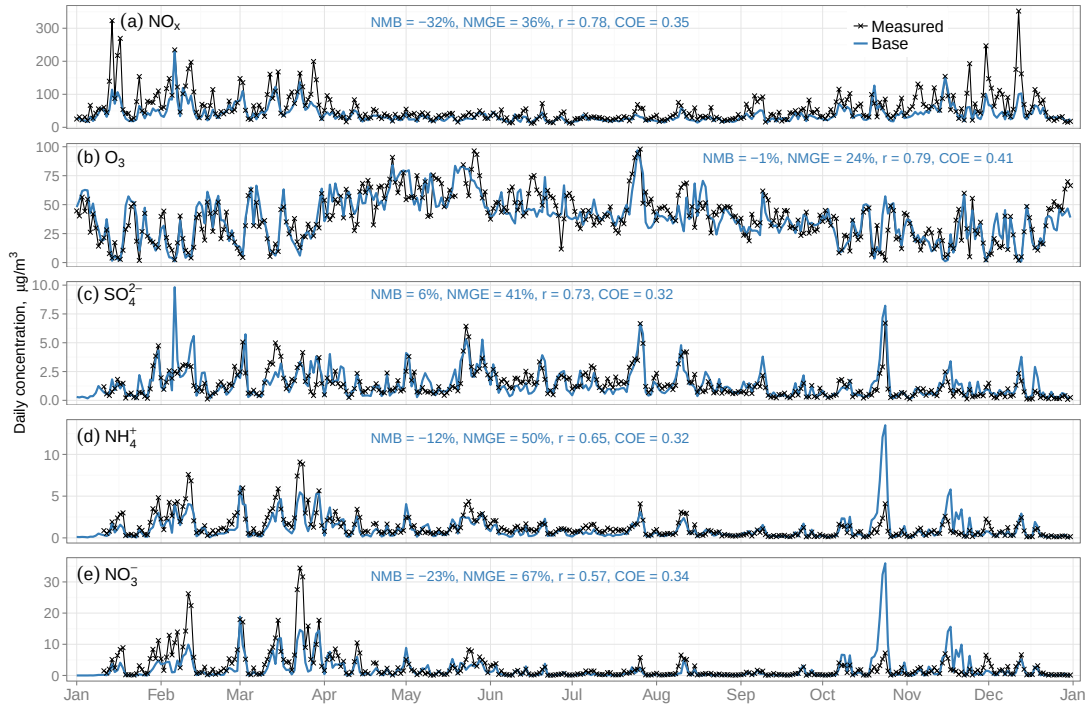

Figure 3.4 *Time-series of measured and modelled daily-average concentrations of (a)* NO_x *(as* NO_2*), (b)* O_3*, (c)* SO_4^{2-}*, (d)* NH_4^+*, and (d)* NO_3^- *at the London North Kensington Urban Background site, 2012. Measurement data of* NO_x *and* O_3 *are from the UK Automated Urban and Rural Network (AURN);* SO_4^{2-}*,* NH_4^+ *and* NO_3^- *were measured with the cToF-AMS (Table 1.3).*

3.3.2 Hourly comparison of secondary OA: summer IOP

Evaluation statistics between hourly measured and modelled SOA concentrations in July and August 2012 (summer IOP) show reassuring agreement (Fig. 3.5). The values of r for the Base run were 0.67 and 0.55 at North Kensington and Harwell respectively. The addDiesel experiment yields a modest improvement in the value of r at North Kensington (to 0.76) and a marked improvement in Harwell (to 0.74). The addDiesel run substantially improves the NMB for SOA at the Harwell and London North Kensington sites from -32% to -5%, and from -35% to 0.1%, respectively (Fig. 3.5). This suggests that ~30% of SOA at both sites during this period can be explained by the diesel IVOCs added into the model using pentadecane as a surrogate. There is also marked improvement of model-measurement COE values at the two sites (Harwell, 0.26 to 0.42, and NK 0.31 to 0.45). The improvement in NMGE is noticeable (Harwell, 54% to 43%, and NK 59% to 47%), but smaller than the improvements in the other metrics. It can be seen from the scatter-plots in Fig. 3.6 that most modelled hourly SOA concentrations fall within a factor of two of the measured concentrations (FAC2 for the addDiesel experiment is 78% at Harwell and 62% at NK).

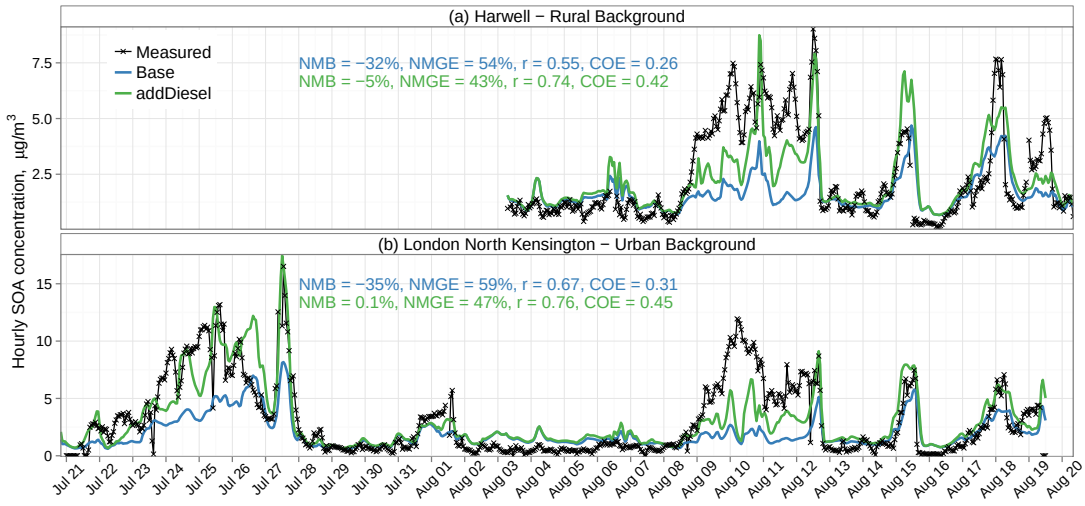

Figure 3.5 *Time-series of measured and modelled hourly-average concentrations at (a) the Harwell Rural Background site, and (b) the London North Kensington Urban Background site during the summer IOP. Note the different scales on the y-axes.*

Measured and modelled mean hour of day variations of SOA concentrations are presented in Fig. 3.7, where it can be seen that measured SOA concentrations do not have a very strong diurnal cycle. Interestingly, both sites exhibit dips in measured SOA concentrations in the morning and early evening. Both measured and modelled SOA concentrations in London North Kensington reach a maximum in the afternoon, but

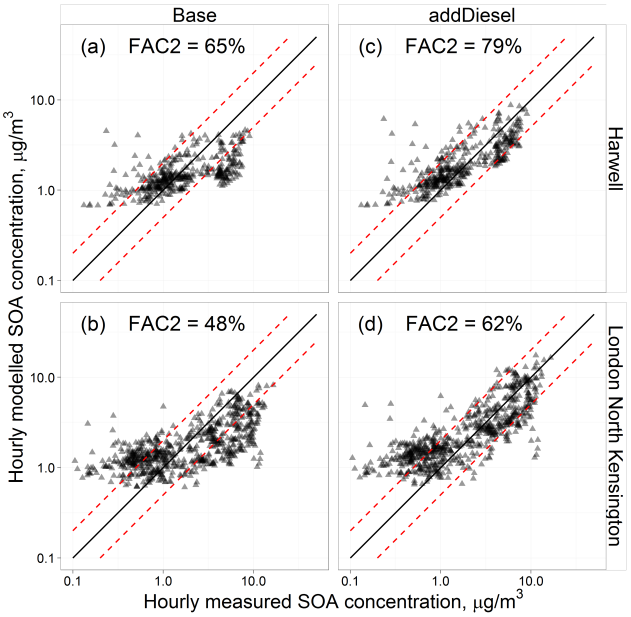

Figure 3.6 *Scatterplots of measured and modelled hourly SOA concentrations during the summer 2012 IOP: (a) Base simulation at the Harwell Rural Background site; (b) Base simulation at the North Kensington Urban Background site; (c) addDiesel simulation at the Harwell Rural Background site; (d) addDiesel simulation at the North Kensington Urban Background site. The straight lines are the 2:1, 1:1, and 1:2 lines.*

SOA of the addDiesel experiment starts this increase earlier than the measurements, meaning that the ASOA production from pentadecane might be too rapid.

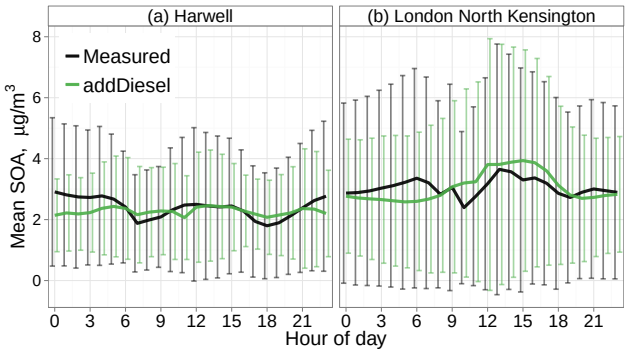

Figure 3.7 *Average hourly profiles of modelled (addDiesel experiment) and measured SOA during the summer IOP. Also shown are the standard deviations for each mean value.*

During the summer IOP, there were two sustained episodes of increased SOA concentrations: 23-Jul to 28-Jul and 9-Aug to 13-Aug (Fig. 3.5). Only London North Kensington had measurements during the first episode and the elevated concentrations were well captured by the addDiesel simulation (including the highest peak of greater than 16 $\mu g\,m^{-3}$: 27-Jul 13:00, Fig. 3.8b). Daily averaged SOA maps (Fig. 3.9) suggest that this first episode arose from a combination of SOA transported from Europe and

SOA produced locally in London. A region of elevated concentration around London exists within a general gradient of SOA from continental Europe to Southern England. Even daily averaged concentrations are spatially variable during this episode meaning that inaccuracies in some of the modelled peaks can be attributed to uncertainties in the underlying meteorological model. Most of the modelled SOA during this episode was of anthropogenic origin with the addDiesel run yielding a significant portion of ASOA from pentadecane.

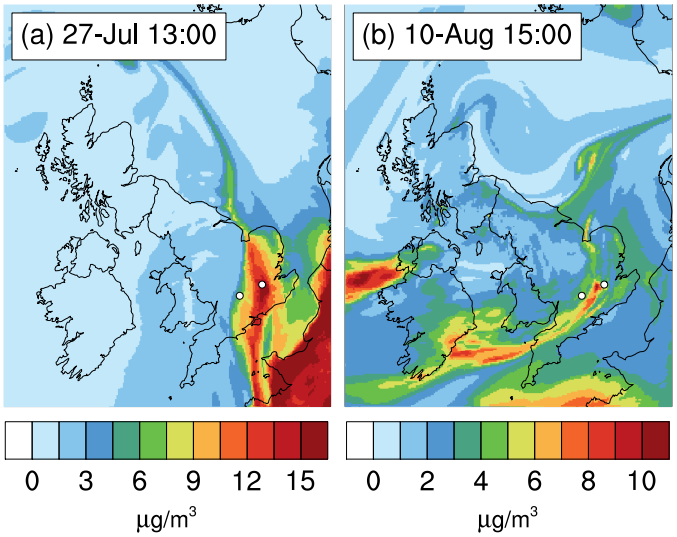

Figure 3.8 *Modelled (addDiesel experiment) hourly concentrations of SOA at the time of the maximum measured hourly SOA value at the London North Kensington site during the first and second SOA episodes of the summer IOP. The white circles mark the measurement site locations, left: Harwell, right: London North Kensington.*

For the second sustained episode of high SOA concentrations, from 9-Aug to 13-Aug, several features remain substantially underestimated even in the addDiesel run. For Harwell, the model does capture two of the highest peaks (10-Aug 22:00 measured: 6.8 $\mu g\,m^{-3}$, addDiesel: 8.5 $\mu g\,m^{-3}$ and 12-Aug 12:00 measured: 7.9 $\mu g\,m^{-3}$, addDiesel: 7.0 $\mu g\,m^{-3}$), but for London North Kensington, the model simulates a minimum during the highest measured concentration (10-Aug 05:00 measured: 11.9 $\mu g\,m^{-3}$, addDiesel: 2.0 $\mu g\,m^{-3}$). The high concentrations during the first two days of this episode were very localised with horizontal widths of just tens of kilometres (Fig. 3.10a,b). There was a build-up of pollution caused by high pressure and low boundary-layer height (BLH), which led to production of ASOA in London. The high variability in the modelled concentrations (for example, the simulated minimum during the measured maximum at North Kensington) is caused by the shifting of this narrow ASOA plume in space (Fig. 3.8b). On 12-Aug, this episode was also subject to SOA contribution from Europe (Fig. 3.10d).

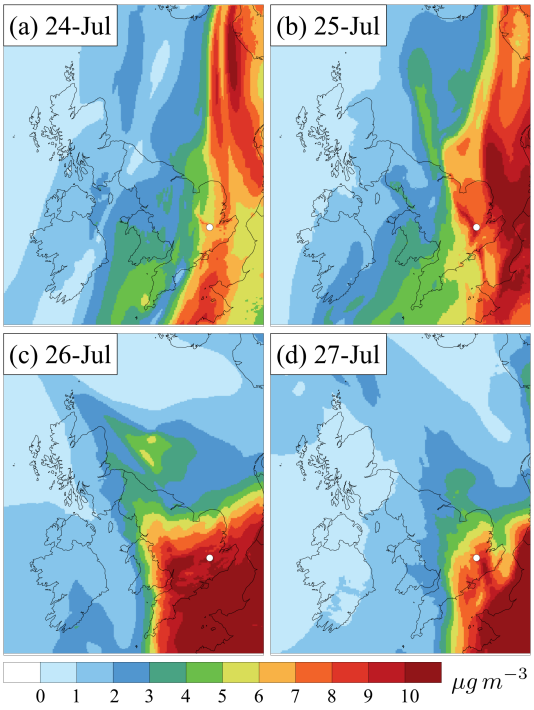

Figure 3.9 *Modelled (addDiesel experiment) daily average concentrations of SOA during the first SOA episode of the summer 2012 IOP. The white circle indicates the location of London North Kensington.*

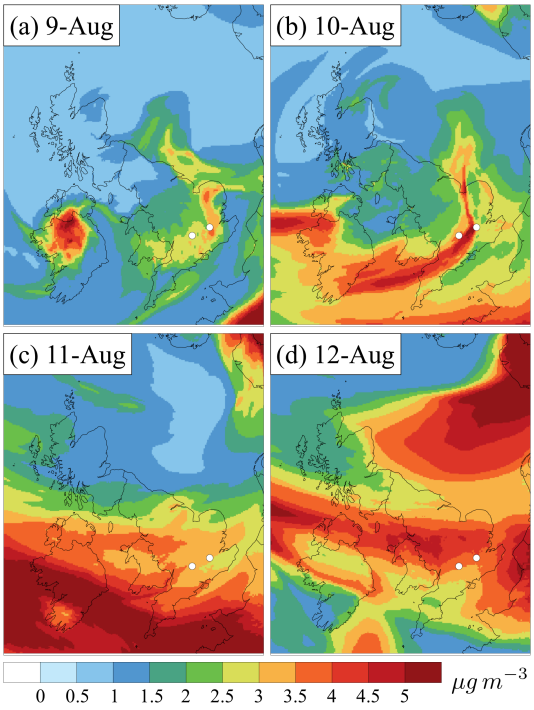

Figure 3.10 *Modelled (addDiesel experiment) daily-average concentrations of SOA during the second SOA episode of the summer 2012 IOP. The white circles mark the measurement site locations, left: Harwell, right: London North Kensington.*

During the period of overlapping measurements at Harwell and North Kensington (3-Aug–18-Aug), both the measurements and the model agree with a modest rural to urban increase. Average measured SOA concentrations were 2.4 $\mu g\,m^{-3}$ and 2.6 $\mu g\,m^{-3}$ for Harwell and North Kensington, respectively, whilst average modelled concentrations were 2.3 $\mu g\,m^{-3}$ and 2.5 $\mu g\,m^{-3}$ (for the addDiesel experiment).

3.3.3 Hourly comparison of secondary OA: winter IOP

Both the Detling and London North Kensington sites exhibit good modelled-measured hourly correlation (r = 0.63 and 0.64, addDiesel run; Fig. 3.11). The addDiesel run decreases the NMB for SOA at these sites from -59% to -30% for Detling, and from -24% to 8% for London North Kensington. This suggests that ~30% of SOA at these sites during this period can be explained by diesel IVOCs. In Detling, there is also a pronounced improvement in the COE, from 0.10 to 0.31. In North Kensington, the COE was already high but is increased from 0.27 to 0.30. It can be seen in Fig. 3.11 as well as Fig. 3.12 that lower concentrations of SOA (19-Jan–27-Jan) are overestimated by the model. This overestimation is caused by the very simplified method of including missing sources of OA using a constant concentration of 0.4 $\mu g\,m^{-3}$ (which is assumed to be highly oxygenated and is therefore included under modelled SOA). As a constant, this background OA does not currently go through atmospheric emission-removal processes in the model. However, the period in question exhibited snowfall, removing

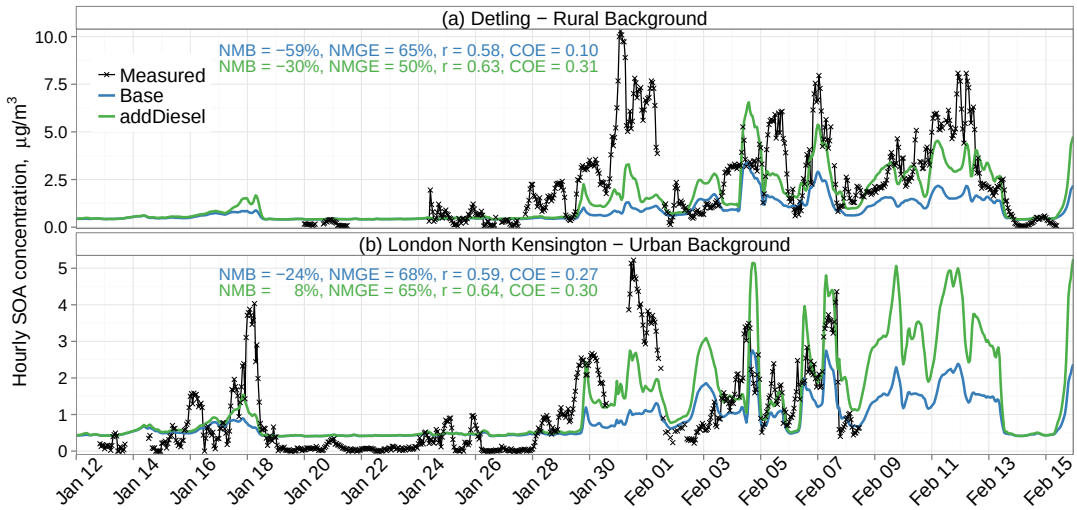

Figure 3.11 *Time-series of measured and modelled hourly-average concentrations at (a) the Detling Rural Background site, and (b) the London North Kensington Urban Background site during the winter 2012 IOP. Note the different scales on the y-axes.*

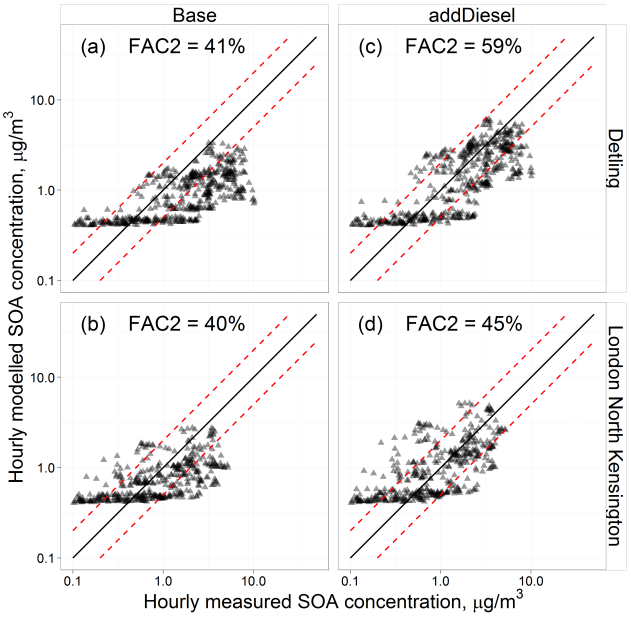

Figure 3.12 *Scatterplots of measured and modelled hourly SOA concentrations during the winter 2012 IOP: (a) Base simulation at the Detling Rural Background site; (b) Base simulation at the North Kensington Urban Background site; (c) addDiesel simulation at the Detling Rural Background site; (d) addDiesel simulation at the North Kensington Urban Background site. The straight lines are the 2:1, 1:1, and 1:2 lines.*

much of the aerosol (as can be seen from the very low concentrations measured in both Detling and London North Kensington, 19-Jan–27-Jan on Fig. 3.11). This inclusion of the background OA as a constant concentration is *intentionally simplistic* (Simpson 2015, personal contact). Until these missing sources (e.g. oceanic material, and spores) are introduced as real emissions with spatial and temporal variation (and with appropriate removal mechanisms), this intentionally simplistic approach does not give the scientific community ungrounded confidence in our modelling capabilities of this component. For example, it is clear from the modelled vs measured hourly scatterplots (Fig. 3.12) how this constant creates 'flatline' minimums for the model at 0.4 $\mu g\,m^{-3}$. Explicit inclusion of additional missing biogenic sources of OA to the model is already part of ongoing development of the model and will be presented in future studies.

During the ClearfLo Winter IOP, measured SOA concentrations were higher in Detling than in North Kensington (Fig. 3.11). This is correctly captured by the simulations and is caused by a steep positive gradient of concentrations from southern England across to the near European continent (Fig. 3.13). The measured Detling/North Kensington SOA ratio (ratio of average concentrations for this period) was 1.8 while the modelled ratio was 1.1, so the model correctly simulates the direction of the spatial gradient, but underestimates its magnitude. For North Kensington, the model also captures that

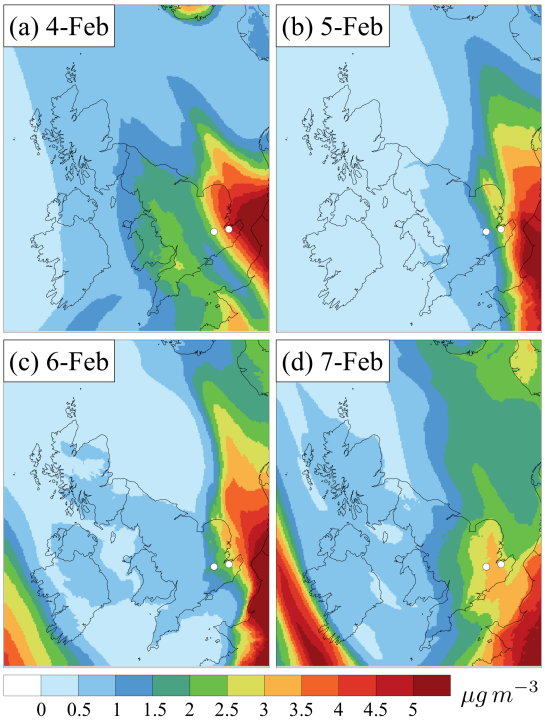

Figure 3.13 *Modelled (addDiesel experiment) daily average concentrations of SOA during the second SOA episode of the winter 2012 IOP. The white circles mark the measurement site locations, left: London North Kensington, right: Detling.*

SOA concentrations are lower on Feb-5 than on Feb-4. In Detling, however, measured concentrations were higher on Feb 5, which the model does not reproduce. During the night of 4-5 February, the wind was very strong ($> 10\ \mathrm{m\,s^{-1}}$) and there was a small shift between the measured wind direction and the wind direction input to EMEP4UK from WRF. As a consequence, the simulated pollution plume was shifted too much to the east (Fig. 3.13b) causing the model-measurement discrepancy on this particular occasion.

Even though the additional diesel IVOCs noticeably increased the modelled SOA concentrations during the winter IOP, there is still a marked underestimation of elevated measured SOA concentrations during 15-Jan–19-Jan and 30-Jan–4-Feb. During these periods, the observed temperature was colder than the average temperature of the winter IOP (Crilley et al., 2015) and peaks in measured SOA also coincide with elevated concentrations of SFOA (Figs. 3.3b and 3.11b). As the modelled SFOA is underestimated by a factor of 4 (NMB of -72%), it is likely that (i) SOA precursor VOC emissions from domestic heating are also underestimated, and (ii) adding missing IVOCs from this emission sector would contribute to the modelled SOA during these periods. It has been recently shown by Denier van der Gon et al. (2015) that the

emission factors used by different European countries for wood combustion PM emissions, even for the same appliance type, can differ by a factor of 5. They constructed a revised inventory, in which each country's emission was updated using an unified emission factor. This resulted in increases of PM (and estimated accompanying IVOC) emission estimates for most countries. Furthermore, London is a *smoke control area* and therefore no residential emissions of SFOA are assumed by the national emissions inventory. Recent studies have, however, suggested that there are indeed local sources of SFOA in London (Crilley et al., 2015; Young et al., 2015a).

3.3.4 Daily and seasonal secondary OA: annual dataset

Time-series of daily averaged modelled and measured SOA concentrations for the whole year are shown in Fig. 3.14. Table 3.2 gives daily modelled vs measured SOA evaluation statistics during different seasons at the North Kensington site. Values for autumn are presented with and without the two extreme points (size of the data set n = 91 and n = 89).

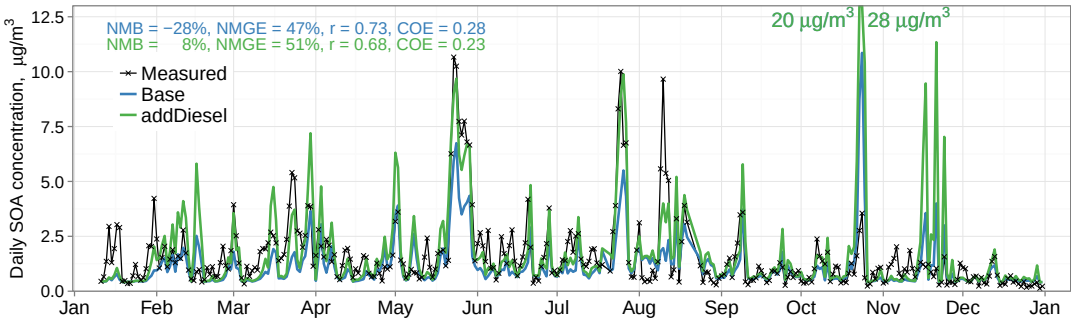

Figure 3.14 *Time-series of measured and modelled daily-average SOA concentrations at the London North Kensington Urban Background site. The two outliers (23 and 24 October, included in the plot as labels) are excluded from the model evaluation statistics presented in the plot.*

For the daily model-measurements comparison, spring has the highest correlation (r = 0.85, both Base and addDiesel; Table 3.2). This can also be seen from the time series (Fig. 3.14: March–May) where both model simulations follow most of the measured peaks. The Base run r-value for spring was already high, but nevertheless, the addDiesel run shows a marked improvement for all other model evaluation statistics. FAC2 is increased by 10%, COE is increased to 0.39, NMB is reduced by 35% and NMGE is reduced by 7%. The NMGE of 38% remaining in the addDiesel model run is probably governed by uncertainties in meteorology, as well as by uncertainties in the temporal and spatial variability of emissions. During summer, the model captures

Table 3.2 *Model-measurements comparison statistics for daily SOA at London North Kensington. Autumn is presented with and without the two outliers (23-Oct and 24-Oct. n = 91 and 89, respectively).*

	Base	addDiesel	Base	addDiesel
	spring (MAM)		summer (JJA)	
n (days)	91		86	
FAC2	64%	74%	60%	79%
NMB	-35%	0.1%	-34%	-5%
NMGE	45%	38%	48%	39%
r	0.85	0.85	0.71	0.82
COE	0.29	0.39	0.26	0.41
	autumn (SON)		winter (JFD)	
n (days)	89		81	
FAC2	82%	74%	70%	69%
NMB	-2%	58%	-28%	6%
NMGE	52%	96%	47%	61%
r	0.38	0.28	0.40	0.40
COE	-0.13	-1.07	0.21	-0.02
	autumn (SON)			
n (days)	91			
FAC2	80%	73%		
NMB	13%	102%		
NMGE	63%	137%		
r	0.58	0.54		
COE	-0.30	-1.84		

the majority of the periods of increased SOA mass well (e.g., Jun-28, Jul-22 - Jul-29, Aug-15, Aug-20, Fig. 3.14: June–August), but there is some model underestimation when SOA concentrations were lower (< 2 $\mu g\,m^{-3}$). As for spring, the addDiesel experiment improves all model evaluation statistics. More detailed hourly analysis of the SOA concentrations during the summer IOP (end of July to August) was presented in Sect. 3.3.2.

The model performance is less good in autumn than during the other seasons. There are some days where the Base case scenario overestimates measured SOA (23–25-Oct, 21-Nov, 24-Nov) with the addDiesel run increasing this further. During these days,

particle nitrate (NO_3^-) and ammonium (NH_4^+) are also substantially overestimated by the model (Fig. 3.4). The enhancement of NH_4^+ is directly linked with the overestimation of NO_3^- as NH_4^+ is only present as ammonium nitrate and ammonium sulphate in this version of the model. This suggests that the overestimations are likely caused by errors occurring during this period in the meteorological forecasts, e.g., missed rain events, rather than by uncertainties in the formation of secondary organic aerosol specifically.

The model evaluation statistics for autumn are strongly influenced by the two modelled values on 23-Oct and 24-Oct (Table 3.2). Removing these two values reduces the seasonal average SOA concentration modelled with the addDiesel run by 33% (2.0 and 1.5 $\mu g\,m^{-3}$ with and without these two points, respectively). Their combined influence on the annual average modelled concentration is 8%, which is substantially more than any other points of the annual dataset.

For the winter months, modelled concentrations in January are much lower than measurements, whereas in February the timing of several peaks is well reproduced and even overestimated by the addDiesel experiment. Detailed hourly analysis of the SOA concentrations during the winter IOP has been presented in Sect. 3.3.3. In December, measured SOA concentrations were much lower than in January and even though the model captures the highest peak, there is some overestimation in the lowest range ($< 0.5\ \mu g\,m^{-3}$).

Figure 3.15 shows annually and seasonally averaged measured and modelled SOA. The difference between the Base and addDiesel experiments illustrate the impact of missing IVOC emissions from diesel-traffic on SOA formation. As was discussed before, and

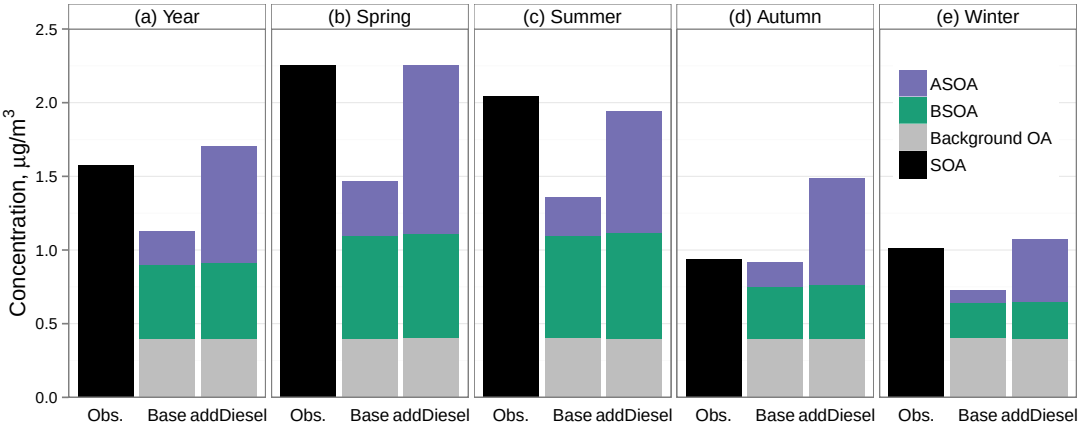

Figure 3.15 *Annually and seasonally averaged measured and modelled concentrations of SOA at the London North Kensington site.*

can be seen from Table 3.2, IVOC precursors from diesel vehicles reduce the NMB by ~30%, which as an annual average is 0.6 $\mu g\,m^{-3}$ of additional SOA. Moreover, the 90-th percentile of daily averaged SOA concentrations of the addDiesel experiment is 3.8 $\mu g\,m^{-3}$ (which is similar to the measured 90th percentile of 3.2 $\mu g\,m^{-3}$), whereas the 90-th percentile of the Base case simulation is 2.2 $\mu g\,m^{-3}$. This means that (i) on 36 days of the year, SOA is a notable component of PM (the annual average $PM_{2.5}$ concentration limit value of the European Union Directive 2008/50/EC is 25 $\mu g\,m^{-3}$), and (ii) during those days, the relative contribution to SOA from diesel IVOCs could be greater than 40% (calculated as the difference between SOA modelled with addDiesel and Base, relative to addDiesel: (addDiesel-Base)/addDiesel). We note that Fig. 3.15a shows that in the addDiesel simulation, the modelled BSOA+Background OA still makes up 53% of the SOA, as an annual average. This value is based on the assignment of the constant background OA in the model to natural SOA, which is what it is intended to represent. Some of this may have some anthropogenic origin, and more research on the missing (or boundary condition) sources that this background constant represents is needed for accurate attribution of the biogenic vs anthropogenic relative contributions.

3.3.5 OM/OC ratios

Measured OM/OC ratios for SOA were generally higher than those modelled (1.99–2.34 vs 1.88–1.97, Table 3.3). Nevertheless, the measured OM/OC ratio at London North Kensington during the summer IOP was the lowest of the measured range: 1.99, which is a close match to modelled SOA OM/OC ratio for that period: 1.97. Model performance for spring and summer was shown to be very good, but it is possible that the missing SOA precursors in the colder months (from domestic heating) could yield SOA with higher initial OM/OC ratios, thereby increasing the annual average value. Furthermore, wintertime simulations of SOA in Paris by Fountoukis et al. (2016) also showed large underestimations and they speculated that this could be pointing towards an SOA formation process during low photochemical activity periods that is currently not simulated in atmospheric chemical transport models.

Table 3.3 *Measured and modelled (addDiesel experiment) OM/OC ratios. Site names are abbreviated as follows: NK - London North Kensington, HAR - Harwell, DET - Detling.*

Pollutant	Site	Period	Meas. OM/OC	Mod. OM/OC
HOA	NK	winter IOP	1.25	1.25
	NK	summer IOP	1.19	
	NK	annual	1.32	
	HAR	summer IOP	1.31	
	DET	winter IOP	1.45	
SFOA	NK	winter IOP	1.62	1.70
	NK	annual	1.78	
	DET	winter IOP	1.64	
SOA	NK	winter IOP	2.03	1.88
	NK	summer IOP	1.99	1.97
	NK	annual	2.25	1.94
	HAR	summer IOP	2.39	1.99
	DET	winter IOP	2.34	1.86

3.3.6 Comparison to the previous (IVOCs=1.5xPOA) approach

Figure 3.16 shows the annual average HOA, SFOA, BSOA and Background OA (BGND OA), and ASOA concentrations at London North Kensington modelled with different assumptions for additional IVOC emissions. As was explained in Sect. 3.2.1, for the UK, the addDiesel experiment adds 90 Gg of diesel-related IVOCs proportionally to road transport emissions (SNAP7), whereas the IVOCs=1.5xPOA approach only adds 5 Gg to SNAP7 and another 26 Gg to other sectors (mainly to SNAP2: residential and non-industrial combustion). Therefore, the addDiesel approach creates a considerably larger amount of SOA from IVOCs (and only from diesel-related IVOCs) than the previous method. The 1.5volPOA experiment was undertaken using the semivolatile treatment of POA emissions. This means that the modelled ASOA from this experiment also includes aged semivolatile POA, possibly giving it potential to create more ASOA than the Base or addDiesel experiments (the organic material added to the model in the 1.5volPOA experiment is 1.0×POA (as

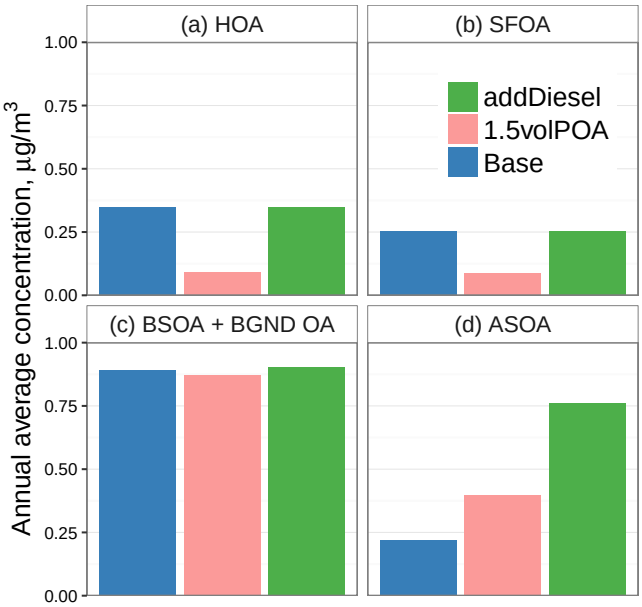

Figure 3.16 *Simulated annual and seasonal average concentrations of OA components (BGND OA stands for Background OA) for the London North Kensington site of three different model experiments: Base - all emissions as in officially reported emissions inventories, POA is treated as non-volatile; 1.5volPOA - semivolatile treatment of POA + IVOC emissions added as 1.5xPOA; addDiesel - Base + IVOC emissions from diesel traffic added proportionally to VOC emissions from the on-road traffic source sector (SNAP7); both the latter additions as described in the main text.*

SVOCs) + 1.5×POA (IVOCs) = 2.5×POA as introduced by Robinson et al. (2007) and Shrivastava et al. (2008)). It can be seen from Figs. 3.16a, b that treating POA as semivolatile leads to much lower concentrations than the nonvolatile treatment (which already underestimates measured concentrations of HOA and SFOA by -54% and -71%, respectively; Fig.3.3). This is not surprising given that the semivolatile treatment of POA assigns only 3% + 6% + 9% of the POA to the three lowest volatility bins with saturation concentrations of 0.01, 0.1 and 1 $\mu g\,m^{-3}$, respectively (as given in Sect. 3.2.1). In a study in Mexico City, Shrivastava et al. (2011) revised this treatment by assuming much higher total semi- and intermediate volatility POA emissions: 7.5× the inventory emissions of (particulate) POA. This was justified by the fact that their emission factors of POA were derived from measurements at urban background sites, but, following Robinson et al. (2007), 2/3 of POA would have evaporated by then. Recently, Shrivastava et al. (2015) also used this factor of 7.5 in global simulations. Emission factors used in European inventories are, however, taken from tailpipe measurements with concentrations sufficiently high that most of the semivolatiles should still be reported in the particulate phase. Therefore the further underestimation of HOA and SFOA concentrations with the volatile treatment could be due to a number of issues: (i) a systematic underestimation of emissions, but for a different reason than

in Shrivastava et al. (2011), (ii) the volatility of POA is overestimated by Robinson et al. (2007), (iii) the evaporation of semivolatile POA emission is too rapid in the model (instantaneous).

Figure 3.16c shows that the lower HOA and SFOA concentrations lead to a very small negative change for the absorptive partitioning of BSOA. Finally, it can be seen from the annual average concentrations of ASOA in Fig. 3.16d that including aged SVOCs and IVOCs in the simulation doubles the modelled ASOA concentration compared to the Base case scenario (ASOA from officially reported anthropogenic VOCs), but that the ASOA in the 1.5volPOA experiment is still much lower than simulated with the addDiesel experiment.

3.4 Discussion

We show that ~30% of SOA in London could be produced from completely new estimates of diesel-related IVOC emissions that are not currently included in the emissions inventories. This is one of a very few studies where IVOC emissions are added proportionally to NMVOC emissions (as opposed to addition proportionally to POA emissions). Moreover, previous studies have added IVOCs proportionally to POA from all sources, whereas this study focuses specifically on the impact of diesel-IVOCs from on-road traffic emissions (IVOCs = 2.3xSNAP7 VOCs). There is reason to believe that higher volatility VOCs are better represented in current emissions inventories than the emissions of PM. Also, the official inventories do not provide the individual contribution of POA to total PM. Therefore, the addition of IVOCs proportionally to NMVOCs may be better constrained than the POA-based approach used in studies so far. The additional emissions are also tied directly to the relevant emission source category.

There are several possible uncertainties in this estimate of additional IVOCs, and subsequent SOA production and ageing. As a first approximation, IVOCs were added to each European country based on the measurements in London. This was justified as the diesel usage in the UK is similar to the European average. Furthermore, different European countries might be using different emissions factors for their estimates of NMVOCs from gasoline and diesel or have a different average fleet age than the UK. It should be noted that two of the most populous countries in Europe - France and Germany - both have a higher diesel penetration than the UK and therefore for western central Europe the addition is rather conservative.

It was seen from the hourly profiles at the London North Kensington site during the summer IOP (Fig. 3.7b) that both the model and the measurements exhibit a small diurnal cycle (peaking in the afternoon). Even though somewhat counter-intuitive (as most of the SOA chemistry is photochemically driven through reaction with the OH radical), an absence of a strong diurnal cycle of SOA has been seen in many European studies (Zhang et al., 2013; Fountoukis et al., 2014; Young et al., 2015a). A relatively small daytime increase of SOA could be explained by the expansion of the boundary layer height (Xu et al., 2015), as well as by contributions from long-range transport. PMF measurements of SOA in Mexico City, on the other hand, revealed a very strong diurnal cycle, peaking around the mid-day (Shrivastava et al., 2011). The fact that during the summer IOP the addDiesel experiment exhibits a slightly stronger diurnal cycle than the measurements (with day-time values slightly overestimated and night-time underestimated) indicates that the SOA yields could be too high. In this work, an SOA density of 1.5 $\mathrm{g\,cm^{-3}}$ is assumed and the yields are increased linearly, as has been done in all other ACTM studies. Actually, increasing the assumed density of SOA from the unit value (1 $\mathrm{g\,cm^{-3}}$) changes the total $\mathrm{C_{OA}}$ (condensed-phase OA) on the Odum mass yield plots (Odum et al., 1996) used to derive the yields from the chamber experiment. Therefore, increasing the yields linearly is not exactly correct (Donahue 2015, personal contact) and further studies and refinement into the calculation of SOA yields and density would be beneficial.

In this work, an ageing rate of $4.0\times10^{-12}\,\mathrm{cm^3\,molecule^{-1}\,s^{-1}}$ was used for both ASOA and BSOA (Lane et al., 2008). This is slower than has been used in some other studies (for example, Tsimpidi et al. (2010) uses $4.0 \times 10^{-11}\,\mathrm{cm^3\,molecule^{-1}\,s^{-1}}$: 10 times faster, or Fountoukis et al. (2011) uses $1.0 \times 10^{-11}\,\mathrm{cm^3\,molecule^{-1}\,s^{-1}}$: 2.5 times faster). A combination of lower initial SOA yields, but slightly higher ageing rates could possibly flatten the diurnal cycle of modelled SOA, matching the measurements better. Therefore, an improvement for the detailed, hourly, evolution could be achieved by a sensitivity study of these yields and ageing rates. This does not, however, change the main scope and results of this paper which illustrate the relative impact of the diesel-IVOCs on SOA formation.

In the current set-up of the EMEP model, only two PM size fractions are simulated: $\mathrm{PM_{2.5}}$ and $\mathrm{PM_{2.5-10}}$, because only two fractions are included in the emissions inventories for PM used in this study. Even though on an annual basis, 90% of $\mathrm{OC_{2.5}}$ is in the sub-micron ($\mathrm{OC_1}$) range (Sect. 3.2.3), the comparison between a modelled $\mathrm{OC_{2.5}}$ and a measured $\mathrm{OC_1}$ could be introducing larger errors during specific days or hours. Therefore, as AMS measurements become more prevalent, emissions

inventories should be reported for all three size classes, PM_1, $\mathrm{PM}_{1-2.5}$, $\mathrm{PM}_{2.5-10}$. This would allow the model to partition SOA into the corresponding fractions, making the direct comparison of modelled SOA_1 to measured SOA_1 possible.

We showed that treating POA as semivolatile and letting it evaporate lead to a great underestimation of HOA and SFOA concentrations compared to measurements at the London North Kensington urban background site. As has been highlighted by a number studies before us (listed in the Introduction), this work also finds that a major source of uncertainty in OA modelling is the volatility of primary emissions, an issue that currently not addressed by official emissions inventories. In the experiment of semivolatile POA (denoted 1.5volPOA), IVOCs were included from all source sectors. This experiment simulated substantially less ASOA than the addition of IVOCs associated with just the traffic source sector. This means that a combination of the POA-based and the new addition of diesel-IVOCs proportionally to NMVOCs would not create a substantial overestimation of SOA concentrations compared to measurements. Nevertheless, further modelling studies (including different assumptions regarding ageing rates, fragmentation, and yields) as well as more measurements of IVOC emissions from different sources are clearly necessary.

In the evaluation of modelled and measured SOA, it was shown that some of the uncertainties in the modelled concentrations are caused by errors in modelled wind vectors, especially during some of the high-pollution episodes discussed in the Results sections of this chapter. For example, there was a very narrow plume created by high-pressure-low-BLH build-up and the positive feedback of the SOA partitioning mechanism. There were also at least two episodes with strong European-imported gradients of SOA over London. During both of these types of episodes, wind speed and direction have the most effect on whether at a specific time and location very high or relatively low concentrations occur. Nevertheless, the underlying meteorological model works well (as demonstrated by comparisons of different pollutants for the whole calendar year), and overall the errors caused by meteorology are believed to be relatively smaller than those introduced by emissions (amount, volatility, composition), or SOA yields and ageing rates.

3.5 Conclusions

This chapter presented annual time series of new high-resolution simulations of SOA formation over the UK that include diesel-related intermediate volatility organic

compound emissions not currently included in the emissions inventory. The derivation of the magnitude of these additional emissions of SOA precursors, as well as evaluation of the model simulated SOA, were both based on measurements made during the Clean Air for London (ClearfLo) campaign in 2012. The IVOC emissions were added in proportion to the VOC emissions from the specifically-relevant on-road traffic source, in contrast to previous studies that have added IVOCs proportionally to POA emissions from all POA sources. Modelled concentrations of SOA were compared with positive matrix factorisation (PMF) analyses of aerosol mass spectrometer (AMS) measurements at a central London urban background location (North Kensington) and at the Detling and Harwell rural background locations outside of London.

The model performance in comparison to relatively more well-known components of air pollution, such as $\mathrm{NO_x}$, $\mathrm{O_3}$ and secondary inorganic aerosol was shown to be very good, providing confidence in the prediction skill of the ACTM system used. Modelled concentrations of SOA were evaluated in four groups: (i) hourly comparison during a summer IOP (Intensive Observation Period), (ii) hourly comparison during a winter IOP, (iii) daily comparison for a full calendar year (including seasonal statistics), and (iv) comparison of OM/OC ratios of all apportioned OA components. To the author's knowledge, this is the first study where modelled OA components are compared with a year-long dataset of PMF-apportioned AMS measurements.

During the period of concurrent measurements at all locations, SOA concentrations at the Detling rural background location were greater than at the central London location. The model showed that this was caused by an intense pollution plume with a strong gradient of SOA from mainland Europe passing over the rural location and demonstrates how short periods of measurements can give a different picture compared with longer-term measurements, as well as the value of atmospheric chemistry-transport modelling for supporting the interpretation of measurements taken at different sites or for short durations.

The model simulations show that these estimates of diesel-related IVOC could explain on average ~30% of the annual SOA in and around London. The 90-th percentile of modelled daily SOA concentrations at the urban background site for the whole year was 3.8 $\mu\mathrm{g\,m^{-3}}$, and the influence of missing diesel-related IVOC precursors was even greater on high percentile SOA days than its contribution to annual average SOA. The magnitudes of these contributions to SOA provide strong additional support for the need to undertake further refinement of the amount and speciation of these precursor emissions for inclusion in official emissions inventories.

Chapter 4

Modelling cooking organic aerosol - estimates of emissions based on measurements at two sites in London

This chapter is based on a research paper accepted for publication in 'Atmospheric Chemistry and Physics' (Ots, R., Vieno, M., Allan, J. D., Reis, S., Nemitz, E., Young, D. E., Coe, H., Di Marco, C., Detournay, A., Mackenzie, I. A., Green, D. C., and Heal, M. R. (2016). Model simulations of cooking organic aerosol (COA) over the UK using estimates of emissions based on measurements at two sites in London, Atmos. Chem. Phys., 1–28, doi: 10.5194/acp-2016-342, accepted for publication in Atmos. Chem. Phys..; see Appendix E). I implemented changes to the model code, ran the model simulations and undertook all data analysis, but the co-authors, namely Dr Mathew Heal, made valuable contributions to the methodology, and the presentation of results through discussions and manuscript editing. In addition, several of the co-authors were involved in the collection and processing the measurements, on which my estimates of COA emissions, and the model-measurement comparisons are based.

4.1 Introduction

In the US, emissions of OA from meat charbroiling (grilling) or frying have been known for decades to be a significant contributor to ambient air quality (Rogge et al., 1991; Hildemann et al., 1991). Consequently, cooking aerosol is included as a component of particulate matter in the US national emission inventory (USEPA, 2004). In Europe, the impact of cooking emissions on ambient air quality via national emissions has so far been neglected. This might be because of an assumption that there is less meat charbroiling in Europe than in the US. However, using positive matrix factorization (PMF) analyses of aerosol mass spectrometer (AMS) measurements, several recent European studies have apportioned a substantial part of submicron OA to cooking. Allan et al. (2010) estimated that the average contribution of COA to OA in Manchester, UK, was 19% whilst in London, UK, it was 22–30%. For Barcelona, Spain, Mohr et al. (2012) reported a 17% contribution to OA from COA, and measurements at different sites in Paris, France, were interpreted as indicating a 15–20% average contribution from COA (Crippa et al., 2013a,b). Allan et al. (2010) also reported that the COA in London is more likely to be produced from vegetable seed oils used during frying, rather than solely from meat cooking.

Based on the aforementioned PMF apportionment measurements of OA components in Paris, Fountoukis et al. (2016) estimated the emissions of COA to be ~80 $\mathrm{mg\,person^{-1}\,day^{-1}}$ on average. Adding these emissions to their model based on population density enabled their simulations to reproduce measured COA concentrations at two sites during the MEGAPOLI campaign. Fountoukis et al. (2016) then added the same 80 $\mathrm{mg\,person^{-1}\,day^{-1}}$ emission of COA to their model for a European domain, and concluded that, based on this estimate, the contribution of COA emissions from other countries to COA concentrations in Paris was between 0.1–0.2 $\mu\mathrm{g\,m^{-3}}$ of $\mathrm{PM_1}$. Discussion of potential uncertainties in the quantification of COA by PMF of AMS measurements is presented later in this paper.

In this work, AMS-derived measurements of COA for a full calendar year at two sites in London during the 2012 Clean Air for London campaign (ClearfLo; Bohnenstengel et al. (2014); Young et al. (2015a)) were combined with gridded UK population density data (Reis et al., 2016) to construct estimates of COA emissions across the UK. The EMEP4UK ACTM (Vieno et al., 2010, 2014, 2016; Ots et al., 2016) was then applied to conduct calibration tests of these novel gridded and temporally-variable emissions of COA, and predictions were compared with a third, independent, dataset of measurements of COA made by AMS in Manchester in Jan–Feb 2007 (Allan et al.,

2010).

4.2 Methods

4.2.1 Chemical and physical properties of COA in the model

A new tracer was added into the model for COA with dry and wet deposition properties similar to other fine primary organic aerosol components (HOA, SFOA). For the split of PM2.5 emissions into this new tracer the emission sector SNAP11 (natural sources) was utilised (technical detail relevant for the EMEP model, see Fig. 2.2 for a visualisation of the "PM split"). As the emissions from SNAP11 are not included in the official national total (anthropogenic) emissions, only SNAP1 to SNAP10 are, the reporting of these emissions is not as coordinated or strictly controlled as the other sectors are. Therefore, alternative datasets consistently compiled for the whole domain (*e.g.* for forest fires, emissions from soil, lightning NO_x) or even explicit calculation schemes (*e.g.* for biogenic VOCs or dust re-suspension) are usually applied in models. Therefore it was possible in this work to adopt the unused definition slots of SNAP11 in the EMEP model for cooking emissions. For example, the initially flat diurnal profile of SNAP11 (Fig. 2.5) was changed to reflect higher emissions during lunch and dinner (explained in more detail in Sect. 4.2.5). The added COA tracer is non-volatile and does not undergo atmospheric ageing, but it is included in the total OA budget for the absorptive partitioning of secondary organic aerosol species of the VBS bins.

4.2.2 AMS measurements used in this chapter

The construction of COA emissions estimates were based on measurements made during the ClearfLo project (Bohnenstengel et al., 2014) at two sites in London, shown in Fig. 4.1. Marylebone Road is a 'kerbside' site on the edge of a heavily-trafficked urban through-road, whilst the North Kensington site is classified as urban background and is situated in the car park of a school. The measurements at Marylebone Road were taken with a Q-AMS (Quadrupole AMS; Jayne et al. (2000)) between 11-Jan-2012 and 1-Feb-2013 and were averaged to hourly values, yielding 5996 data points (Detournay et al. (2015); several gaps in the measured data were caused by problems with the instrument computer). The measurements at North Kensington were taken with a

cToF-AMS (compact Time of Flight AMS; DeCarlo et al. (2006)) between 11-Jan-2012 and 23-Jan-2013, and with a HR-ToF-AMS between 21-Jul-2012 and 19-Aug-2012 (High-Resolution ToF-AMS), hourly averaging yielded 8035 data points (Young et al., 2015a). The annual average (for 2012) concentrations of COA derived from the AMS measurements were 2.2 $\mu g\,m^{-3}$ at Marylebone Road, and 0.8 $\mu g\,m^{-3}$ at North Kensington. Figure 4.3 shows a satellite image of the Marylebone Road measurement site with food-related commercial establishments (cafes, restaurants, etc.), as known to Google, marked. (The accuracy or comprehensiveness of these establishments marked on Google Maps has not been verified, but are presented to illustrate the number of food outlets in the area.) There is no direct source of cooking emissions close to the Marylebone Road measurement site, so the measured concentrations, although high, are likely to represent an average of the many COA emissions sources in the vicinity.

Positive matrix factorisation (PMF) seeks to reproduce the measured time series of the organic mass spectrum through a linear composition of a (user-selectable) number of factor spectra (representing different OA types or sources) and their mass contribution, taking into account the precision associated with each measurement. Subjectivity is minimised by comparison of concentration time-series with independent measurements and assessment of the robustness of the solution, e.g. through boot-strapping. COA has been identified as a contributor to urban OA measurements because it exhibits a distinct diurnal cycle and the associated factor spectrum is very similar to that of lab-generated cooking oil aerosol (Allan et al., 2010). Nevertheless, there are some inherent uncertainties involved in deriving COA concentrations from AMS measurements. For example, AMS measurements need to be corrected for the fraction of aerosol that is not effectively vaporised due to bounce from the hot surface involved in the AMS's detection mechanism. Whilst this is well characterised for typical, internally-mixed ambient aerosols (e.g. Middlebrook et al. (2012)), it is possible that the COA measured by the AMS is not well mixed with other aerosol components and could therefore be detected at a higher efficiency. If this were the case, AMS measurements may overestimate COA concentrations by up to a factor of 2.

Indeed, a study comparing AMS-PMF derived concentrations of PM components with those estimated based on measurements and a chemical mass balance (CMB) model at the North Kensington site during a 2-week period in the same campaign used in this study concluded that AMS derived COA was on average 1.6 times higher than the CMB derived values, but good correlation was seen (a linear fit of $\mathrm{AMS_{COA}} = 2.24 \times \mathrm{CMB_{COA}} - 0.33\ \mu g\,m^{-3}$, with r = 0.89), Yin et al. (2015)), which is consistent with the AMS collection efficiency (CE) being higher than the usual

Figure 4.1 *Residential population density in central London with a 1 km × 1 km resolution in the OSGB36 (Ordinance Survey Great Britain 1936) projection. Also shown are the measurement sites (points), and the EMEP4UK 5 km × 5 km grid used in this study (black lines). Underlying map from © OpenStreetMap contributors.*

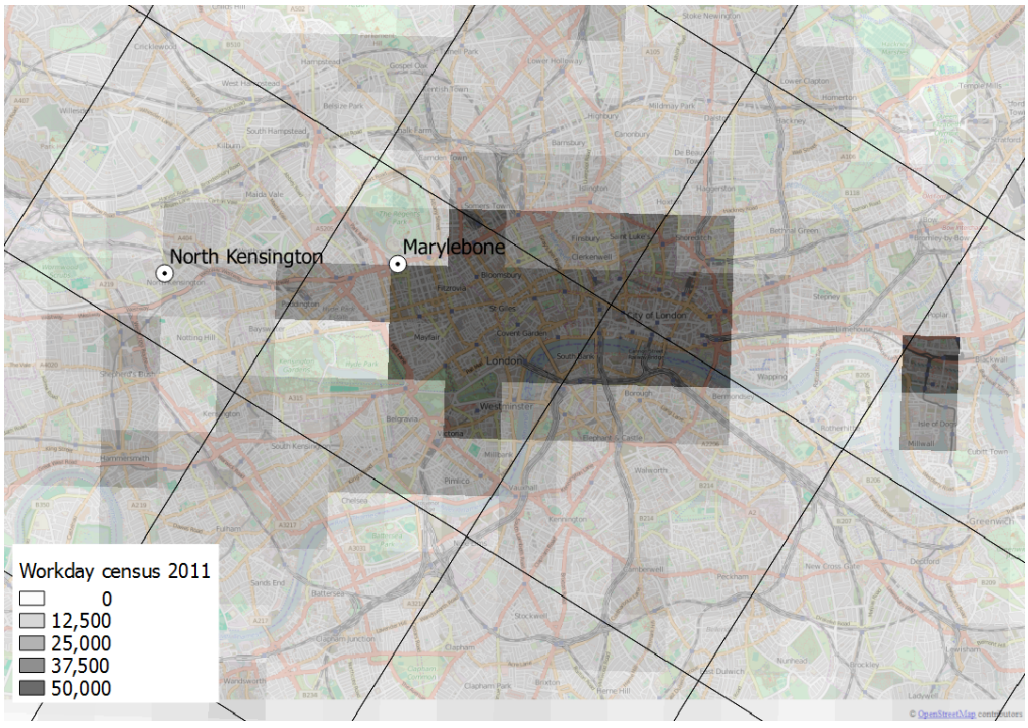

Figure 4.2 *Similar to Fig. 4.1, but for workday population density (note the different scale compared with Fig. 4.1). Underlying map from © OpenStreetMap contributors.*

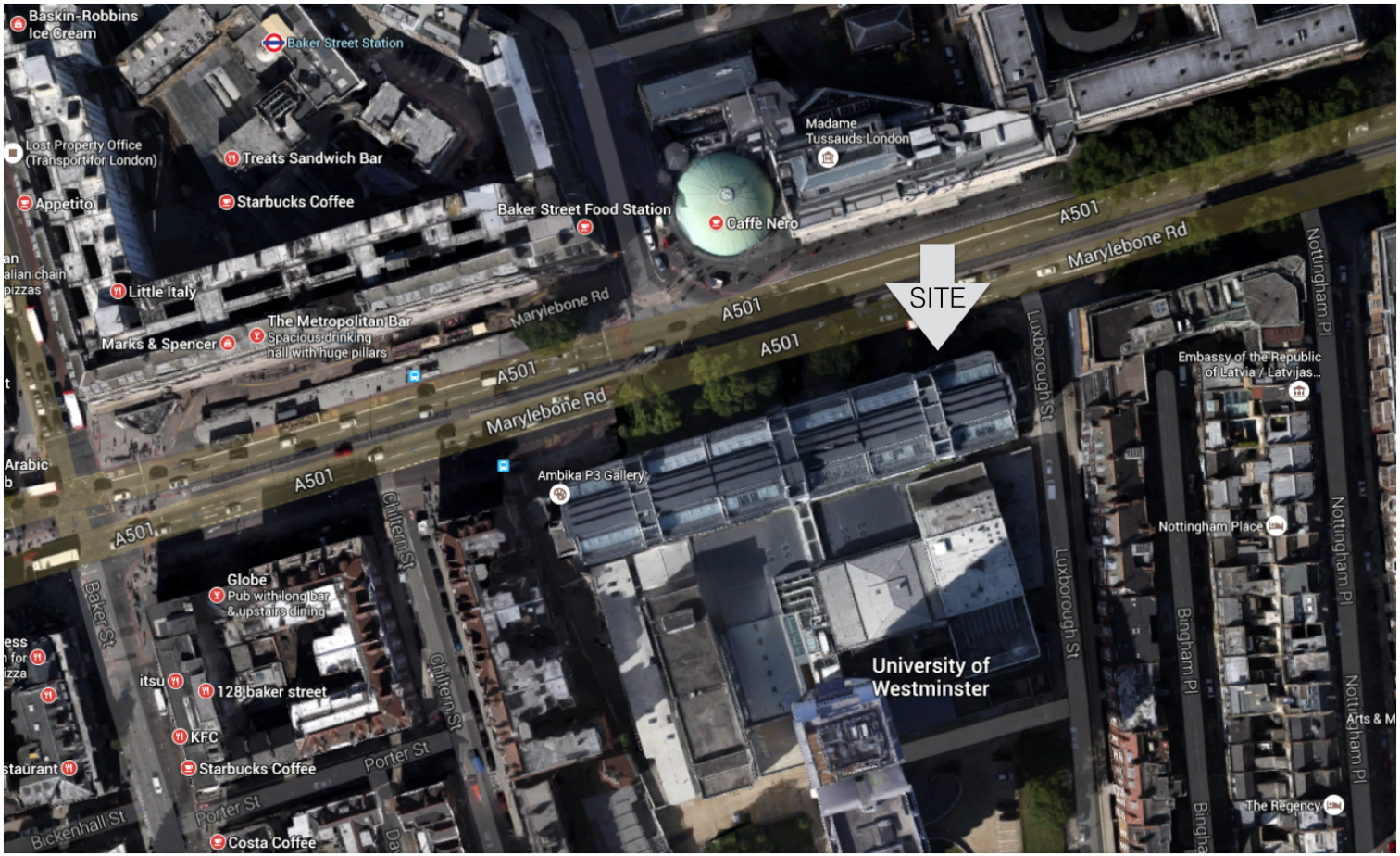

Figure 4.3 *Location of the Marylebone Road measurement site with some of the cafes and restaurants in the area marked. Imagery © 2015 Google Earth, map data © 2015 Google; last accessed on 10-Dec-2015.*

0.5. There are also additional sources of uncertainty with PMF, in particular rotational ambiguity, which can cause both over- and underestimates (Allan et al., 2010; Paatero et al., 2002). However, the CMB approach is also not without its uncertainties, in particular that the COA marker(s) used in the CMB may not be fully representative, and because of the need to scale marker concentration to COA concentration.

In summary, the full quantification of COA by AMS (and any other approach) requires further research but it is currently more likely that the AMS overestimates the COA than underestimates it.

4.2.3 Spatial distribution of COA emissions

Figure 4.1 shows the residential population density data in the central London area at 1 km $\times$ 1 km resolution, overlaid by the EMEP4UK grid cells (5 km $\times$ 5 km), and Fig. 4.2 the equivalent workday population density[1]. These datasets were compiled by Reis et al. (2016) based on the 2011 UK Census, with population data provided on output area level, spatially distributed on a 1 km $\times$ 1 km grid for England, Wales and Northern Ireland using the Land Cover Map 2007 land use classes 'urban', 'suburban' and 'urban industrial'.

The North Kensington and Marylebone Road measurement sites are situated in different model grid cells. The Marylebone Road grid cell includes most of the very central part of London, with many popular tourist attractions such as Madam Tussauds, Buckingham Palace, Big Ben and the Houses of Parliament, and the London Eye. Even though there are no gridded data of 'tourist population density', the workday population density data include indication for tourist numbers as many of the jobs (and therefore the workday population density) in this area will be directly related to, or indirectly dependent on, the tourism sector. The total workday population for the grid cell of the Marylebone Road site is more than 3 times higher than for the grid cell for the North Kensington site. The residential population density in the North Kensington grid cell, however, is higher than in the Marylebone Road grid cell. The annual-average measured COA concentration at the Marylebone Road site was 2.8 times higher than at the North Kensington site, very similar to the ratio in gridded workday population density. Therefore, workday population density was chosen as the spatial distribution

[1]The *workday population* is a redistribution of the usually resident population to their place of work, while residents who are not in work remain at their area of residence. The workday population of an area is defined as *"all usual residents aged 16 and above who are in employment and whose workplace is in the area, and all other usual residents of any age who are not in employment but are resident in the area"* (Source: Office for National Statistics, http://www.ons.gov.uk/ons/index.html).

weighting to apply to COA emissions in the model input.

At present, gridded workday census data are only available for England, Wales, and Northern Ireland, so for Scotland the residential population data had to be used instead. The finer resolution (1 km) information of the COA emissions gridded to population density data was aggregated appropriately to the coarser model resolution during input data preparation.

4.2.4 Annual total emitted COA

Based on sensitivity tests (Table 4.1), the annual total COA emissions for the UK applied to the model was set to 7.4 Gg. (The spatial distribution applied to these emissions is explained in the previous section, the temporal variation is explained in the following section.) This is a 9% addition to the UK national total $\mathrm{PM}_{2.5}$ emissions for the year 2012 (82 Gg, NAEI (2013)). This emission corresponds to about 320 $\mathrm{mg\,person^{-1}\,day^{-1}}$ (for a population of 63 million), which is 4 times higher than estimated by Fountoukis et al. (2016) for France. This difference might be explained by differences in cuisines - it is possible that relatively more grilled, fried and, in particular, deep-fried food is consumed in the UK than in France. Furthermore, it is also possible that the difference in the measurement site locations relative to the very centre of either megacity, and the representativeness of the measurement location to model grid average, could increase or decrease the estimate made for the whole country.

Table 4.1 *Results of sensitivity tests for setting the annual total COA emission for the UK (gridded to workday population density). Model biases of COA concentrations at these sites are shown for the total emissions of 2 Gg, 8 Gg, and 7.4 Gg. A total emission of 7.4 Gg was chosen and is used in the rest of the simulations presented in this work.*

Site	Measured	Modelled		
		2 Gg	+8 Gg	+7.4 Gg
North Kensington	0.8 $\mu\mathrm{g\,m^{-3}}$	-70%	18%	8%
Marylebone Road	2.2 $\mu\mathrm{g\,m^{-3}}$	-75%	-2%	-4%

4.2.5 Diurnal variation of COA emissions

The average diurnal profiles of measured COA concentrations at the Marylebone Road and North Kensington sites are shown in Figs. 4.4a and 4.4b. The measured diurnal cycle of COA concentrations at Marylebone Road was taken as a basis for a temporal emission profile. Marylebone Road was chosen because the concentrations are substantially higher than at North Kensington and show a stronger diurnal variation with more pronounced peaks around both the lunchtime (12:00–14:00) and evening (dinnertime, 18:00–21:00) periods. Even though the diurnal COA concentration variation at Marylebone Road is clearly driven by these meal times, it is further influenced by atmospheric processes such as changing boundary layer height and dispersion, potentially introducing a non-linearity between emissions and concentrations. Therefore, the model was used to assess these processes using

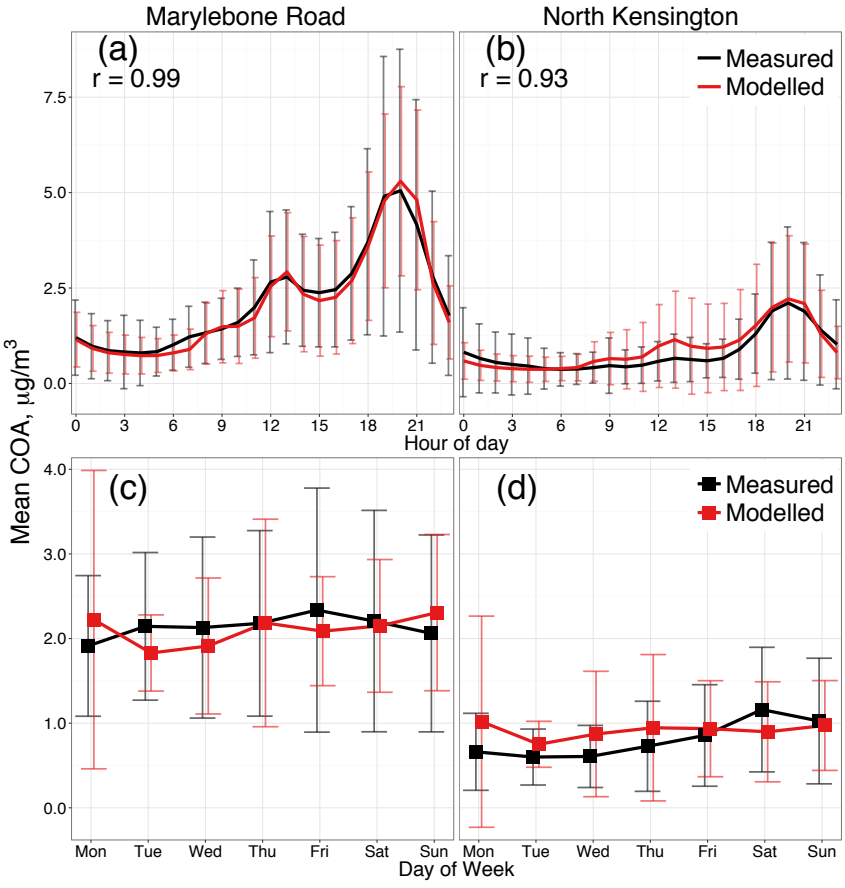

Figure 4.4 *Average temporal profiles of COA concentrations at the two sites in central London in 2012: (a) diurnal profile at the Marylebone Road site, (b) diurnal profile at the North Kensington site, (c) day-of-week profile at the Marylebone Road site, (d) day-of-week profile at the North Kensington site. The timestamp of panels (a) and (b) is at the beginning of the hour. Also shown are standard deviations for each mean value.*

sensitivity runs with different diurnal emission profiles. As a first test, the diurnal profile of COA emissions was set exactly to the measured profile at Marylebone Road, with separate profiles for weekdays and weekend days (the lunchtime peak is more pronounced on weekdays than on weekends). Further sensitivity runs with modified diurnal emission profiles were conducted with the goal of optimising modelled-measured agreement simultaneously at both the Marylebone Road and North Kensington measurement sites. These sensitivity runs and the final diurnal weekday and weekend diurnal emission profiles selected are explained in detail in the Supplementary Information. The emissions total was applied to all seven days of the week because the measurements showed only very small day-of-the-week trends (Fig. 4.4c and d) and differed between the two measurement sites. No seasonality (or monthly) variation was assigned to the emission profile under the assumption that cooking is a consistent year-round activity. It is, however, recognised that cooking emissions may also be strongly affected by tourist population density and may thus have some degree of seasonality. For example, the 2012 Summer Olympics took place in London from 25-July to 12-August attracting 680,000 overseas tourists alone (for National Statistics, 2012).

4.2.6 Summary of the newly composed COA emissions

- The emissions were spatially gridded to workday population density, not residential population density, as this captured the relative difference between observed annual average COA concentrations between the central, commercially-based (Marylebone Road site) and the residential (North Kensington site) areas.
- The annual total COA emission for the UK was based on a series of sensitivity runs to minimise total bias for both sites. The final amount was 7.4 Gg per year, which is an almost 10% addition to the officially reported total $\mathrm{PM}_{2.5}$ emissions (82 Gg in 2012). This corresponds to about 320 $\mathrm{mg\,person^{-1}\,day^{-1}}$ on average.
- The diurnal profile of COA emissions (i.e. the relative increase of emissions during lunch or dinner) was mainly based on the observations at Marylebone Road (as the concentrations were higher and the emission profile was therefore more pronounced at the very central location). Slightly different diurnal cycles were assigned to weekday and weekend COA emissions, but no day-of-the-week or monthly variations were applied to the emissions.

The annual gridded UK COA emissions used in the model simulations are shown in

Fig. 4.5a, and the resulting annual-average modelled COA surface concentrations (for 2012) are shown in Fig. 4.5b.

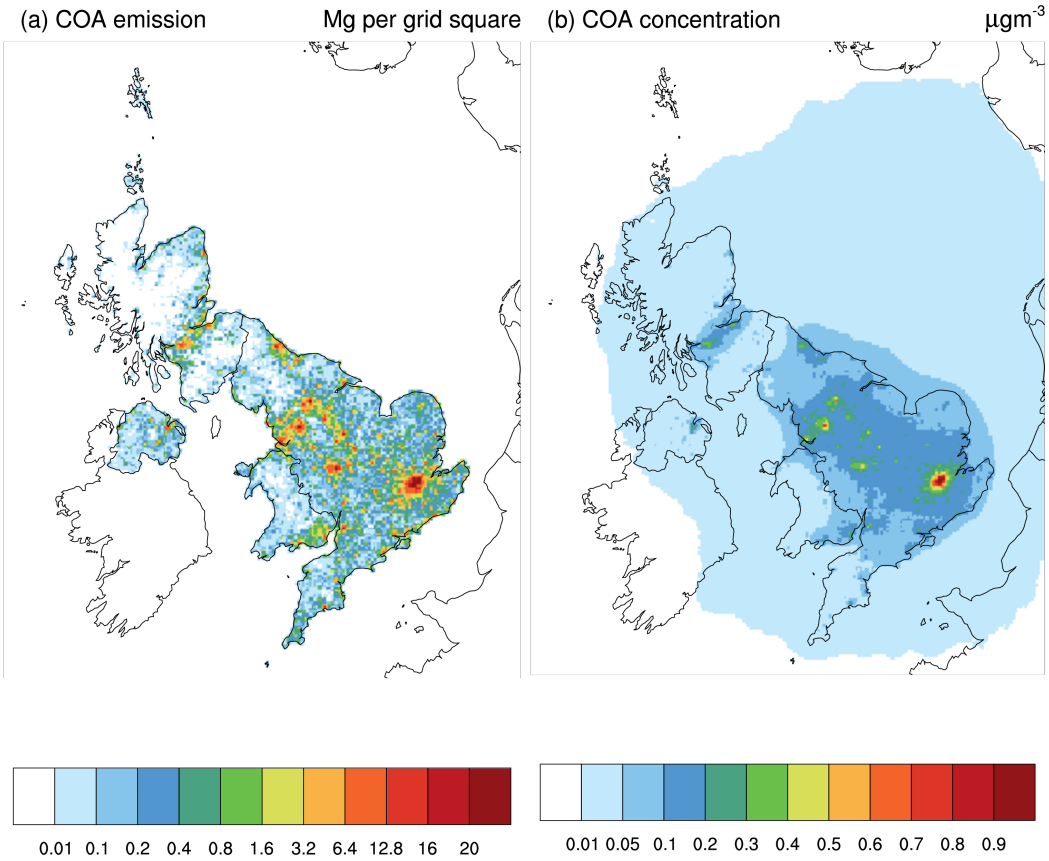

Figure 4.5 *(a) total COA emissions for the year 2012 (Mg per 5 km × 5 km grid cell), (b) annual average concentrations ($\mu g\ m^{-3}$).*

4.3 Results and Discussion

The results section is organised as follows. First, hourly concentrations and average diurnal profiles of measured and modelled COA at the two sites in London are evaluated. Second, an evaluation of daily-averaged measured and modelled COA is presented. These analyses are undertaken for the same sites that were used to estimate the COA emissions. In the third part of the results section, the modelled concentrations are evaluated against a separate, short (two-week) period of measurements from a different location, the centre of the city of Manchester. Finally, modelled concentrations of COA in other major UK cities, as well as in the vicinity of London are discussed.

4.3.1 Hourly comparison of measured and modelled COA concentrations in London

The average hourly profiles (diurnal cycles) of measured and modelled COA concentrations at the Marylebone Road and North Kensington sites are shown in Fig. 4.4a and b, respectively. As explained above, the diurnal COA emission profile applied to the model was mainly based on measurements at the Marylebone Road site. Since COA measurements at this site had a notable lunchtime peak, the modelled lunchtime peak at North Kensington (12:00–14:00, Fig. 4.4b) is slightly elevated compared with the measurements, but, overall, measured and modelled diurnal cycles are in very good agreement (r = 0.99 for Marylebone Road; r = 0.93 for North Kensington).

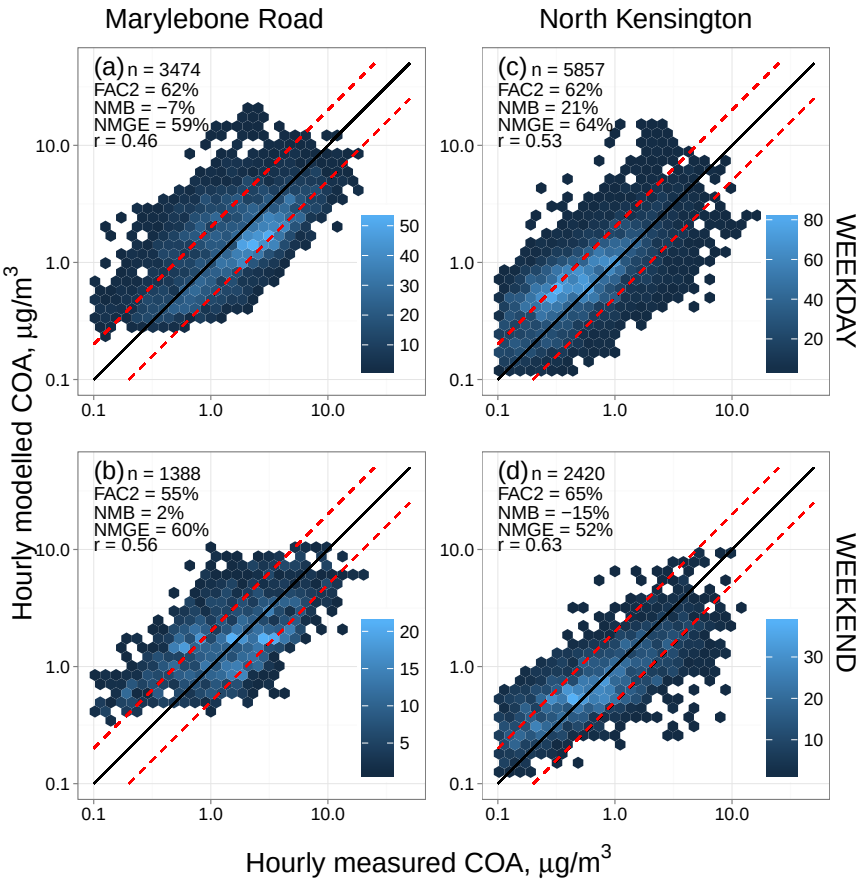

Figure 4.6 *Data density scatterplots of measured versus modelled hourly COA concentrations for approximately one year at two sites in London: (a) Marylebone Road on weekdays, (b) Marylebone Road on weekends, (c) North Kensington on weekdays, (d) North Kensington on weekends. The colour scales indicate number of instances in a hexagonal (concentrations) bin. The straight lines are the 2:1, 1:1, and 1:2 lines. Note that on this Fig. the NMB for Marylebone Road for weekdays is -7%, but calculating the same statistic based on the numbers in Table 4.2 gives a NMB of -5%. This small discrepancy is caused by the rounding of concentrations for Table 4.2.*

Scatterplots of modelled and measured hourly COA concentrations at the Marylebone Road and North Kensington sites, with weekdays and weekends separated, are shown in Fig. 4.6 (the time series of these hourly data are shown in Figs. B5–B8). The average concentrations for each panel of Fig. 4.6 are given in Table 4.2. At the Marylebone Road site, neither the hourly evaluation statistics, nor the mean COA concentrations, show a difference between weekdays and weekends. However, differences in the statistics are observed between weekdays and weekends at the North Kensington site: mean COA concentration for weekdays is 0.7 $\mu g\,m^{-3}$, whereas for weekends it is 1.1 $\mu g\,m^{-3}$. As no day-of-the-week variation was applied to total daily emissions (only to the weekday/weekend diurnal emission profiles), the model can not reproduce this difference (both weekday and weekend mean simulated COA concentrations are 0.9 $\mu g\,m^{-3}$). It is possible in the model to give emissions from each source sector a weekly cycle. This is done for several sectors already. For example, road transport emissions are higher during weekdays, whereas residential heating emissions are higher during the weekends. For cooking emissions, a weekly cycle might be justified for more office dominated areas (like the North Kensington area), but not for the very central commercial and recreational area where the Marylebone Road site is located. It is possible that central London is an exception and that overall, it would be better to assign a weekly cycle to emissions from cooking activities (as it is possible that in every other city than the capital, weekends are busier than weekdays in terms of eating out and therefore a day-of-week factor would be justified). Therefore, more measurements (or alternatively, statistics about the spatial and temporal variability of restaurant customer numbers during different days of the week) should be collected.

Table 4.2 *Measured and modelled mean concentrations of COA for approximately one year at two sites in London for weekdays (Monday–Friday) and weekends (Saturday–Sunday). Values in brackets are the 95% confidence interval of the mean. The number of (hourly) data points used for calculating each mean are given in Fig. 4.6.*

	Marylebone Road		North Kensington	
	Meas.	Mod.	Meas.	Mod.
Weekdays [$\mu g\,m^{-3}$]	2.2 (2.1–2.3)	2.1 (2.0–2.2)	0.7 (0.7–0.7)	0.9 (0.9–1.0)
Weekend [$\mu g\,m^{-3}$]	2.1 (2.0–2.3)	2.2 (2.1–2.3)	1.1 (1.0–1.2)	0.9 (0.9–1.0)

Overall, the hourly evaluation statistics are similar for both sites (Fig. 4.6): FAC2 is 62% (weekdays) and 55% (weekends) for Marylebone Road, and 62% (weekdays) and 65% (weekend) for North Kensington; NMGE is 69% and 60% for Marylebone Road and 64% and 52% for North Kensington; *r*-values are 0.46 and 0.56 for Marylebone Road and 0.53 and 0.63 for North Kensington. The conclusion is that the diurnal emission profiles derived as model input for COA emissions result in similar model performance for both types of area.

4.3.2 Evaluation of daily-averaged COA concentrations in London

Time series of daily averaged modelled and measured COA concentrations along with daily evaluation statistics for the two sites in London are shown in Fig. 4.7. Based on the hourly evaluation in the previous section, some disagreement can be expected at the North Kensington site by not including in the model any difference between weekday and weekend emissions. Despite this, it was shown that the hourly evaluation statistics were similar for both sites. However, North Kensington and Marylebone Road show very different results for the daily evaluation. For the North Kensington site, daily performance is satisfactory (Fig. 4.7b), with an *r*-value of 0.56 and a COE of 0.19. The NMGE of 43% could be attributed to the uncertainties in the COA emissions (including the weekdays vs weekends difference), as well as uncertainties in the meteorological driver. For Marylebone Road on the other hand (Fig. 4.7a), the model does not satisfactorily simulate the measured daily variation of COA concentrations (r = 0.11, COE = -0.22).

Figures 4.8a–d show polar plots of measured and modelled COA concentrations for the North Kensington and Marylebone Road sites. Wind data are from the the Heathrow Airport meteorological station (Met Office, 2012), about 20 km to the west of central London. Meteorological observations from the airport, rather than more local measurements, are used as the airport measurements are unaffected by large buildings and are likely to be more representative of larger scale wind over Greater London. For comparability, the same wind data are used for both measured and modelled concentrations. Furthermore, the days with missing measurements (Fig. 4.7, especially important for the Marylebone Road site) are also removed from the modelled concentrations polar plots. However, it should be noted that the datasets used in these plots still differ in size between the two sites (n days = 191 at Marylebone Road and n days = 340 at North Kensington).

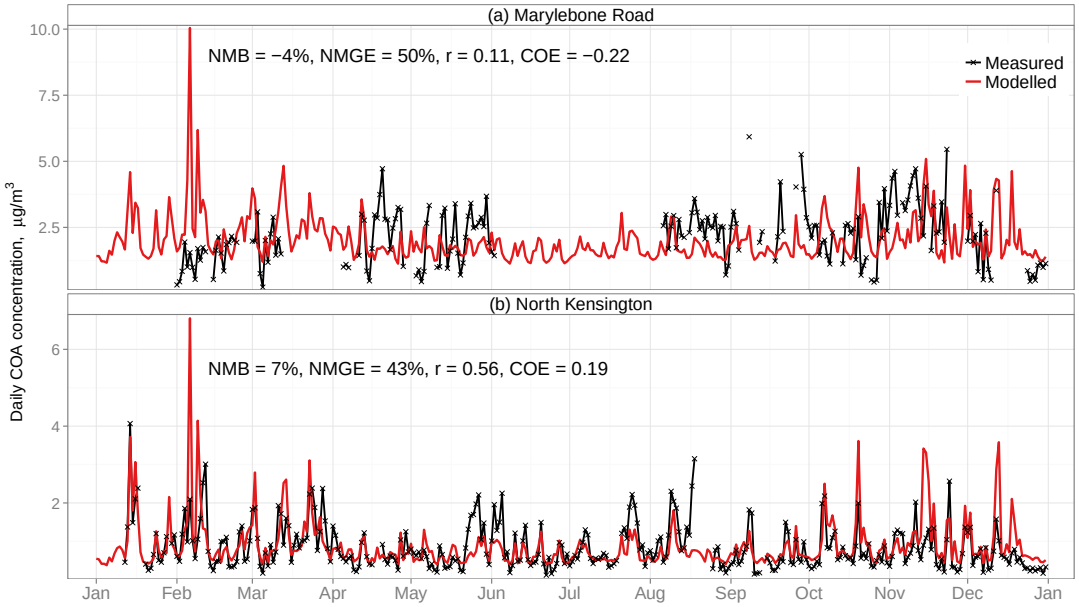

Figure 4.7 *Time-series of measured and modelled daily averaged COA concentrations at the (a) Marylebone Road, and the (b) North Kensington measurement sites, year 2012.*

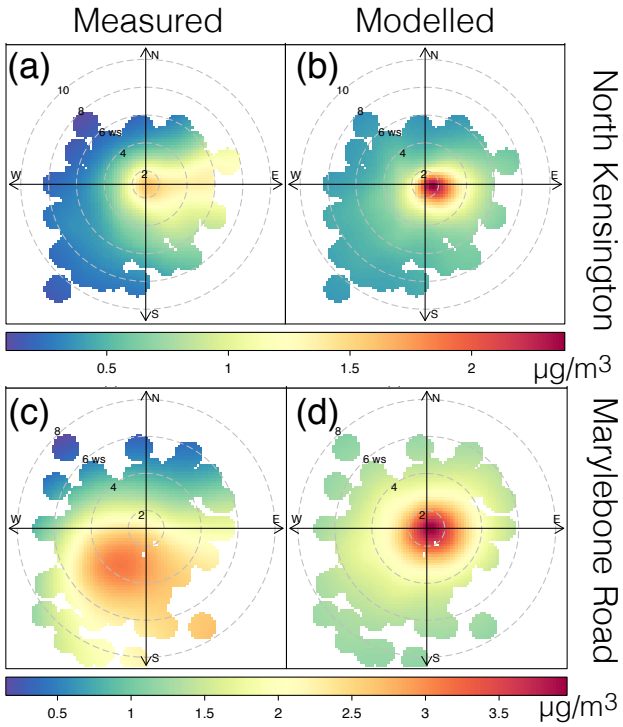

Figure 4.8 *Polar plots of daily averaged COA concentrations for wind speed (ws, $\mathrm{m\,s^{-1}}$) and direction measured at the Heathrow Airport meteorological station (Met Office, 2012). (a) measured and (b) modelled concentrations at the North Kensington site. (c) measured and (d) modelled concentrations at the Marylebone Road site.*

It can be seen from Figs. 4.8a and 4.8b that at the North Kensington site both measurements and model show higher concentrations when the wind is from the east. This is expected as North Kensington is slightly to the west of central London (Fig. 4.1) and therefore wind from the east has passed over more local emission sources. However, the polar plots for Marylebone Road show substantial differences between measured and modelled concentrations. The model simulates higher daily COA concentrations at lower wind speeds from all directions (Fig. 4.8d). In contrast, the measurements show a gradient of higher concentrations when winds are southerly and lower concentrations for northerly winds (Fig. 4.8c). This latter pattern is similar to polar plots of measured NO_x concentrations at the same site. A detailed map of the Marylebone Road location is shown in Fig. 4.9. Although the measurement site is located on the south side of the busy street, highest concentrations of traffic-related pollutants are seen during southerly winds due to street canyon recirculation (Carslaw and Beevers, 2013). This similarity in the patterns of NO_x and COA at this site could indicate that some of the OA apportioned as COA in the PMF analysis might actually be HOA (hydrocarbon-like OA; a primary OA component from fossil fuel combustion). Indeed, based on measurements in Pasadena, California, Hayes et al. (2013) observed that the correlation between HOA+COA and CO is stronger than the correlation between just HOA and CO (0.71 vs 0.59). They also speculated this could mean the COA component identified may also include some particulate mass from non-cooking sources such as traffic.

Figure 4.9 *Location of the Marylebone Road measurement site, arrows indicate the West and South directions from the site. The measurement station is on the southern pavement of the street. Map from © OpenStreetMap contributors.*

Scatterplots of daily-averaged modelled and measured concentrations at the Marylebone Road site conditioned by four divisions of wind directions are shown in Fig. 4.10. The FAC2, *r*-value, and the number of data points are also presented in each panel.

During the period of measurements at Marylebone Road in 2012 (total number of days with measurements was 191) the prevalent daily-averaged wind direction was SW (91 days). The model generally underestimates daily COA concentrations when wind was from this direction (Fig. 4.10c: most points below the 1:1 line), but most points are still within a factor of two of the measurements (Fig. 4.10c: FAC2 = 80%). FAC2 values are noticeably lower for the northerly directions (Fig. 4.10a (NW): FAC2 = 67%, Fig. 4.10b (NE): FAC2 = 42%), with the model generally overestimating COA concentrations on days when the prevalent wind direction was northerly. There is a large park (Regent's Park) just to the north of the Marylebone Road measurement site, explaining why lower concentrations are measured from that direction. The model can not of course resolve this 'sub-grid' variation (the model's horizontal resolution is 5 km×5 km, as shown in Fig. 4.1) and thus misses the effects of the park.

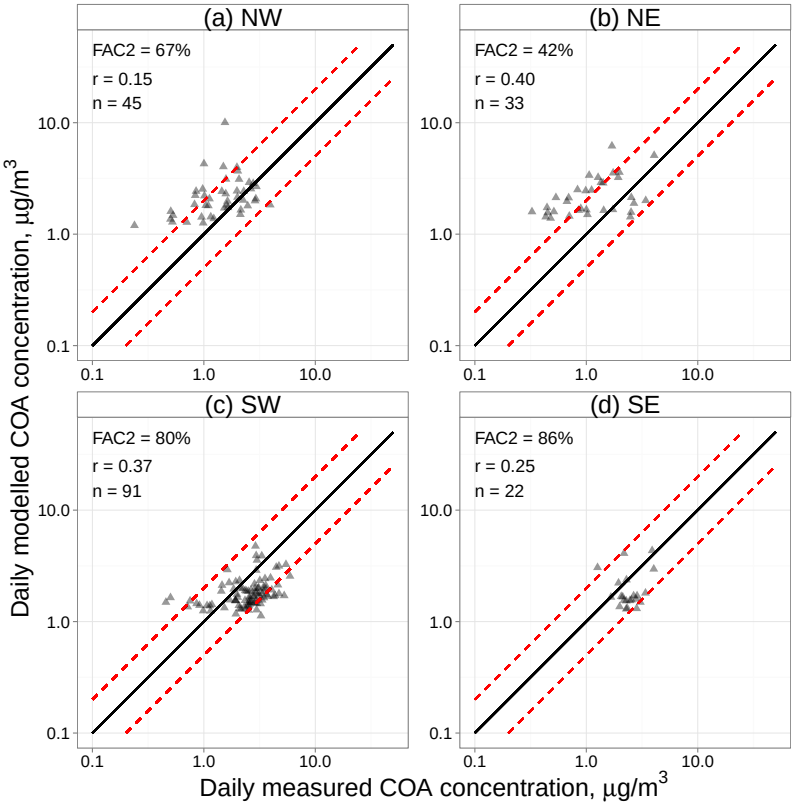

Figure 4.10 *Scatterplots of daily-averaged modelled versus measured concentrations at the Marylebone Road site panelled by four divisions of wind directions measured at the Heathrow Airport meteorological station (Met Office, 2012): (a) from 270°–360° (denoted NW: north west), (b) from 0°–90° (denoted NE: north east), (c) from 180°–270° (denoted SW: south west), (d) from 90°–180° (denoted SE: south east).*

Scatterplots of the daily-averaged modelled and measured concentrations at the Marylebone Road site panelled instead by wind speed quantiles but coloured by wind directions are shown in Fig. 4.11. The number of data points on each quantile panel

is equal, but the number of points with the same colouring is largest for the SW direction (180°–270° from north), as was shown in Fig. 4.10. During low wind speeds (Fig. 4.11a), COA concentrations for winds from the NE and NW directions are overestimated, but concentrations for winds from the SW and SE directions are well reproduced by the model. For all other wind speeds (Fig. 4.11b, c and d) COA concentrations for winds from the northerly directions are overestimated, but COA concentrations for winds from the southerly directions are underestimated. It is an interesting, but currently unexplained observation, that COA concentrations are not underestimated when winds from the southerly directions are of low wind speed.

Whilst the use of the synoptic wind from Heathrow Airport will represent medium to far-field influences more accurately, the funnelling of the air flow by the street canyon will affect the contribution from very local sources and the degree of ventilation vs. build-up of material emitted from within the canyon. These effects are likely to lead to

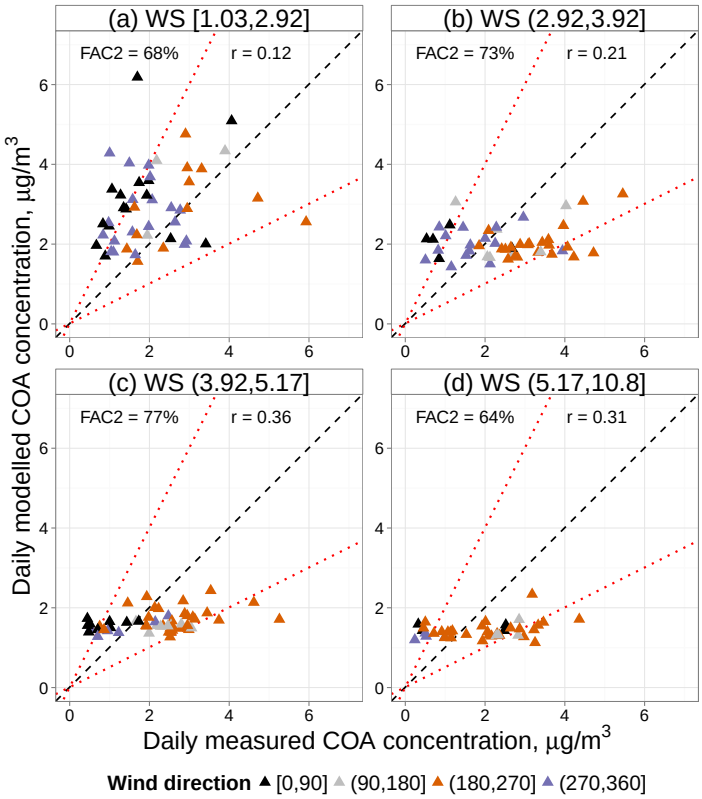

Figure 4.11 *Scatterplots of daily-averaged modelled versus measured concentrations at the Marylebone Road site panelled by wind speed (WS) quartiles measured at the Heathrow Airport meteorological station (Met Office, 2012): (a) first quartile, (b) second quartile, (c) third quartile, (d) fourth quartile; units of wind speeds displayed on panel labels* $\mathrm{m\,s^{-1}}$*. Points are coloured by wind directions (see Fig. 4.10 for number of points from each direction), units: degrees from north.*

a more variable concentration at the Marylebone Road roadside site than at the North Kensington background site. Measurements at different locations and more modelling studies (including different models, for example an urban dispersion model) of COA concentrations in London, as well as in other cities would be necessary to draw further conclusions about the variability of COA concentrations in a street canyon situation.

4.3.3 Comparison with COA measurements in Manchester in 2007

In this section, modelled concentrations (using the emissions based on measurements in London, 2012) are compared with a two-week period of AMS and PMF apportionment measurements in Manchester, Jan–Feb 2007 (taken with a cToF-AMS; Allan et al. (2010)). The Manchester measurement site location, as well as gridded workday population density (1 km $\times$ 1 km resolution) overlaid with the modelling grid (5 km $\times$ 5 km) is shown in Fig. 4.12. The model grid cell in which the measurement site is situated includes an area of a few km in width where the workday population density is several times higher than in the rest of the 5 km $\times$ 5 km cell (this is very central Manchester around the main train station). Since the measurement site was also located in this high workday population density area it is likely that the measured concentrations represent the highest COA concentrations in Manchester, in contrast, the model simulates an average concentration for the whole grid cell which will be lower than at the sub-grid measurement hot-spot. It should also be noted that the Manchester measurement site is located 0.5 km from a 'Chinatown', which could have a direct influence on the measured COA concentrations due to its high number of restaurants and deep-frying.

The time series of hourly-averaged measured and modelled concentrations during the 2-week period of measurements in Manchester are shown in Fig. 4.13a. Average diurnal cycles are shown in Fig. 4.13b, and a scatterplot of daily averaged concentrations in Fig. 4.13c. Modelled concentrations are a factor of 2 lower than measurements (NMB = -50%), likely due to the sub-grid modelling issue discussed above. Nevertheless, there is very good measurement-model correlation (r = 0.80 for diurnal profiles, r = 0.63 for hourly-averaged concentrations, r = 0.86 for daily-averaged concentrations). This indicates that the diurnal profile for COA emissions derived based on measurements in London is also suitable for use in other areas. However, the results suggest that because London is a megacity, the high concentrations in the central area can on average be captured by simulations with

Figure 4.12 *Workday population density in Manchester with a 1 km × 1 km resolution in the OSGB36 (Ordinance Survey Great Britain 1936) projection. Also shown is the measurement site (point), and the EMEP4UK 5 km × 5 km grid used in this study (black lines). Underlying map from © OpenStreetMap contributors.*

the 5 km × 5 km horizontal resolution, whereas for Manchester, a finer set-up (~1-2 km for example) would be needed. Nevertheless, the modelled concentrations are still useful in representing the spatially-averaged concentrations within the whole grid cell. Even allowing for the model resolution, the negative bias between model and measurement suggests that the per capita emissions estimate for COA derived from the London measurements is not an overestimate for COA emissions in Manchester (setting aside the discussion that both London and Manchester AMS measurements maybe be overestimates of COA).

4.3.4 Maximum modelled COA concentrations in London, Manchester, Leeds, and Birmingham

Some statistics for the range of daily-average COA concentrations at the two London sites are given in Table 4.3. The modelled and measured mean values match closely, with a bias of -0.1 $\mu g\,m^{-3}$ for the Marylebone Road site, and +0.1 $\mu g\,m^{-3}$ for the North Kensington site. For the Marylebone grid cell, two sets of statistics of modelled concentrations are given: one matched for data availability with measurements (i.e. missing January, most of March, June and July, other odd days), and one for the full calendar year. The influence of the missing periods is small in this case (full year mean is 2.0 $\mu g\,m^{-3}$, measurements-matched mean is 2.1 $\mu g\,m^{-3}$).

The model grid cell encompassing the Marylebone Road site has the highest annual average modelled COA concentration in London, and indeed across the whole of the UK. Therefore, these statistics (both measured and modelled) likely represent the maximum contribution cooking emissions might have on a 5 km $\times$ 5 km area. The annual average COA concentration of 2 $\mu g\,m^{-3}$ in central London is relevant as that constitutes 20% of the WHO $PM_{2.5}$ air quality guideline of 10 $\mu g\,m^{-3}$ for example.

Figure 4.14 shows the time series of daily-averaged modelled concentrations for 2012 for the other most populous cities in the the UK - Birmingham, Manchester, and Leeds (Glasgow is omitted as the workday population data were not yet available for Scotland). The data shown are for the grid cell over these cities with the largest annual-average COA concentrations. The higher COA concentrations in these cities are also visible in the annual average map of modelled COA surface concentrations in Fig. 4.15b. Based on the gridded workday population density in Manchester and the

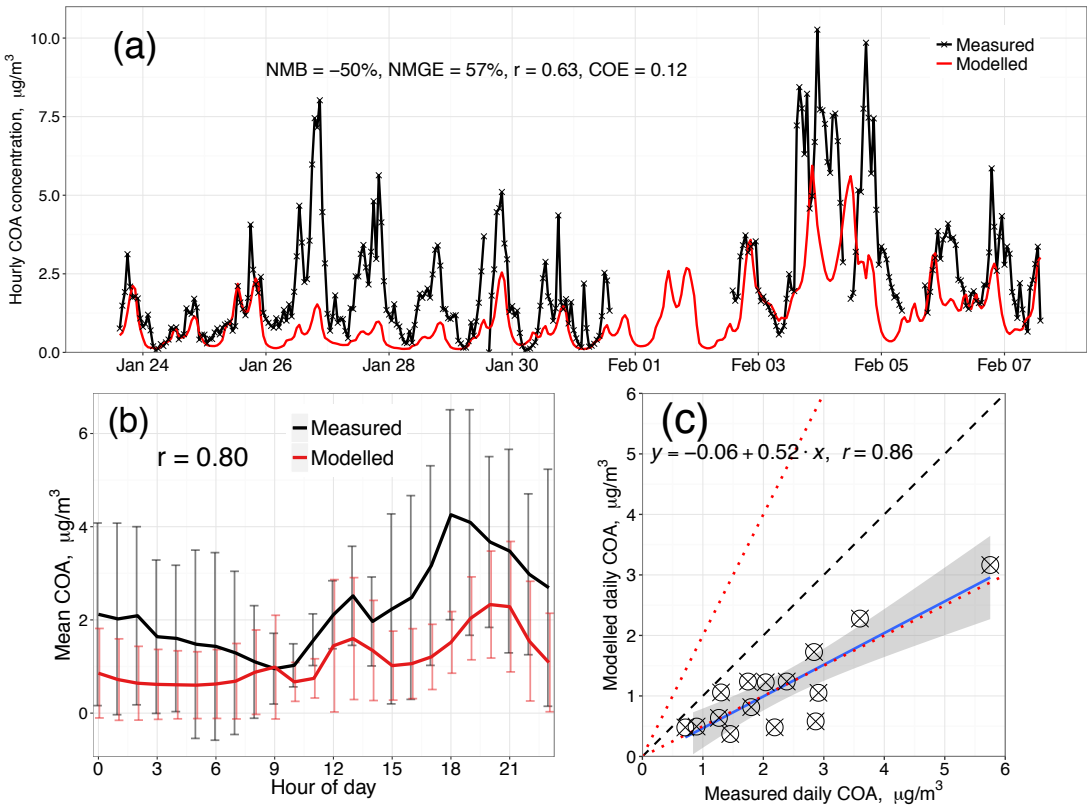

Figure 4.13 *Comparison of modelled COA concentrations with an independent dataset of AMS measurements in Manchester, 2007. (a) Time series of measured and modelled hourly averaged COA concentrations. (b) Average diurnal profiles of measured and modelled COA (the timestamp is at the beginning of the hour, also shown are standard deviations for each mean value). (c) Scatterplots of daily-averaged modelled versus measured concentrations (the dotted and dashed lines are the 2:1, 1:1, and 1:2 lines, the blue line is the linear fit, the shading is the 95% confidence interval of the fit).*

Table 4.3 *Statistics for measured and modelled daily averaged COA concentrations at the two sites in London (site abbreviation as follows: MARY - Marylebone Road, NKEN - North Kensington). Up10 is the 90th percentile (upper 10% of the values), and Up5 is the 95th percentile (upper 5% of the values). The time-series of these values are shown in Fig. 4.7. Values in the "Modelled" line are for model values matched for data availability with the measurements. As Marylebone Road exhibits a few longer periods with missing measurements, modelled stats for the full year are also presented (red line in Fig. 4.7a). All units in* $\mu g\,m^{-3}$.

		Mean	Median	Up10	Up5	Maximum
MARY	Meas.	2.2	2.1	3.5	4.1	5.9
	Mod.	2.1	1.8	3.2	3.9	10.0
	Mod. (full year)	2.0	1.8	3.1	3.7	10.0
NKEN	Meas.	0.8	0.6	1.7	2.0	4.1
	Mod.	0.9	0.7	1.4	2.0	6.8

results shown in the previous section, it is likely that these simulated 5 km $\times$ 5 km concentrations do not capture the central hot-spots of cities smaller than London, but capture the average of an area wider than the centre itself.

It can be seen from Fig. 4.14 that COA exhibits a seasonal cycle whereby modelled surface concentrations are higher during winter than in summer. As the emissions addition did not include monthly or seasonal variation, this effect is purely meteorology and deposition driven. For example, a lower and more stable atmospheric boundary layer increases concentrations allowing for build-up of pollution. There is also a small positive effect on the dry deposition fluxes during the summer as the canopy has less quasi-laminar resistance, leading to more deposition and decreased ambient concentrations.

As an annual average in 2012, modelled COA contributed 0.5–0.7 $\mu g\,m^{-3}$ in these cities (data given in Fig. 4.14). On 36 days of 2012 (90th percentile, denoted Up10 in Fig. 4.14), modelled COA concentrations are over 0.9 $\mu g\,m^{-3}$ in Leeds and Birmingham, and over 1.3 $\mu g\,m^{-3}$ in Manchester. As a 95th percentile of daily averages for 2012, modelled COA contributed 1.3, 2,2 and 2.9 $\mu g\,m^{-3}$ in Leeds, Birmingham and Manchester, respectively.

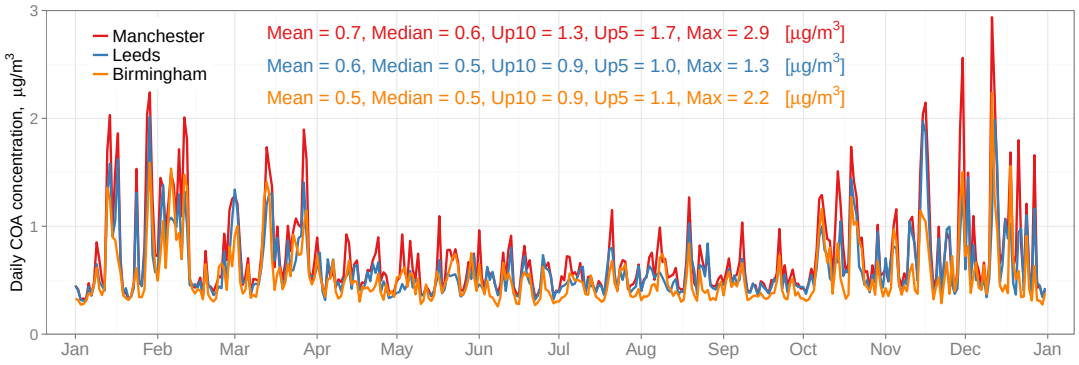

Figure 4.14 *Time series of modelled daily-averaged COA concentrations for Manchester, Leeds, and Birmingham, year 2012. Up10 is the 90th percentile (upper 10% of the values), and Up5 is the 95th percentile (upper 5% of the values). The locations of these cities are shown in Fig. 4.15.*

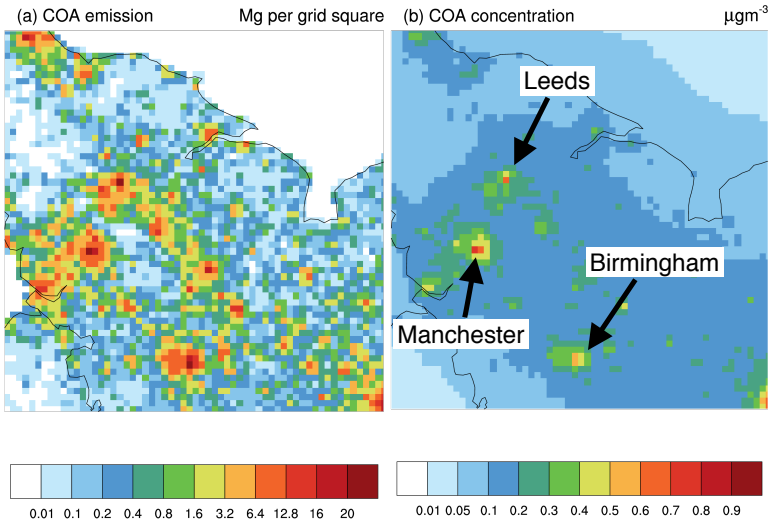

Figure 4.15 *As Fig. 4.5, but zoomed in on northern England to show three other major cities with large estimated COA emissions: Manchester, Leeds, and Birmingham. (a) total COA emissions for the year 2012 (Mg per 5 km × 5 km grid cell, note the non-linear scale), (b) annual average concentrations ($\mu g\,m^{-3}$).*

4.3.5 COA concentrations in the vicinity of London

The map of UK modelled surface concentrations of COA presented in Fig. 4.5b shows that the impact of cooking emissions on an annual average basis is spatially very limited, as COA concentrations drop markedly outside the highly populated urban areas. There are no PMF apportionment measurements of COA concentrations reported outside UK urban areas, but daily-averaged modelled concentrations (for 2012) at Harwell are shown in Fig. 4.16a for an illustration of anticipated non-urban COA concentrations (Harwell is an EMEP supersite ~80 km west of central London,

its exact location is marked on maps in Fig. 4.17). Harwell was also a measurement site during the ClearfLo project. The modelled time series indicate that the COA concentrations at Harwell are relatively small and episodic. In fact, their characteristic diurnal signature is entirely lost (Fig. 4.16b) and their time-series becomes very similar to that of other emissions dominated by population density. This is the reason why PMF commonly fails to resolve COA and hydrocarbon-like organic aerosol (HOA, dominated by vehicular emissions) at rural sites.

The modelled COA concentrations for Harwell are similar to the COA concentration derived by Yin et al. (2015) with the chemical mass balance (CMB) method for the same site. For the period 12-Jan-2012 to 8-Feb-2012 Yin et al. (2015) estimate COA of 0.13 $\mu g\,m^{-3}$ (note text in this paper also refers to a COA average value of 0.12 $\mu g\,m^{-3}$); the model here yields a concentration of 0.17 $\mu g\,m^{-3}$ for the same period, 0.12 $\mu g\,m^{-3}$ for the full year average.

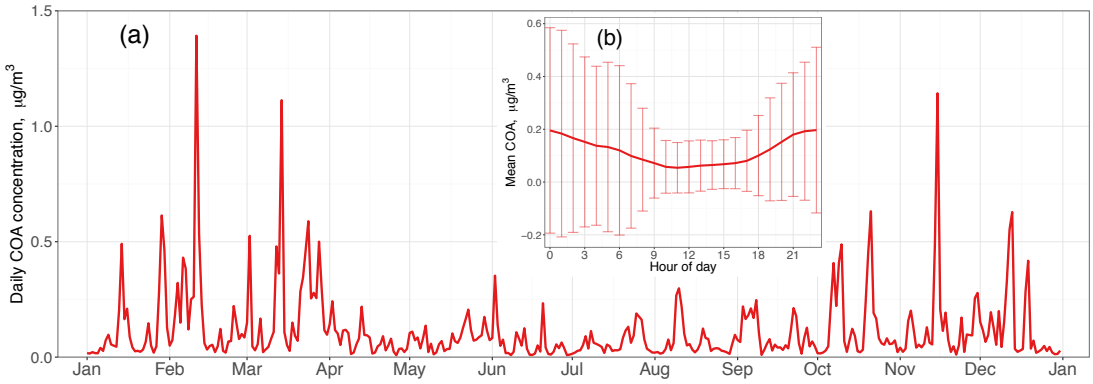

Figure 4.16 *Modelled COA concentrations for the Harwell EMEP supersite location (a rural background site ~80 km from central London), year 2012. (a) Time series of modelled daily averaged COA concentrations. (b) Average diurnal profiles (the timestamp is at the beginning of the hour, also shown are standard deviations for each mean value).*

Modelled surface concentrations near the Greater London area for the 18 highest days (95th percentile: 0.43 $\mu g\,m^{-3}$ for Harwell) are shown in Fig. 4.17. Most of the higher concentrations at these location come from London, with the exception of 11-Feb and 12-Feb, when some traces of COA concentrations arrive from northern England. Furthermore, as even the 95th percentile of daily averaged COA concentrations in the vicinity of London sites is rather low, compared with the COA concentrations experienced within the large urban areas, this demonstrates that the impact of cooking emissions is also spatially very limited on a daily basis.

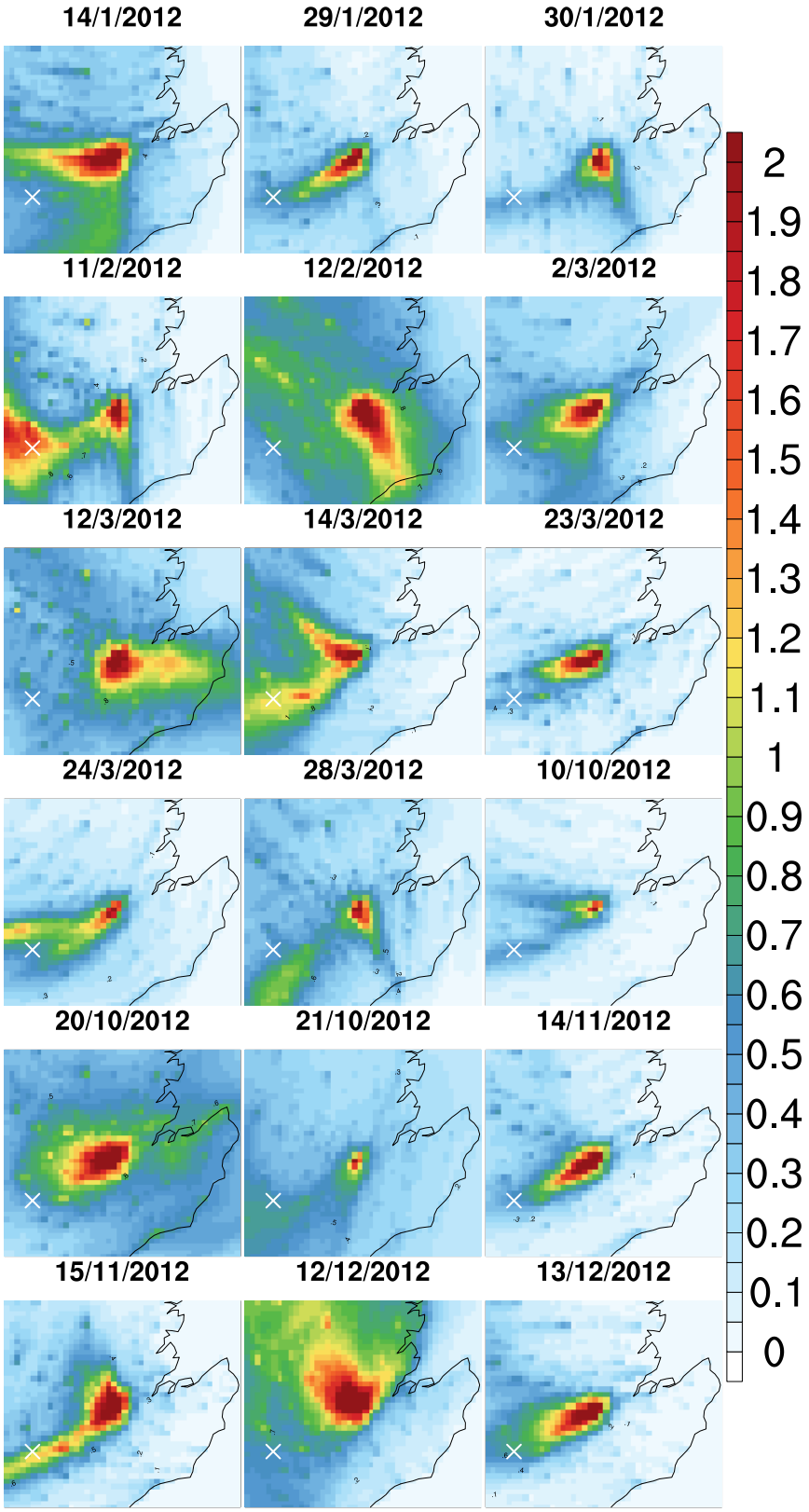

Figure 4.17 *Daily COA modelled surface concentration maps for the 18 days (95th percentile of the year) when modelled COA concentrations for the Harwell location (marked with a white cross) were highest, units:* $\mu g\ m^{-3}$.

4.4 Conclusions

In this chapter, spatially resolved estimates of emissions of cooking organic aerosol (COA) which are currently not included in European emissions inventories were generated for the UK. The magnitude and spatial and diurnal distributions of COA emissions have been derived from determinations of COA concentrations by positive-matrix factorisation (PMF) of aerosol mass spectrometer (AMS) measurements at two sites in London for the full calendar year 2012 (Marylebone Road, a kerbside site in central London; and North Kensington, an urban background site in a residential area close to central London).

An evaluation of daily concentrations in London revealed different results for the two sites. For the North Kensington site, the model captured day-to-day variability throughout the year (r = 0.56, COE = 0.19), whereas for the Marylebone Road site, the model could not simulate observed inter-day variability (r = 0.11, COE = -0.22). Based on polar plots of measured wind directions, the likely source of this disagreement is a sub-(model)-grid effect at the Marylebone Road site and local air flows. Comparing model results with measurements for another time period and location (Manchester, Jan–Feb 2007) suggests that the diurnal profile of COA emissions derived from 2012 measurements at Marylebone Road is suitable for simulating COA concentrations at other central urban areas.

It is shown that in London, annual average COA concentrations are between 1–2 $\mu g\,m^{-3}$ (urban background site to urban central site). Both the measurements and modelled concentrations agree that the 95th percentile of daily averaged COA concentrations at the different locations is 2–4 $\mu g\,m^{-3}$. For three other major cities, Manchester, Leeds and Birmingham, modelled annual average concentrations of COA were between 0.5–0.7 $\mu g\,m^{-3}$, but it should be noted that the model simulates the average concentration of the 5 km $\times$ 5 km grid cells, whereas it was shown for Manchester that cities can exhibit a central hot-spot of smaller scale (1–2 km in dimension). Therefore in some urban centres the contribution might be bigger than is modelled here.

The impact of COA concentrations is spatially very limited as the modelled concentrations drop markedly outside the highly populated urban areas. For example, the simulations estimated an annual average COA concentration of 0.12 $\mu g\,m^{-3}$ for the EMEP supersite Harwell (classified as rural background), which is ~80 km west of central London. This is comparable to estimates of COA concentrations at

Harwell derived from a chemical mass balance (CMB) model applied to two weeks of measurements.

It is noted that it is possible that AMS-PMF measurements of COA concentrations might be overestimated by up to a factor of 2. This means that the emission estimate of 7.4 Gg of COA per year (about 320 $\mathrm{mg\,person^{-1}\,day^{-1}}$) could be a factor of 2 too high (but since COA is a primary PM emission, modelled COA concentrations scale linearly with changes in COA emission amount in the model). If this were the case then, depending on the degree of overestimation, COA would still an important contributor of PM in very central areas, but possibly less so in wider urban or suburban areas.

In short, the spatially and temporally resolved COA emissions developed here for the UK can contribute to closing the gap between modelled and observed concentrations of orgnic aerosol and to total PM mass concentrations in urban areas.

Chapter 5

A model investigation of carbonaceous aerosol from residential solid fuel burning with different assumptions for the spatial distribution of emissions

5.1 Introduction

Residential wood burning is estimated to be the single largest anthropogenic primary source of OC, making up 60% of total OC emissions from European countries (Denier van der Gon et al., 2015; Bergström, 2015). In some countries, in addition to wood, coal is also burned in residential and other small combustion plants. Several AMS-PMF apportionment measurements have thus attributed OA from this source as solid fuel OA (SFOA), which is a more general version of the commonly known biomass burning OA (BBOA) factor (Allan et al., 2010; Young et al., 2015a). Globally, solid fuel burning from residential heating as well as from food cooking activities is a major source of both indoor and outdoor $\mathrm{PM}_{2.5}$ air pollution. As developed countries commit to renewable energy targets, the use of wood and biomass in residential heating is likely to increase (replacing some of the natural gas based heating systems; WHO (2015)). Some residential solid fuel burning in urban areas can also be attributed to recreational reasons, e.g. for decoration (Fuller et al., 2013).

Since the Great Smog of 1952 in London, several legislative interventions have substantially reduced the use of solid fuels in residential heating by subsidising the increased availability of oil and natural gas, as well as the implementation of smoke control areas (Fuller et al., 2013). For example, almost all of London is a smoke control area whereby the use of solid fuel burning is prohibited, unless it is undertaken in approved wood burners (Fuller et al., 2013). This control is only applied on appliances with a chimney, incidental sources such as bonfires or barbecues are allowed.

There is evidence, however, that the smoke control legislation is no longer actively enforced. Several recent studies have reported substantial local contributions of solid fuel burning in London coinciding with days of low temperature (Fuller et al., 2014; Crilley et al., 2015). This is relevant as, currently, the National Atmospheric Emissions Inventory (NAEI) assumes zero residential emissions of non-approved solid fuel burning in smoke control areas (i.e. that the law is being followed). Furthermore, the NAEI only includes estimates of emissions from officially sold solid fuels (NAEI, 2013), but there is reason to believe that much of fuel wood is non-commercial and falls outside of the economic administration (Denier van der Gon et al., 2015). For example, a recent UK Wood Use Survey concluded that the official national consumption of domestic wood fuel is underestimated by a factor of 3 (Waters, 2016). Furthermore, the survey showed that 31% of wood fuel is sourced from the informal grey market of wood (i.e. own garden, other landowners garden, waste wood, etc.).

The results of this survey are completely in line with recent evaluations of wood burning emissions in Belgium, where it was also concluded that their official inventory has underestimated the amount of wood burned in residential settings by more than a factor of 3 (Lefebvre et al., 2016). Belgium has since included these increased emissions estimates (including both official sales as well as non-commercial wood sources) in the amount reported to the Centre on Emission Inventories and Projections (CEIP) of the EMEP programme, and the authors of that study urge countries that currently do not make estimates of non-officially traded or sourced wood to follow their example.

It was shown in a previous chapter where model-measurement comparisons of several different pollutants were presented (Sect. 3.3.1) that modelled SFOA at the London North Kensington site is hugely underestimated compared to yearlong PMF apportionment of AMS measurements (NMB of -71%). Therefore, in this chapter, four model experiments were constructed to explore potential find an explanations for this.

5.2 Methods

The Base case scenario uses the same emissions inventory as in Chapter 3, but with a small enhancement for the daily variation in emissions - degree-day factors (Simpson et al., 2012). Degree-day factors modulate the daily variation in emissions from the SNAP2 sector according to ambient temperature (i.e. increasing the emissions during colder days). SNAP2 includes $\mathrm{PM}_{2.5}$ emissions from both residential and small (non-industrial) commercial combustion, but the residential part dominates with annual emissions for 2012 of 19 Gg from residential, 1 Gg from commercial and 5 Gg from stationary military combustion (NAEI, 2013). This means that applying the degree-day factors (aimed to capture increased residential heating on colder days) to the whole of SNAP2 does not introduce big additional uncertainty relating to the temperature-related variations in emissions for the commercial component of SNAP2.

A degree-day is defined as $H_{dd,j} = max(18°C - T_j^{24h}, 1)$, where *j* is the day number and T^{24h} is the daily averaged temperature in $°C$. These degree-days are divided by the annual mean $\left(\overline{H_{jj}}\right)$ to obtain degree-day factors (Simpson et al., 2012). For this work, degree-day factors pre-calculated by the EMEP MSC-W Centre based on ECMWF meteorological simulations for the 50 km $\times$ 50 km domain (Schulz et al., 2013) were disaggregated using the simple area-weighting method assuming homogeneity for degree-day factors within the 50 km to 5 km conversion.

In the second scenario (Base4x), emissions from SNAP2 were increased by a factor of 4 (based on the NMB of -71% at the London North Kensington site). SNAP2 is the only sector with SFOA emissions in the set-up used (Sect. 2.3: Emissions, and Fig.2.2).

For the Redist experiment, the annual reported $\mathrm{PM}_{2.5}$ emissions from SNAP2 were re-gridded linearly to residential population density (census data from Reis et al. (2016)) as this would 'over-write' the assumption made by the NAEI that only smokeless fuels are used in smoke control areas.

Finally, the fourth test was a hybrid of the Base and Redist experiments, where, for each grid cell, half the emissions of Base and half of Redist (of the SNAP2 sector) were added together: combRedist$_{emis}$ = 0.5$\times$ Base$_{emis}$ + 0.5$\times$ Redist$_{emis}$. The experiments Base, Redist, and combRedist therefore include an equal total emission amount, the only difference is in their spatial distribution. All four experiments use the same temporal variation for SNAP2, including degree-day factors. The emissions used for

the four experiments are summarised in Table 5.1. In all of these experiments, SFOA is assumed to be non-volatile.

The emission maps of these four experiments are shown in Fig. 5.1, and the resulting modelled annual average concentrations in Fig. 5.2. The measurements used to evaluate the modelled surface concentrations from experiments were described in Chapters 3 and 4. In short, the following AMS-PMF datasets from the ClearfLo campaign were used: cToF-AMS at the London North Kensington urban background site (yearlong, used in daily evaluation), Q-AMS at the London Marylebone Road kerbside site (yearlong), HR-ToF-AMS at the London North Kensington site (winter IOP), HR-ToF-AMS at the Harwell rural background site (winter IOP), and HR-ToF-AMS at the Detling rural background site (winter IOP).

Table 5.1 *Summary of the four experiments for $PM_{2.5}$ emissions from SNAP2. In the model, $PM_{2.5}$ is split into three components as follows: 48% is SFOA, 26% EC, and 26% other/mineral PM. For more information see Sect. 2.3 and Fig.2.2.*

Experiment	Total $\mathrm{PM}_{2.5}$ emission	Spatial distribution
Base	25 Gg	NAEI
Base4x	100 Gg	NAEI
Redist	25 Gg	Population density
combRedist	25 Gg	NAEI + Population density

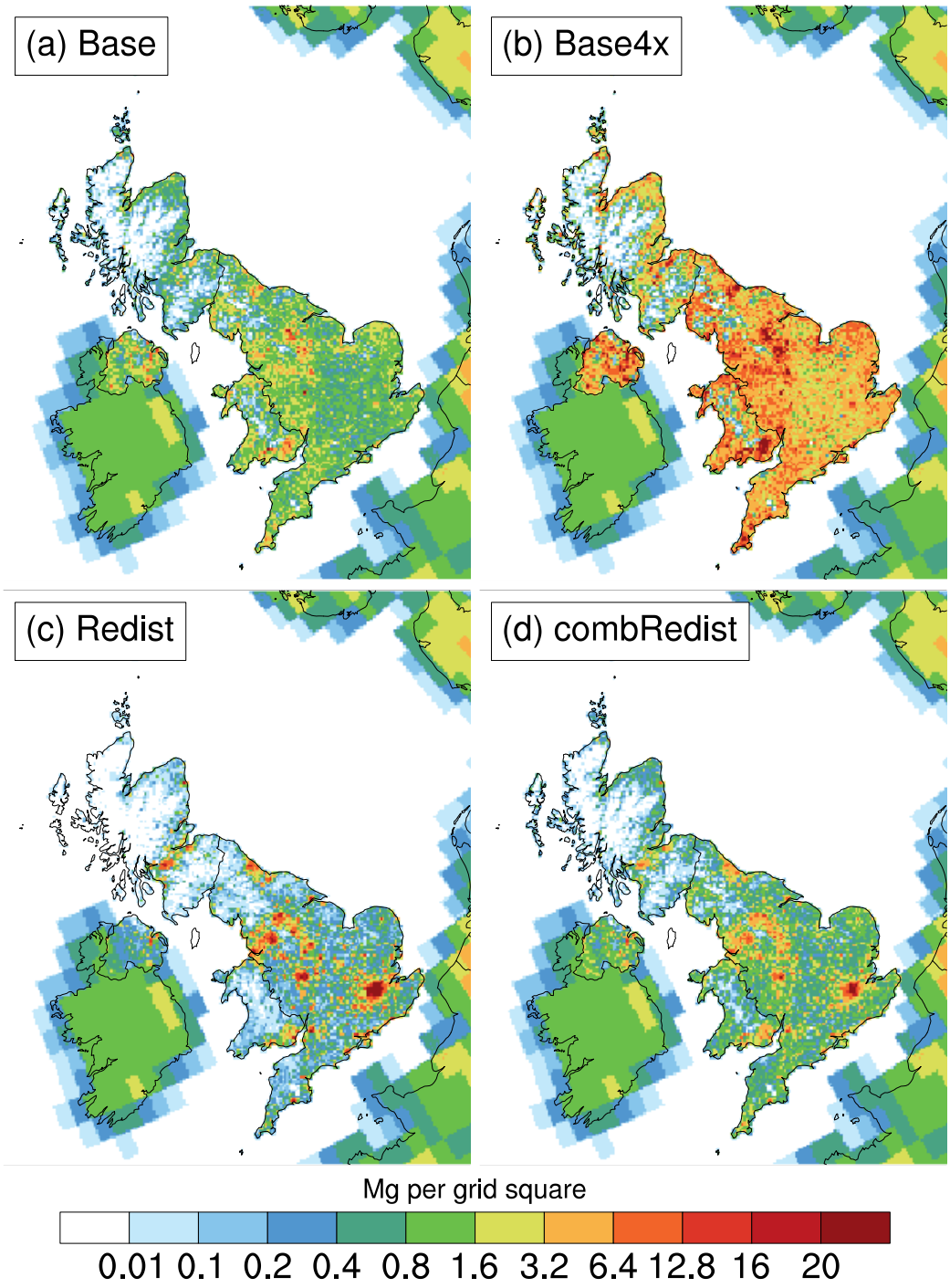

Figure 5.1 *Total SFOA emissions (defined as 48% of $PM_{2.5}$ from SNAP2) for the year 2012 in the inner nesting domain for the four scenarios of this study: (a) Base: as in the NAEI, (b) Base4x: Base increased by a factor of 4 over the whole of UK, (c) Redist: UK emissions redistributed to residential population density (national total same as Base), (d) combRedist: half of the total emission redistributed to residential population density, half as reported by NAEI (a combination of (a) and (c), national total same as either). All UK emissions are aggregated to the 5 km × 5 km grid from an initial resolution of 1 km × 1 km reported by the NAEI. The emission resolution is 0.1° × 0.1° for other countries (as in CEIP). Note the non-linear scale.*

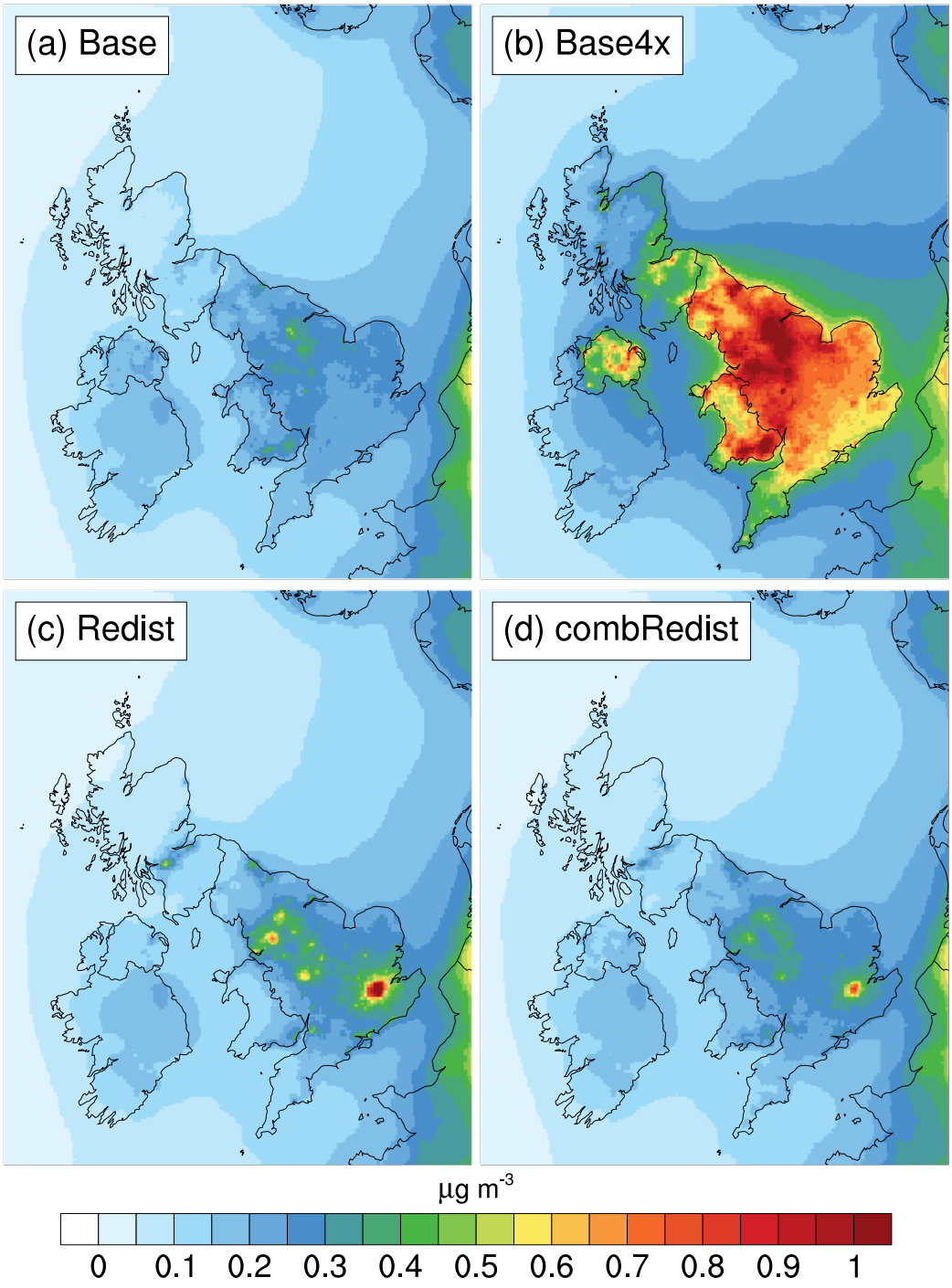

Figure 5.2 *Annual average modelled SFOA concentrations for the year 2012 using the emission scenarios as in Fig. 5.1: (a) Base: as in the NAEI, (b) Base4x: Base increased by a factor of 4 over the whole of UK, (c) Redist: UK emissions redistributed to residential population density (national total same as Base), (d) combRedist: half of the total emission redistributed to residential population density, half as reported by NAEI (a combination of (a) and (c), national total emission same as either).*

5.3 Results and Discussion

Figure 5.2 shows the annual averaged modelled SFOA surface concentrations for the year 2012. In the model, SFOA is emitted as 48% of $\mathrm{PM}_{2.5}$ from the SNAP2 source sector, and it is traced as a non-volatile and chemically inert specie (but it is included in the total OA budget for the absorptive partitioning of secondary organic aerosol species). It can be seen that, on annual average, the gradients of SFOA surface concentrations as indicators of European transport are mainly visible over the North Sea. Over the UK, concentrations follow the pattern of national (i.e. local) emissions, whereas the spatial distributions of the experiments regarding the national emissions are substantially different. The Base and Base4x scenarios (spatially gridded as reported by the NAEI) set most emissions to Northern England, Wales and Northern Ireland, leaving London, Manchester, Leeds, Birmingham, Glasgow, etc. almost unnoticeable (as these, and many more urban locations, are smoke control areas). In contrast, the Redist experiment highlights all of these urban areas, because the SFOA emissions were redistributed linearly to residential population density. The combRedist experiment shows these residential hot-spots while also retaining some of the spatial pattern from the officially reported distribution.

5.3.1 Daily evaluation - London Marylebone Road and North Kensington annual datasets

Time-series of measured and modelled (all four experiments) daily-average SFOA concentrations for the London Marylebone Road and North Kensington sites are shown in Fig. 5.3. Model-measurements evaluation statistics are also presented. The difference between the Base experiment time series in Fig. 5.3b and in Fig. 3.3b is due to the use of degree-day factors. For convenience, the evaluation statistics for the Base emissions experiments with degree-day factors are (values in brackets are from the Base run in Fig. 3.3b): NMB = -69% (-71%), NMGE = 69% (72%), r = 0.73 (0.72), COE = 0.03 (0.01). The improvement in all four of the statistics is small. Degree-day factors do not change the annual total SFOA emission, they only modulate the daily variation of emissions. Therefore, the positive change of 2% in the NMB means that degree-day factors increased SFOA concentrations in some of the air masses arriving at the London North Kensington measurement site during the year 2012.

Almost all of the experiments result in better modelled daily-average SFOA con-

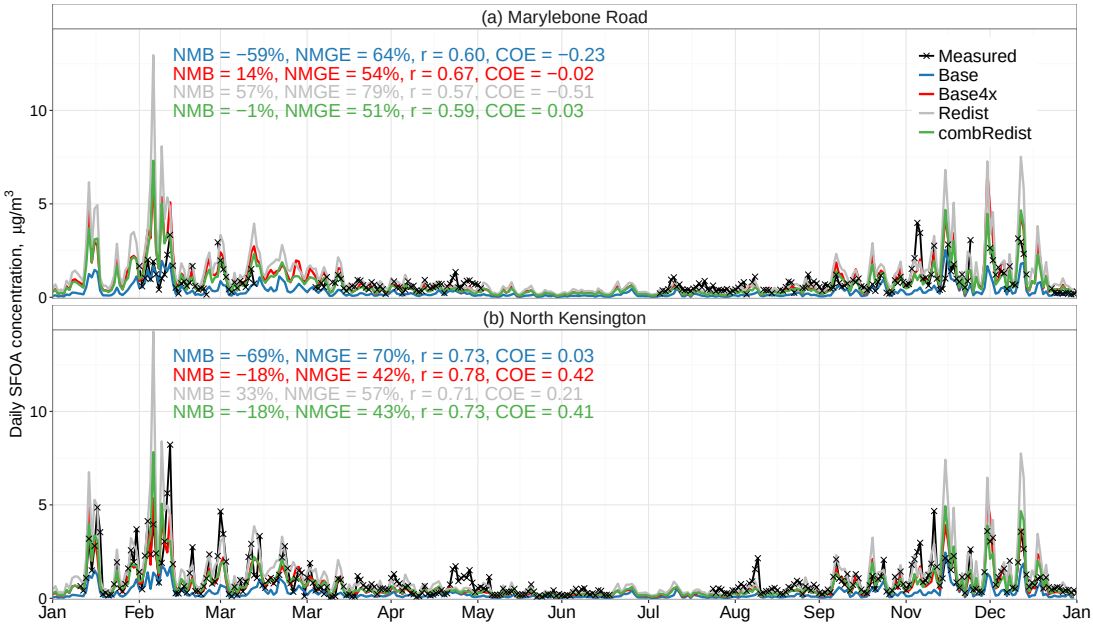

Figure 5.3 *Time-series of measured and modelled daily-average SFOA concentrations at the (a) Marylebone Road, and (b) North Kensington measurement sites, year 2012. For clarity, the Base4x and combRedist experiments are also plotted separately in Figs. 5.4 and 5.5.*

centrations compared to measurements at the two sites. The only exception is the Redist simulation at Marylebone Road, where the underestimation of the Base case is replaced with an equivalent overestimation (NMB of -59% and $+57\%$, Base and Redist, respectively). There is a small decrease in the *r*-value, and an increase of the NMGE, which is caused by the modelled values of Redist being greater than those of the Base experiment. For the London North Kensington site, the Redist experiment is an improvement compared to the Base run, although the concentrations are also overestimated (NMB = $+33\%$, Redist). This is expected, as areas with high population densities would include large apartment buildings which are unlikely to have individual fireplaces. Therefore a completely linear redistribution of residential emissions is not correct, but this experiment was included to give an indication of the maximum effect that population density could have on SFOA concentrations. Furthermore, this experiment is also part of the combRedist emission test.

Figures 5.4 and 5.5 are the same as Fig. 5.3, but separated for the Base4x and combRedist experiments, respectively. Also marked is the annual bonfire celebration of Guy Fawkes Night (5th of November) to draw attention to an increase in SFOA emissions that can not be simulated with the model, given that the temporal variation is prescribed using a regular approach (i.e. hour-of-day, day-of-week, month-of-year) which does not include information about specific days and events.

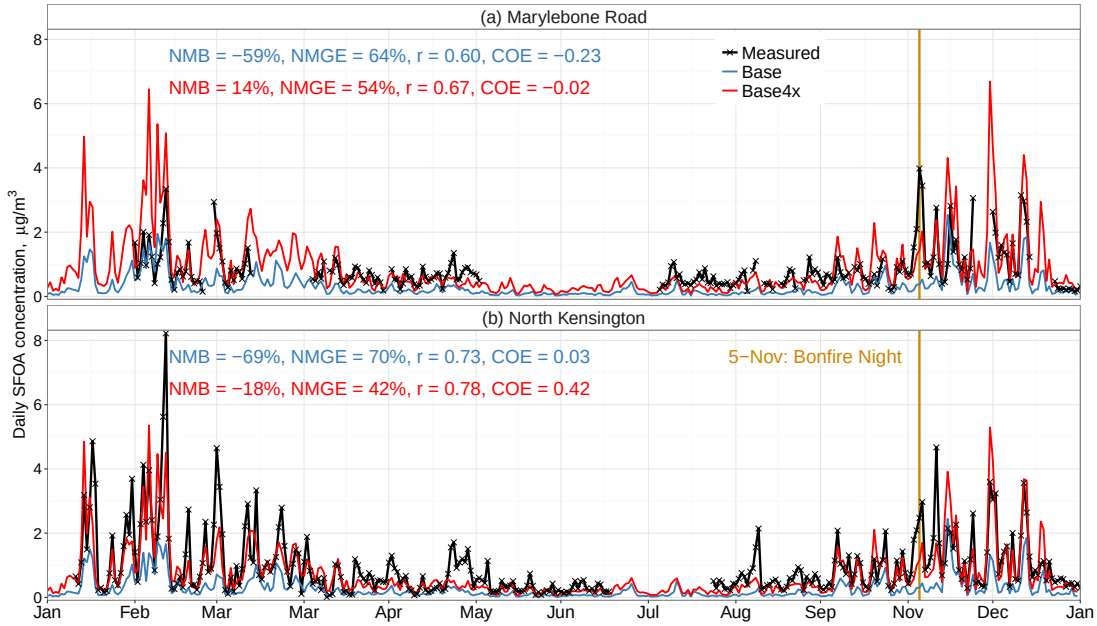

Figure 5.4 *Same as Fig. 5.3, but for the Base and Base4x experiments. The vertical line marks the date of the 'bonfire night', November 5th.*

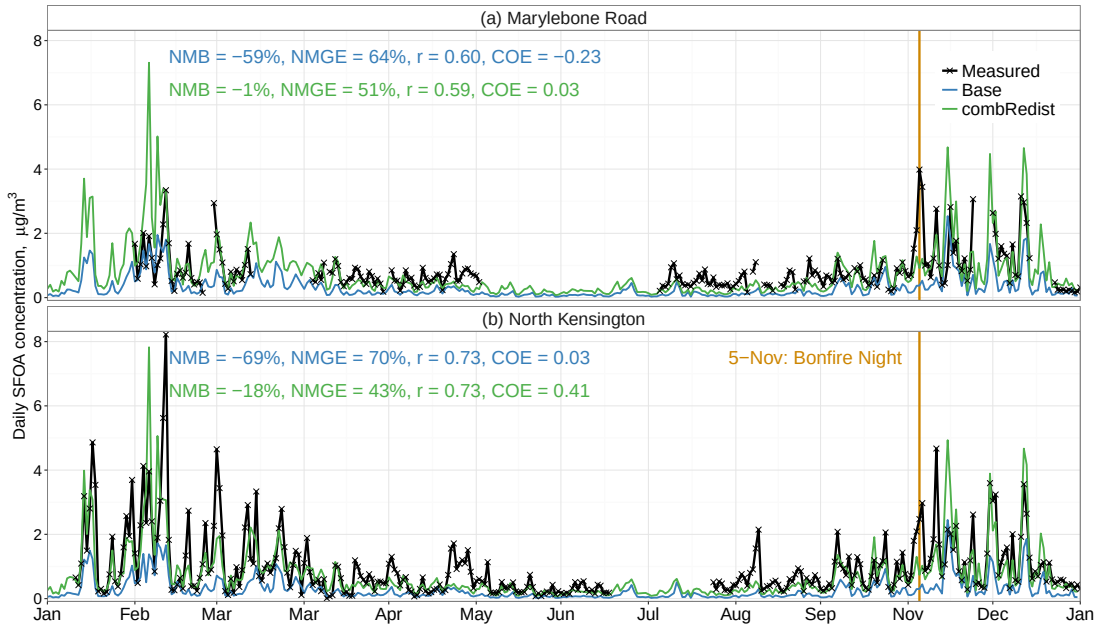

Figure 5.5 *Same as Fig. 5.3, but for the Base and combRedist experiments. The vertical line marks the date of the 'bonfire night', November 5th.*

Both the Base4x and combRedist experiments have better predictive abilities compared to AMS+PMF measured concentrations of SFOA at these two sites in London than the Base case emissions simulation. The NMGE at the Marylebone Road site is reduced to 54% (Base4x) or 51% (combRedist), compared to 64% for the Base case simulation. At the North Kensington site, NMGE is reduced to 42% (Base4x) or 43% (combRedist), compared to 70% for the Base case simulation. The Base4x results in improvements in the *r*-value: 0.67 (Base: 0.60) and 0.78 (Base: 0.73) at Marylebone and North Kensington, respectively, whereas with the combRedist emissions, the *r*-values of daily-average concentrations remain the same as Base: 0.59 (0.60) and 0.73 (0.73), at Marylebone Road and North Kensington, respectively. The improvement in COE values is similar for both experiments (Fig. 5.3) at both sites. Both experiments decreased the NMB at North Kensington to -18% (Base4x and combRedist) from -69% (Base), whereas at Marylebone Road, the Base4x reaches an overestimation of NMB = $+14\%$ while the combRedist matches the measured mean SFOA: NMB = -1% (NMB of Base at the Marylebone Road measurement site: -59%). It should be noted, however, that there are several days in November and December where both the Base4x and combRedist experiments overestimate SFOA concentrations compared to measurements, thus compensating for the NMB.

In summary, in comparison with daily-average measurements of SFOA concentrations at two sites in London the Base4x and the combRedist experiments resulted in similar improvements in NMGE and COE, the Base4x experiment had better *r*-values, and the combRedist experiment better matched the annual mean concentrations of SFOA at the two sites. Nevertheless, it should be noted that AMS-PMF apportionment measurements are also subject to uncertainty which limits the expected correlation with the model (for more information about this see Sect. 3.2.3 and Fig. 1.8).

The following sections in this chapter evaluate these experiments in comparison to hourly-average measurements taken with the High Resolution (HR-ToF-AMS) instruments during the ClearfLo winter Intensive Observation Period (IOP), which included two rural background sites - Harwell and Detling - as well as the London North Kensington site.

5.3.2 Hourly averaged diurnal profiles of SFOA concentrations

Hourly averaged diurnal profiles of SFOA concentrations at the ClearfLo winter IOP sites are shown in Fig. 5.6. The diurnal variation in emissions from different source sectors (same for all countries) was presented in Fig. 2.5, where it can be seen that the hourly emission factors used for SNAP2 assume similar emissions for morning and evening. The hourly averaged profiles of measured concentrations at the rural background sites (Detling and Harwell), and the urban background site (North Kensington) all indicate a substantial increase in the evening (after 18:00), and a very small increase at 9:00 (Fig. 5.6). This clear discrepancy in the prescription of this emission profile for the UK will have a detrimental effect on all of the model evaluation statistics, except NMB.

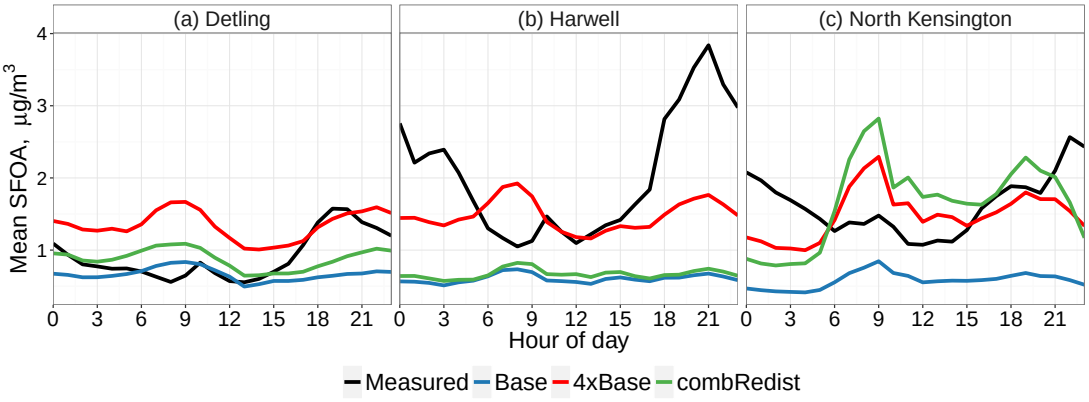

Figure 5.6 *Hourly-averaged diurnal profiles of SFOA concentrations at the (a) Detling, (b) Harwell, and (c) North Kensington measurement sites, winter IOP 2012.*

5.3.3 High SFOA episode: 13-Jan–18-Jan, 2012

Time-series of hourly-average measured and modelled (Base, Base4x, and combRedist experiments) SFOA concentrations at the ClearfLo winter IOP sites are shown in Fig. 5.7, note the period of 13-Jan–18-Jan. The y-axis scales of the three panels (Figs. 5.7abc) vary greatly, especially for the Harwell measurement site. This is due to very high concentrations during this period, at this site in particular. Detling did not have measurements during these days, but North Kensington also exhibits elevated concentrations on some of these days, especially on 17-Jan. During this episode, both the Base4x and combRedist experiments simulate similar concentrations for the North

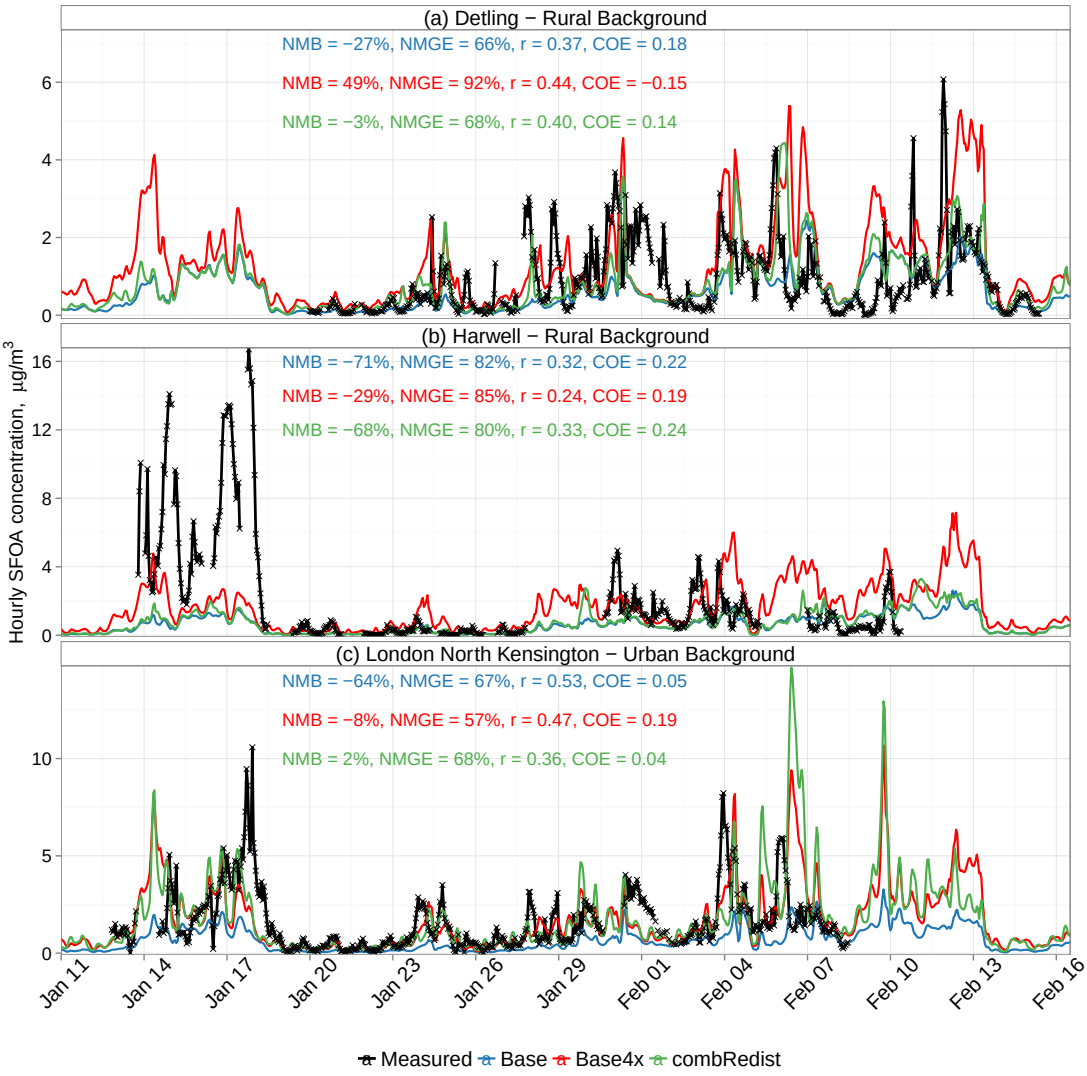

Figure 5.7 *Time-series of measured and modelled hourly average SFOA concentrations at the (a) Detling, (b) Harwell, and (c) London North Kensington measurement sites, year 2012. Note the different scales on the y-axis.*

Kensington site, whereas for Harwell, the Base4x results in higher concentrations than combRedist and is therefore slightly closer to the very high measured concentrations.

Daily-average maps of modelled SFOA surface concentrations during these days are shown in Fig. 5.8 (Base4x experiment), and Fig. 5.9 (combRedist experiment). Time-series of daily-average concentrations during the winter IOP are shown in Fig. 5.10 (using a threshold of 75% of valid hourly values to derive a daily average). It was demonstrated in Chapter 3 that a rural background site can on occasions exhibit substantially higher concentrations than central London due to atmospheric import of polluted air masses from Europe creating a strong spatial gradient. The daily-average concentration maps, however, do not indicate European gradients over Southern

England during these days. Nevertheless, these locations did experience a sustained high-pressure area during these days. Sustained high pressure usually leads to a very stable atmosphere with descending air masses. Therefore, these high concentrations could have been caused by meteorological build-up, and it is possible the model set-up underestimated the strength of this effect.

In summary, the exceptional concentrations measured at Harwell could have been caused by (i) missing local sources in the area, or (ii) over-reporting of the concentrations by AMS measurements or by the PMF analysis applied to apportion measured OA into its components, (iii) meteorological build-up, (iv) or a combination of these. Overall, however, the specific origin of the large discrepancy between model and measurements at the Harwell site during these four days remains unknown.

5.3.4 Hourly evaluation statistics during the rest of the ClearfLo winter IOP, 2012

Table 5.2 presents the hourly evaluation statistics at the Detling, Harwell, and London North Kensington sites during the winter IOP (as in Fig. 5.7) but excluding the largely unexplained high SFOA concentrations episode between 13-Jan–18-Jan. These *r*-values (0.35–0.53; range of hourly *r*-values for all three sites) are lower than the daily *r*-values shown in Figs. 5.4 and 5.5 (0.59–0.78). This is not unexpected, as based on Sect. 5.3.2 the diurnal emissions profile used for all European countries assigning equal amounts of residential combustion emissions to the morning and evening does not match the measured SFOA profiles at these three sites.

For Detling, the Base case run underestimates the mean measured SFOA concentration by -27%, the Base4x experiment results in an overestimation of $+49\%$, and the combRedist yields a close match with -3%. For Harwell, the Base scenario has a NMB of -36%, which turns into an overestimation of $+64\%$ with the Base4x experiment, whereas the combRedist emissions have a very minor effect on modelled concentrations at Harwell (NMB of -31%; the other evaluation statistics of combRedist are also close to those of the Base case run). At the North Kensington site, hourly comparison shows similar results for the two experiments as was seen in the daily evaluation as both emissions cases capture the mean concentration well, but the Base4x yields a better *r*-value than combRedist.

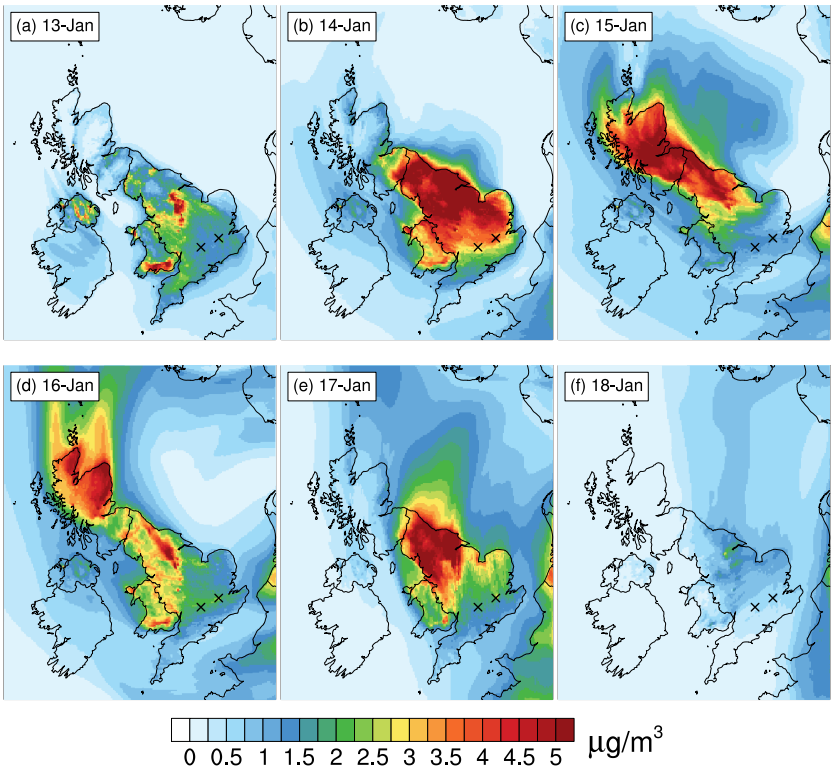

Figure 5.8 *Daily-average modelled (Base4x experiment) SFOA surface concentrations during the episode of high SFOA concentrations at the beginning of the winter IOP, year 2012. The black crosses mark the measurement site locations, left: Harwell, right: London North Kensington.*

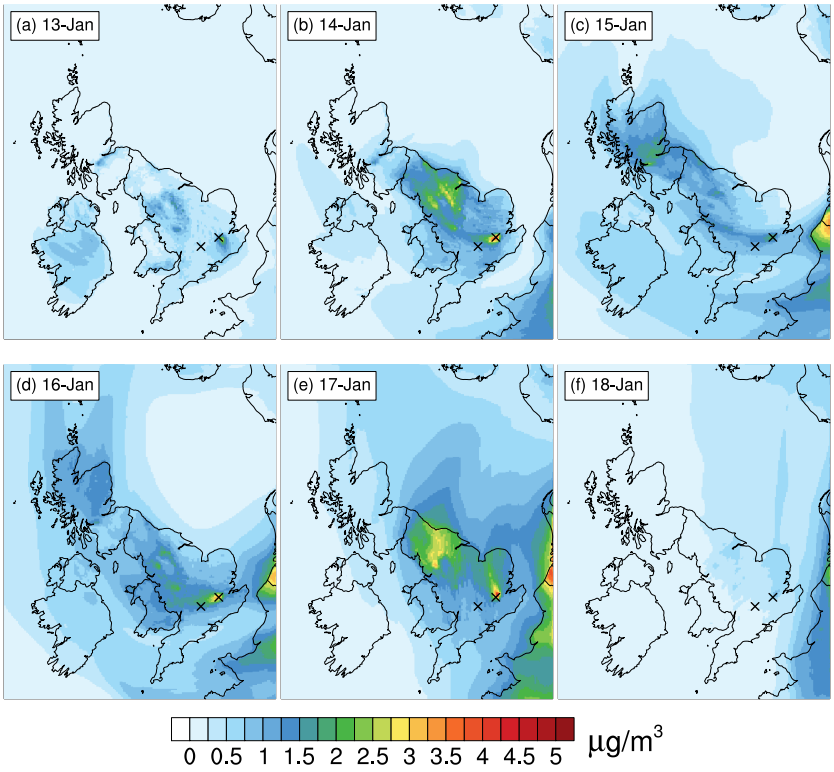

Figure 5.9 *Same as Fig. 5.8, but for the combRedist experiment.*

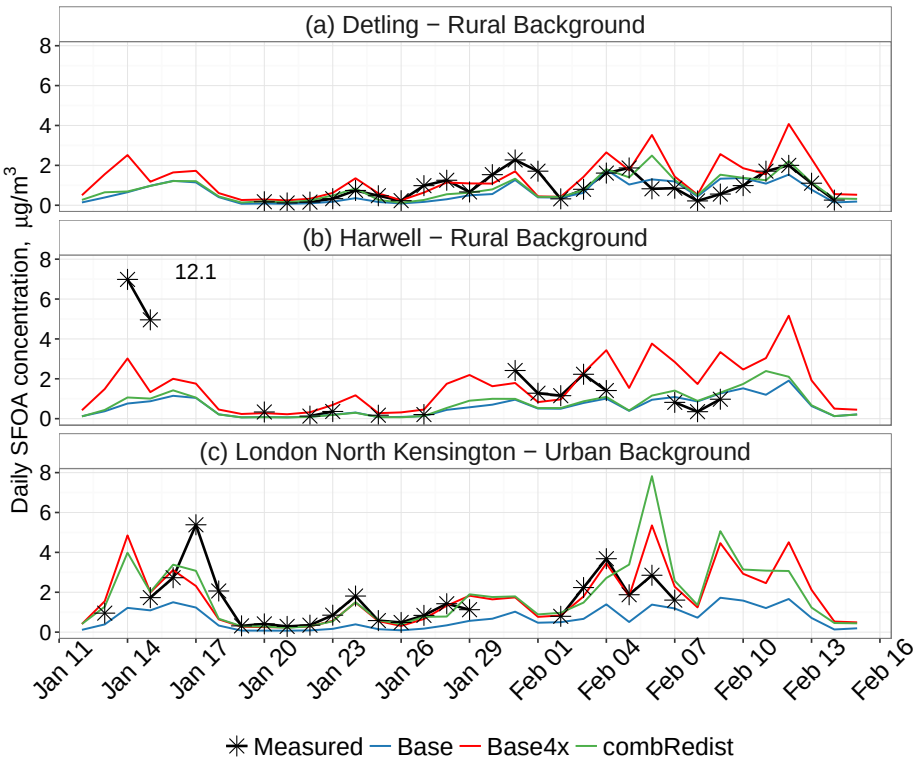

Figure 5.10 *Daily-average measured and modelled SFOA concentrations at the (a) Detling, (b) Harwell, and (c) North Kensington measurement sites, year 2012.*

Table 5.2 *Evaluation statistics for modelled vs measured hourly-average concentrations of SFOA during the ClearfLo winter IOP measurement sites as in Fig. 5.7, but excluding the period of 13-Jan–18-Jan.*

Site	Experiment	NMB	NMGE	r	COE
Detling	Base	-27%	66%	0.37	0.18
	Base4x	49%	92%	0.44	-0.15
	combRedist	-3%	68%	0.40	0.14
Harwell	Base	-36%	69%	0.43	0.18
	Base4x	64%	105%	0.42	-0.24
	combRedist	-31%	68%	0.44	0.19
North Kensington	Base	-64%	66%	0.53	0.06
	Base4x	-1%	56%	0.53	0.20
	combRedist	12%	73%	0.35	-0.04

5.3.5 Comparison of modelled EC with measured EC and BC

Site locations for the black carbon (BC) measurement network in 2012 are shown in Fig. 5.11. Three of these sites (Harwell, London North Kensington, and London Marylebone Road) also have daily-average filter measurements of elemental carbon (EC). Comparisons of the measurements of EC-R (measured EC corrected using reflectance), EC-T (corrected using transmittance), and BC are presented in Appendix C. Substantial discrepancies (at times, more than a factor of 2 for daily average concentrations) are shown even for the same instrument measuring the same pollutant with a different correction method (EC-R vs EC-T), and the direction (i.e. which one is higher, which lower) and the magnitude of discrepancies differ during different seasons or for measurement sites. Therefore, detailed (i.e. hourly or daily) model-measurement evaluation is not justified, and only seasonal-averaged concentrations - allowing for some of the reasons for these differences to cancel each other out - are presented in this section.

Seasonal-average measured concentrations of BC, EC-R, EC-T, and modelled concentrations of EC for the three sites that include different types of measurements of what is essentially the same thing are shown in Fig. 5.12. In addition to emissions from domestic heating, these concentrations also include all other EC, mainly from traffic. Note that the comparison of the pollutant levels measured at the Marylebone Road kerbside site and concentrations measured for that grid cell are not warranted, but they are included to give an indication of the range of concentrations in a megacity.

For Harwell, modelled concentrations from the Base and combRedist experiments are very similar, but the Base4x is higher (all data-sets were made to be of equal size, i.e. days with missing or with measurements below limit of detection EC-R or EC-T values were also removed from measured BC as well as the modelled time series). It was shown above that, in comparison to measured SFOA concentrations, the Base4x experiment overestimates wood and coal burning concentrations at the two rural sites near London (Harwell and Detling). Fig. 5.12 shows that the Base and combRedist modelled EC concentrations are close to measured EC-R during all seasons except autumn for which overestimations of several pollutants for many different days and periods have been presented in Chapter 3. Overall, BC measurements yield higher concentrations than measured or modelled EC, but during winter, measured BC, measured EC-R and modelled EC (Base or combRedist experiments) are a close match, whereas measured EC-T is substantially lower.

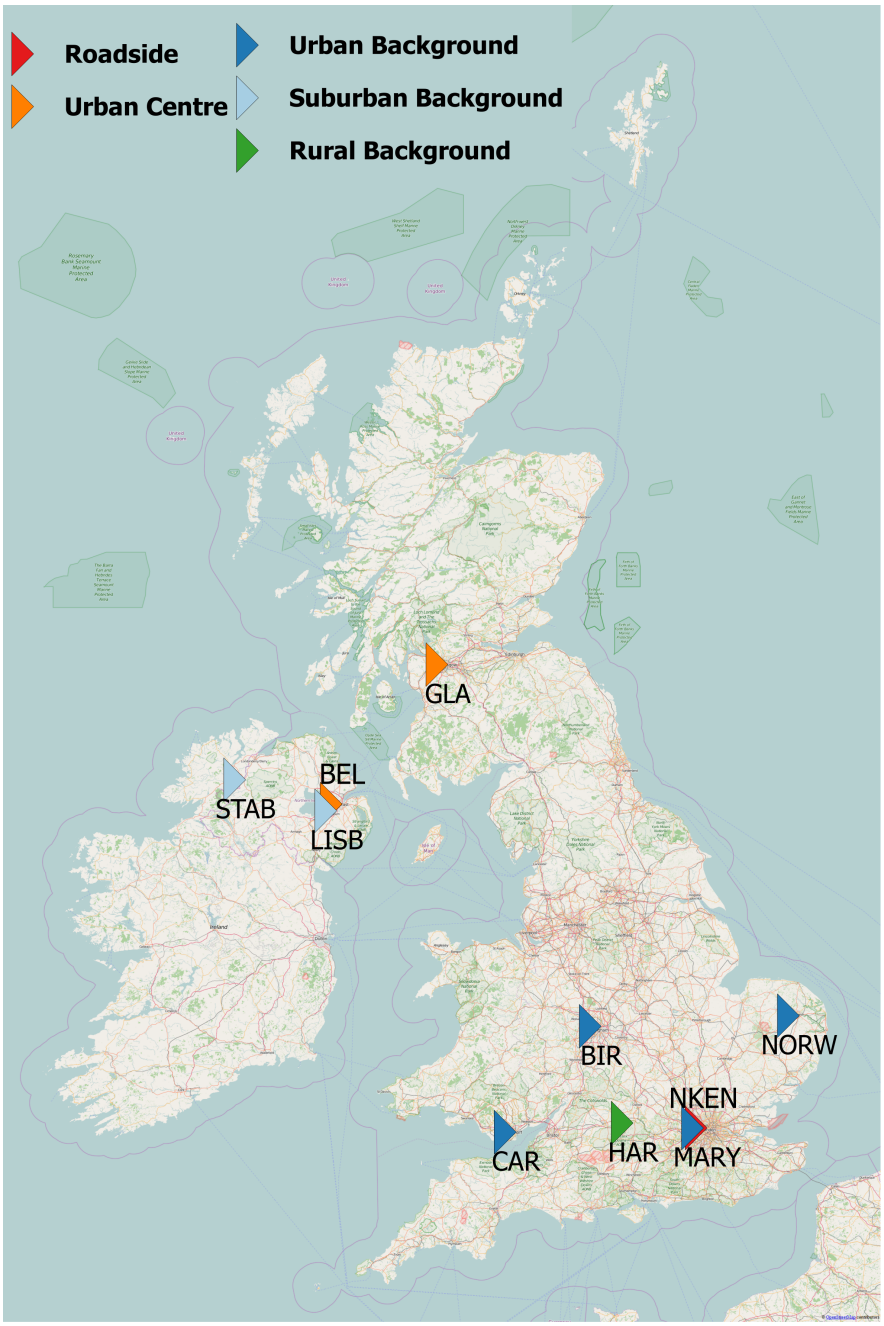

Figure 5.11 *BC-network measurement site locations in 2012. Site names are abbreviated as follows: GLA - Glasgow Centre, STAB - Strabane, BEL - Belfast Centre, LISB - Lisburn Dunmurry, BIR - Birmingham Tyburn, NORW - Norwich Lakenfields, CAR - Cardiff, HAR - Harwell, NKEN - London North Kensington, MARY - London Marylebone Road. Underlying map from © OpenStreetMap contributors.*

At North Kensington, both the Base4x and combRedist experiments result in similarly higher concentrations than the Base run, and these experiments match the measurements of EC-R well. At Marylebone Road, modelled concentrations are substantially lower than what is measured. This is expected as Marylebone Road is a roadside site

with heavy traffic flows and the concentrations captured at the measurement site are therefore much higher than a 5 km $\times$ 5 km $\times$ 40 m model grid value average.

Keeping in mind that measurements of BC are on average higher than measurements of EC-T or EC-R, seasonal-average concentrations of BC and modelled EC at all the BC network measurement sites are presented in Fig. 5.13 (Harwell, North Kensington, and Marylebone road are omitted from this plot as their BC measurements were presented in Fig. 5.12). There are no sites for which the combRedist yields a lower modelled concentration than the Base run. Therefore, based on BC measurements at these sites in different parts of the UK, the experiments conducted for the investigation of spatial distribution of residential wood and coal burning do not result in unrealistic EC concentrations. The three Northern-Irish sites (BEL, LISB, and STAB on Fig. 5.13) exhibit an even stronger seasonal cycle than the other sites (i.e. relatively greater increase for autumn and winter), possibly indicating stronger traditions of residential coal-burning.

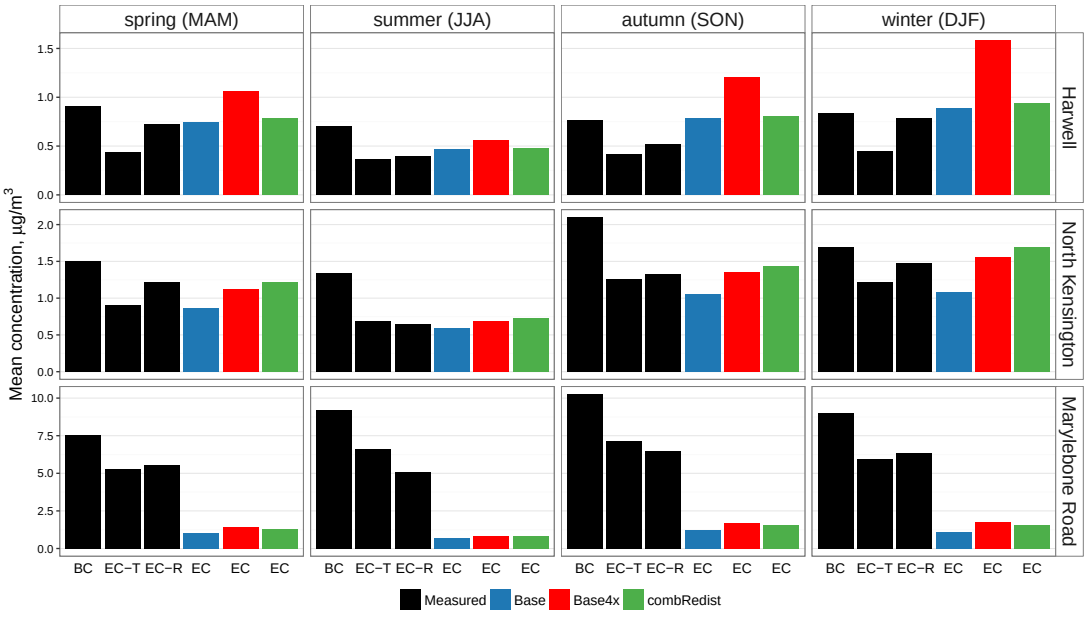

Figure 5.12 *Seasonal-average concentrations of measured BC, EC-R, EC-T, and modelled EC concentrations at the three measurement sites that measure both BC and EC, year 2012.*

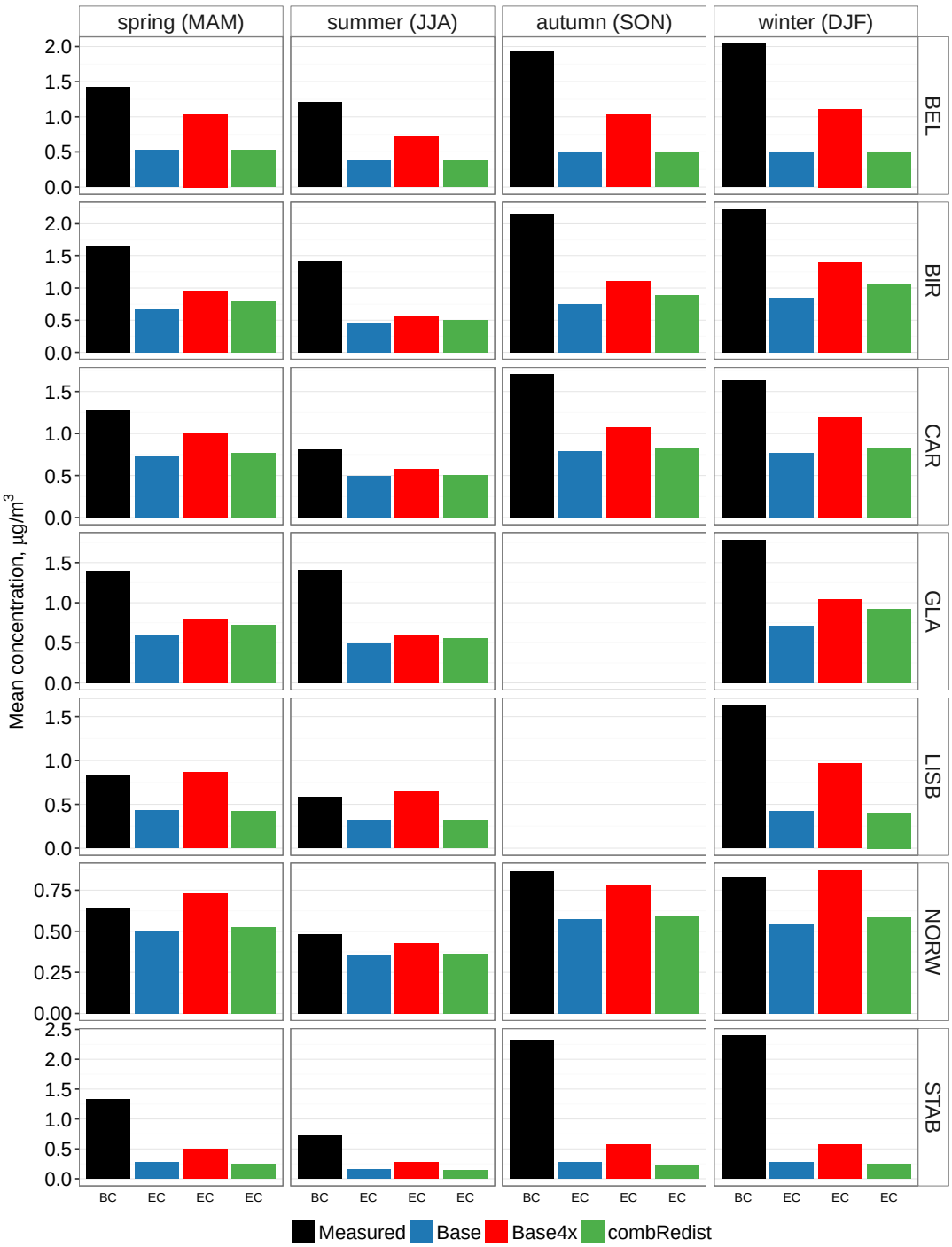

Figure 5.13 *Seasonal-average concentrations of measured BC and modelled EC concentrations at the BC-network measurement sites, year 2012. Site name abbreviations are given in Fig. 5.11.*

5.4 Conclusions

In this chapter, different assumptions for the spatial distribution and total emitted amount of PM emissions from solid fuel burning were carried out. These experiments were based on the large underestimations of SFOA concentrations that were seen in comparison with measurements using the officially reported emissions inventory (a NMB of -71% at the London North Kensington urban background site, for example). The two main scenarios considered were Base4x, and combRedist. For Base4x, officially reported $\mathrm{PM2.5}$ from the SNAP2 source sector (residential and other non-industrial combustion) were increased by a factor of 4. For the combRedist experiment, half of the emissions from SNAP2 were redistributed linearly to residential population density to comprise emissions for smoke control areas. The emission total of combRedist is the same as officially reported (equal to Base, 4 times less than in Base4x).

In comparison with AMS-PMF measurements of SFOA in and around London, it was concluded that Base4x yielded better daily and hourly correlations than the combRedist. Therefore, for certain air masses, the spatial distribution reported by the national emissions inventory is sound. The Base4x did, however, overestimate SFOA concentrations at the rural sites, whereas the combRedist captured mean measured concentrations at the different sites better. The combRedist is intentionally simplistic (i.e. exactly 50% was reassigned), but a better agreement might be, for example, Base2x + 30% redistributed to population density (or limitless combinations of Base emissions and redistribution to include emissions for smoke control areas). Furthermore, the experiments undertaken here only deal with potential discrepancies in the national atmospheric emissions inventory, but the concentrations that are measured at these sites are a result of sources, meteorology (e.g. advection), and dry and wet deposition — both of which also depend on meteorology. Therefore, future work on the modelling capabilities of SFOA concentrations should also assess, and if possible validate, the accuracy the different drivers of atmospheric pollutant concentrations.

Modelled concentrations of EC (which includes all combustion sources, not just solid fuel burning) were compared with different measurements: EC-R, EC-T, and BC. Substantial discrepancies were seen between the different measurements of this component and, therefore, detailed comparison with the model was not presented. However, based on seasonal-average concentrations at the BC network sites over the UK, it was shown that the concentrations derived from the combRedist experiments

were reasonable, and, therefore, some redistribution of SNAP2 emissions into smoke control areas appears justified.

Chapter 6

Conclusions and future work

This work examined and refined different sources of carbonaceous aerosols using the EMEP4UK modelling system, making use of state of the art measurement datasets. Although the study area was focused on pollutant concentrations over the British Isles, all of the components examined here are of great relevance to the air quality in other countries as well — in Europe and globally. Therefore, the inclusion of these improvements into other air quality models and official emissions' inventories is advised.

Notwithstanding the uncertainties in defining and measuring the carbonaceous component of particulate matter (PM), there is a general tendency for atmospheric chemical transport models to underestimate observed amounts of organic aerosol (OA). Most traditional offline filter measurements can only quantify total OC and EC concentrations (and the OC concentrations must also then be scaled to yield OA), whereas modern online measurements of OA with the Aerosol Mass Spectrometer combined with positive matrix factorization analysis (AMS-PMF), for example, have facilitated the subdivision of the OA component into empirical categories. These include:

- HOA - hydrocarbon-like organic aerosol (primary OA from fossil fuel combustion, especially from traffic sources);
- SFOA - solid-fuel organic aerosol (wood and coal burning);
- OOA - oxygenated organic aerosol (OOA, in this work referred to as secondary OA - SOA);

- COA - cooking OA (from charbroiling, or frying and deep-frying).

These measurements present an opportunity to more rigorously test model simulations of carbonaceous components and thus aid further development of PM modelling capability. The continuous year-long dataset of AMS-PMF measurements at an urban background site in London (North Kensington) is the first of its kind (for its length), and therefore, the work presented here is the first time model simulations have been compared with a full annual cycle of OA apportionment measurements. A further feature of the Clean Air for London (ClearFlo) campaign during which this dataset was collected were additional AMS-PMF datasets collected at another site in central London (Marylebone Road), and at two rural sites (Detling and Harwell) to the east and to the west of Greater London, respectively.

The motivation for this study is illustrated in Fig. 6.1 which shows the annual average measured OA component concentrations at the London North Kensington site in 2012 (the annual average measured $\mathrm{PM}_{2.5}$ at this site in 2012 was 15 $\mu\mathrm{g\,m^{-3}}$, and thus the 4 $\mu\mathrm{g\,m^{-3}}$ of OA is a substantial proportion of the $\mathrm{PM}_{2.5}$). Also shown are component concentrations simulated with the Base case experiment using current official emissions estimates, i.e. the starting point of this work. It can be seen that all simulated components were underestimated compared to measurements, and that COA is entirely missing from the emissions inventory used for this model simulation. The overall aim of this work was to investigate the model-measurement discrepancy apparent on Fig. 6.1.

6.1 Summary of the results

The first part of this work considered the SOA component. The measured annual average SOA concentration at the London North Kensington site was 1.6 $\mu\mathrm{g\,m^{-3}}$. The Base run simulated 1.1 $\mu\mathrm{g\,m^{-3}}$, but with the addition of missing SOA precursors from diesel vehicles, the new modelled mean SOA concentration is much closer to the measured value: 1.7 $\mu\mathrm{g\,m^{-3}}$ (Fig. 6.2a). Furthermore, the hourly and daily evaluation of the model-measurement comparison showed good agreement, giving confidence in the overall prediction skill of the model and set-up used. The addition was based on comprehensive measurements of volatile organic compounds (VOCs) and intermediate volatility organic compounds (IVOCs) in London during the same campaign. The amount of these missing SOA precursors was added into the model proportionally to current traffic emissions of VOCs (diesel-IVOCs = 2.3 $\times$ traffic-VOCs). This was

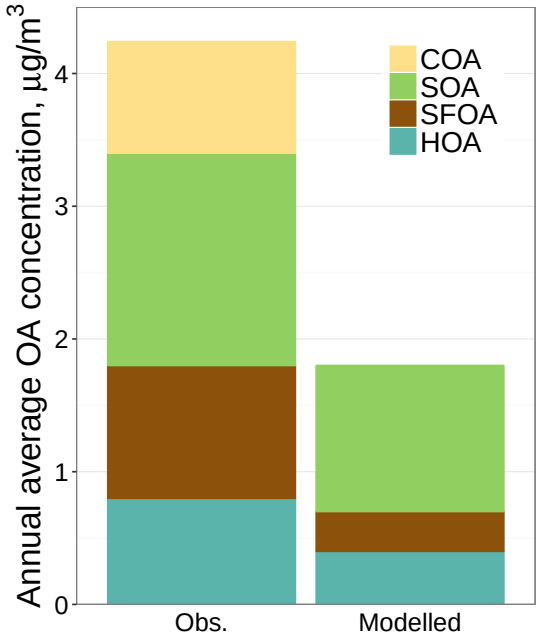

Figure 6.1 *Annual average measured (Obs.) and modelled OA component concentrations at the London North Kensington measurement site, 2012 (modelled concentrations are from the Base case experiment of Chapter 3, i.e. the starting point of this work).*

a more directly-quantitative and source-specific approach to adding these additional SOA precursors than has been undertaken in previous OA modelling studies.

During the period of concurrent measurements, SOA concentrations at the Detling rural background location east of London were greater than at the central London North Kensington location. The model shows that this was caused by an intense pollution plume with a strong gradient of imported SOA passing over the rural location. This demonstrates the value of modelling for supporting the interpretation of measurements taken at different sites or for short durations.

The model simulations show that these estimates of diesel-related IVOC could explain on average ~30% of the annual SOA in and around London. The 90-th percentile of modelled daily SOA concentrations at the urban background site for the whole year was 3.8 $\mu g\,m^{-3}$, and the influence of missing diesel-related IVOC precursors was even greater on high percentile SOA days than its contribution to annual average SOA. The magnitudes of these contributions to SOA provide strong additional support for the need to undertake further refinement of the amount and speciation of these precursor emissions for inclusion in official emissions inventories.

Secondly, the spatially and temporally resolved COA emissions developed here can contribute to closing the gap between modelled and observed concentrations of car-

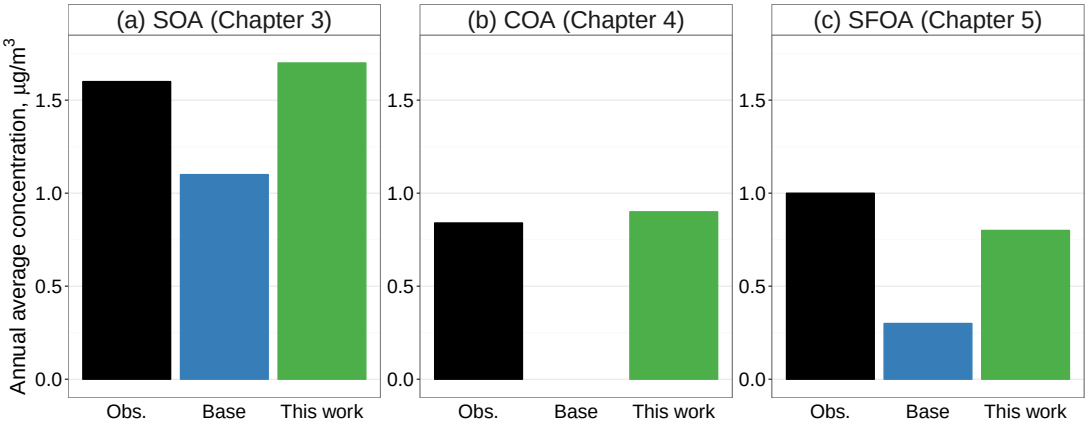

Figure 6.2 *Annual average measured and modelled OA component concentrations as in the three main chapters (London North Kensington site, 2012): (a) secondary organic aerosol (SOA) - Chapter 3, (b) cooking organic aerosol (COA) - Chapter 4, (c) solid fuel organic aerosol (SFOA) - Chapter 5.*

bonaceous aerosol and to total PM mass concentrations in urban areas (see Fig. 6.2b; annual average measured COA concentration at the London North Kensington site was 0.8 $\mu g\,m^{-3}$, modelled 0.9 $\mu g\,m^{-3}$). The final COA emission source strength of 320 $mg\,person^{-1}\,day^{-1}$, and the spatial distribution of these emissions on the basis of workday population density (as opposed to residential population density), were derived by iteration and evaluation of model-measurement comparisons of the magnitudes and diurnal profiles of COA at the two central London sites.

It is shown that in London, annual average COA concentrations are between 1–2 $\mu g\,m^{-3}$ (urban background site to urban central site). Both the measurements and modelled concentrations agree that the 95th percentile of daily averaged COA concentrations at the different locations is 2–4 $\mu g\,m^{-3}$. For three other major cities, Manchester, Leeds and Birmingham, modelled annual average concentrations of COA were between 0.5–0.7 $\mu g\,m^{-3}$, but it should be noted that the model simulates the average concentration of the 5 km $\times$ 5 km grid cells, whereas it was shown for Manchester that cities can exhibit a central hot-spot of smaller scale (1–2 km in dimension). Therefore in some urban centres the contribution might be bigger than is modelled here.

The impact of COA concentrations is spatially very limited as the modelled concentrations drop markedly outside the highly populated urban areas. For example, the simulations estimated an annual average COA concentration of 0.12 $\mu g\,m^{-3}$ for the EMEP supersite Harwell (classified as rural background), which is ~80 km west of central London. This is comparable to estimates of COA concentrations at Harwell derived from a chemical mass balance (CMB) model applied to two weeks of

measurements.

Finally, redistributing 50% of non-industrial wood and coal burning emissions to residential population density (thus over-writing, in part, the assumption made by the national emissions inventory that that only smokeless fuels are burned in smoke control areas) increased the mean modelled SFOA concentration for the London North Kensington site to 0.8 $\mu g\,m^{-3}$, from the Base run value (using the emissions' spatial distribution and total as officially reported) of just 0.3 $\mu g\,m^{-3}$. For comparison, the measured annual mean concentration of SFOA at this site was 1.0 $\mu g\,m^{-3}$ (Fig. 6.2c). Based on the model evaluation presented, redistribution of SFOA emissions into smoke control areas is justified, but further refinement of the amount, as well as the temporal emission profile of this component is necessary.

The total effect of the three refinements to modelled OA undertaken in this work, in comparison again to the measured OA at the North Kensington site, is shown in Fig. 6.3. It can be seen that this work has provided insight into the nature and magnitude of missing, under-represented, and spatially inappropriately-distributed emissions of primary OA and OA precursors compared with the official emissions used in the Base case simulation at the start of this work.

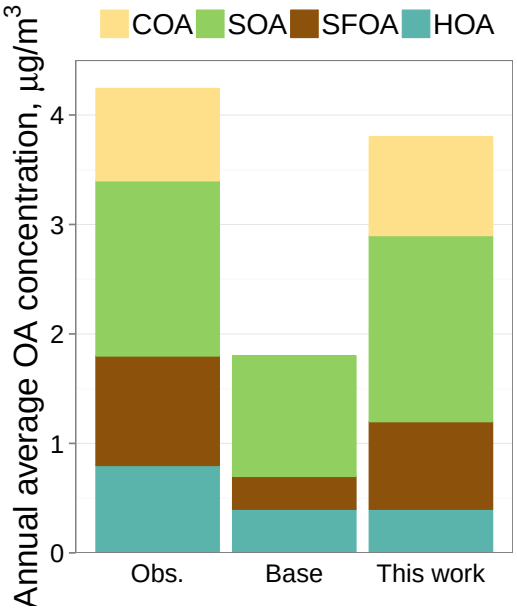

Figure 6.3 *Annual average measured (Obs.) and modelled OA component concentrations at the London North Kensington site, 2012. Separate figures of the components changed in this study were given in Fig. 6.2.*

6.2 Future work

There are several aspects of the emissions, and the description of evolution and secondary formation of carbonaceous PM in atmospheric chemical transport models that remain subject to improvement. First and foremost is the volatility distribution of primary emissions. Following the paper by Robinson et al. (2007), tens of modelling studies have highlighted the severe uncertainties associated with the volatility distribution currently used (as in Sect. 3.3.6). More measurements, both laboratory and ambient, are needed to better quantify and describe the organic component with its various different sources.

Second, the atmospheric ageing rates that reduce the volatility of semivolatile compounds used in different studies can differ by a factor of 10. Furthermore, a 1-D volatility basis set (VBS) approach for simulating SOA production from precursors, ageing, and gas-aerosol partitioning of semivolatile species only works in the direction of reducing volatility. In reality, some highly oxygenated species might fragment, thus becoming more volatile again. The 2-D VBS framework, which allows for fragmentation (Donahue et al., 2012), has not yet been implemented in any chemical transport model due to its computational costs, as well as further uncertainties in the additional input data required for this more complex system (e.g. the oxygen to carbon ratio of each VOC degradation pathway).

Now that the modelled concentrations of OA are comparable to the observations (Fig. 6.3), a logical continuation of this work would be to use the model for estimating the relative impacts of specific countries, regions, or cities on the carbonaceous component of PM air quality. Furthermore, with the model, simulated maps of hourly PM component concentrations are available for the whole modelling domain, not just for measurement site locations (or for short periods of measurement campaigns). For example, Fig. 6.4 shows daily-average SFOA concentrations emitted from different regions in Europe for an arbitrary day. In the set-up used here where primary OA was treated as a non-volatile chemically inert species, it is possible to trace its emissions from different countries within a single model run. For more complex, chemically active pollutants, such as SOA, several sensitivity runs with altered emission sources could be conducted for the assessment of different contributions to the total SOA budget.

However, all of the experiments undertaken in this thesis only deal with problems with the emissions, but atmospheric concentrations are a result of sources, meteorology,

and removal processes. Therefore, future work on air quality modelling should also attempt to refine the accuracy of all the different drivers of atmospheric pollutant concentrations. This would also lead to more accurate estimations of pollutant lifetimes and budget calculations that are necessary for mitigation strategies.

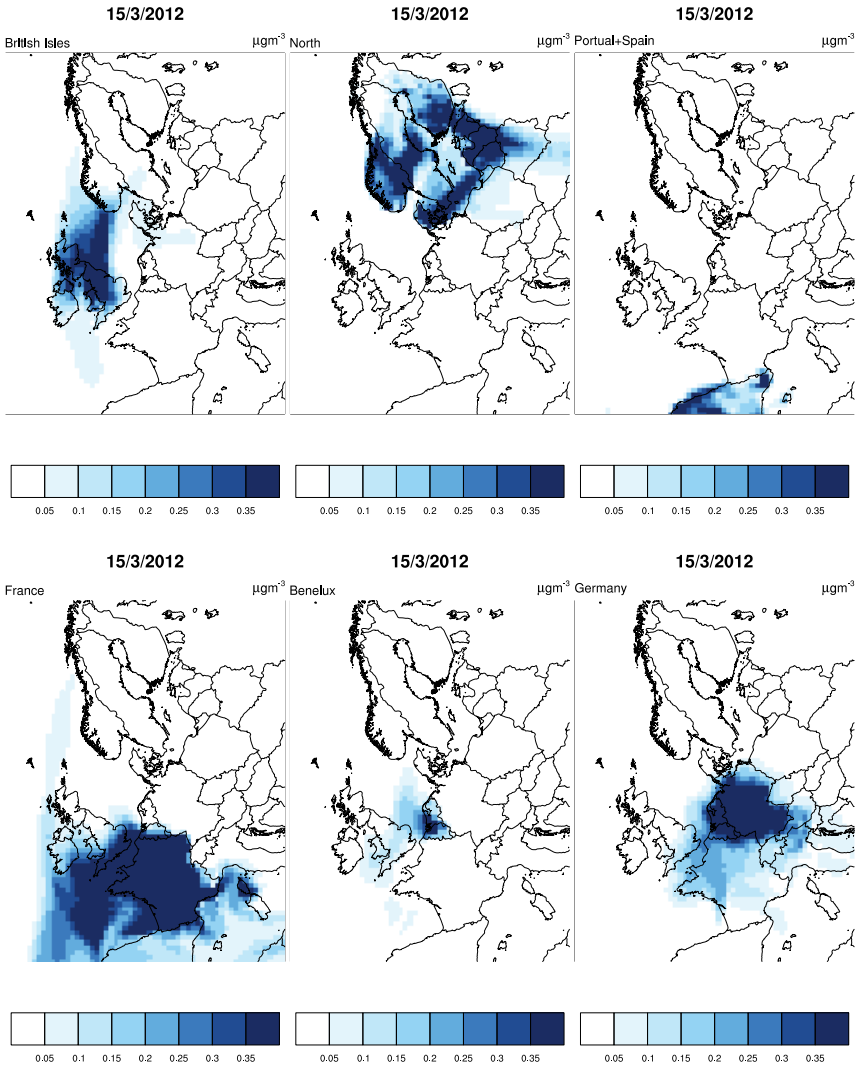

Figure 6.4 *Daily-average modelled surface concentrations of SFOA from the different regions named at the top of each panel.*

References

Aiken, A. C., DeCarlo, P. F., Kroll, J. H., Worsnop, D. R., Huffman, J. A., Docherty, K. S., Ulbrich, I. M., Mohr, C., Kimmel, J. R., Sueper, D., Sun, Y., Zhang, Q., Trimborn, A., Northway, M., Ziemann, P. J., Canagaratna, M. R., Onasch, T. B., Alfarra, M. R., Prevot, A. S. H., Dommen, J., Duplissy, J., Metzger, A., Baltensperger, U., and Jimenez, J. L. (2008). O/C and OM/OC ratios of primary, secondary, and ambient organic aerosols with High-Resolution Time-of-Flight aerosol mass spectrometry. *Environmental Science & Technology*, 42(12):4478–4485.

Aksoyoglu, S., Keller, J., Barmpadimos, I., Oderbolz, D., Lanz, V. A., Prévôt, A. S. H., and Baltensperger, U. (2011). Aerosol modelling in europe with a focus on switzerland during summer and winter episodes. *Atmos. Chem. Phys.*, 11(14):7355–7373.

Allan, J. D., Williams, P. I., Morgan, W. T., Martin, C. L., Flynn, M. J., Lee, J., Nemitz, E., Phillips, G. J., Gallagher, M. W., and Coe, H. (2010). Contributions from transport, solid fuel burning and cooking to primary organic aerosols in two UK cities. *Atmos. Chem. Phys.*, 10(2):647–668.

Andreae, M. O. and Rosenfeld, D. (2008). Aerosol–cloud–precipitation interactions. part 1. the nature and sources of cloud-active aerosols. *Earth-Science Reviews*, 89:13–41.

Andreas, E. L. (1998). A new sea spray generation function for wind speeds up to 32 m/s. *Journal of Physical Oceanography*, 28(11):2175–2184.

Atkinson, R. and Arey, J. (2003). Atmospheric degradation of volatile organic compounds. *Chemical Reviews*, 103(12):4605–4638.

Bahreini, R., Middlebrook, A. M., de Gouw, J. A., Warneke, C., Trainer, M., Brock, C. A., Stark, H., Brown, S. S., Dube, W. P., Gilman, J. B., Hall, K., Holloway,

J. S., Kuster, W. C., Perring, A. E., Prevot, A. S. H., Schwarz, J. P., Spackman, J. R., Szidat, S., Wagner, N. L., Weber, R. J., Zotter, P., and Parrish, D. D. (2012). Gasoline emissions dominate over diesel in formation of secondary organic aerosol mass. *Geophysical Research Letters*, 39(6):L06805.

Begue, N., Tulet, P., Chaboureau, J. P., Roberts, G., Gomes, L., and Mallet, M. (2012). Long-range transport of saharan dust over northwestern europe during EUCAARI 2008 campaign: Evolution of dust optical properties by scavenging. *Journal of Geophysical Research-Atmospheres*, 117.

Bergström, R. (2015). *Carbonaceous Aerosol in Europe Out of the Woods and into the Blue?* PhD thesis, University of Gothenburgh.

Bergström, R., Denier van der Gon, H. A. C., Prévôt, A. S., Yttri, K. E., and Simpson, D. (2012). Modelling of organic aerosols over Europe (2002-2007) using a volatility basis set (VBS) framework: application of different assumptions regarding the formation of secondary organic aerosol. *Atmos. Chem. Phys.*, 12:8499–8527.

Bergström, R., Hallquist, M., Simpson, D., Wildt, J., and Mentel, T. F. (2014). Biotic stress: a significant contributor to organic aerosol in europe? *Atmos. Chem. Phys.*, 14(24):13643–13660.

Blanchard, D. C. and Woodcock, A. H. (1957). Bubble formation and modification in the sea and its meteorological significance. *Tellus*, 9:145–158.

Bohnenstengel, S. I., Belcher, S. E., Aiken, A., Allan, J. D., Allen, G., Bacak, A., Bannan, T. J., Barlow, J. F., Beddows, D. C. S., Bloss, W. J., Booth, A. M., Chemel, C., Coceal, O., Di Marco, C. F., Dubey, M. K., Faloon, K. H., Fleming, Z. L., Furger, M., Gietl, J. K., Graves, R. R., Green, D. C., Grimmond, C. S. B., Halios, C. H., Hamilton, J. F., Harrison, R. M., Heal, M. R., Heard, D. E., Helfter, C., Herndon, S. C., Holmes, R. E., Hopkins, J. R., Jones, A. M., Kelly, F. J., Kotthaus, S., Langford, B., Lee, J. D., Leigh, R. J., Lewis, A. C., Lidster, R. T., Lopez-Hilfiker, F. D., McQuaid, J. B., Mohr, C., Monks, P. S., Nemitz, E., Ng, N. L., Percival, C. J., Prévôt, A. S. H., Ricketts, H. M. A., Sokhi, R., Stone, D., Thornton, J. A., Tremper, A. H., Valach, A. C., Visser, S., Whalley, L. K., Williams, L. R., Xu, L., Young, D. E., and Zotter, P. (2014). Meteorology, air quality, and health in london: The ClearfLo project. *Bulletin of the American Meteorological Society*, 96(5):779–804.

Cames, M. and Helmers, E. (2013). Critical evaluation of the european diesel car boom - global comparison, environmental effects and various national strategies. *Environmental Sciences Europe*, 25(1):15.

Canagaratna, M. R., Jayne, J., Jimenez, J., Allan, J., Alfarra, M., Zhang, Q., Onasch, T., Drewnick, F., Coe, H., Middlebrook, A., Delia, A., Williams, L., Trimborn, A., Northway, M., DeCarlo, P., Kolb, C., Davidovits, P., and Worsnop, D. (2007). Chemical and microphysical characterization of ambient aerosols with the aerodyne aerosol mass spectrometer. *Mass Spectrometry Reviews*, 26(2):185–222.

Canagaratna, M. R., Jimenez, J. L., Kroll, J. H., Chen, Q., Kessler, S. H., Massoli, P., Hildebrandt Ruiz, L., Fortner, E., Williams, L. R., Wilson, K. R., Surratt, J. D., Donahue, N. M., Jayne, J. T., and Worsnop, D. R. (2015). Elemental ratio measurements of organic compounds using aerosol mass spectrometry: characterization, improved calibration, and implications. *Atmos. Chem. Phys.*, 15(1):253–272.

Carslaw, D. C. and Beevers, S. D. (2013). Characterising and understanding emission sources using bivariate polar plots and k-means clustering. *Environmental Modelling & Software*, 40:325–329.

CEIP (2015). WebDab EMEP database: Emissions as used in EMEP models. http://www.ceip.at/ms/ceip_home1/ceip_home/webdab_emepdatabase/. Emis. data downloaded on 15.07.2015.

Chhabra, P. S., Flagan, R. C., and Seinfeld, J. H. (2010). Elemental analysis of chamber organic aerosol using an aerodyne high-resolution aerosol mass spectrometer. *Atmos. Chem. Phys.*, 10(9):4111–4131.

Chow, J. C., Watson, J. G., Chen, L. A., Arnott, W. P., Moosmüller, H., and Fung, K. (2004). Equivalence of elemental carbon by Thermal/Optical reflectance and transmittance with different temperature protocols. *Environmental Science & Technology*, 38(16):4414–4422.

Crilley, L. R., Bloss, W. J., Yin, J., Beddows, D. C. S., Harrison, R. M., Allan, J. D., Young, D. E., Flynn, M., Williams, P., Zotter, P., Prevot, A. S. H., Heal, M. R., Barlow, J. F., Halios, C. H., Lee, J. D., Szidat, S., and Mohr, C. (2015). Sources and contributions of wood smoke during winter in london: assessing local and regional influences. *Atmos. Chem. Phys.*, 15(6):3149–3171.

Crippa, M., Canonaco, F., Slowik, J. G., El Haddad, I., DeCarlo, P. F., Mohr, C., Heringa, M. F., Chirico, R., Marchand, N., Temime-Roussel, B., Abidi, E., Poulain, L., Wiedensohler, A., Baltensperger, U., and Prévôt, A. S. H. (2013a). Primary and secondary organic aerosol origin by combined gas-particle phase source apportionment. *Atmos. Chem. Phys.*, 13(16):8411–8426.

Crippa, M., DeCarlo, P. F., Slowik, J. G., Mohr, C., Heringa, M. F., Chirico, R., Poulain, L., Freutel, F., Sciare, J., Cozic, J., Di Marco, C. F., Elsasser, M., Nicolas, J. B., Marchand, N., Abidi, E., Wiedensohler, A., Drewnick, F., Schneider, J., Borrmann, S., Nemitz, E., Zimmermann, R., Jaffrezo, J., Prévôt, A. S. H., and Baltensperger, U. (2013b). Wintertime aerosol chemical composition and source apportionment of the organic fraction in the metropolitan area of paris. *Atmos. Chem. Phys.*, 13(2):961–981.

DeCarlo, P. F., Kimmel, J. R., Trimborn, A., Northway, M. J., Jayne, J. T., Aiken, A. C., Gonin, M., Fuhrer, K., Horvath, T., Docherty, K. S., Worsnop, D. R., and Jimenez, J. L. (2006). Field-Deployable, High-Resolution, Time-of-Flight aerosol mass spectrometer. *Analytical Chemistry*, 78(24):8281–8289.

Denier van der Gon, H. A. C., Bergström, R., Fountoukis, C., Johansson, C., Pandis, S. N., Simpson, D., and Visschedijk, A. J. H. (2015). Particulate emissions from residential wood combustion in europe – revised estimates and an evaluation. *Atmos. Chem. Phys.*, 15(11):6503–6519.

Detournay, A., Nemitz, E., Di Marco, C. F., and et al. (2015). A 1-year study of submicron aerosol composition at a kerbside location in london. *In Preparation*.

Di Marco, C. F., Nemitz, E., and et al. (2015). Chemical characterisation of the aerosol at a background site in southern england with emphasis on the organic fraction and nitrogen compounds. *In Preparation*.

Donahue, N. M., Kroll, J. H., Pandis, S. N., and Robinson, A. L. (2012). A two-dimensional volatility basis set – part 2: Diagnostics of organic-aerosol evolution. *Atmos. Chem. Phys.*, 12(2):615–634.

Donahue, N. M., Robinson, A. L., and Pandis, S. N. (2009). Atmospheric organic particulate matter: From smoke to secondary organic aerosol. *Atmospheric Environment*, 43:94–106.

Donahue, N. M., Robinson, A. L., Stanier, C. O., and Pandis, S. N. (2006). Coupled partitioning, dilution, and chemical aging of semivolatile organics. *Environmental Science & Technology*, 40:2635–2643.

Dunmore, R. E., Hopkins, J. R., Lidster, R. T., Lee, J. D., Evans, M. J., Rickard, A. R., Lewis, A. C., and Hamilton, J. F. (2015). Diesel-related hydrocarbons can dominate gas phase reactive carbon in megacities. *Atmos. Chem. Phys.*, 15(17):9983–9996.

EEA (2013). EMEP/EEA air pollutant emission inventory guidebook - 2013. http://www.eea.europa.eu/publications/emep-eea-guidebook-2013.

EEA, E. E. A. (2010). Dieselisation in the european economic area. Technical report.

Entec (2010). UK ship emissions inventory, final report. Technical report. Crown copyright.

Exxon Mobil (2014). The outlook for energy: A view to 2040. Technical report, Exxon Mobil Corporation, Texas.

Fecan, F., Marticorena, B., and Bergametti, G. (1999). Parametrization of the increase of the aeolian erosion threshold wind friction velocity due to soil moisture for arid and semi-arid areas. *Annales Geophysicae-Atmospheres Hydrospheres and Space Sciences*, 17:149–157.

for National Statistics, U. O. (2012). Overseas travel and tourism - monthly release, august 2012. Technical report.

Fountoukis, C., Megaritis, A. G., Skyllakou, K., Charalampidis, P. E., Denier van der Gon, H. A. C., Crippa, M., Prévôt, A. S. H., Fachinger, F., Wiedensohler, A., Pilinis, C., and Pandis, S. N. (2016). Simulating the formation of carbonaceous aerosol in a european megacity (Paris) during the MEGAPOLI summer and winter campaigns. *Atmos. Chem. Phys.*, 16(6):3727–3741.

Fountoukis, C., Megaritis, A. G., Skyllakou, K., Charalampidis, P. E., Pilinis, C., Denier van der Gon, H. A. C., Crippa, M., Canonaco, F., Mohr, C., Prévôt, A. S. H., Allan, J. D., Poulain, L., Petäjä, T., Tiitta, P., Carbone, S., Kiendler-Scharr, A., Nemitz, E., O'Dowd, C., Swietlicki, E., and Pandis, S. N. (2014). Organic aerosol concentration and composition over europe: insights from comparison of regional model predictions with aerosol mass spectrometer factor analysis. *Atmos. Chem. Phys.*, 14(17):9061–9076.

Fountoukis, C., Racherla, P. N., Denier van der Gon, H. A. C., Polymeneas, P., Charalampidis, P. E., Pilinis, C., Wiedensohler, A., Dall'Osto, M., O'Dowd, C., and Pandis, S. N. (2011). Evaluation of a three-dimensional chemical transport model (PMCAMx) in the european domain during the EUCAARI may 2008 campaign. *Atmos. Chem. Phys.*, 11(20):10331–10347.

Fuller, G. W., Sciare, J., Lutz, M., Moukhtar, S., and Wagener, S. (2013). New directions: Time to tackle urban wood burning? *Atmospheric Environment*, 68:295–296.

Fuller, G. W., Tremper, A. H., Baker, T. D., Yttri, K. E., and Butterfield, D. (2014). Contribution of wood burning to PM10 in london. *Atmospheric Environment*, 87:87–94.

Genberg, J., Hyder, M., Stenström, K., Bergström, R., Simpson, D., Fors, E. O., Jönsson, J. r., and Swietlicki, E. (2011). Source apportionment of carbonaceous aerosol in southern sweden. *Atmos. Chem. Phys.*, 11(22):11387–11400.

Gentner, D. R., Isaacman, G., Worton, D. R., Chan, A. W. H., Dallmann, T. R., Davis, L., Liu, S., Day, D. A., Russell, L. M., Wilson, K. R., Weber, R., Guha, A., Harley, R. A., and Goldstein, A. H. (2012). Elucidating secondary organic aerosol from diesel and gasoline vehicles through detailed characterization of organic carbon emissions. *Proceedings of the National Academy of Sciences*, 109(45):18318–18323. PMID: 23091031.

Goldstein, A. H. and Galbally, I. E. (2007). Known and unexplored organic constituents in the earth's atmosphere. *Environmental Science & Technology*, 41(5):1514–1521.

Grieshop, A. P., Logue, J. M., Donahue, N. M., and Robinson, A. L. (2009). Laboratory investigation of photochemical oxidation of organic aerosol from wood fires 1: measurement and simulation of organic aerosol evolution. *Atmos. Chem. Phys.*, 9(4):1263–1277.

Harrison, R. M. and Yin, J. (2008). Sources and processes affecting carbonaceous aerosol in central england. *Atmospheric Environment*, 42(7):1413–1423.

Hayes, P. L., Ortega, A. M., Cubison, M. J., Froyd, K. D., Zhao, Y., Cliff, S. S., Hu, W. W., Toohey, D. W., Flynn, J. H., Lefer, B. L., Grossberg, N., Alvarez, S., Rappenglück, B., Taylor, J. W., Allan, J. D., Holloway, J. S., Gilman, J. B., Kuster, W. C., de Gouw, J. A., Massoli, P., Zhang, X., Liu, J., Weber, R. J., Corrigan, A. L., Russell, L. M., Isaacman, G., Worton, D. R., Kreisberg, N. M., Goldstein, A. H., Thalman, R., Waxman, E. M., Volkamer, R., Lin, Y. H., Surratt, J. D., Kleindienst, T. E., Offenberg, J. H., Dusanter, S., Griffith, S., Stevens, P. S., Brioude, J., Angevine, W. M., and Jimenez, J. L. (2013). Organic aerosol composition and sources in pasadena, california, during the 2010 CalNex campaign. *Journal of Geophysical Research: Atmospheres*, 118(16):9233–9257.

Heal, M. R., Kumar, P., and Harrison, R. M. (2012). Particles, air quality, policy and health. *Chemical Society Reviews*, 41:6606–6630.

Heal, M. R. and Quincey, P. (2012). The relationship between black carbon concentration and black smoke: A more general approach. *Atmospheric Environment*, 54:538–544.

Hildemann, L. M., Markowski, G. R., Jones, M. C., and Cass, G. R. (1991). Submicrometer aerosol mass distributions of emissions from boilers, fireplaces, automobiles, diesel trucks, and Meat-Cooking operations. *Aerosol Science and Technology*, 14(1):138–152.

Hinds, W. C. (1999). *Aerosol technology : properties, behavior, and measurement of airborne particles*. Wiley.

Hodzic, A., Jimenez, J. L., Madronich, S., Canagaratna, M. R., DeCarlo, P. F., Kleinman, L., and Fast, J. (2010). Modeling organic aerosols in a megacity: potential contribution of semi-volatile and intermediate volatility primary organic compounds to secondary organic aerosol formation. *Atmos. Chem. Phys.*, 10(12):5491–5514.

Hodzic, A., Kasibhatla, P. S., Jo, D. S., Cappa, C. D., Jimenez, J. L., Madronich, S., and Park, R. J. (2016). Rethinking the global secondary organic aerosol (SOA) budget: stronger production, faster removal, shorter lifetime. *Atmospheric Chemistry and Physics*, 16(12):7917–7941.

Jathar, S. H., Farina, S. C., Robinson, A. L., and Adams, P. J. (2011). The influence of semi-volatile and reactive primary emissions on the abundance and properties of global organic aerosol. *Atmos. Chem. Phys.*, 11(15):7727–7746.

Jathar, S. H., Gordon, T. D., Hennigan, C. J., Pye, H. O. T., Pouliot, G., Adams, P. J., Donahue, N. M., and Robinson, A. L. (2014). Unspeciated organic emissions from combustion sources and their influence on the secondary organic aerosol budget in the united states. *Proceedings of the National Academy of Sciences*, 111(29):10473–10478. PMID: 25002466.

Jayne, J. T., Leard, D. C., Zhang, X., Davidovits, P., Smith, K. A., Kolb, C. E., and Worsnop, D. R. (2000). Development of an aerosol mass spectrometer for size and composition analysis of submicron particles. *Aerosol Science and Technology*, 33(1-2):49–70.

Koo, B., Knipping, E., and Yarwood, G. (2014). 1.5-Dimensional volatility basis set approach for modeling organic aerosol in CAMx and CMAQ. *Atmospheric Environment*, 95:158–164.

Kroll, J. H. and Seinfeld, J. H. (2008). Chemistry of secondary organic aerosol: Formation and evolution of low-volatility organics in the atmosphere. *Atmospheric Environment*, 42:3593–3624.

Kuenen, J. J. P., Visschedijk, A. J. H., Jozwicka, M., and Denier van der Gon, H. A. C. (2014). TNO-MACC_II emission inventory; a multi-year (2003–2009) consistent high-resolution european emission inventory for air quality modelling. *Atmos. Chem. Phys.*, 14(20):10963–10976.

Laj, P., Klausen, J., Bilde, M., Plaß-Duelmer, C., Pappalardo, G., Clerbaux, C., Baltensperger, U., Hjorth, J., Simpson, D., Reimann, S., Coheur, P. F., Richter, A., De Mazière, M., Rudich, Y., McFiggans, G., Torseth, K., Wiedensohler, A., Morin, S., Schulz, M., Allan, J. D., Attié, J. L., Barnes, I., Birmili, W., Cammas, J. P., Dommen, J., Dorn, H. P., Fowler, D., Fuzzi, S., Glasius, M., Granier, C., Hermann, M., Isaksen, I. S. A., Kinne, S., Koren, I., Madonna, F., Maione, M., Massling, A., Moehler, O., Mona, L., Monks, P. S., Müller, D., Müller, T., Orphal, J., Peuch, V. H., Stratmann, F., Tanré, D., Tyndall, G., Abo Riziq, A., Van Roozendael, M., Villani, P., Wehner, B., Wex, H., and Zardini, A. A. (2009). Measuring atmospheric composition change. *Atmospheric Environment*, 43(33):5351–5414.

Lane, T. E., Donahue, N. M., and Pandis, S. N. (2008). Simulating secondary organic aerosol formation using the volatility basis-set approach in a chemical transport model. *Atmospheric Environment*, 42(32):7439–7451.

Lanz, V. A., Prévôt, A. S. H., Alfarra, M. R., Weimer, S., Mohr, C., DeCarlo, P. F., Gianini, M. F. D., Hueglin, C., Schneider, J., Favez, O., D'Anna, B., George, C., and Baltensperger, U. (2010). Characterization of aerosol chemical composition with aerosol mass spectrometry in central europe: an overview. *Atmos. Chem. Phys.*, 10(21):10453–10471.

Lefebvre, W., Fierens, F., Vanpoucke, C., Renders, N., Jespers, K., Vercauteren, J., Deutsch, F., and Janssen, S. (2016). The effect of wood burning on particulate matter concentrations in flanders, belgium. In Steyn, D. G. and Chaumerliac, N., editors, *Air Pollution Modeling and its Application XXIV*, Springer Proceedings in Complexity, pages 459–464. Springer International Publishing. DOI: 10.1007/978-3-319-24478-5_73.

Legates, D. R. and McCabe, G. J. (2013). A refined index of model performance: a rejoinder. *International Journal of Climatology*, 33(4):1053–1056.

Lelieveld, J., Gromov, S., Pozzer, A., and Taraborrelli, D. (2016). Global tropospheric hydroxyl distribution, budget and reactivity. *Atmospheric Chemistry and Physics*, 16(19):12477–12493.

Lide, D. R. and Weast, R. C. (1993). *CRC handbook of chemistry and physics*. CRC Press.

Lin, G., Sillman, S., Penner, J. E., and Ito, A. (2014). Global modeling of SOA: the use of different mechanisms for aqueous-phase formation. *Atmos. Chem. Phys.*, 14(11):5451–5475.

Marticorena, B. and Bergametti, G. (1995). Modeling the atmospheric dust cycle .1. design of a Soil-Derived dust emission scheme. *Journal of Geophysical Research-Atmospheres*, 100:16415–16430.

Menut, L., Goussebaile, A., Bessagnet, B., Khvorostiyanov, D., and Ung, A. (2012). Impact of realistic hourly emissions profiles on air pollutants concentrations modelled with CHIMERE. *Atmospheric Environment*, 49:233–244.

Met Office (2012). Met Office integrated data archive system (MIDAS) land and marine surface stations data (1853-current). Technical report, NCAS British Atmospheric Data Centre.

Middlebrook, A. M., Bahreini, R., Jimenez, J. L., and Canagaratna, M. R. (2012). Evaluation of Composition-Dependent collection efficiencies for the aerodyne aerosol mass spectrometer using field data. *Aerosol Science and Technology*, 46(3):258–271.

Miller, M. R., McLean, S. G., Duffin, R., Lawal, A. O., Araujo, J. A., Shaw, C. A., Mills, N. L., Donaldson, K., Newby, D. E., and Hadoke, P. W. (2013). Diesel exhaust particulate increases the size and complexity of lesions in atherosclerotic mice. *Particle and Fibre Toxicology*, 10:61.

Mohr, C., DeCarlo, P. F., Heringa, M. F., Chirico, R., Slowik, J. G., Richter, R., Reche, C., Alastuey, A., Querol, X., Seco, R., Peñuelas, J., Jiménez, J. L., Crippa, M., Zimmermann, R., Baltensperger, U., and Prévôt, A. S. H. (2012). Identification and quantification of organic aerosol from cooking and other sources in barcelona using aerosol mass spectrometer data. *Atmos. Chem. Phys.*, 12(4):1649–1665.

Murphy, B. N. and Pandis, S. N. (2009). Simulating the formation of semivolatile primary and secondary organic aerosol in a regional chemical transport model. *Environmental Science & Technology*, 43:4722–4728.

NAEI (2013). UK emission mapping methodology 2009.

NCAR (2008). A description of the advanced research WRF version 3. Technical report.

NCEP (2000). *NCEP FNL Operational Model Global Tropospheric Analyses, continuing from July 1999*. Research Data Archive at the National Center for Atmospheric Research, Computational and Information Systems Laboratory, Boulder CO.

Ng, N. L., Canagaratna, M. R., Jimenez, J. L., Zhang, Q., Ulbrich, I. M., and Worsnop, D. R. (2011). Real-Time methods for estimating organic component mass concentrations from aerosol mass spectrometer data. *Environmental Science & Technology*, 45(3):910–916.

Ng, N. L., Canagaratna, M. R., Zhang, Q., Jimenez, J. L., Tian, J., Ulbrich, I. M., Kroll, J. H., Docherty, K. S., Chhabra, P. S., Bahreini, R., Murphhy, S. M., Seinfeld, J. H., Hildebrandt, L., Donahue, N. M., DeCarlo, P. F., Lanz, V. A., Prévôt, A. S. H., Dinar, E., Rudich, Y., and Worsnop, D. R. (2010). Organic aerosol components observed in northern hemispheric datasets from aerosol mass spectrometry. *Atmos. Chem. Phys.*, 10(10):4625–4641.

Odum, J. R., Hoffmann, T., Bowman, F., Collins, D., Flagan, R. C., and Seinfeld, J. H. (1996). Gas/Particle partitioning and secondary organic aerosol yields. *Environmental Science & Technology*, 30(8):2580–2585.

Ots, R., Young, D. E., Vieno, M., Xu, L., Dunmore, R. E., Allan, J. D., Coe, H., Williams, L. R., Herndon, S. C., Ng, N. L., Hamilton, J. F., Bergström, R., Di Marco, C., Nemitz, E., Mackenzie, I. A., Kuenen, J. J. P., Green, D. C., Reis, S., and Heal, M. R. (2016). Simulating secondary organic aerosol from missing diesel-related intermediate-volatility organic compound emissions during the clean air for london (ClearfLo) campaign. *Atmos. Chem. Phys.*, 16(10):6453–6473.

Paatero, P. (1997). Least squares formulation of robust non-negative factor analysis. *Chemometrics and Intelligent Laboratory Systems*, 37(1):23–35.

Paatero, P., Hopke, P. K., Song, X., and Ramadan, Z. (2002). Understanding and controlling rotations in factor analytic models. *Chemometrics and Intelligent Laboratory Systems*, 60(1–2):253–264.

Paatero, P. and Tapper, U. (1994). Positive matrix factorization: A non-negative factor model with optimal utilization of error estimates of data values. *Environmetrics*, 5(2):111–126.

Pan, X., Chin, M., Gautam, R., Bian, H., Kim, D., Colarco, P. R., Diehl, T. L., Takemura, T., Pozzoli, L., Tsigaridis, K., Bauer, S., and Bellouin, N. (2015). A multi-model evaluation of aerosols over south asia: common problems and possible causes. *Atmos. Chem. Phys.*, 15(10):5903–5928.

Pankow, J. F. (1994). An Absorption-Model of Gas-Particle partitioning of Organic-Compounds in the atmosphere. *Atmospheric Environment*, 28:185–188.

Passant, N. R. (2002). Speciation of UK emissions of non-methane volatile organic compounds. Technical report, AEA Technology Report ENV- 05452002, Culham, Abington, UK.

Pöschl, U. (2005). Atmospheric aerosols: Composition, transformation, climate and health effects. *Angewandte Chemie-International Edition*, 44:7520–7540.

Presto, A. A., Miracolo, M. A., Donahue, N. M., and Robinson, A. L. (2010). Secondary organic aerosol formation from High-NOx Photo-Oxidation of low volatility precursors: n-Alkanes. *Environmental Science & Technology*, 44(6):2029–2034.

Pye, H. O. T. and Seinfeld, J. H. (2010). A global perspective on aerosol from low-volatility organic compounds. *Atmos. Chem. Phys.*, 10(9):4377–4401.

Quincey, P., Butterfield, D., Green, D., Coyle, M., and Cape, J. N. (2009). An evaluation of measurement methods for organic, elemental and black carbon in ambient air monitoring sites. *Atmospheric Environment*, 43(32):5085–5091.

Redington, A. L. and Derwent, R. G. (2013). Modelling secondary organic aerosol in the united kingdom. *Atmospheric Environment*, 64:349–357.

Reis, S., Blank, P., Friedrich, R., Smiatek, G., José, R. S., Peña, J. I., Pérez, J. L., González, R. M., Lewyckyj, N., Colles, A., Janssen, L., Mensink, C., Reis, S., Blank, P., Wickert, B., Friedrich, R., Müezzinoğlu, A., Elbir, T., Dinçer, F., Bayram, A., Odabasi, M., Cetin, E., and Seyfioglu, R. (2004). Emission models and tools. In Friedrich, P. D. R. and Reis, D. W. S., editors, *Emissions of Air Pollutants*, pages 279–335. Springer Berlin Heidelberg.

Reis, S., Steinle, S., Carnell, E. J., Leaver, D., Vieno, M., Beck, R., and Dragosits, U. (2016). UK gridded population based on census 2011 and land cover map 2007. *NERC Environmental Information Data Centre*.

Robinson, A. L., Donahue, N. M., Shrivastava, M. K., Weitkamp, E. A., Sage, A. M., Grieshop, A. P., Lane, T. E., Pierce, J. R., and Pandis, S. N. (2007). Rethinking organic aerosols: Semivolatile emissions and photochemical aging. *Science*, 315:1259–1262.

Rogge, W. F., Hildemann, L. M., Mazurek, M. A., Cass, G. R., and Simoneit, B. R. T. (1991). Sources of fine organic aerosol. 1. charbroilers and meat cooking operations. *Environmental Science & Technology*, 25(6):1112–1125.

Schauer, J. J., Kleeman, M. J., Cass, G. R., and Simoneit, B. R. T. (1999). Measurement of emissions from air pollution sources. 1. c1 through c29 organic compounds from meat charbroiling. *Environmental Science & Technology*, 33(10):1566–1577.

Schulz, M., Gauss, M., Benedictow, A., Jonson, J. E., Tsyro, S., Nyiri, A., Simpson, D., Steensen, B. M., Klein, H., Valdebenito, A., Wind, P., Kirkevåg, A., Griesfeller, J., Bartnicki, J., Olivie, D., Grini, A., Iversen, T., Seland, ., Semeena, S. V., Fagerli, H., Aas, W., Hjellbrekke, A., Mareckova, K., Wankmuller, R., Schneider, P., Solberg, S., Svendby, T., Liu, L., Posch, M., Vieno, M., Reis, S., Kryza, M., Werner, M., and Walaszek, K. (2013). Transboundary acidification, eutrophication and ground level ozone in europe in 2011. Technical report, Norwegian Meteorological Institute.

Seinfeld, J. H. and Pandis, S. N. (2006). *Atmospheric chemistry and physics : from air pollution to climate change*. Wiley.

Shrivastava, M., Easter, R., Liu, X., Zelenyuk, A., Singh, B., Zhang, K., Ma, P., Chand, D., Ghan, S., Jimenez, J. L., Zhang, Q., Fast, J., Rasch, P. J., and Tiitta, P. (2015). Global transformation and fate of SOA: implications of low volatility SOA and Gas-Phase fragmentation reactions. *Journal of Geophysical Research: Atmospheres*, page 2014JD022563.

Shrivastava, M., Fast, J., Easter, R., Gustafson Jr., W. I., Zaveri, R. A., Jimenez, J. L., Saide, P., and Hodzic, A. (2011). Modeling organic aerosols in a megacity: comparison of simple and complex representations of the volatility basis set approach. *Atmos. Chem. Phys.*, 11(13):6639–6662.

Shrivastava, M. K., Lane, T. E., Donahue, N. M., Pandis, S. N., and Robinson, A. L. (2008). Effects of gas particle partitioning and aging of primary emissions on urban and regional organic aerosol concentrations. *Journal of Geophysical Research-Atmospheres*, 113.

Simpson, D., Benedictow, A., Berge, H., Bergström, R., Emberson, L. D., Fagerli, H., Flechard, C. R., Hayman, G. D., Gauss, M., Jonson, J. E., Jenkin, M. E., Nyíri, A., Richter, C., Semeena, S. V., Tsyro, S., Tuovinen, J. P., Valdebenito, A., and Wind, P. (2012). The EMEP MSC-W chemical transport model - technical description. *Atmos. Chem. Phys.*, 12:7825–7865.

Sofiev, M., Soares, J., Prank, M., Leeuw, G. d., and Kukkonen, J. (2011). A regional-to-global model of emission and transport of sea salt particles in the atmosphere. *Journal of Geophysical Research-Atmospheres*, 116.

Spracklen, D. V., Jimenez, J. L., Carslaw, K. S., Worsnop, D. R., Evans, M. J., Mann, G. W., Zhang, Q., Canagaratna, M. R., Allan, J., Coe, H., McFiggans, G., Rap, A., and Forster, P. (2011). Aerosol mass spectrometer constraint on the global secondary organic aerosol budget. *Atmos. Chem. Phys.*, 11(23):12109–12136.

Stockwell, W. R. and Calvert, J. G. (1983). The mechanism of the HO-SO2 reaction. *Atmospheric Environment (1967)*, 17:2231–2235.

Toll, V., Reis, K., Ots, R., Kaasik, M., Männik, A., Prank, M., and Sofiev, M. (2015). SILAM and MACC reanalysis aerosol data used for simulating the aerosol direct radiative effect with the NWP model HARMONIE for summer 2010 wildfire case in russia. *Atmospheric Environment*, 121:75–85.

Tsigaridis, K., Daskalakis, N., Kanakidou, M., Adams, P. J., Artaxo, P., Bahadur, R., Balkanski, Y., Bauer, S. E., Bellouin, N., Benedetti, A., Bergman, T., Berntsen, T. K., Beukes, J. P., Bian, H., Carslaw, K. S., Chin, M., Curci, G., Diehl, T., Easter, R. C., Ghan, S. J., Gong, S. L., Hodzic, A., Hoyle, C. R., Iversen, T., Jathar, S. H., Jimenez, J. L., Kaiser, J. W., Kirkevåg, A., Koch, D., Kokkola, H., Lee, Y. H., Lin, G., Liu, X., Luo, G., Ma, X., Mann, G. W., Mihalopoulos, N., Morcrette, J., Müller, J., Myhre, G., Myriokefalitakis, S., Ng, N. L., O'Donnell, D., Penner, J. E., Pozzoli, L., Pringle, K. J., Russell, L. M., Schulz, M., Sciare, J., Seland, ., Shindell, D. T., Sillman, S., Skeie, R. B., Spracklen, D., Stavrakou, T., Steenrod, S. D., Takemura, T., Tiitta, P., Tilmes, S., Tost, H., van Noije, T., van Zyl, P. G., von Salzen, K., Yu, F., Wang, Z., Wang, Z., Zaveri, R. A., Zhang, H., Zhang, K., Zhang, Q., and Zhang, X. (2014). The AeroCom evaluation and intercomparison of organic aerosol in global models. *Atmos. Chem. Phys.*, 14(19):10845–10895.

Tsimpidi, A. P., Karydis, V. A., Pandis, S. N., and Lelieveld, J. (2016). Global combustion sources of organic aerosols: Model comparison with 84 AMS factor analysis data sets. *Atmospheric Chemistry and Physics Discussions*, pages 1–51.

Tsimpidi, A. P., Karydis, V. A., Zavala, M., Lei, W., Molina, L., Ulbrich, I. M., Jimenez, J. L., and Pandis, S. N. (2010). Evaluation of the volatility basis-set approach for the simulation of organic aerosol formation in the mexico city metropolitan area. *Atmos. Chem. Phys.*, 10(2):525–546.

Ulbrich, I. M., Canagaratna, M. R., Zhang, Q., Worsnop, D. R., and Jimenez, J. L. (2009). Interpretation of organic components from positive matrix factorization of aerosol mass spectrometric data. *Atmos. Chem. Phys.*, 9(9):2891–2918.

USEPA (2004). 2002 national emission inventory (NEI) preparation plan. Technical report, USEPA.

Varga, G., Kovacs, J., and Ujvari, G. (2013). Analysis of saharan dust intrusions into the carpathian basin (Central europe) over the period of 1979-2011. *Global and Planetary Change*, 100:333–342.

Verwer, J., Blom, J., and Hundsdorfer, W. (1996). An implicit-explicit approach for atmospheric transport-chemistry problems. *Applied Numerical Mathematics*, 20(1-2):191–209.

Verwer, J. and Simpson, D. (1995). Explicit methods for stiff ODEs from atmospheric chemistry. *Applied Numerical Mathematics*, 18(1-3):413–430.

Vieno, M., Dore, A. J., Stevenson, D. S., Doherty, R., Heal, M. R., Reis, S., Hallsworth, S., Tarrason, L., Wind, P., Fowler, D., Simpson, D., and Sutton, M. A. (2010). Modelling surface ozone during the 2003 heat-wave in the UK. *Atmos. Chem. and Phys.*, 10:7963–7978.

Vieno, M., Heal, M. R., Hallsworth, S., Famulari, D., Doherty, R. M., Dore, A. J., Tang, Y. S., Braban, C. F., Leaver, D., Sutton, M. A., and Reis, S. (2014). The role of long-range transport and domestic emissions in determining atmospheric secondary inorganic particle concentrations across the UK. *Atmos. Chem. Phys.*, 14(16):8435–8447.

Vieno, M., Heal, M. R., Twigg, M. M., MacKenzie, I. A., Braban, C. F., Lingard, J. J. N., Ritchie, S., Beck, R. C., Móring, A., Ots, R., Marco, C. F. D., Nemitz, E., Sutton, M. A., and Reis, S. (2016). The UK particulate matter air pollution episode

of March–April 2014: more than saharan dust. *Environmental Research Letters*, 11(4):044004.

Waters, L. (2016). Summary results of the domestic wood use survery. Technical report, Renewable Energy Statistics.

WHO (2006). Air quality guidelines. global update 2005. Technical report, World Health Organisation Regional Office for Europe, Copenhagen, Denmark.

WHO (2013). Review of evidence on health aspects of air pollution – REVIHAAP project. Technical report, World Health Organisation Regional Office for Europe, Copenhagen, Denmark.

WHO (2015). Residential heating with wood and coal: health impacts and policy options in europe and north america. Technical report, World Health Organisation, Copenhagen, Denmark.

Wiedinmyer, C., Akagi, S. K., Yokelson, R. J., Emmons, L. K., Al-Saadi, J. A., Orlando, J. J., and Soja, A. J. (2011). The fire INventory from NCAR (FINN): a high resolution global model to estimate the emissions from open burning. *Geosci. Model Dev.*, 4(3):625–641.

Xu, L., Suresh, S., Guo, H., Weber, R. J., and Ng, N. L. (2015). Aerosol characterization over the southeastern united states using high-resolution aerosol mass spectrometry: spatial and seasonal variation of aerosol composition and sources with a focus on organic nitrates. *Atmos. Chem. Phys.*, 15(13):7307–7336.

Xu, L., Williams, L. R., Young, D. E., Allan, J. D., Coe, H., Massoli, P., Fortner, E., Chhabra, P., Herndon, S., Brooks, W. A., Jayne, J. T., Worsnop, D. R., Aiken, A. C., Liu, S., Gorkowski, K., Dubey, M. K., Fleming, Z. L., Visser, S., Prévôt, A. S. H., and Ng, N. L. (2016). Wintertime aerosol chemical composition, volatility, and spatial variability in the greater london area. *Atmos. Chem. Phys.*, 16(2):1139–1160.

Yin, J., Cumberland, S. A., Harrison, R. M., Allan, J., Young, D. E., Williams, P. I., and Coe, H. (2015). Receptor modelling of fine particles in southern england using CMB including comparison with AMS-PMF factors. *Atmos. Chem. Phys.*, 15(4):2139–2158.

Young, D. E., Allan, J. D., Williams, P. I., Green, D. C., Flynn, M. J., Harrison, R. M., Yin, J., Gallagher, M. W., and Coe, H. (2015a). Investigating the annual behaviour

of submicron secondary inorganic and organic aerosols in london. *Atmos. Chem. Phys.*, 15(11):6351–6366.

Young, D. E., Allan, J. D., Williams, P. I., Green, D. C., Harrison, R. M., Yin, J., Flynn, M. J., Gallagher, M. W., and Coe, H. (2015b). Investigating a two-component model of solid fuel organic aerosol in london: processes, PM1 contributions, and seasonality. *Atmos. Chem. Phys.*, 15(5):2429–2443.

Zhang, Q., Jimenez, J. L., Canagaratna, M. R., Allan, J. D., Coe, H., Ulbrich, I., Alfarra, M. R., Takami, A., Middlebrook, A. M., Sun, Y. L., Dzepina, K., Dunlea, E., Docherty, K., DeCarlo, P. F., Salcedo, D., Onasch, T., Jayne, J. T., Miyoshi, T., Shimono, A., Hatakeyama, S., Takegawa, N., Kondo, Y., Schneider, J., Drewnick, F., Borrmann, S., Weimer, S., Demerjian, K., Williams, P., Bower, K., Bahreini, R., Cottrell, L., Griffin, R. J., Rautiainen, J., Sun, J. Y., Zhang, Y. M., and Worsnop, D. R. (2007). Ubiquity and dominance of oxygenated species in organic aerosols in anthropogenically-influenced northern hemisphere midlatitudes. *Geophysical Research Letters*, 34(13):L13801.

Zhang, Q. J., Beekmann, M., Drewnick, F., Freutel, F., Schneider, J., Crippa, M., Prevot, A. S. H., Baltensperger, U., Poulain, L., Wiedensohler, A., Sciare, J., Gros, V., Borbon, A., Colomb, A., Michoud, V., Doussin, J., Denier van der Gon, H. A. C., Haeffelin, M., Dupont, J., Siour, G., Petetin, H., Bessagnet, B., Pandis, S. N., Hodzic, A., Sanchez, O., Honoré, C., and Perrussel, O. (2013). Formation of organic aerosol in the paris region during the MEGAPOLI summer campaign: evaluation of the volatility-basis-set approach within the CHIMERE model. *Atmos. Chem. Phys.*, 13(11):5767–5790.

Ziemann, P. J. and Atkinson, R. (2012). Kinetics, products, and mechanisms of secondary organic aerosol formation. *Chemical Society Reviews*, 41:6582–6605.

Appendix A

Adding pentadecane into the EMEP model

This appendix describes the inclusion of a new species and its SOA yields to the EMEP model.

A.1 Adding pentadecane to a .species file

GenChem is a helper program for the EMEP model. The GenChem Perl+shell script reads in two types of text files, .species and .reactions, and creates the appropriate FORTRAN code that can then be compiled as part of the EMEP model.

```
C15H32,1,C15H32,212.4,xx,xx,0,0,0,xx,xx,,"
```

A.2 Adding pentadecane to a .reactions file

```
rcemis:C15H32   =   C15H32 ;

* Yields Presto 2010
* These yields were from C15H32 (M 212.41), so scaled for our C (12) and non_C (1) to
    ↪ get moles; assuming an OM/OC of 1.7
2.07e-11   OH   +   C15H32   =   0.69 ASOC_ng100 + 5.77 NON_C_ASOA_ng100 + 1.11
    ↪ ASOC_ug1 + 9.31 NON_C_ASOA_ug1 + 6.40 ASOC_ug10 + 53.79 NON_C_ASOA_ug10 + 4.69
    ↪ ASOC_ug1e2 + 39.36 NON_C_ASOA_ug1e2 ;
```

A.3 Increasing all NMVOCs from SNAP7 by 3.3 times - femis.dat file

The femis.dat file can be used to scale emissions from any country or SNAP sector up or down. This is often used for emission-scenario tests.

```
Name  7        sox       nox        co       voc       nh3       pm25       pmco
 0    7        1.0       1.0       1.0       3.3       1.0        1.0        1.0
```

A.4 Retaining the emissions of all other components - emisplit.dat file

The emissplit.dat file is used to split the total NMVOC emissions into surrogate species (groups). For the EmCHem09 chemical scheme, this includes 14 groups. To include pentadecane, a surrogate for diesel-IVOCs, all other NMVOCs in the emisplit file had to be scaled down by 3.3 (they were increased in femis.dat so this scales them back to the original, reported, value). C15H32 was then be added as 70% of total NMVOCs from this sector (an increase of 3.3 times means an addition of 2.3, and 2.3 is 70% of 3.3):

```
# VOC splits for EmChem09
# Produced by Garry Hayman from NAEI2000_09Nov 2009
# Riinu Ots added C12H26 to multiply snap7 emissions with 3.3, for whole europe
# "Riinu Ots therefore divided all other species with 3.3, to scale to new emission
    ↪ total"
: MASS_ASSUMED 0
99 99   C2H6     NC4H10   C2H4    C3H6     C5H8   OXYL   CH3OH   C2H5OH   HCHO
    ↪ CH3CHO    MEK   GLYOX   MGLYOX  C15H32 UNREAC \#HEADERS
0  7    1.421    10.794   1.999   3.205   0.000   10.309   0.000   0.000    0.794
    ↪ 0.766   0.124   0.000   0.000   70   0.000
```

Appendix B

Cooking aerosol emission sensitivity tests

B.1 Temporal emission profile

As was explained in Section 4.2, the measured diurnal profile of COA at the Marylebone Road site was used as a basis for an emission profile for the atmospheric chemistry transport model (ACTM). The normalised emission diurnal profiles (for weekdays and weekends), denoted *Test1 (asMeasured)*, is given in Table B.1, and is shown in Fig. B.1. COA emissions are gridded to workday population density for an annual total of 7.4 Gg for the UK as this value minimised the biases compared to annual measurements at the 2 sites. Emitting COA in the model using the measured profile already yields near perfect correlation coefficients between the measured and modelled diurnal cycles at the measurement stations (0.96 and 0.97 for Marylebone Road weekdays and weekends, respectively, and 0.98 for North Kensington for both weekdays and weekends), as well as good COE values (0.71 and 0.71 for Marylebone Road, and 0.33 and 0.67 for North Kensington; Fig. B.2). However, Fig. B.2 also shows that at Marylebone Road, the modelled lunchtime peak is underestimated. Therefore, sensitivity runs with altered emission profiles were conducted.

Based on the results of the 'asMeasured' test (Fig. B.2), for the first sensitivity experiment the lunchtime emission was increased and night-time emission decreased. For the weekend profile, dinner emission was also increased slightly. These changes were normalised, meaning that the total amount of COA emitted each day remained

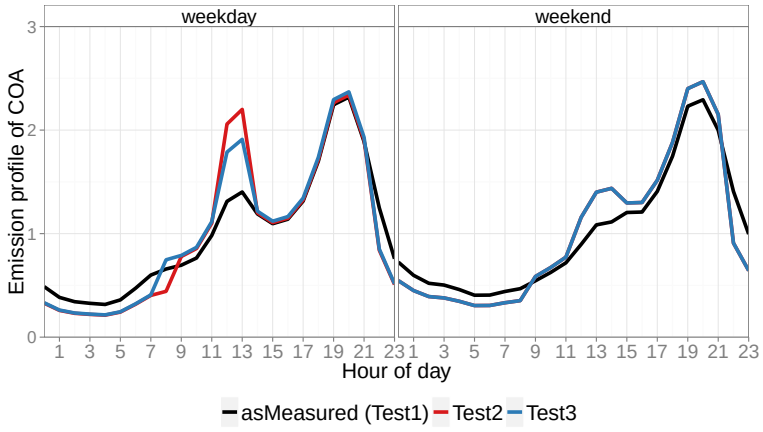

Figure B.1 *Diurnal normalised emission profiles for COA used in sensitivity runs. The timestamp is at the beginning of the hour. The specific hourly values are are also given in Table B.1.*

the same. The resulting emission profiles, denoted *Test2*, are given in Table B.1, and are shown in Fig. B.1. Average hourly profiles modelled for the two measurement station grid cells with the Test2 emission profiles are shown in Fig. B.3. There is an improvement for the Marylebone Road site (r-values increase to 0.98 and 0.99 for the weekdays and weekend profiles, respectively; COE values are increased to 0.78 and 0.85, weekdays and weekends, respectively; Fig. B.3a and b). For North Kensington, however, these metrics are slightly worsened by the Test2 run, but still remain high (r-values of 0.91 and 0.94, COE values of 0.30 and 0.58; Fig. B.3cd).

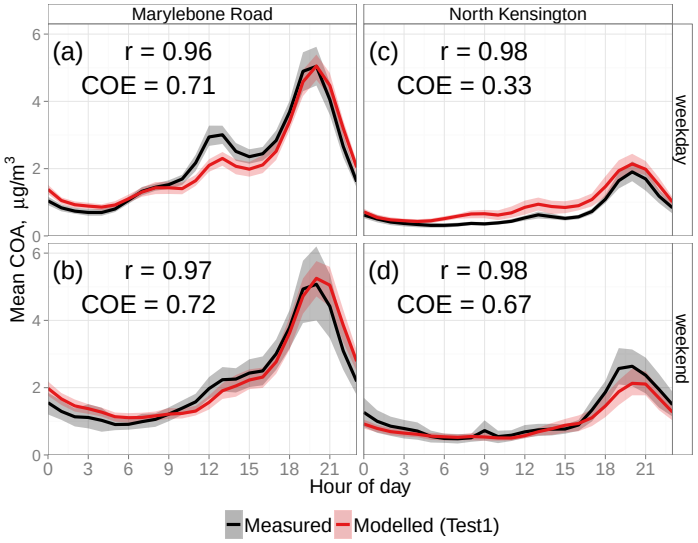

Figure B.2 *Average hourly profiles of measured and modelled COA using the first iteration diurnal emission profiles (Test1: asMeasured). The shading is the 95% confidence interval. Timestamp is at the beginning of the hour.*

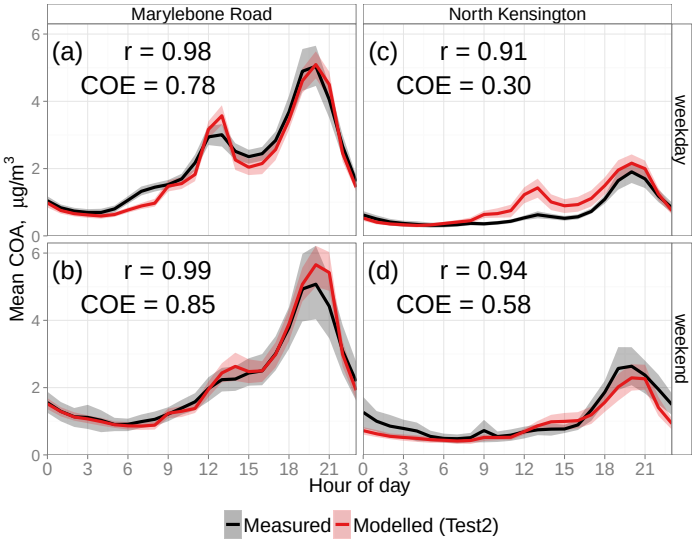

Figure B.3 *Similar to Fig.B.2, but with modified diurnal emission profiles (Test2).*

Based on the results of Test2, for the final sensitivity experiment the lunchtime emission was decreased relative to Test2 and breakfast emission was elevated slightly. The weekend profile was left identical to Test2. The resulting emission profiles, denoted *Test3*, are given in Table B.1, and are shown in Fig. B.1. Average hourly profiles of COA concentrations modelled with these emission profiles are shown in Fig. B.4. This profile was chosen as the final profile for COA emissions and further evaluation of modelled COA concentrations at these sites is presented in Chapter 4.

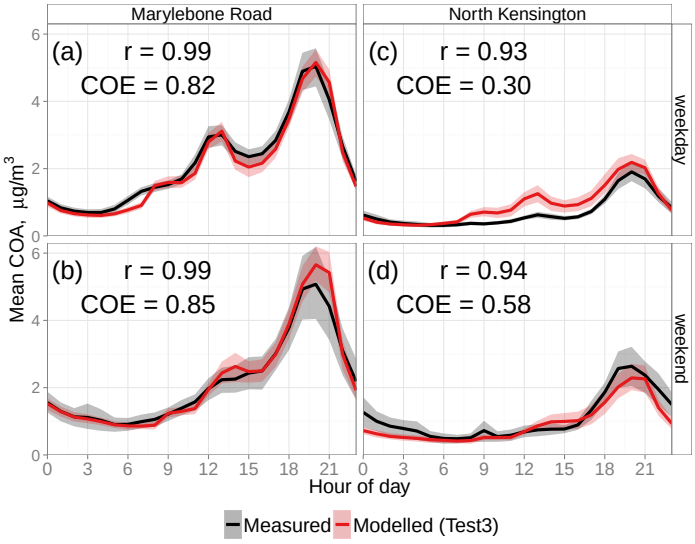

Figure B.4 *Similar to Fig.B.2, but with modified diurnal emission profiles (Test3).*

Table B.1 *Different normalised diurnal emission profiles for COA emissions used in sensitivity runs. The timestamp is at the beginning of the hour. Note that the weekend values for Test2 and Test3 are identical.*

	Test1 (as measured)		Test2		Test3 (final)	
	weekdays	weekend	weekdays	weekend	weekdays	weekend
0:00	0.49	0.72	0.32	0.55	0.33	0.55
1:00	0.38	0.60	0.26	0.45	0.26	0.45
2:00	0.34	0.52	0.23	0.39	0.23	0.39
3:00	0.33	0.50	0.22	0.38	0.22	0.38
4:00	0.32	0.46	0.21	0.35	0.21	0.35
5:00	0.36	0.40	0.24	0.30	0.25	0.30
6:00	0.47	0.41	0.32	0.30	0.32	0.30
7:00	0.60	0.44	0.40	0.33	0.41	0.33
8:00	0.66	0.47	0.44	0.35	0.75	0.35
9:00	0.69	0.54	0.78	0.59	0.79	0.59
10:00	0.76	0.63	0.86	0.67	0.87	0.67
11:00	0.98	0.72	1.10	0.77	1.12	0.77
12:00	1.31	0.90	2.06	1.16	1.79	1.16
13:00	1.40	1.08	2.20	1.40	1.91	1.40
14:00	1.19	1.11	1.20	1.44	1.22	1.44
15:00	1.10	1.20	1.11	1.30	1.12	1.30
16:00	1.14	1.21	1.15	1.30	1.16	1.30
17:00	1.31	1.41	1.33	1.52	1.34	1.52
18:00	1.70	1.75	1.72	1.88	1.74	1.88
19:00	2.25	2.23	2.26	2.40	2.29	2.40
20:00	2.32	2.29	2.34	2.47	2.37	2.47
21:00	1.89	2.00	1.90	2.15	1.93	2.15
22:00	1.25	1.41	0.84	0.91	0.85	0.91
23:00	0.76	1.00	0.51	0.64	0.52	0.64
SUM	24.00	24.00	24.00	24.00	24.00	24.00

B.1.1 Hourly time-plots

Hourly averaged time-plots of modelled and measured COA concentrations for the whole year are shown in Figs. B.5 and B.6 (Marylebone Road) and Figs. B.7 and B.8 (North Kensington).

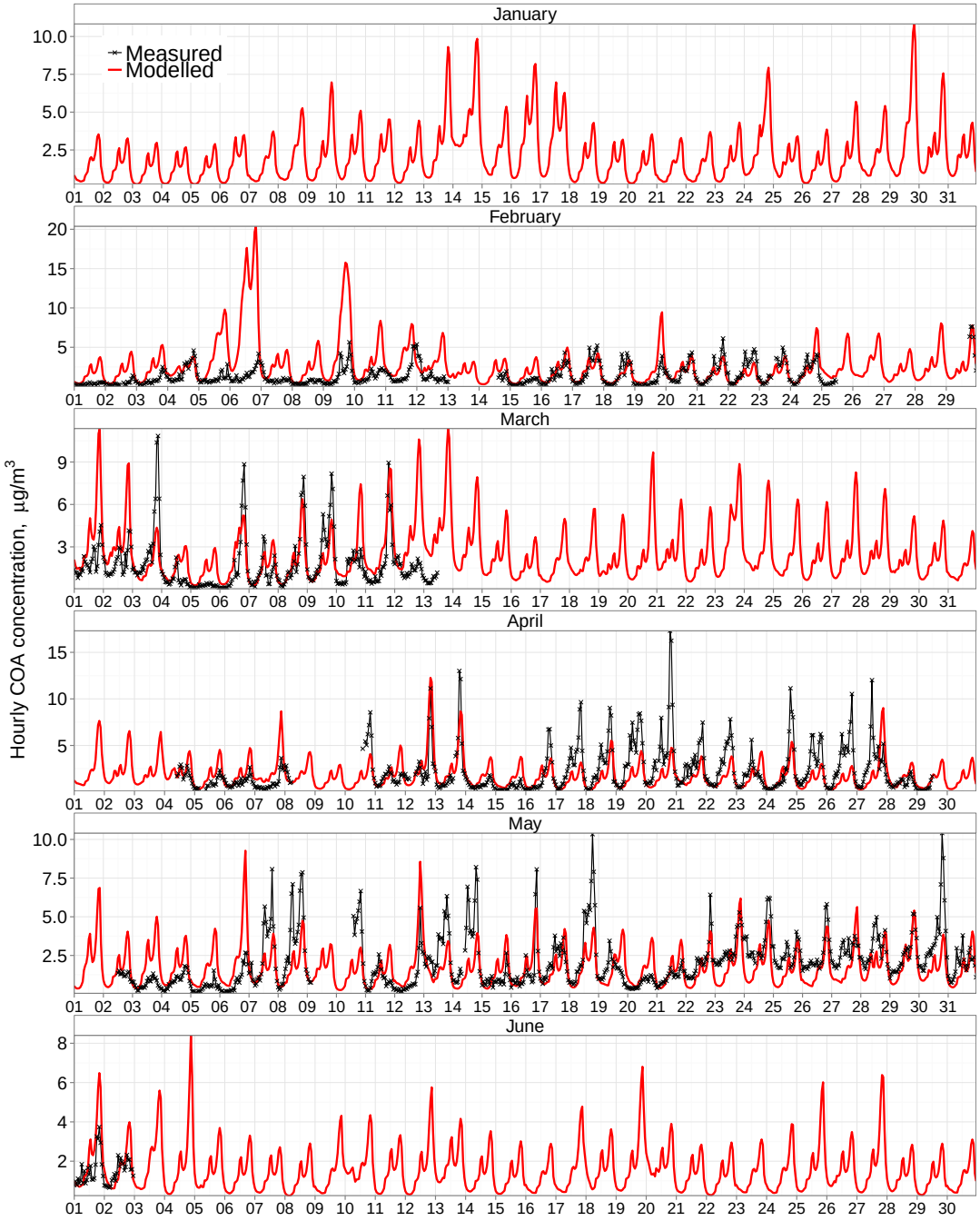

Figure B.5 *Hourly time-plots of measured and modelled COA concentrations at the Marylebone Road measurement site for January–June 2012.*

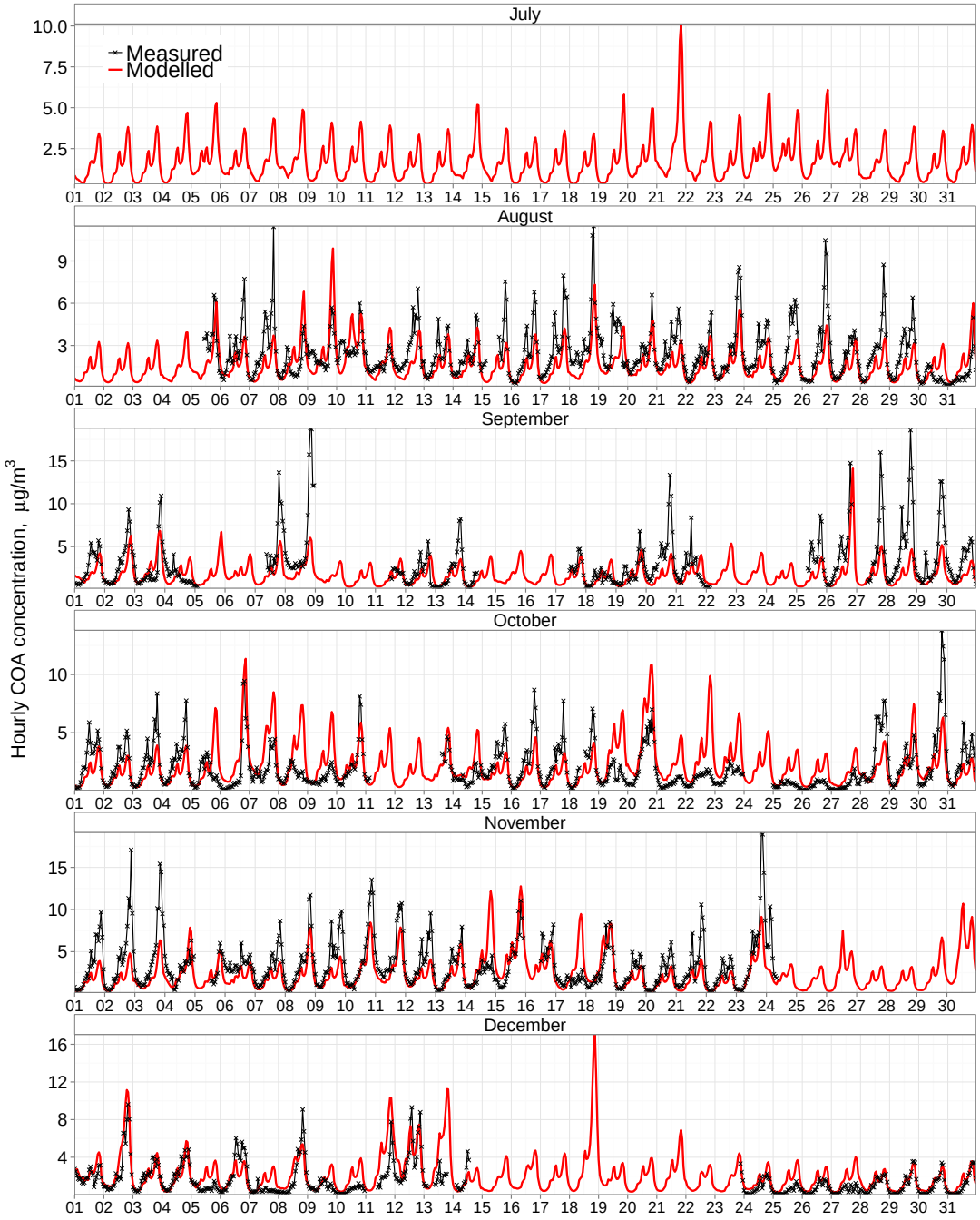

Figure B.6 *Hourly time-plots of measured and modelled COA concentrations at the Marylebone Road measurement site for July–December 2012.*

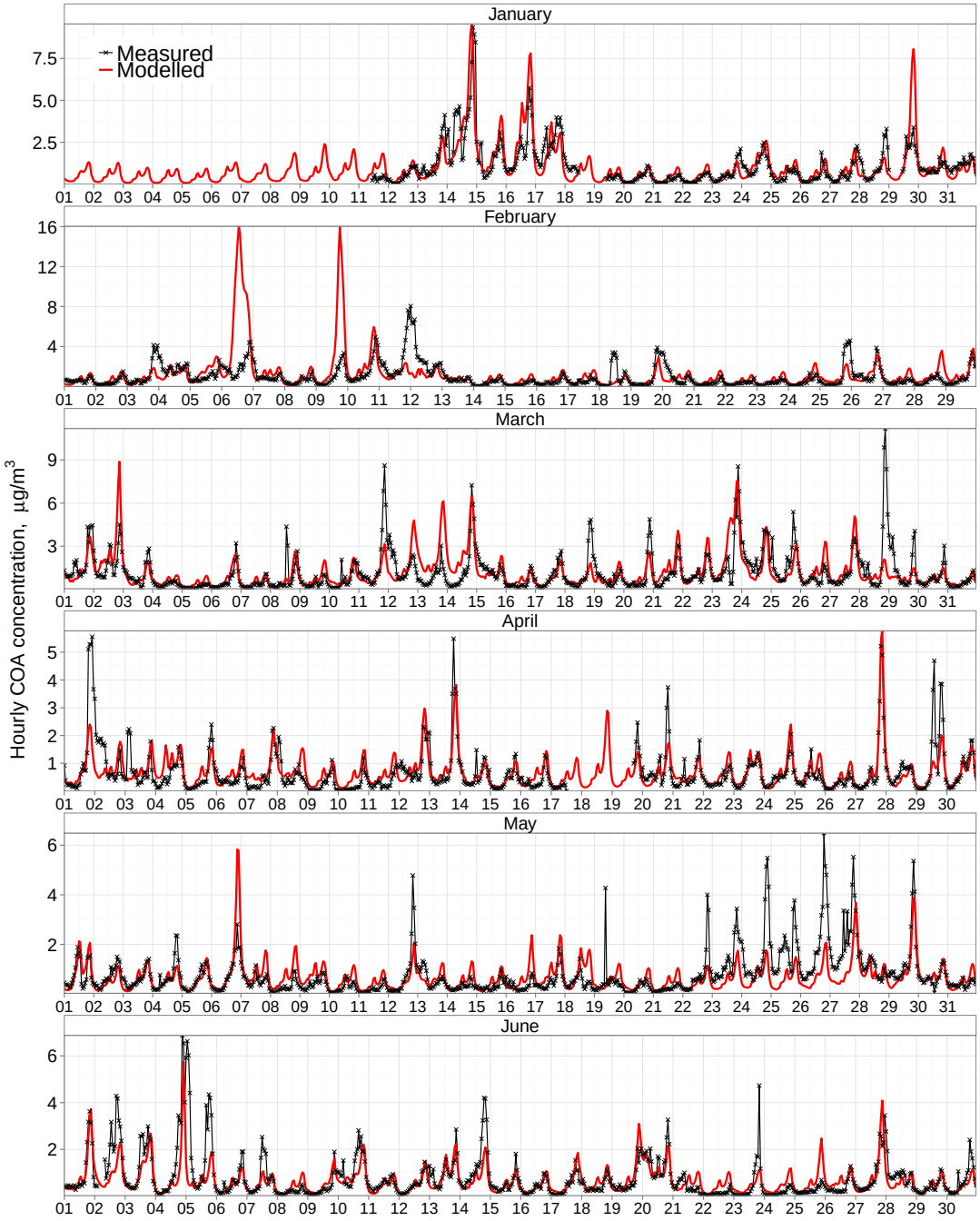

Figure B.7 *Hourly time-plots of measured and modelled COA concentrations at the North Kensington measurement site for January–June 2012.*

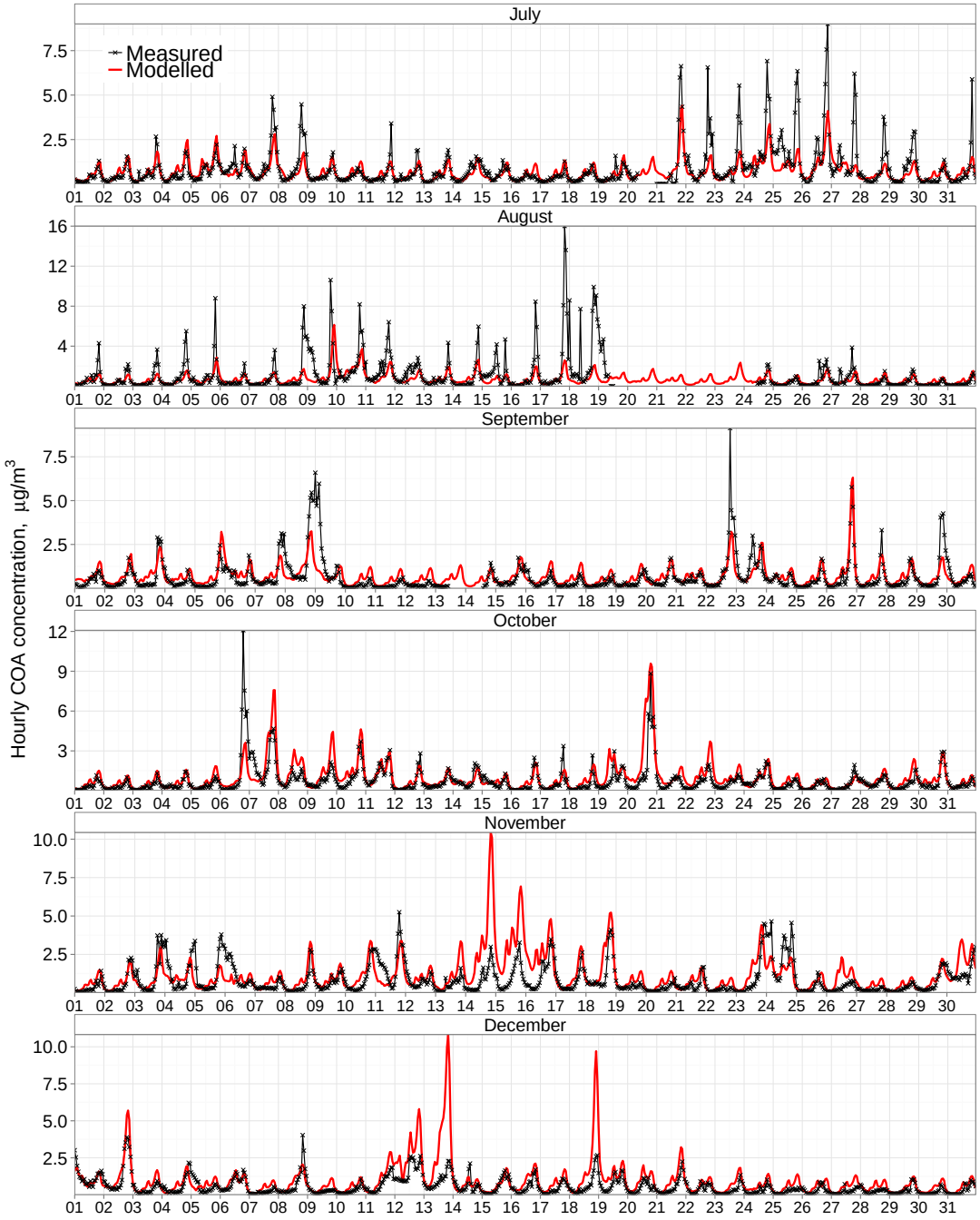

Figure B.8 *Hourly time plots of measured and modelled COA concentrations at the North Kensington measurement site for July–December 2012.*

Appendix C

Measured EC-R, EC-T, BC

C.1 Measurements of EC

The UK Particulate Concentrations and Numbers collects daily samples of PM_{10} onto binder-free pure quartz filters using a Partisol 2025 sampler at three measurement stations: London Marylebone Road (kerbside), London North-Kensington (urban background) and Harwell (rural background). These filters are analysed at the UK National Physics Laboratory (on a Sunset Laboratory Carbon Aerosol Analysis Lab instrument). The protocol used to quantify TC of that sample is a variation of the NIOSH protocol known as Quartz (Quincey et al., 2009). During the heating of the sample, some organic matter will be converted to elemental carbon by pyrolysis. This conversion is monitored by continuously measuring the transmittance (T) or reflectance (R) of the sample. The T or R signal is used to correct the assigned particles of TC into OC and EC by taking account of carbonaceous material that was OC, but become pyrolised into EC during the heating process. However, the quantification of the pyrolysed OC differs whether T or R is used, adding uncertainty to the measurements.

Figure C.1 illustrates the uncertainty of EC split from TC using reflectance (EC-R) and EC split from TC using transmittance (EC-T). For Harwell and North Kensington, EC-R is higher than EC-T (on average over the full dataset) which is similar to the findings of Chow et al. (2004). However, it can be noted that for both Harwell and North Kensington, in the lower range ($<$ ~0.4 $\mu g\,m^{-3}$ for Harwell, $<$ ~0.6 $\mu g\,m^{-3}$ for North Kensington), EC-T is higher than EC-R, whereas above these values, EC-R is

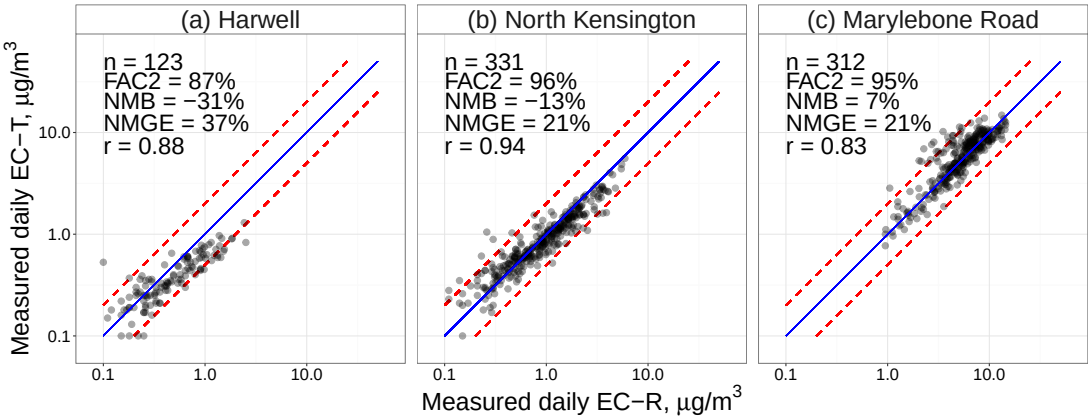

Figure C.1 *Scatterplot of measured daily-average EC split from TC using reflectance (EC-R) against EC split from TC using transmittance (EC-T), year 2012. Data below the detection limit ($< 0.1\ \mu g\ m^{-3}$) have been removed, leading to the lower number of data points for Harwell.*

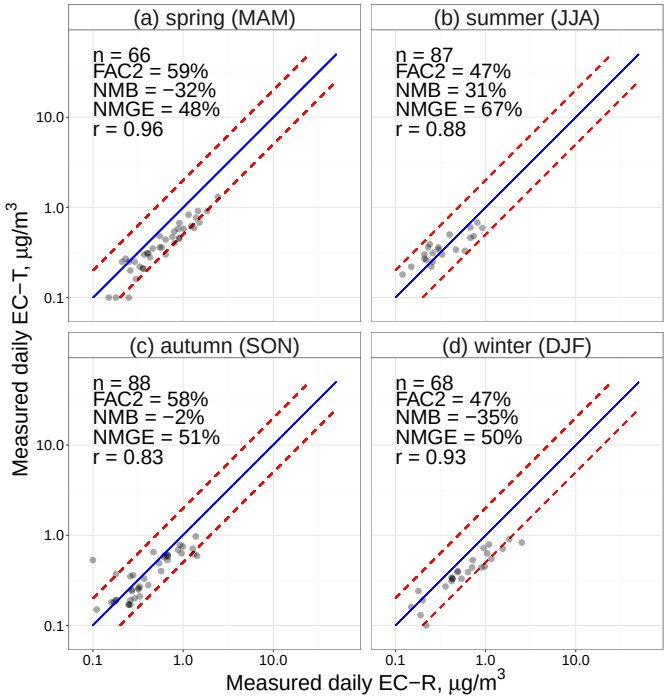

Figure C.2 *Scatterplot of measured daily-average EC split from TC using reflectance (EC-R) against EC split from TC using transmittance (EC-T) at the Harwell site split by seasons, year 2012.*

higher than EC-T.

Figures C.2, C.3, and C.3 split the points in Fig. C.1 into seasons for Harwell, North Kensington, and Marylebone Road, respectively. In spring and winter, EC-T is lower than EC-R (NMB from -7% to -35%), whereas during summer EC-T is higher than EC-R (NMB from +19% to +31%). In autumn, average measured concentrations of

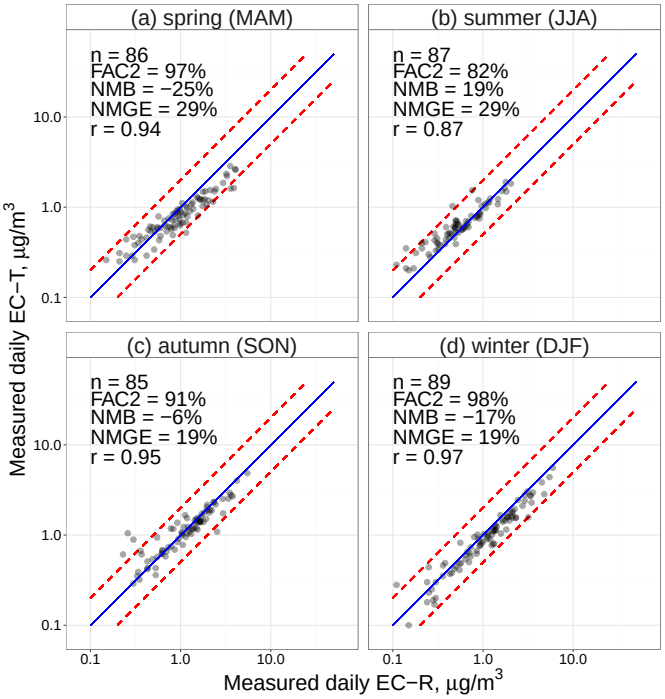

Figure C.3 *Scatterplot of measured daily-average EC split from TC using reflectance (EC-R) against EC split from TC using transmittance (EC-T) at the North Kensington site split by seasons, year 2012.*

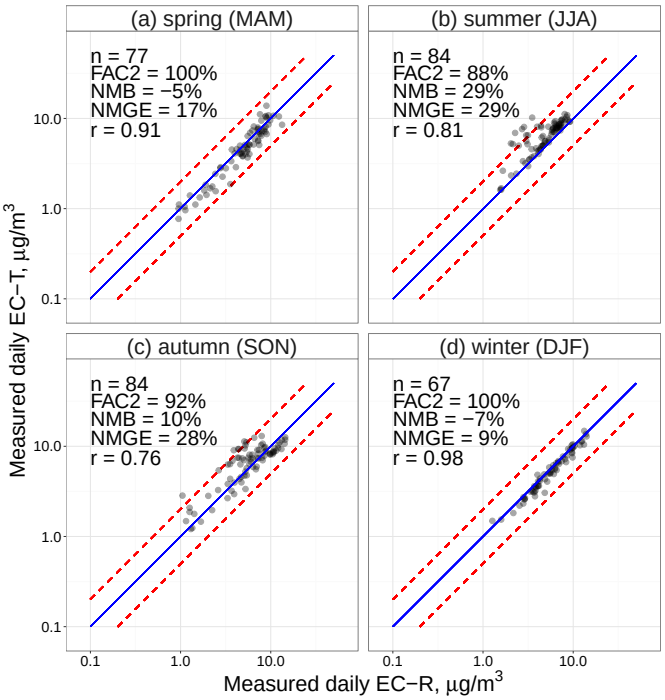

Figure C.4 *Scatterplot of measured daily-average EC split from TC using reflectance (EC-R) against EC split from TC using transmittance (EC-T) at the Marylebone Road site split by seasons, year 2012.*

EC-R and EC-T are most similar (NMB from -2% to +10%), but substantial scatter can be seen for some days as measured concentrations of EC-T and EC-R can differ from each other by more than a factor of 2. These clear similar findings at all three sites suggest that the different methods for quantifying of EC with the same instrument are dependent on season.

C.2 Measurements of BC

Measurements of black carbon involve the collection of $\mathrm{PM}_{2.5}$ onto a quartz tape, for which the absorption coefficient α [m^{-1}] is measured by a single-pass transmission of 880 nm light (compared to a clean sample, using the area and volume of the sample as well). The measurements are reported with an hourly timestep. The main uncertainties associated with BC measurements are (Heal and Quincey, 2012):

- Atmospheric oxidation changes the mass extinction coefficient of the sample (making it appear less dark).
- Variations in the size distribution of the particles leading to variations in the mass extinction coefficient.
- Variations in the external and internal mixing with other particles in the sample leading to variations in the optical properties of the sample.

It is not possible to take these factors into account operationally, as they differ on every single sample. Therefore a single mass extinction coefficient is used throughout BC measurements.

C.3 Measured BC vs measured EC

Figure C.5 shows daily-average time-series of measured EC-R and BC for the three measurement sites that have both sets of measurements. For Jan–March and Oct–Dec, measurements of BC and EC-R at the Harwell and North Kensington sites are a very close match to each other, whereas from April to September, BC is consistently higher than EC-R. At Marylebone Road, winter and early spring months (which exhibit good agreement between BC and EC-R for the North Kensington and Harwell sites) have

better agreement than the summer, but BC is overestimated compared to EC-R for throughout the year.

C.4 Conclusions

There are several inherit and methodologically obtained uncertainties in quantifying the refractory part of carbonaceous aerosol: elemental or black carbon. Overall, the mean absolute values of the different measurements relate to each other as follows: BC $>$ EC-R $>$ EC-T, but the magnitudes of the differences, and in some cases also the order vary for seasons and for individual sites.

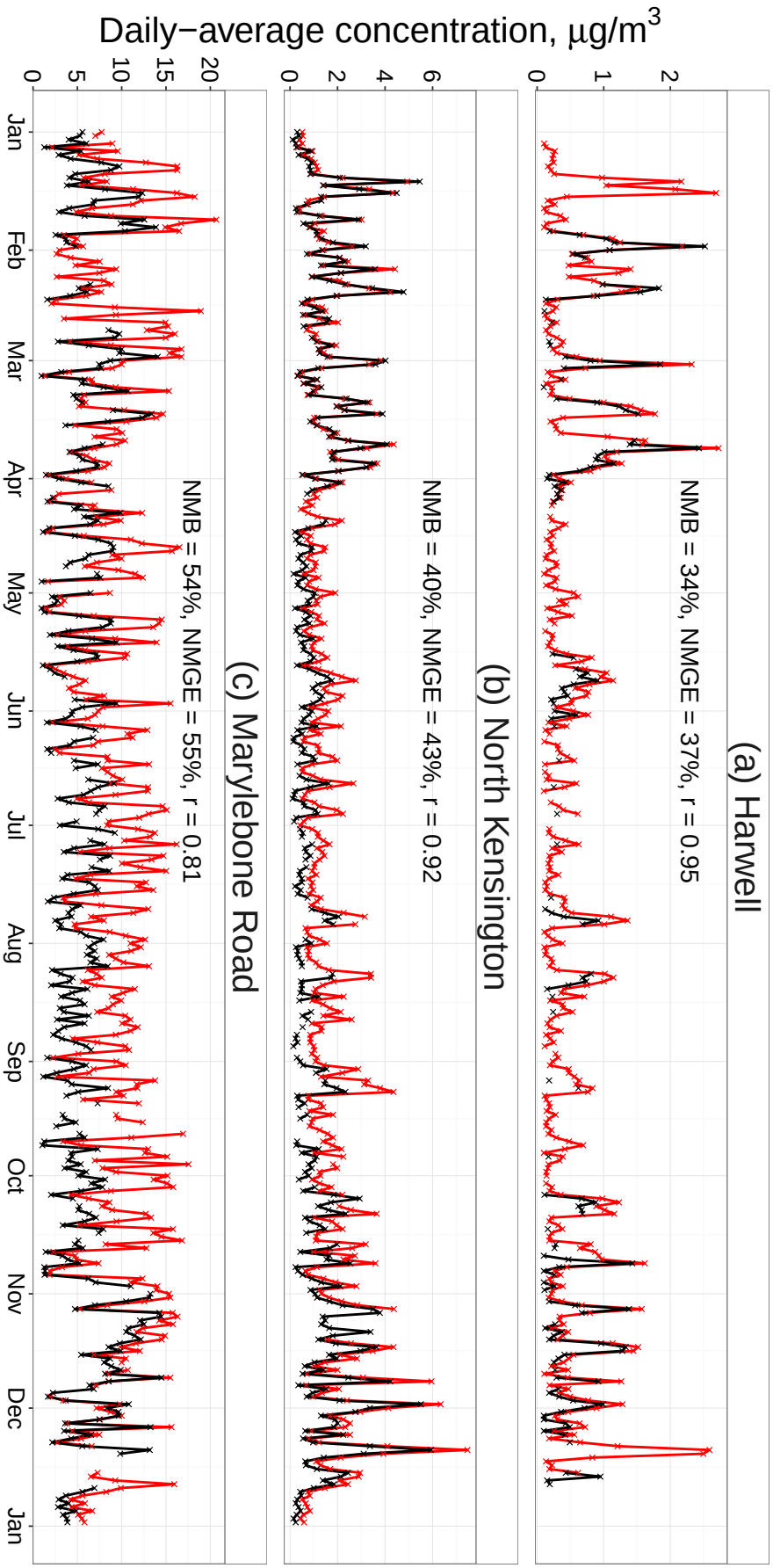

Figure C.5 *Time-series of daily-average measured EC-R and BC concentrations at the (a) Harwell, (b) North Kensington, and (c) Marylebone Road measurement sites, year 2012.*

Appendix D

Publication

This appendix contains the peer-review publication which formed the basis for Chapter 3.

Ots, R., Young, D. E., Vieno, M., Xu, L., Dunmore, R. E., Allan, J. D., Coe, H., Williams, L. R., Herndon, S. C., Ng, N. L., Hamilton, J. F., Bergstrm, R., Di Marco, C., Nemitz, E., Mackenzie, I. A., Kuenen, J. J. P., Green, D. C., Reis, S., and Heal, M. R. (2016). Simulating secondary organic aerosol from missing diesel-related intermediate-volatility organic compound emissions during the Clean Air for London (ClearfLo) campaign, 16, 6453-6473, *Atmos. Chem. Phys.*, doi: 10.5194/acp-2015-920.

Atmos. Chem. Phys., 16, 6453–6473, 2016
www.atmos-chem-phys.net/16/6453/2016/
doi:10.5194/acp-16-6453-2016

Atmospheric Chemistry and Physics
Open Access
EGU

Simulating secondary organic aerosol from missing diesel-related intermediate-volatility organic compound emissions during the Clean Air for London (ClearfLo) campaign

Riinu Ots[1,2], Dominique E. Young[3,a], Massimo Vieno[2], Lu Xu[4], Rachel E. Dunmore[5], James D. Allan[3,6], Hugh Coe[3], Leah R. Williams[7], Scott C. Herndon[7], Nga L. Ng[4,8], Jacqueline F. Hamilton[5], Robert Bergström[9,10], Chiara Di Marco[2], Eiko Nemitz[2], Ian A. Mackenzie[11], Jeroen J. P. Kuenen[12], David C. Green[13], Stefan Reis[2,14], and Mathew R. Heal[1]

[1]School of Chemistry, University of Edinburgh, Edinburgh, UK
[2]Natural Environment Research Council, Centre for Ecology & Hydrology, Penicuik, UK
[3]School of Earth, Atmospheric and Environmental Sciences, University of Manchester, Manchester, UK
[4]School of Chemical and Biomolecular Engineering, Georgia Institute of Technology, Atlanta, GA, USA
[5]Wolfson Atmospheric Chemistry Laboratories, Department of Chemistry, University of York, York, UK
[6]National Centre for Atmospheric Science, University of Manchester, Manchester, UK
[7]Aerodyne Research, Inc., Billerica, MA, USA
[8]School of Earth and Atmospheric Sciences, Georgia Institute of Technology, Atlanta, GA, USA
[9]Swedish Meteorological and Hydrological Institute, Norrköping, Sweden
[10]Department of Chemistry and Molecular Biology, University of Gothenburg, Gothenburg, Sweden
[11]School of GeoSciences, University of Edinburgh, Edinburgh, UK
[12]TNO, Department of Climate, Air and Sustainability, Utrecht, the Netherlands
[13]MRC PHE Centre for Environment and Health, King's College London, London, UK
[14]University of Exeter Medical School, Knowledge Spa, Truro, UK
[a]now at: Department of Environmental Toxicology, University of California, Davis, CA, USA

Correspondence to: Mathew R. Heal (m.heal@ed.ac.uk) and Riinu Ots (r.ots@ed.ac.uk)

Received: 12 November 2015 – Published in Atmos. Chem. Phys. Discuss.: 18 January 2016
Revised: 26 April 2016 – Accepted: 11 May 2016 – Published: 27 May 2016

Abstract. We present high-resolution (5 km × 5 km) atmospheric chemical transport model (ACTM) simulations of the impact of newly estimated traffic-related emissions on secondary organic aerosol (SOA) formation over the UK for 2012. Our simulations include additional diesel-related intermediate-volatility organic compound (IVOC) emissions derived directly from comprehensive field measurements at an urban background site in London during the 2012 Clean Air for London (ClearfLo) campaign. Our IVOC emissions are added proportionally to VOC emissions, as opposed to proportionally to primary organic aerosol (POA) as has been done by previous ACTM studies seeking to simulate the effects of these missing emissions. Modelled concentrations are evaluated against hourly and daily measurements of organic aerosol (OA) components derived from aerosol mass spectrometer (AMS) measurements also made during the ClearfLo campaign at three sites in the London area. According to the model simulations, diesel-related IVOCs can explain on average ∼ 30 % of the annual SOA in and around London. Furthermore, the 90th percentile of modelled daily SOA concentrations for the whole year is 3.8 µg m^{-3}, constituting a notable addition to total particulate matter. More measurements of these precursors (currently not included in official emissions inventories) is recommended. During the period of concurrent measurements, SOA concentrations at the Detling rural background location east of London were greater than at the central London location. The model shows that this was caused by an intense pollution plume with a

Published by Copernicus Publications on behalf of the European Geosciences Union.

strong gradient of imported SOA passing over the rural location. This demonstrates the value of modelling for supporting the interpretation of measurements taken at different sites or for short durations.

1 Introduction

Ambient airborne particulate matter (PM) has diverse sources and physicochemical properties. It affects the transport, transformation, and deposition of chemical species, and has significant impacts on radiative forcing and on human health (Pöschl, 2005; USEPA, 2009). The elemental and organic carbon (EC and OC) components constitute a substantial proportion of total particle mass (USEPA, 2009; Putaud et al., 2010; AQEG, 2012). However, the characterization and source apportionment of the organic component remains a major challenge (Fuzzi et al., 2006; Hallquist et al., 2009; Jimenez et al., 2009). Understanding the sources of this organic aerosol (OA) is important in order to devise effective reduction strategies for ambient PM concentrations (Heal et al., 2012).

Organic aerosol is typically a complex mixture of thousands of organic species, the majority of which are present at low concentrations (less than a few ng m^{-3}). Current levels of scientific understanding, instrumentation, and modelling capability mean that explicit measurement and modelling of all individual OA species is not feasible at present. Measurement of OA by on-line mass spectrometry, such as with the Aerodyne aerosol mass spectrometer (AMS; Canagaratna et al., 2007), and consideration of individual organic marker ions coupled with multivariate statistical techniques such as positive matrix factorization (PMF; Paatero and Tapper, 1994; Paatero, 1997) have facilitated the subdivision of the OA component into empirical categories. These include hydrocarbon-like organic aerosol (HOA), oxygenated organic aerosol (OOA, which can be further split into low-volatility and semi-volatile oxygenated organic aerosol: LV-OOA and SV-OOA), solid-fuel organic aerosol (SFOA) or biomass burning organic aerosol (BBOA), cooking organic aerosol (COA), and a number of other categories (Ulbrich et al., 2009; Ng et al., 2010, 2011; Lanz et al., 2010; Young et al., 2015a). The SFOA factor includes biomass aerosols that are the so-called BBOA as well as OA from coal and charcoal combustion (Allan et al., 2010).

Even allowing for the uncertainties in defining and measuring OA components, there is a general tendency for atmospheric chemical transport model (ACTM) simulations to underestimate observed amounts of OA and SOA. For example, the AeroCom (Aerosol Comparisons between Observations and Models) project, which includes ~ 30 global ACTMs and global circulation models (GCMs), has concluded that the amount of OA present in the atmosphere remains largely underestimated (Tsigaridis et al., 2014). Similarly, in an evaluation of seven global models, Pan et al. (2015) reported a systematic underestimation of OA over South Asia. Global modelling studies of SOA specifically have demonstrated huge uncertainties (up to 10-fold) in total simulated SOA budgets (Pye and Seinfeld, 2010; Spracklen et al., 2011; Jathar et al., 2011).

Several regional ACTM studies have also reported an underestimation of total OA (Simpson et al., 2007; Murphy and Pandis, 2009; Hodzic et al., 2010; Aksoyoglu et al., 2011; Jathar et al., 2011; Bergström et al., 2012; Koo et al., 2014) and SOA (Hodzic et al., 2010; Shrivastava et al., 2011; Zhang et al., 2013; Fountoukis et al., 2014), with normalized mean biases (NMBs) often in the range of -30 to -50 %. In some cases, this underestimation has been shown to be due to problems with the underlying emission inventories, particularly for domestic wood burning in wintertime (Simpson et al., 2007; Denier van der Gon et al., 2015). There may also be sources of biogenic secondary organic aerosol (BSOA) arising from previously neglected VOC emissions such as those induced by biotic stress (Berg et al., 2013; Bergström et al., 2014).

Currently, ACTMs cannot explicitly simulate all the kinetic and thermodynamic processes associated with the evolving gas-phase chemistry of semi-volatile organic compounds and their partitioning to the particle phase (Donahue et al., 2014). A widely used heuristic parametrization for simulating OA is the volatility basis set (Donahue et al., 2011, 2012). The volatility (in this case the saturation concentration at 298 K, C^*) of gas-phase organic compounds are sorted into bins: low-volatility organic compounds (LVOCs, $C^* \leq 0.1\,\mu g\,m^{-3}$; with no lower C^*, this category also incorporates extremely low-volatility organic compounds, ELVOCs), semi-volatile organic compounds (SVOCs, $C^* = 1\text{–}10^3\,\mu g\,m^{-3}$), intermediate-volatility organic compounds (IVOCs, $C^* = 10^4\text{–}10^6\,\mu g\,m^{-3}$), and volatile organic compounds (VOCs, $C^* \geq 10^7$). Thus, organic compounds are distributed across a continuum from particles to gases. Under typical ambient conditions, all LVOCs, some of the SVOCs, and essentially none of the IVOCs or VOCs are in the condensed phase (Donahue et al., 2006).

Current emissions inventories, however, only report estimates for VOCs ($C^* \geq 10^7\,\mu g\,m^{-3}$) and for the particle fraction of the emissions of species with lower volatilities. The main reason for this is that compounds with intermediate volatility (SVOCs and IVOCs) are difficult to quantify, and this is currently not routinely undertaken.

Robinson et al. (2007) and Shrivastava et al. (2008) estimated the mass of emitted IVOCs to be 1.5 times that of POA emissions. In their study, this addition of IVOCs $= 1.5 \times$ POA was applied to all sources of POA – from diesel to biomass burning. They based this estimation on chassis dynamometer tailpipe measurements by Schauer et al. (1999). Since then, several regional and global ACTM applications have adopted this factor of 1.5 (e.g. Murphy

and Pandis, 2009; Tsimpidi et al., 2010, 2016; Hodzic et al., 2010; Jathar et al., 2011; Fountoukis et al., 2011; Genberg et al., 2011; Bergström et al., 2012; Zhang et al., 2013; Koo et al., 2014). A number of studies, including many of those cited above reporting model underestimation of OA, have highlighted the need for improved measurement and speciation of SVOCs and IVOCs and for these species to be reported in inventories.

Jathar et al. (2014) performed emissions and smog chamber experiments on SOA production from petrol and diesel vehicles. Diesel contains hydrocarbons with a higher carbon number (C_8–C_{20}) than petrol (mainly C_4–C_{10}). The typical method used for hydrocarbon analysis is gas chromatography (GC); however, as the carbon number increases, the number of potential structural isomers increases exponentially, meaning GC is unable to distinguish individual species in the intermediate-volatility range (Goldstein and Galbally, 2007). The total carbon of this unresolved complex mixture was estimated and Jathar et al. (2014) concluded that these unspeciated organic gases dominate SOA production compared with SOA from the speciated precursors commonly included in emissions inventories (single-ring aromatics, isoprene, terpenes, and large alkenes). Jathar et al. (2014) also performed box-model simulations of the SOA budget for the US, with the addition of unspeciated emissions based on measurements by Schauer et al. (1999), and concluded that petrol contributes much more to SOA than does diesel. This result is similar to that of Bahreini et al. (2012), who, based on measurements in the Los Angeles Basin, California (CA), concluded that the contribution of diesel emissions to SOA was zero within measurement uncertainty. Conversely, Gentner et al. (2012) reported that diesel was responsible for 65–90 % of vehicular-derived SOA based on measurements of gas-phase organic carbon in the Caldecoff Tunnel, CA, and in Bakersfield, CA, and on estimations of SOA yields. The huge dissimilarity in these conclusions, even in the same state in the US, emphasizes the need for continued research into petrol- and diesel-related SOA formation. Furthermore, the US and Europe have very different diesel vehicle profiles: in the US, a negligible proportion of passenger cars are diesel (3 %), whilst on average across Europe 33 % of passenger cars are diesel and this proportion is increasing (Cames and Helmers, 2013). Globally, the demand for diesel fuel is increasing and by 2020 it is expected to overtake petrol as the principal transport fuel used worldwide (Exxon Mobil, 2014).

In this study, we present new high-resolution simulations of SOA formation in a 3-D ACTM model which includes additional diesel-related IVOC emissions derived directly from comprehensive field measurements of IVOCS and VOCs at an urban background site in central London (Dunmore et al., 2015) during the Clean Air for London (ClearfLo) campaign in 2012 (Bohnenstengel et al., 2014). Modelled concentrations are compared with OA components derived by PMF analysis of AMS measurements during the same campaign, including comparisons with the long-term measurements (full year) as well as the two month-long intensive observation periods (IOPs) in winter and summer.

2 Methods

2.1 Model description

The EMEP4UK model is a regional application of the EMEP MSC-W (European Monitoring and Evaluation Programme Meteorological Sythesizing Centre-West) model. The EMEP MSC-W model is a 3-D Eulerian model that has been used for both scientific studies and policy making in Europe. A detailed description of the EMEP MSC-W model, including references to evaluation and application studies, is available in Simpson et al. (2012), Schulz et al. (2013), and at http://www.emep.int. The EMEP4UK model is described in Vieno et al. (2010, 2014), and the model used here is based on version v4.5.

The EMEP4UK model uses one-way nesting from a 50 km × 50 km greater European domain to a nested 5 km × 5 km area covering the British Isles and parts of the near continent. The model has 21 vertical levels, extending from the ground to 100 hPa. The lowest vertical layer is ∼ 40 m thick, meaning that modelled surface concentrations represent the average for a 5 km × 5 km × 40 m grid cell. The model time step varies from 20 s (chemistry) to 5 and 20 min for advection in the inner and outer domains, respectively. The chemical scheme used in this study is EMEP-EmChem09soa with the MARS equilibrium module for gas–aerosol partitioning of secondary inorganic aerosol (Binkowski and Shankar, 1995; Simpson et al., 2012).

The model was driven by output from the Weather Research and Forecasting (WRF) model (http://www.wrf-model.org, version 3.1.1) including data assimilation of 6-hourly model meteorological reanalysis from the US National Center for Environmental Prediction (NCEP)/National Center for Atmospheric Research (NCAR) Global Forecast System (GFS) at 1° resolution (NCEP, 2000). The WRF configuration was as follows: *Lin Purdue* for microphysics; *Grell-3* for cumulus parametrization; *Goddart Shortwave* for radiation physics; and Yonsey University (YSU) for planetary boundary layer (PBL) height (see NCAR, 2008, for further information). This configuration is identical to that presented in Vieno et al. (2010), where it is shown to perform very well in comparison with measurements. No further evaluation is presented here.

2.2 Emissions

Gridded anthropogenic emissions of NO_x ($NO + NO_2$), SO_2, NH_3, CO, NMVOCs (non-methane VOCs), $PM_{2.5}$ (PM with aerodynamic diameter < 2.5 µm) and PM_{10} (PM with aerodynamic diameter < 10 µm) were obtained from NAEI (National Atmospheric Emissions Inventory, NAEI, 2013, for the

Table 1. SNAP source sectors as specified in the emissions input to the model (CEIP, 2015).

SNAP1	Combustion in energy and transformation industries
SNAP2	Residential and non-industrial combustion
SNAP3	Combustion in manufacturing industry
SNAP4	Production processes
SNAP5	Extraction and distribution of fossil fuels
SNAP6	Solvent and other product use
SNAP7	Road transport
SNAP8	Other mobile sources and machinery
SNAP9	Waste treatment and disposal
SNAP10	Agriculture

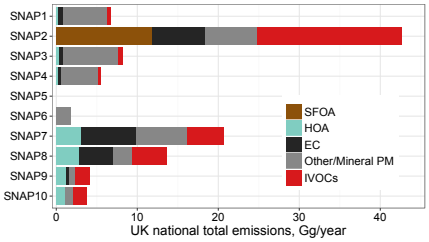

Figure 1. Annual UK $PM_{2.5}$ emissions by SNAP sector (Table 1) as specified in the NAEI (for year 2012), with each sector split into POA (HOA or SFOA), EC, and remaining PM following Kuenen et al. (2014). The red bars are additional IVOCs (not included in official emission totals) that can be estimated as $1.5 \times$ the POA mass in that sector. They are included in this plot to give an indication of the relative mass of IVOC additions that have been used in other studies.

UK and from CEIP (EMEP Centre on Emission Inventories and Projections; CEIP, 2015) for the rest of the model domain. All emissions are apportioned across a standard set of emission source sectors, following the sector structure defined in the Selected Nomenclature for Air Pollutant (SNAP; EEA, 2013; Table 1), consistently applied across the whole domain.

Primary PM emissions reported as $PM_{2.5}$ and PM_{10} in the NAEI and CEIP were speciated into EC, OA from fossil fuel combustion, OA from domestic combustion, and remaining primary PM by source sectors (using splits developed by Kuenen et al., 2014, as in Fig. 1). Default speciation of NMVOC emissions into 14 surrogate groups was used (Simpson et al., 2012). International shipping emissions from Entec UK Limited (now Amec Foster Wheeler) were used (Entec, 2010). The annual sectoral total emissions are temporally distributed to hourly resolution using hour-of-day, day-of-week, and monthly emission factors for each source sector as incorporated in the EMEP ACTM (Simpson et al., 2012). Daily emissions of all the aforementioned trace gases and particles from natural fires were taken from the Fire INventory from NCAR version 1.0 (FINNv1; Wiedinmyer et al., 2011). Monthly NO_x emissions from in-flight aircraft, soil, and lightning, as well as biogenic emissions of dimethyl sulfide (DMS), are included as described in Simpson et al. (2012). Biogenic emissions of isoprene and monoterpenes are calculated by the model for every grid cell and time step. Estimated emissions of wind-blown dust and sea salt are also included, but these have no impact on the model simulations of OA (Simpson et al., 2012).

2.3 SOA production in the model

The EMEP MSC-W model uses the 1-D volatility basis set (VBS; Donahue et al., 2006) approach for SOA formation, ageing and phase partitioning. The implementation of the VBS framework within the model, including various options for the treatment of volatility distributions and ageing reactions is described by Bergström et al. (2012).

In the model set-up used here, POA is treated as non-volatile and inert, as is currently assumed by emissions inventories. Having POA be non-volatile allows us to better identify and isolate the SOA formed from our additional diesel IVOCs. Furthermore, it has been demonstrated by Shrivastava et al. (2011) that a two-species VBS simulates an evolution of oxygen : carbon ratios (O : C) similar to the nine-species VBS approach. The two bins of Shrivastava et al. (2011) were of volatility 0.01 and 10^5, which, because material with the lower volatility is always completely in the particle phase under ambient conditions, is similar to our non-volatile treatment of POA.

Five volatility bins ($C^* = 0.1$, 1, 10, 100, $1000\,\mu g\,m^{-3}$) are used for SOA production and ageing. The SOA yields for alkanes, alkenes, aromatics, isoprene, and terpenes under high- and low-NO_x conditions were taken from Tsimpidi et al. (2010). Note that Tsimpidi et al. (2010) reported yields for the four VBS bins between 1 and $1000\,\mu g\,m^{-3}$. In this work, the lowest VBS bin ($0.1\,\mu g\,m^{-3}$) is used for the ageing reactions, as well as for SOA from the additional diesel IVOCs (explained in the next section). SOA from alkanes, alkenes, and terpenes is assumed to have an initial organic matter to organic carbon ratio (OM / OC ratio) of 1.7, while that from isoprene and aromatics is assumed to be 2.0 and 2.1, respectively (Bergström et al., 2012; Chhabra et al., 2010). For comparison, HOA and SFOA were assumed to have OM / OC ratios of 1.25 and 1.70, respectively (as in Bergström et al., 2012, based on Aiken et al., 2008). Both anthropogenic SOA (ASOA; from alkanes, alkenes, and aromatics) and BSOA (from isoprene and terpenes) undergo atmospheric ageing by the hydroxyl (OH) radical in the model (with rate coefficient of $4.0 \times 10^{-12}\,cm^3\,molecule^{-1}\,s^{-1}$; Lane et al., 2008), resulting in a shift into the next lower volatility bin and a mass increase of 7.5 %.

A constant background OA of $0.4\,\mu g\,m^{-3}$ is used to represent the contribution of OA sources not explicitly included in the model (e.g. oceanic sources or spores; Bergström et al.,

Table 2. Comparison of diesel and petrol NMVOCs in the UK National Atmospheric Emissions Inventory (NAEI) with the urban background ambient concentrations measured during the ClearfLo winter intensive observation period in London.

	NAEI 2012 (emission)	Measurements* (concentration)
Diesel (I)VOCs	8 Gg yr^{-1}	107 µg m^{-3}
Petrol VOCs	31 Gg yr^{-1}	33 µg m^{-3}
Diesel/petrol	0.26	3.2

* Dunmore et al. (2015).

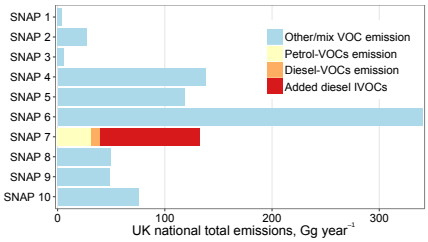

Figure 2. Annual UK NMVOC emissions by SNAP sector (Table 1) as specified in the NAEI (for the year 2012), with the SNAP7 emissions subdivided into petrol and diesel vehicles, and with the additional diesel-associated IVOC emissions input to the model in this study shown in red.

2014). This background OA is assumed to be highly oxygenated and is therefore included under modelled SOA when comparing with observations (with an OM / OC ratio of 2.0 it is also assumed to be non-volatile).

2.4 Additional IVOCs from diesel

Current emissions inventories report highly volatile anthropogenic VOCs of $C^* \geq 10^7$ µg m^{-3} (Passant, 2002). However, diesel vehicles also produce substantial emissions of species with intermediate volatility in the range $10^5 \leq C^* \leq 10^6$ µg m^{-3} (IVOCs), as has been shown by Dunmore et al. (2015) from measurements made at an urban background site in central London during the ClearfLo project.

In this study, aliphatic IVOC emissions from diesel vehicles were introduced into the model proportionally to on-road transport VOC emissions, using *n*-pentadecane ($C_{15}H_{32}$) as a surrogate for the following reasons. First, the amount of alkenes in diesel fuel is low (< 5 %; Gentner et al., 2012), so an alkane is the most appropriate surrogate. Second, all *n*-alkanes up to *n*-dodecane were individually speciated and quantified during two month-long intensive observation periods (IOPs) during the ClearfLo project and there were strong correlations between all *n*-alkanes that have a predominately diesel source (Dunmore et al., 2015). Third, the rate constant for the linear alkane is a reasonable representation of the rate constant for all the (unmeasured) branched and cyclic isomers, as demonstrated by Dunmore et al. (2015) for the C_{12} *n*-alkane, dodecane. The bulk of diesel emissions, however, are likely to have higher carbon numbers than were measured by a comprehensive two-dimensional gas chromatography (GC × GC) system (Dunmore et al., 2015). The rate coefficient for the reaction between *n*-pentadecane and OH has been measured in a number of studies ($k = 2.07 \times 10^{-11}$ cm^3 molecule^{-1} s^{-1}; Atkinson and Arey, 2003) unlike for the majority of branched isomers in this range. Furthermore, measurements of diesel fuel composition have shown that the average carbon number on a percentage weight basis was 14.94 (Gentner et al., 2012), so *n*-pentadecane was considered to be an appropriate surrogate for diesel emissions in general.

In the NAEI, emissions from petrol vehicles dominate the NMVOC emissions from road traffic, but measurements during the ClearfLo winter IOP showed that NMVOCs assigned to diesel vehicles dominated traffic-related NMVOC concentrations. The amount of pentadecane emitted in the model was therefore set to match the measured diesel-(I)VOC (IVOCs + VOCs) to petrol-VOC ratio (Table 2, Fig. 2). This pentadecane addition was then applied to every country in the model domain using the same factor as for the UK. This first approximation is justified because the fleet share of diesel vehicles in the UK is similar to the European average (∼ 30 %; EEA, 2010), but it can introduce errors for specific countries.

For the oxidation products of $C_{15}H_{32}$, SOA mass yields were taken from Presto et al. (2010): 0.044, 0.071, 0.41, and 0.30 for the 0.1, 1, 10, and 100 µg m^{-3} bins, respectively (Presto et al., 2010, did not report a yield for the 1000 µg m^{-3} bin). These yields are reported for SOA with unit density (1 g cm^{-3}). In this work, SOA density was assumed to be 1.5 g cm^{-3} (Tsimpidi et al., 2010; Bergström et al., 2012) and the yields were increased accordingly.

For the UK, our approach adds 90 Gg of diesel-IVOC emission for the year 2012 (Fig. 2). The 1.5 × POA approach (Shrivastava et al., 2008, based on measurements by Schauer et al., 1999) would only add 31 Gg (Fig. 1). Part of this discrepancy could be attributable to the different methods and circumstances used to derive the additions (this work: 5 weeks of ambient measurements in a megacity; previous estimate: tailpipe laboratory measurements using different instruments). Another possible reason for the difference is an underestimate in POA emissions in the inventory; more POA would increase the amount of proportionally added IVOCs. However, Dunmore et al. (2015) show that lower-carbon-number (and higher-volatility) NMVOCs measured during the ClearfLo campaign were consistent with emissions estimates. This lends confidence to adding IVOCs proportionally to reported NMVOC emissions, rather than

proportionally to POA emissions. Nevertheless, we have also performed a model run using the POA-based IVOC estimate, also including the semi-volatile treatment of POA. The emitted semi-volatile POA (SVOCs) and 1.5 × POA IVOCs are assigned to nine VBS bins – 0.03 × POA, 0.06 × POA, 0.09 × POA, 0.14 × POA, 0.18 × POA, 0.30 × POA, 0.40 × POA, 0.50 × POA, 0.80 × POA to the bins 0.01–10^6, respectively – totalling 2.5×POA (Shrivastava et al., 2008). Both SVOCs and IVOCs then go through atmospheric ageing with OH ($k = 4.0 \times 10^{-11}$ cm^3 molecule^{-1} s^{-1}; Shrivastava et al., 2008). In this case, the additional IVOCs were calculated from POA from all sources, not just traffic-related. Note that in the UK, most of the additional IVOCs of the POA-based approach would come from SNAP2 (residential and non-industrial combustion emissions; Fig. 1): 18 Gg, whereas only 5 Gg would be added to SNAP7 (road transport; and 8 Gg to remaining sectors). SVOCs and IVOCs that have undergone at least one ageing shift and are in the particulate phase are included under SOA (in addition to ASOA and BSOA from VOCs as in the Base case). Due to the very different absolute amounts and source categories (the latter of which also leads to differences in the spatial pattern and temporal variation of the additional emissions), detailed comparison of the two different additions is not justified, and only annual total OA component budgets of the different addition methodologies are presented.

2.5 Summary of model experiments

Three runs of the EMEP4UK modelling system were performed for 2012:

- Base: all anthropogenic emissions as in officially reported inventories; emissions of biogenic VOCs are calculated by the model for each advection time step.
- addDiesel: Base + additional diesel IVOCs added proportionally to NMVOC emissions from traffic (2.3 × SNAP7). The additional IVOCs were treated using *n*-pentadecane as surrogate species. The semi-volatile VBS species formed after oxidation of *n*-pentadecane were treated in the same way as the ASOA species from VOC oxidation (the same ageing rate and mass increase due to oxygen addition; see Sect. 2.3).
- 1.5volPOA: semi-volatile treatment of POA + additional IVOCs added proportionally to all POA emissions (1.5 × POA; as in Shrivastava et al., 2008, based on measurements by Schauer et al., 1999). Inclusion of anthropogenic and biogenic VOCs as in Base.

2.6 Comparison with measurements

Modelled $OA_{2.5}$ (OA with diameter < 2.5 µm) is compared with non-refractory submicron ($NR\text{-}PM_1$) OA measured by

Figure 3. Locations of measurement sites used in this study. London North Kensington is an urban background site, and Harwell and Detling are rural background sites. Underlying map from ©OpenStreetMap contributors.

Aerodyne AMS instruments at an urban background site in central London and at two rural sites (Xu et al., 2016; Young et al., 2015a, b; Bohnenstengel et al., 2014; site locations are shown in Fig. 3). The error introduced to the comparison by the different size fractions is believed to be small, as measurements at an urban background site in Birmingham, England have shown that 90 % of organic carbon in $PM_{2.5}$ is in the submicron fraction (Harrison and Yin, 2008).

Different types of AMS were deployed in this campaign. At the London North Kensington site a compact time-of-flight AMS (cToF-AMS) was deployed for a full calendar year (January 2012–January 2013), and a high-resolution time-of-flight AMS (HR-ToF-AMS) was also deployed for the IOPs at the same site. A HR-ToF-AMS was deployed in Detling during the winter IOP, and in Harwell during the summer IOP. PMF analysis was applied to each of the data sets to apportion measured OA into different components (Ulbrich et al., 2009). A detailed description of the derivation and optimization of the factors retrieved from the AMS data at Detling can be found in Xu et al. (2016), at London North Kensington in Young et al. (2015a, b) (all three of these analyses were performed with the PMF2 solver), and at Harwell in Di Marco et al. (2016) (using the ME-2 solver). The OM / OC ratios for each of the PMF data sets presented in this study were calculated with the Improved-Ambient method from Canagaratna et al. (2015). A summary of the instruments, measurement periods, and resolved PMF factors is given in Table 3. As our emissions inventory does not include cooking OA (NAEI, 2013), this factor could not be compared with the model.

When AMS measurements and their PMF apportionments are compared, some disagreement is observed, as shown for the two instruments measuring at the same time at the same location at London North Kensington. This is in part due to

Table 3. AMS measurements and resolved PMF factors during the ClearfLo campaign and the allocation of the PMF factors to SOA for comparison with model simulations. Site locations are shown in Fig. 3. Site names are abbreviated as follows: NK – London North Kensington; DET – Detling; HAR – Harwell.

				PMF factors	
Period	Site	Dates (year 2012)	Instrument	Primary	Secondary
Winter IOP	NK	13 Jan–8 Feb	HR-ToF-AMS	HOA, SFOA1, SFOA2, COA	OOA
	DET	20 Jan–14 Feb	HR-ToF-AMS	HOA, SFOA	OOA
Summer IOP	NK	21 Jul–19 Aug	HR-ToF-AMS	HOA, COA, unknown	SV-OOA, LV-OOA
	HAR	3 Aug–20 Aug	HR-ToF-AMS	HOA	SV-OOA, LV-OOA, N-OOA
Annual	NK	11 Jan–24 Jan (2013)*	cToF-AMS	HOA, SFOA**, COA	OOA1, OO2**

* As the cToF-AMS was retuned before the summer IOP and retuned to the previous tuning at the end of the IOP, the subsequent data could not be used in the PMF analysis (see Young et al. (2015a) for details). However, for the purpose of the comparison in this study, data from the HR-ToF-AMS, deployed at the same site during the summer IOP, were used to fill in this period. ** PMF analysis revealed the SFOA and OOA2 factors were convolved due to their similar, strong diurnal cycles. Daily averages have been used to estimate their concentrations (Young et al., 2015a).

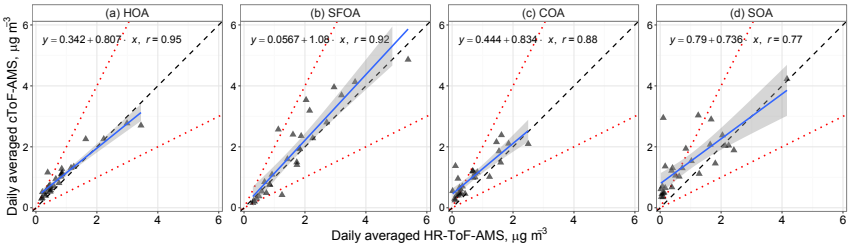

Figure 4. Scatter plots of PMF-derived OA component concentrations – **(a)** HOA, **(b)** SFOA, **(c)** COA, and **(d)** SOA – based on different AMS instruments at the London North Kensington site during the winter IOP. The dashed lines are the 2 : 1, 1 : 1, and 1 : 2 lines.

the differences in the types of AMS used, where more chemical information is retrieved from the HR-ToF-AMS, which can subsequently lead to differences in the derived PMF factors from the individual data sets. It should also be kept in mind that PMF was run on each of the full data sets, covering a full year for the cToF-AMS and only four weeks for each of the HR-ToF-AMS IOPs; thus, it is not necessarily expected that the same PMF factors would be derived from the different data sets. Nevertheless, strong correlations between daily averaged primary OA components from the two instruments deployed at the London North Kensington site during the winter IOP are observed (0.95, 0.92, and 0.88 for HOA, SFOA, and COA, respectively), with less strong correlations for SOA (0.77). Scatter plots of these PMF derived OA component concentrations resolved for the cToF-AMS data and HR-ToF-AMS are shown in Fig. 4. This inherent uncertainty in the measurements constrains the expected correlation with the model.

The following numerical metrics were used for model evaluation:

- FAC2 (factor of 2): the proportion of modelled concentrations that are within a factor of 2 of the measured concentrations.
- NMB: normalized mean bias.
- NMGE: normalized mean gross error, which is defined as

$$\mathrm{NMGE} = \frac{\frac{1}{n}\sum_{i=1}^{n}|M_i - O_i|}{\overline{O}}, \quad (1)$$

  where M_i is the ith modelled value, O_i is the corresponding measured value, $\overline{O}$ is the mean measured value, and n in the total number of observations.
- r: correlation coefficient.
- COE: coefficient of efficiency, which is defined as

$$\mathrm{COE} = 1.0 - \frac{\sum_{i=1}^{n}|M_i - O_i|}{\sum_{i=1}^{n}|O_i - \overline{O}|}. \quad (2)$$

A COE of 1 indicates perfect agreement between model and measurements. Although the COE does not have a lower bound, a zero or negative COE implies that the model cannot

explain any of the variation in the observations (Legates and McCabe, 2013).

Seasons are defined as follows: winter – December–January–February (DJF); spring – March–April–May (MAM); summer – June–July–August (JJA); and autumn – September–October–November (SON).

3 Results

The comparisons between the model results and measurements are presented in the following order. First, comparisons are presented for primary OA, NO_x, O_3, and for secondary inorganic aerosol (SIA) to give an overview of the overall performance of the modelling system. Second, the hourly concentrations of SOA during the two IOPs are evaluated, demonstrating the agreement between the model and measurements at high temporal resolution. Third, the year-long daily SOA concentrations are compared and the relative impact of diesel VOCs on SOA production in London is shown. Fourth, modelled and measured OM / OC ratios are shown. Finally, annual total ASOA from our method and the previous 1.5 × POA approach are compared.

3.1 POA, NO_x, O_3, SIA: annual data set

Figure 5 shows the year-long comparison between the daily averaged model results and the cToF-AMS measurements at the London North Kensington site. The model underestimates primary OA (HOA and SFOA) concentrations (NMB of −54 and −71 %, respectively) but shows good daily correlations (r values of 0.53 and 0.72, respectively). The underestimation of HOA may be caused by a combination of lack of model resolution (e.g. the minor road close to the measurement site can not be resolved with the 5 km grid), and underestimation of PM emissions. Modelled NO_x concentrations are relatively less underestimated in comparison to measurements (NMB of −32 %, Fig. 6a), suggesting that HOA emissions may be more underestimated than the emissions of NO_x. Concentrations of secondary inorganic pollutants are simulated well by the model in the gas phase (Fig. 6b, with a NMB of −1 % for ozone) and for inorganic PM constituents (Fig. 6c–d), with NMBs of 6 % for SO_4^{2-}, −12 % for NH_4^+, and −23 % for NO_3^-.

3.2 Hourly comparison of secondary OA: summer IOP

Evaluation statistics between hourly measured and modelled SOA concentrations in July and August 2012 (summer IOP) show excellent agreement (Fig. 7). The values of r for the Base run were 0.67 and 0.55 at North Kensington and Harwell, respectively. The addDiesel experiment yields a modest improvement in the value of r at North Kensington (to 0.76) and a marked improvement in Harwell (to 0.74). The addDiesel run substantially improves the NMB for SOA at the Harwell and London North Kensington sites from −32 to −5 % and from −35 to 0.1 %, respectively (Fig. 7). This means that ∼ 30 % of SOA at both sites during this period can be explained by the diesel IVOCs added into the model using pentadecane as a surrogate. There is also marked improvement of model–measurement COE values at the two sites (Harwell, 0.26 to 0.42; NK, 0.31 to 0.45). The improvement in NMGE is noticeable (Harwell, 54 to 43 %; NK, 59 to 47 %), but smaller than the improvements in the other metrics. It can be seen from the scatter plots in Fig. 8 that most modelled hourly SOA concentrations fall within a factor of 2 of the measured concentrations (FAC2 for the addDiesel experiment is 78 % at Harwell and 62 % at NK).

Measured and modelled mean hour-of-day variations of SOA concentrations are presented in Fig. 9, where it can be seen that measured SOA concentrations do not have a very strong diurnal cycle. Interestingly, both sites exhibit dips in measured SOA concentrations in the morning and early evening. Both measured and modelled SOA concentrations in London North Kensington reach a maximum in the afternoon, but SOA of the addDiesel experiment starts this increase earlier than the measurements, meaning that our ASOA production from pentadecane might be too rapid.

During the summer IOP, there were two sustained episodes of increased SOA concentrations: 23 to 28 July and 9 to 13 August (Fig. 7). Only London North Kensington had measurements during the first episode and the elevated concentrations were well captured by the addDiesel simulation (including the highest peak of greater than 16 µg m^{-3}: 27 July 13:00 GMT, Fig. 10b). Daily averaged SOA maps (Fig. 11) suggest that this first episode arose from a combination of SOA transported from Europe and SOA produced locally in London. A region of elevated concentration around London exists within a general gradient of SOA from continental Europe to southern England. Even daily averaged concentrations are spatially variable during this episode meaning that inaccuracies in some of the modelled peaks can be attributed to uncertainties in the underlying meteorological model. Most of the modelled SOA during this episode was of anthropogenic origin with the addDiesel run yielding a significant portion of ASOA from pentadecane.

For the second sustained episode of high SOA concentrations, from 9 to 13 August, several features remain substantially underestimated even in the addDiesel run. For Harwell, the model captures two of the highest peaks (10 August 22:00 GMT measured: 6.8 µg m^{-3}, addDiesel: 8.5 µg m^{-3}; 12 August 12:00 GMT measured: 7.9 µg m^{-3}, addDiesel: 7.0 µg m^{-3}), but for London North Kensington, the model simulates a minimum during the highest measured concentration (10 August 05:00 GMT measured: 11.9 µg m^{-3}, addDiesel: 2.0 µg m^{-3}). The high concentrations during the first 2 days of this episode were very localized with horizontal widths of just tens of kilometres (Fig. 12a and b). There was a build-up of pollution caused by high pressure and low boundary layer height (BLH), which led to production of ASOA in London. The high variability in the modelled con-

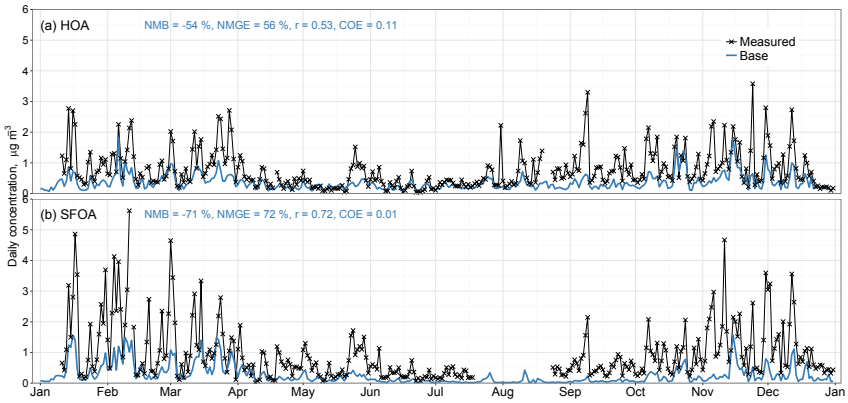

Figure 5. Time series of measured and modelled daily average concentrations of **(a)** HOA, and **(b)** SFOA at the London North Kensington urban background site, 2012, measured with the cToF-AMS (Table 3).

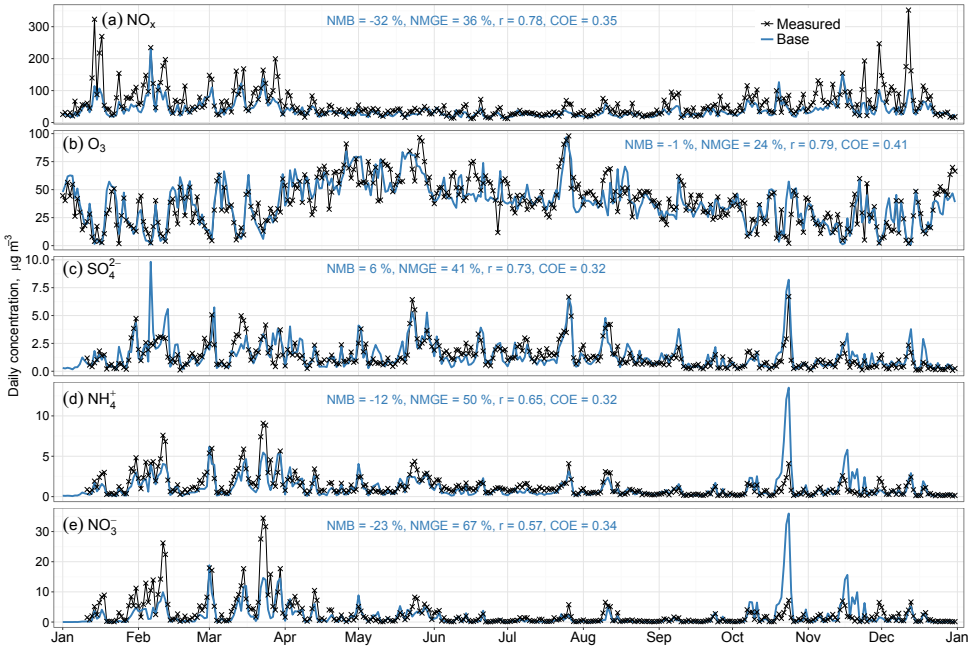

Figure 6. Time series of measured and modelled daily average concentrations of **(a)** NO_x (as NO_2), **(b)** O_3, **(c)** SO_4^{2-}, **(d)** NH_4^+, and **(d)** NO_3^- at the London North Kensington urban background site, 2012. Measurement data of NO_x and O_3 are from the UK Automated Urban and Rural Network (AURN); SO_4^{2-}, NH_4^+, and NO_3^- were measured with the cToF-AMS (Table 3).

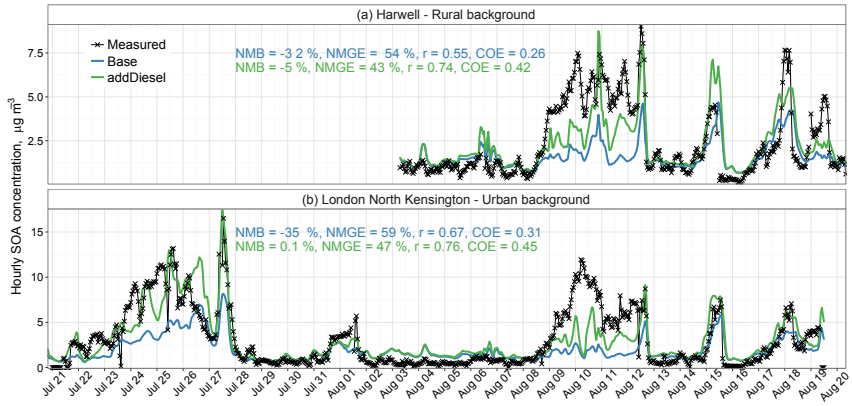

Figure 7. Time series of measured and modelled hourly average concentrations at **(a)** the Harwell rural background site, and **(b)** the London North Kensington urban background site during the summer IOP. Note the different scales on the *y* axes.

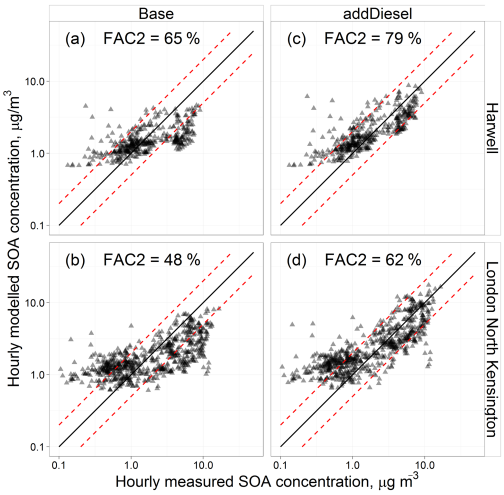

Figure 8. Scatter plots of measured and modelled hourly SOA concentrations during the summer 2012 IOP: **(a)** Base simulation at the Harwell rural background site; **(b)** Base simulation at the North Kensington urban background site; **(c)** addDiesel simulation at the Harwell rural background site; **(d)** addDiesel simulation at the North Kensington urban background site. The straight lines are the 2 : 1, 1 : 1, and 1 : 2 lines.

centrations (for example, the simulated minimum during the measured maximum at North Kensington) is caused by the shifting of this narrow ASOA plume in space (Fig. 10b). On 12 August, this episode was also subject to SOA contribution from Europe (Fig. 12d).

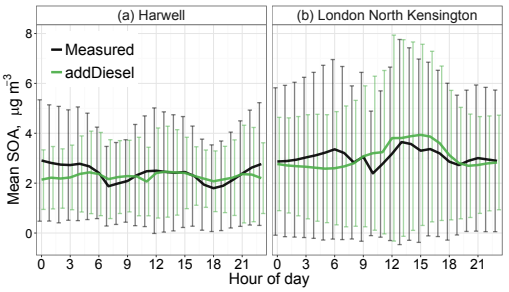

Figure 9. Average hourly profiles of modelled (addDiesel experiment) and measured SOA during the summer IOP. Also shown are the standard deviations for each mean value.

During the period of overlapping measurements at Harwell and North Kensington (3–18 August), both the measurements and the model agree with a modest rural to urban increase. Average measured SOA concentrations were 2.4 and 2.6 µg m^{-3} for Harwell and North Kensington, respectively, whilst average modelled concentrations were 2.3 and 2.5 µg m^{-3} (for the addDiesel experiment).

3.3 Hourly comparison of secondary OA: winter IOP

Both the Detling and London North Kensington sites exhibit good model–measurement hourly correlation ($r = 0.63$ and 0.64, addDiesel run; Fig. 13). The addDiesel run decreases the NMB for SOA at these sites from −59 to −30 % for Detling, and from −24 to 8 % for London North Kensington. This means that ∼ 30 % of SOA at these sites during this period can be explained by diesel IVOCs. In Detling, there is also a pronounced improvement in the COE,

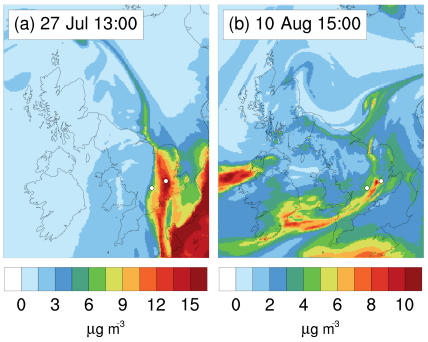

Figure 10. Modelled (addDiesel experiment) hourly concentrations of SOA at the time of the maximum measured hourly SOA value at the London North Kensington site during the first and second SOA episodes of the summer IOP. The white circles mark the measurement site locations – left: Harwell; right: London North Kensington.

from 0.10 to 0.31. In North Kensington, the COE was already high but is increased from 0.27 to 0.30. It can be seen in Fig. 13 as well as Fig. 14 that lower concentrations of SOA (19—27 January) are overestimated by the model. This overestimation is caused by the very simplified method of including missing sources of OA using a constant concentration of 0.4 µg m^{-3} (which is assumed to be highly oxygenated and is therefore included under modelled SOA). As a constant, this background OA does not currently go through atmospheric emission-removal processes in the model. However, the period in question exhibited snowfall, removing much of the aerosol (as can be seen from the very low concentrations measured in both Detling and London North Kensington). Explicit inclusion of additional missing biogenic sources of OA to the model is already part of ongoing development of the model and will be presented in future studies.

During the ClearfLo Winter IOP, measured SOA concentrations were higher in Detling than in North Kensington (Fig. 13). This is correctly captured by the simulations and is caused by a steep positive gradient of concentrations from southern England across to the near European continent (Fig. 15). The measured Detling / North Kensington SOA ratio (ratio of average concentrations for this period) was 1.8, while the modelled ratio was 1.1, so the model correctly simulates the direction of the spatial gradient, but underestimates its magnitude. For North Kensington, the model also captures that SOA concentrations are lower on 5 February than on 4 February. In Detling, however, measured concentrations were higher on 5 February, which the model does not reproduce. During the night of 4–5 February, the wind was very strong (> 10 m s^{-1}) and there was a small shift between the measured wind direction and the wind direction input to EMEP4UK from WRF. As a consequence, the simulated pollution plume was shifted too much to the east (Fig. 15b), causing the model–measurement discrepancy on this particular occasion.

Even though the additional diesel IVOCs noticeably increased the modelled SOA concentrations during the winter IOP, there is still a marked underestimation of elevated measured SOA concentrations during 15–19 January and 30 January–4 February. During these periods, the observed temperature was colder than the average temperature of the winter IOP (Crilley et al., 2015) and peaks in measured SOA also coincide with elevated concentrations of SFOA (Figs. 5b and 13b). As our modelled SFOA is underestimated by a factor of 4 (NMB of −72 %), it is likely that (i) SOA precursor VOC emissions from domestic heating are also underestimated, and (ii) adding missing IVOCs from this emission sector would contribute to the modelled SOA during these periods. It has been recently shown by Denier van der Gon et al. (2015) that the emission factors used by different European countries for wood combustion PM emissions, even for the same appliance type, can differ by a factor of 5. They constructed a revised inventory, in which each country's emission was updated using an unified emission factor. This resulted in increases of PM (and estimated accompanying IVOC) emission estimates for most countries. Furthermore, London is a *smoke control area* and therefore no residential emissions of SFOA are assumed by the national emissions inventory. Recent studies have, however, suggested that there are indeed local sources of SFOA in London (Crilley et al., 2015; Young et al., 2015a).

3.4 Daily and seasonal secondary OA: annual data set

Time series of daily averaged modelled and measured SOA concentrations for the whole year are shown in Fig. 16. Table 4 gives daily modelled vs. measured SOA evaluation statistics during different seasons at the North Kensington site. Values for autumn are presented with and without the two extreme points (size of the data set $n = 91$ and $n = 89$).

For the daily model–measurement comparison, spring has the highest correlation ($r = 0.85$, both Base and addDiesel; Table 4). This can also be seen from the time series (Fig. 16: March–May) where both model simulations follow most of the measured peaks. The Base run r value for spring was already high, but, nevertheless, the addDiesel run shows a marked improvement for all other model evaluation statistics. FAC2 is increased by 10 %, COE is increased to 0.39, NMB is reduced by 35 %, and NMGE is reduced by 7 %. The NMGE of 38 % remaining in the addDiesel model run is probably governed by uncertainties in meteorology, as well as by uncertainties in the temporal and spatial variability of emissions. During summer, the model captures the majority of the periods of increased SOA mass well (e.g. 28 June, 22–29 July, 15 and 20 August; Fig. 16: June–August), but there is some model underestimation when SOA concentrations were lower (< 2 µg m^{-3}). As for spring, the addDiesel experiment improves all model evaluation statistics. More detailed

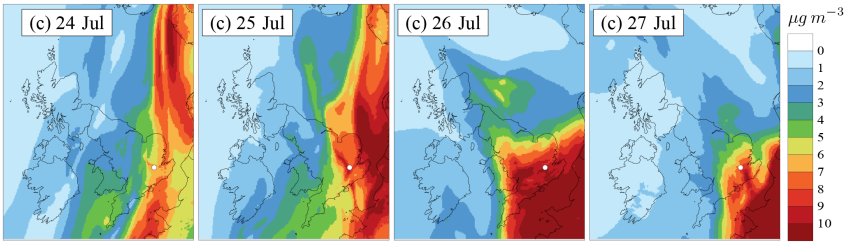

Figure 11. Modelled (addDiesel experiment) daily average concentrations of SOA during the first SOA episode of the summer 2012 IOP. The white circle indicates the location of London North Kensington.

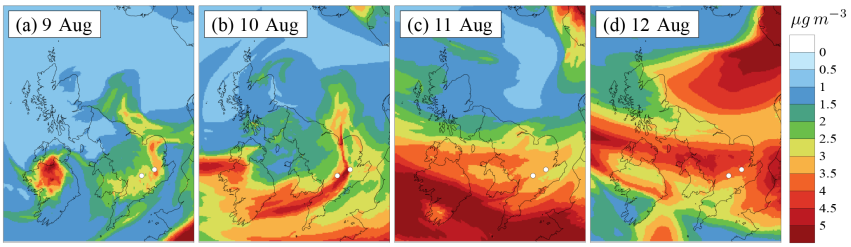

Figure 12. Modelled (addDiesel experiment) daily average concentrations of SOA during the second SOA episode of the summer 2012 IOP. The white circles mark the measurement site locations – left: Harwell; right: London North Kensington.

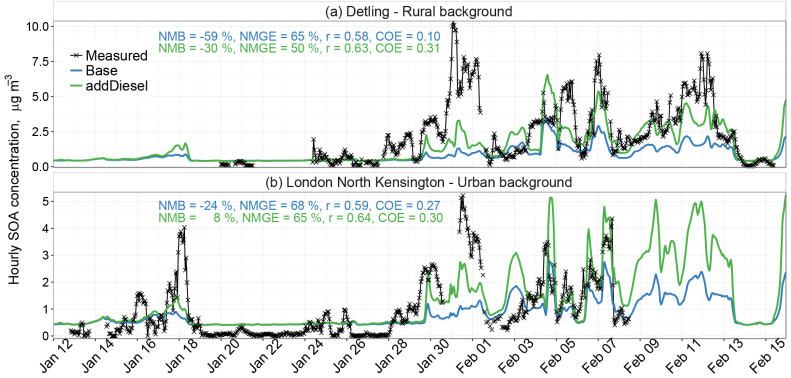

Figure 13. Time series of measured and modelled hourly average concentrations at **(a)** the Detling rural background site, and **(b)** the London North Kensington urban background site during the winter 2012 IOP. Note the different scales on the *y* axes.

hourly analysis of the SOA concentrations during the summer IOP (end of July to August) was presented in Sect. 3.2.

The model performance is less good in autumn than during the other seasons. There are some days where the Base case scenario overestimates measured SOA (23–25 October, 21 and 24 November) with the addDiesel run increasing this further. During these days, particle nitrate (NO_3^-) and ammonium (NH_4^+) are also substantially overestimated by the model (Fig. 6). This suggests that the overestimations are likely caused by errors occurring during this period in the meteorological forecasts, e.g. missed rain events, rather than by uncertainties in the formation of secondary organic aerosol specifically.

The model evaluation statistics for autumn are strongly influenced by the two modelled values on 23 and 24 October (Table 4). Removing these two values reduces the seasonal

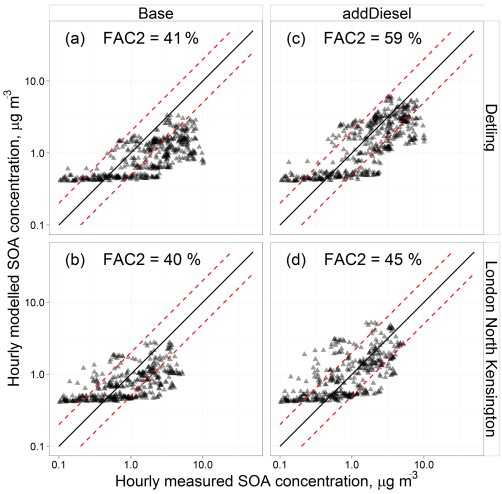

Figure 14. Scatter plots of measured and modelled hourly SOA concentrations during the winter 2012 IOP: **(a)** Base simulation at the Detling rural background site; **(b)** Base simulation at the North Kensington urban background site; **(c)** addDiesel simulation at the Detling rural background site; **(d)** addDiesel simulation at the North Kensington urban background site. The straight lines are the 2 : 1, 1 : 1, and 1 : 2 lines.

Table 4. Model–measurement comparison statistics for daily SOA at London North Kensington. Autumn is presented with and without the two outliers (23 and 24 October $n = 91$ and 89, respectively).

	Base	addDiesel	Base	addDiesel
	spring (MAM)		summer (JJA)	
n (days)	91		86	
FAC2	64 %	74 %	60 %	79 %
NMB	−35 %	0.1 %	−34 %	−5 %
NMGE	45 %	38 %	48 %	39 %
r	0.85	0.85	0.71	0.82
COE	0.29	0.39	0.26	0.41
	autumn (SON)		winter (JFD)	
n (days)	89		81	
FAC2	82 %	74 %	70 %	69 %
NMB	−2 %	58 %	−28 %	6 %
NMGE	52 %	96 %	47 %	61 %
r	0.38	0.28	0.40	0.40
COE	−0.13	−1.07	0.21	−0.02
	autumn (SON)			
n (days)	91			
FAC2	80 %	73 %		
NMB	13 %	102 %		
NMGE	63 %	137 %		
r	0.58	0.54		
COE	−0.30	−1.84		

average SOA concentration modelled with the addDiesel run by 33 % (2.0 and 1.5 µg m^{-3} with and without these two points, respectively). Their combined influence on the annual average modelled concentration is 8 %, which is substantially more than any other points of the annual data set.

For the winter months, modelled concentrations in January are much lower than measurements, whereas in February the timing of several peaks is well reproduced and even overestimated by the addDiesel experiment. Detailed hourly analysis of the SOA concentrations during the winter IOP has been presented in Sect. 3.3. In December, measured SOA concentrations were much lower than in January, and even though the model captures the highest peak, there is some overestimation in the lowest range (< 0.5 µg m^{-3}).

Figure 17 shows annually and seasonally averaged measured and modelled SOA. The difference between the Base and addDiesel experiments illustrate the impact of missing IVOC emissions from diesel traffic on SOA formation. As was discussed before, and can be seen from Table 4, IVOC precursors from diesel vehicles reduce the NMB by ∼ 30 %, which as an annual average is 0.6 µg m^{-3} of additional SOA. Moreover, the 90th percentile of daily averaged SOA concentrations of the addDiesel experiment is 3.8 µg m^{-3} (which is similar to the measured 90th percentile of 3.2 µg m^{-3}), whereas the 90th percentile of the Base case simulation is 2.2 µg m^{-3}. This means that (i), on 36 days of the year, SOA is a notable component of PM (the annual average $PM_{2.5}$ concentration limit value of the European Union Directive 2008/50/EC is 25 µg m^{-3}) and that (ii), during those days, the relative contribution to SOA from diesel IVOCs could be greater than 40 % (calculated as the difference between SOA modelled with addDiesel and Base, relative to addDiesel: (addDiesel-Base)/addDiesel). We note that Fig. 17a shows in the addDiesel simulation that the modelled BSOA + Background OA still makes up 53 % of the SOA, as an annual average. This value is based on the assignment of the constant background OA in the model to natural SOA, which is what it is intended to represent. This may have some anthropogenic origin, and more research on the missing (or boundary condition) sources that this background constant represents is needed for accurate attribution of the biogenic vs. anthropogenic relative contributions.

3.5 OM / OC ratios

Measured OM / OC ratios for SOA were generally higher than those modelled (1.99–2.34 vs. 1.88–1.97, Table 5). Nevertheless, the measured OM / OC ratio at London North Kensington during the summer IOP was the lowest of the measured range, 1.99, which is a close match to modelled SOA OM / OC ratio for that period, 1.97. Model performance for spring and summer was shown to be very good, but

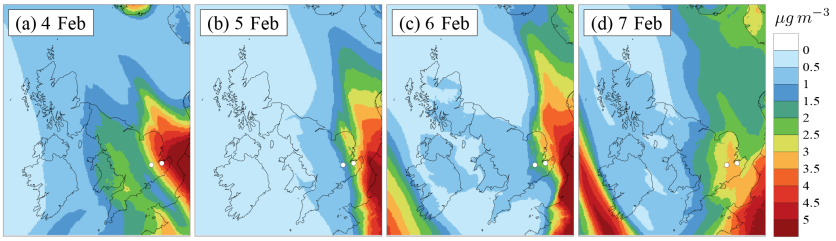

Figure 15. Modelled (addDiesel experiment) daily average concentrations of SOA during the second SOA episode of the winter 2012 IOP. The white circles mark the measurement site locations – left: London North Kensington; right: Detling.

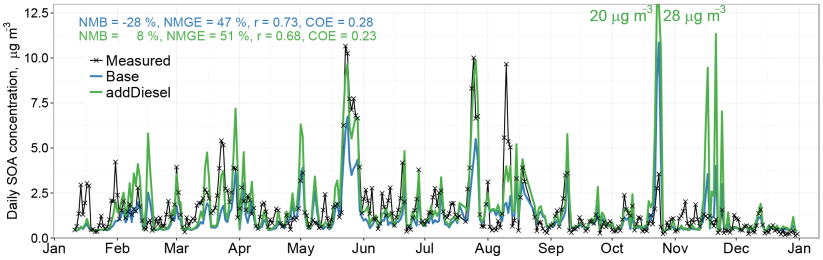

Figure 16. Time series of measured and modelled daily average SOA concentrations at the London North Kensington urban background site. The two outliers (23 and 24 October, included in the plot as labels) are excluded from the model evaluation statistics presented in the plot.

Table 5. Measured and modelled (addDiesel experiment) OM / OC ratios. Site name abbreviations are given in Table 3.

Pollutant	Site	Period	Meas. OM / OC	Mod. OM / OC
HOA	NK	winter IOP	1.25	1.25
	NK	summer IOP	1.19	
	NK	annual	1.32	
	HAR	summer IOP	1.31	
	DET	winter IOP	1.45	
SFOA	NK	winter IOP	1.62	1.70
	NK	annual	1.78	
	DET	winter IOP	1.64	
SOA	NK	winter IOP	2.03	1.88
	NK	summer IOP	1.99	1.97
	NK	annual	2.25	1.94
	HAR	summer IOP	2.39	1.99
	DET	winter IOP	2.34	1.86

it is possible that the missing SOA precursors in the colder months (from domestic heating) could yield SOA with higher initial OM / OC ratios, thereby increasing the annual average value. Furthermore, wintertime simulations of SOA in Paris by Fountoukis et al. (2016) also showed large underestimations, and they speculated that this could be pointing towards an SOA formation process during periods of low photochemical activity that is currently not simulated in atmospheric chemical transport models.

3.6 Comparison to the previous (IVOCs = 1.5 × POA) approach

Figure 18 shows the annual average HOA, SFOA, BSOA and background OA (BGND OA), and ASOA concentrations at London North Kensington modelled with different assumptions for additional IVOC emissions. As was explained in Sect. 2.4, for the UK, the addDiesel experiment adds 90 Gg of diesel-related IVOCs proportionally to road transport emissions (SNAP7), whereas the IVOCs = 1.5 × POA approach only adds 5 Gg to SNAP7 and another 26 Gg to other sectors (mainly to SNAP2: residential and non-industrial combustion). Therefore, our approach creates a considerably larger amount of SOA from IVOCs (and only from diesel-related IVOCs) than the previous method. The 1.5volPOA experiment was undertaken using the semi-volatile treatment of POA emissions. This means that the modelled ASOA from this experiment also includes aged semi-volatile POA, possibly giving it potential to create more ASOA than the Base or addDiesel experiments (the organic material added to the model in the 1.5volPOA experiment is 1.0 × POA (as SVOCs) + 1.5 × POA (IVOCs) = 2.5 × POA as introduced by Robinson et al. (2007) and Shrivastava et al. (2008)). It

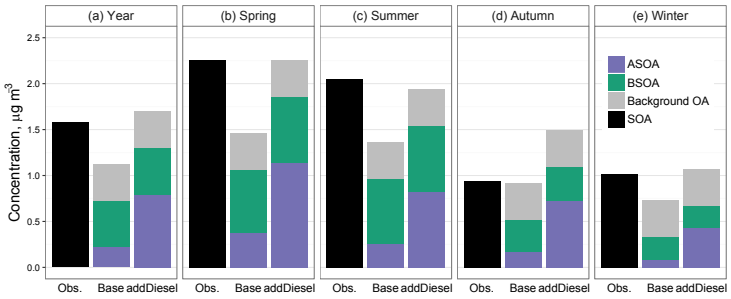

Figure 17. Annually and seasonally averaged measured and modelled concentrations of SOA at the London North Kensington site.

can be seen from Fig. 18a and b that treating POA as semi-volatile leads to much lower concentrations than the non-volatile treatment (which already underestimates measured concentrations of HOA and SFOA by -54 and $-71\,\%$, respectively; Fig. 5). This is not surprising given that the semi-volatile treatment of POA assigns only $3\,\% + 6\,\% + 9\,\%$ of the POA to the three lowest volatility bins with saturation concentrations of 0.01, 0.1, and $1\,\mu g\,m^{-3}$, respectively (as given in Sect. 2.4). In a study in Mexico City, Shrivastava et al. (2011) revised this treatment by assuming much higher total semi-volatile and intermediate-volatility POA emissions: $7.5\times$ the inventory emissions of (particulate) POA. This was justified by the fact that their emission factors of POA were derived from measurements at urban background sites, but, following Robinson et al. (2007), two-thirds of POA would have evaporated by then. Recently, Shrivastava et al. (2015) also used this factor of 7.5 in global simulations. Emission factors used in European inventories are, however, taken from tailpipe measurements with concentrations sufficiently high that most of the semi-volatiles should still be reported in the particulate phase. Therefore the further underestimation of HOA and SFOA concentrations with the volatile treatment could be due to a number of issues: (i) a systematic underestimation of emissions, but for a different reason than in Shrivastava et al. (2011); (ii) the volatility of POA is overestimated by Robinson et al. (2007), or (iii) the evaporation of semi-volatile POA emission is too rapid in the model (instantaneous in our set-up).

Figure 18c shows that the lower HOA and SFOA concentrations lead to a very small negative change for the absorptive partitioning of BSOA. Finally, it can be seen from the annual average concentrations of ASOA in Fig. 18d that including aged SVOCs and IVOCs in the simulation doubles the modelled ASOA concentration compared to the Base case scenario (ASOA from officially reported anthropogenic VOCs) but that the ASOA in our 1.5volPOA experiment is still much lower than simulated with our addDiesel experiment.

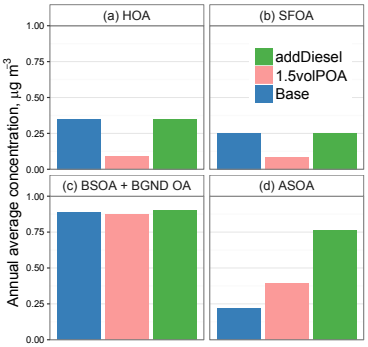

Figure 18. Simulated annual and seasonal average concentrations of OA components (BGND OA stands for background OA) for the London North Kensington site of three different model experiments: Base – all emissions as in officially reported emissions inventories, and POA is treated as non-volatile; 1.5volPOA – semi-volatile treatment of POA + IVOC emissions added as $1.5\times$ POA; addDiesel – Base + IVOC emissions from diesel traffic added proportionally to VOC emissions from the on-road traffic source sector (SNAP7). The last two additions are as described in the main text.

4 Discussion

We show that $\sim 30\,\%$ of SOA in London could be produced from completely new estimates of diesel-related IVOC emissions that are not currently included in the emissions inventories. This is one of a very few studies where IVOC emissions are added proportionally to NMVOC emissions (as opposed to addition proportionally to POA emissions). Moreover, previous studies have added IVOCs proportionally to POA from all sources, whereas this study focuses specifically on the impact of diesel IVOCs from on-road traffic emissions (IVOCs $= 2.3\times$ SNAP7 VOCs). There is reason to believe that higher-volatility VOCs are better represented in current emissions inventories than the emissions of PM. Also, the official inventories do not provide the individual contribu-

tion of POA to total PM. Therefore, the addition of IVOCs proportionally to NMVOCs may be better constrained than the POA-based approach used in studies so far. The additional emissions are also tied directly to the relevant emission source category.

There are several possible uncertainties in our estimate of additional IVOCs, and subsequent SOA production and ageing. As a first approximation, we added IVOCs to each European country based on our measurements in London. This was justified as the diesel usage in the UK is similar to the European average. Furthermore, different European countries might be using different emissions factors for their estimates of NMVOCs from petrol and diesel or have a different average fleet age than the UK. It should be noted that two of the most populous countries in Europe – France and Germany – both have a higher diesel penetration than the UK ,and therefore for western central Europe our addition is rather conservative.

It was seen from the hourly profiles at the London North Kensington site during the summer IOP (Fig. 9b) that both the model and the measurements exhibit a small diurnal cycle (peaking in the afternoon). Even though somewhat counter-intuitive (as most of the SOA chemistry is photochemically driven through reaction with the OH radical), an absence of a strong diurnal cycle of SOA has been seen in many European studies (Zhang et al., 2013; Fountoukis et al., 2014; Young et al., 2015a). A relatively small daytime increase in SOA could be explained by the expansion of the boundary layer height (Xu et al., 2015), as well as by contributions from long-range transport. PMF measurements of SOA in Mexico City, on the other hand, revealed a very strong diurnal cycle, peaking around midday (Shrivastava et al., 2011). The fact that during the summer IOP our addDiesel experiment exhibits a slightly stronger diurnal cycle than the measurements (with daytime values slightly overestimated and nighttime underestimated) indicates that the SOA yields could be too high. We assumed an SOA density of $1.5\,\mathrm{g\,cm^{-3}}$ and increased the yields linearly, as has been done in all other ACTM studies. Actually, increasing the assumed density of SOA from the unit value ($1\,\mathrm{g\,cm^{-3}}$) changes the total C_{OA} (condensed-phase OA) on the Odum mass yield plots (Odum et al., 1996) used to derive the yields from the chamber experiment. Therefore, increasing the yields linearly is not exactly correct (N. M. Donahue, personal communication, 2015) and further studies and refinement into the calculation of SOA yields and density would be beneficial.

We use an ageing rate of $4.0 \times 10^{-12}\,\mathrm{cm^3\,molecule^{-1}\,s^{-1}}$ for both ASOA and BSOA (Lane et al., 2008). This is slower than has been used in some other studies (for example, Tsimpidi et al., 2010, use $4.0 \times 10^{-11}\,\mathrm{cm^3\,molecule^{-1}\,s^{-1}}$, which is 10 times faster, and Fountoukis et al., 2011, use $1.0 \times 10^{-11}\,\mathrm{cm^3\,molecule^{-1}\,s^{-1}}$, which is 2.5 times faster). A combination of lower initial SOA yields but slightly higher ageing rates could possibly flatten the diurnal cycle of our modelled SOA, matching the measurements better. Therefore, an improvement for the detailed, hourly evolution could be achieved by a sensitivity study of these yields and ageing rates. This does not, however, change the main scope and results of this paper which illustrate the relative impact of the diesel IVOCs on SOA formation.

In the current set-up of the EMEP model, only two PM size fractions are simulated – $PM_{2.5}$ and $PM_{2.5-10}$ – because only two fractions are included in the emissions inventories for PM used in this study. Even though on an annual basis 90 % of $OC_{2.5}$ is in the submicron (OC_1) range (Sect. 2.6), the comparison between a modelled $OC_{2.5}$ and a measured OC_1 could be introducing larger errors during specific days or hours. Therefore, as AMS measurements become more prevalent, emissions inventories should be reported for all three size classes, PM_1, $PM_{1-2.5}$, and $PM_{2.5-10}$. This would allow the model to partition SOA into the corresponding fractions, making the direct comparison of modelled SOA_1 to measured SOA_1 possible.

We showed that treating POA as semi-volatile and letting it evaporate led to a great underestimation of HOA and SFOA concentrations compared to measurements at the London North Kensington urban background site. As has been highlighted by a number studies before us (listed in the Introduction), we would also emphasize that a major source of uncertainty in OA modelling is the volatility of primary emissions, an issue that is currently not addressed by official emissions inventories. In our experiment of semi-volatile POA (denoted 1.5volPOA), IVOCs were included from all source sectors. This experiment simulated substantially less ASOA than our addition of IVOCs associated with just the traffic source sector. This means that a combination of the POA-based IVOCs and our addition of diesel IVOCs proportional to NMVOCs would not create a substantial overestimation of SOA concentrations compared to measurements. Nevertheless, further modelling studies (including different assumptions regarding ageing rates, fragmentation, and yields) as well as more measurements of IVOC emissions from different sources are clearly necessary.

In the evaluation of modelled and measured SOA, it was shown that some of the uncertainties in the modelled concentrations are caused by errors in modelled wind vectors. Nevertheless, the underlying meteorological model works well (as demonstrated by comparisons of different pollutants for the whole calendar year), and overall the errors caused by meteorology are believed to be relatively smaller than those introduced by emissions (amount, volatility, composition), or SOA yields and ageing rates.

5 Conclusions

This study presents annual time series of new high-resolution simulations of SOA formation over the UK (using the EMEP4UK Eulerian atmospheric chemical transport model) that include diesel-related IVOC emissions not currently in-

cluded in the emissions inventory. The derivation of the magnitude of these additional emissions of SOA precursors and the evaluation of the model simulated SOA were both based on measurements made during the Clean Air for London (ClearfLo) campaign in 2012. The IVOC emissions were added in proportion to the VOC emissions from the specifically relevant on-road traffic source, in contrast to previous studies that have added IVOCs proportionally to primary organic aerosol (POA) emissions from all POA sources. Modelled concentrations of SOA were compared with positive matrix factorization (PMF) analyses of aerosol mass spectrometer (AMS) measurements at a central London urban background location (North Kensington) and at the Detling and Harwell rural background locations outside of London.

The model performance in comparison to relatively more well-known components of air pollution, such as NO_x, O_3, and secondary inorganic aerosol, was shown to be very good, providing confidence in the prediction skill of the ACTM system used. Modelled concentrations of SOA were evaluated in four groups: (i) hourly comparison during a summer IOP (intensive observation period), (ii) hourly comparison during a winter IOP, (iii) daily comparison for a full calendar year (including seasonal statistics), and (iv) comparison of OM / OC ratios of all apportioned OA components. To our knowledge, this is the first study where modelled OA components are compared with a year-long data set of PMF-apportioned AMS measurements.

During the period of concurrent measurements at all locations, SOA concentrations at the Detling rural background location were greater than at the central London location. The model showed that this was caused by an intense pollution plume with a strong gradient of SOA from mainland Europe passing over the rural location and demonstrates how short periods of measurements can give a different picture compared with longer-term measurements, as well as the value of atmospheric chemistry transport modelling for supporting the interpretation of measurements taken at different sites or for short durations.

The model simulations show that these estimates of diesel-related IVOCs could explain on average $\sim 30\,\%$ of the annual SOA in and around London. The 90th percentile of modelled daily SOA concentrations at the urban background site for the whole year was $3.8\,\mu g\,m^{-3}$, and the influence of missing diesel-related IVOC precursors was even greater on high percentile SOA days than its contribution to annual average SOA. The magnitudes of these contributions to SOA provide strong additional support for the need to undertake further refinement of the amount and speciation of these precursor emissions for inclusion in official emissions inventories.

Data availability

Processed measurement data used in this study are available through the ClearfLo project archive at the British Atmospheric Data Centre (http://badc.nerc.ac.uk/browse/badc/clearflo). The model data (input, code, relevant output) are archived at the University of Edinburgh, and Centre for Ecology&Hydrology and are available on request.

Acknowledgements. The authors acknowledge the UK Department for Environment, Food and Rural Affairs (Defra) and the Devolved Administrations for several projects: development of the EMEP4UK model (AQ0727); access to the AURN data, which were obtained from uk-air.defra.gov.uk and are subject to Crown 2014 copyright, Defra, licensed under the Open Government Licence (OGL); and partial support for the aerosol measurements. Partial support for the EMEP4UK modelling from the European Commission FP7 ECLAIRE project is gratefully acknowledged. This work was supported in part by the UK Natural Environment Research Council (NERC) ClearfLo project (grant ref. NE/H008136/1). Riinu Ots was supported by a PhD studentship (University of Edinburgh and NERC-CEH contract 587/NEC03805). Dominique E. Young was supported by a NERC PhD studentship (ref. NE/I528142/1). Rachel E. Dunmore was supported by a NERC PhD studentship (ref. NE/J500197/1). Nga L. Ng, Lu Xu, Leah R. Williams, and Scott C. Herndon were supported by the US Department of Energy (grant no. DE-SC000602). The authors would like to thank David Simpson for helpful advice about the EMEP model.

NCAR command language (NCL) was used to produce the maps (NCAR, 2015), and R, openair, and ggplot2 were used for the analysis and all other plots (R Core Team, 2014; Carslaw and Ropkins, 2012; Wickham, 2009).

Edited by: M. Kanakidou

References

Aiken, A. C., DeCarlo, P. F., Kroll, J. H., Worsnop, D. R., Huffman, J. A., Docherty, K. S., Ulbrich, I. M., Mohr, C., Kimmel, J. R., Sueper, D., Sun, Y., Zhang, Q., Trimborn, A., Northway, M., Ziemann, P. J., Canagaratna, M. R., Onasch, T. B., Alfarra, M. R., Prevot, A. S. H., Dommen, J., Duplissy, J., Metzger, A., Baltensperger, U., and Jimenez, J. L.: O / C and OM / OC Ratios of Primary, Secondary, and Ambient Organic Aerosols with High-Resolution Time-of-Flight Aerosol Mass Spectrometry, Environ. Sci. Technol., 42, 4478–4485, doi:10.1021/es703009q, 2008.

Aksoyoglu, S., Keller, J., Barmpadimos, I., Oderbolz, D., Lanz, V. A., Prévôt, A. S. H., and Baltensperger, U.: Aerosol modelling in Europe with a focus on Switzerland during summer and winter episodes, Atmos. Chem. Phys., 11, 7355–7373, doi:10.5194/acp-11-7355-2011, 2011.

Allan, J. D., Williams, P. I., Morgan, W. T., Martin, C. L., Flynn, M. J., Lee, J., Nemitz, E., Phillips, G. J., Gallagher, M. W., and Coe, H.: Contributions from transport, solid fuel burning and cooking to primary organic aerosols in two UK cities, Atmos. Chem. Phys., 10, 647–668, doi:10.5194/acp-10-647-2010, 2010.

AQEG: Report: Fine Particulate Matter ($PM_{2.5}$) in the United – Defra, UK, http://uk-air.defra.gov.uk/library/reports?report_id=727 (last access: 24 May 2016), 2012.

Atkinson, R. and Arey, J.: Atmospheric Degradation of Volatile Organic Compounds, Chem. Rev., 103, 4605–4638, doi:10.1021/cr0206420, 2003.

Bahreini, R., Middlebrook, A. M., de Gouw, J. A., Warneke, C., Trainer, M., Brock, C. A., Stark, H., Brown, S. S., Dube, W. P., Gilman, J. B., Hall, K., Holloway, J. S., Kuster, W. C., Perring, A. E., Prevot, A. S. H., Schwarz, J. P., Spackman, J. R., Szidat, S., Wagner, N. L., Weber, R. J., Zotter, P., and Parrish, D. D.: Gasoline emissions dominate over diesel in formation of secondary organic aerosol mass, Geophys. Res. Lett., 39, L06805, doi:10.1029/2011GL050718, 2012.

Berg, A. R., Heald, C. L., Huff Hartz, K. E., Hallar, A. G., Meddens, A. J. H., Hicke, J. A., Lamarque, J., and Tilmes, S.: The impact of bark beetle infestations on monoterpene emissions and secondary organic aerosol formation in western North America, Atmos. Chem. Phys., 13, 3149–3161, doi:10.5194/acp-13-3149-2013, 2013.

Bergström, R., Denier van der Gon, H. A. C., Prévôt, A. S., Yttri, K. E., and Simpson, D.: Modelling of organic aerosols over Europe (2002–2007) using a volatility basis set (VBS) framework: application of different assumptions regarding the formation of secondary organic aerosol, Atmos. Chem. Phys., 12, 8499–8527, doi:10.5194/acp-12-8499-2012, 2012.

Bergström, R., Hallquist, M., Simpson, D., Wildt, J., and Mentel, T. F.: Biotic stress: a significant contributor to organic aerosol in Europe?, Atmos. Chem. Phys., 14, 13643–13660, doi:10.5194/acp-14-13643-2014, 2014.

Binkowski, F. S. and Shankar, U.: The Regional Particulate Matter Model: 1. Model description and preliminary results, J. Geophys. Res.-Atmos., 100, 26191–26209, doi:10.1029/95JD02093, 1995.

Bohnenstengel, S. I., Belcher, S. E., Aiken, A., Allan, J. D., Allen, G., Bacak, A., Bannan, T. J., Barlow, J. F., Beddows, D. C. S., Bloss, W. J., Booth, A. M., Chemel, C., Coceal, O., Di Marco, C. F., Dubey, M. K., Faloon, K. H., Fleming, Z. L., Furger, M., Gietl, J. K., Graves, R. R., Green, D. C., Grimmond, C. S. B., Halios, C. H., Hamilton, J. F., Harrison, R. M., Heal, M. R., Heard, D. E., Helfter, C., Herndon, S. C., Holmes, R. E., Hopkins, J. R., Jones, A. M., Kelly, F. J., Kotthaus, S., Langford, B., Lee, J. D., Leigh, R. J., Lewis, A. C., Lidster, R. T., Lopez-Hilfiker, F. D., McQuaid, J. B., Mohr, C., Monks, P. S., Nemitz, E., Ng, N. L., Percival, C. J., Prévôt, A. S. H., Ricketts, H. M. A., Sokhi, R., Stone, D., Thornton, J. A., Tremper, A. H., Valach, A. C., Visser, S., Whalley, L. K., Williams, L. R., Xu, L., Young, D. E., and Zotter, P.: Meteorology, Air Quality, and Health in London: The ClearfLo Project, B. Am. Meteorol. Soc., 96, 779–804, doi:10.1175/BAMS-D-12-00245.1, 2014.

Cames, M. and Helmers, E.: Critical evaluation of the European diesel car boom – global comparison, environmental effects and various national strategies, Environ. Sci. Europe, 25, 1–22, doi:10.1186/2190-4715-25-15, 2013.

Canagaratna, M. R., Jayne, J., Jimenez, J., Allan, J., Alfarra, M., Zhang, Q., Onasch, T., Drewnick, F., Coe, H., Middlebrook, A., Delia, A., Williams, L., Trimborn, A., Northway, M., DeCarlo, P., Kolb, C., Davidovits, P., and Worsnop, D.: Chemical and microphysical characterization of ambient aerosols with the aerodyne aerosol mass spectrometer, Mass Spectrom. Rev., 26, 185–222, doi:10.1002/mas.20115, 2007.

Canagaratna, M. R., Jimenez, J. L., Kroll, J. H., Chen, Q., Kessler, S. H., Massoli, P., Hildebrandt Ruiz, L., Fortner, E., Williams, L. R., Wilson, K. R., Surratt, J. D., Donahue, N. M., Jayne, J. T., and Worsnop, D. R.: Elemental ratio measurements of organic compounds using aerosol mass spectrometry: characterization, improved calibration, and implications, Atmos. Chem. Phys., 15, 253–272, doi:10.5194/acp-15-253-2015, 2015.

Carslaw, D. C. and Ropkins, K.: openair – An R package for air quality data analysis, Environ. Model. Softw., 27–28, 52–61, doi:10.1016/j.envsoft.2011.09.008, 2012.

CEIP: WebDab EMEP database: Emissions as used in EMEP models, http://www.ceip.at/ms/ceip_home1/ceip_home/webdab_emepdatabase/, last access: 15 July 2015.

Chhabra, P. S., Flagan, R. C., and Seinfeld, J. H.: Elemental analysis of chamber organic aerosol using an aerodyne high-resolution aerosol mass spectrometer, Atmos. Chem. Phys., 10, 4111–4131, doi:10.5194/acp-10-4111-2010, 2010.

Crilley, L. R., Bloss, W. J., Yin, J., Beddows, D. C. S., Harrison, R. M., Allan, J. D., Young, D. E., Flynn, M., Williams, P., Zotter, P., Prevot, A. S. H., Heal, M. R., Barlow, J. F., Halios, C. H., Lee, J. D., Szidat, S., and Mohr, C.: Sources and contributions of wood smoke during winter in London: assessing local and regional influences, Atmos. Chem. Phys., 15, 3149–3171, doi:10.5194/acp-15-3149-2015, 2015.

Denier van der Gon, H. A. C., Bergström, R., Fountoukis, C., Johansson, C., Pandis, S. N., Simpson, D., and Visschedijk, A. J. H.: Particulate emissions from residential wood combustion in Europe – revised estimates and an evaluation, Atmos. Chem. Phys., 15, 6503–6519, doi:10.5194/acp-15-6503-2015, 2015.

Di Marco, C. F., Nemitz, E., Twigg, M. M., Langford, B., Lingard, J. J. N., and Ritchie, S.: Chemical characterisation of the aerosol at a background site in southern England with emphasis on the organic fraction and nitrogen compounds, in preparation, 2016.

Donahue, N. M., Robinson, A. L., Stanier, C. O., and Pandis, S. N.: Coupled Partitioning, Dilution, and Chemical Aging of Semivolatile Organics, Environ. Sci. Technol., 40, 2635–2643, doi:10.1021/es052297c, 2006.

Donahue, N. M., Epstein, S. A., Pandis, S. N., and Robinson, A. L.: A two-dimensional volatility basis set: 1. organic-aerosol mixing thermodynamics, Atmos. Chem. Phys., 11, 3303–3318, doi:10.5194/acp-11-3303-2011, 2011.

Donahue, N. M., Kroll, J. H., Pandis, S. N., and Robinson, A. L.: A two-dimensional volatility basis set – Part 2: Diagnostics of organic-aerosol evolution, Atmos. Chem. Phys., 12, 615–634, doi:10.5194/acp-12-615-2012, 2012.

Donahue, N. M., Robinson, A. L., Trump, E. R., Riipinen, I., and Kroll, J. H.: Volatility and Aging of Atmospheric Organic Aerosol, in: Atmospheric and Aerosol Chemistry, no. 339 in Topics in Current Chemistry, edited by: McNeill, V. F. and Ariya, P. A., Springer, Berlin, Heidelberg, 97–143, 2014.

Dunmore, R. E., Hopkins, J. R., Lidster, R. T., Lee, J. D., Evans, M. J., Rickard, A. R., Lewis, A. C., and Hamilton, J. F.: Diesel-related hydrocarbons can dominate gas phase reactive carbon in megacities, Atmos. Chem. Phys., 15, 9983–9996, doi:10.5194/acp-15-9983-2015, 2015.

EEA: Dieselisation in the European Economic Area, Tech. rep., http://www.eea.europa.eu/data-and-maps/figures/dieselisation-in-the-eea (last access: 24 May 2016), 2010.

EEA: EMEP/EEA air pollutant emission inventory guidebook – 2013, http://www.eea.europa.eu/publications/emep-eea-guidebook-2013 (last access: 24 May 2016), 2013.

Entec: UK ship emissions inventory, final report, Tech. rep., crown copyright, http://uk-air.defra.gov.uk/assets/documents/reports/cat15/1012131459_21897_Final_Report_291110.pdf, (last access: 24 May 2016), 2010.

Exxon Mobil: The Outlook for Energy: A view to 2040, Tech. rep., Exxon Mobil Corporation, Texas, available at: http://cdn.exxonmobil.com/~/media/global/files/outlook-for-energy/2015-outlook-for-energy_print-resolution.pdf (last access: 24 May 2016), 2014.

Fountoukis, C., Racherla, P. N., Denier van der Gon, H. A. C., Polymeneas, P., Charalampidis, P. E., Pilinis, C., Wiedensohler, A., Dall'Osto, M., O'Dowd, C., and Pandis, S. N.: Evaluation of a three-dimensional chemical transport model (PMCAMx) in the European domain during the EUCAARI May 2008 campaign, Atmos. Chem. Phys., 11, 10331–10347, doi:10.5194/acp-11-10331-2011, 2011.

Fountoukis, C., Megaritis, A. G., Skyllakou, K., Charalampidis, P. E., Pilinis, C., Denier van der Gon, H. A. C., Crippa, M., Canonaco, F., Mohr, C., Prévôt, A. S. H., Allan, J. D., Poulain, L., Petäjä, T., Tiitta, P., Carbone, S., Kiendler-Scharr, A., Nemitz, E., O'Dowd, C., Swietlicki, E., and Pandis, S. N.: Organic aerosol concentration and composition over Europe: insights from comparison of regional model predictions with aerosol mass spectrometer factor analysis, Atmos. Chem. Phys., 14, 9061–9076, doi:10.5194/acp-14-9061-2014, 2014.

Fountoukis, C., Megaritis, A. G., Skyllakou, K., Charalampidis, P. E., Denier van der Gon, H. A. C., Crippa, M., Prévôt, A. S. H., Fachinger, F., Wiedensohler, A., Pilinis, C., and Pandis, S. N.: Simulating the formation of carbonaceous aerosol in a European Megacity (Paris) during the MEGAPOLI summer and winter campaigns, Atmos. Chem. Phys., 16, 3727–3741, doi:10.5194/acp-16-3727-2016, 2016.

Fuzzi, S., Andreae, M. O., Huebert, B. J., Kulmala, M., Bond, T. C., Boy, M., Doherty, S. J., Guenther, A., Kanakidou, M., Kawamura, K., Kerminen, V., Lohmann, U., Russell, L. M., and Pöschl, U.: Critical assessment of the current state of scientific knowledge, terminology, and research needs concerning the role of organic aerosols in the atmosphere, climate, and global change, Atmos. Chem. Phys., 6, 2017–2038, doi:10.5194/acp-6-2017-2006, 2006.

Genberg, J., Hyder, M., Stenström, K., Bergström, R., Simpson, D., Fors, E. O., Jönsson, J. R., and Swietlicki, E.: Source apportionment of carbonaceous aerosol in southern Sweden, Atmos. Chem. Phys., 11, 11387–11400, doi:10.5194/acp-11-11387-2011, 2011.

Gentner, D. R., Isaacman, G., Worton, D. R., Chan, A. W. H., Dallmann, T. R., Davis, L., Liu, S., Day, D. A., Russell, L. M., Wilson, K. R., Weber, R., Guha, A., Harley, R. A., and Goldstein, A. H.: Elucidating secondary organic aerosol from diesel and gasoline vehicles through detailed characterization of organic carbon emissions, P. Natl. Acad. Sci. USA, 109, 18318–18323, doi:10.1073/pnas.1212272109, 2012.

Goldstein, A. H. and Galbally, I. E.: Known and Unexplored Organic Constituents in the Earth's Atmosphere, Enviro. Sci. Technol., 41, 1514–1521, doi:10.1021/es072476p, 2007.

Hallquist, M., Wenger, J. C., Baltensperger, U., Rudich, Y., Simpson, D., Claeys, M., Dommen, J., Donahue, N. M., George, C., Goldstein, A. H., Hamilton, J. F., Herrmann, H., Hoffmann, T., Iinuma, Y., Jang, M., Jenkin, M. E., Jimenez, J. L., Kiendler-Scharr, A., Maenhaut, W., McFiggans, G., Mentel, T. F., Monod, A., Prévôt, A. S. ., Seinfeld, J. H., Surratt, J. D., Szmigielski, R., and Wildt, J.: The formation, properties and impact of secondary organic aerosol: current and emerging issues, Atmos. Chem. Phys., 9, 5155–5236, doi:10.5194/acp-9-5155-2009, 2009.

Harrison, R. M. and Yin, J.: Sources and processes affecting carbonaceous aerosol in central England, Atmos. Environ., 42, 1413–1423, doi:10.1016/j.atmosenv.2007.11.004, 2008.

Heal, M. R., Kumar, P., and Harrison, R. M.: Particles, air quality, policy and health, Chem. Soc. Rev., 41, 6606–6630, doi:10.1039/c2cs35076a, 2012.

Hodzic, A., Jimenez, J. L., Madronich, S., Canagaratna, M. R., DeCarlo, P. F., Kleinman, L., and Fast, J.: Modeling organic aerosols in a megacity: potential contribution of semi-volatile and intermediate volatility primary organic compounds to secondary organic aerosol formation, Atmos. Chem. Phys., 10, 5491–5514, doi:10.5194/acp-10-5491-2010, 2010.

Jathar, S. H., Farina, S. C., Robinson, A. L., and Adams, P. J.: The influence of semi-volatile and reactive primary emissions on the abundance and properties of global organic aerosol, Atmos. Chem. Phys., 11, 7727–7746, doi:10.5194/acp-11-7727-2011, 2011.

Jathar, S. H., Gordon, T. D., Hennigan, C. J., Pye, H. O. T., Pouliot, G., Adams, P. J., Donahue, N. M., and Robinson, A. L.: Unspeciated organic emissions from combustion sources and their influence on the secondary organic aerosol budget in the United States, P. Natl. Acad. Sci. USA, 111, 10473–10478, doi:10.1073/pnas.1323740111, 2014.

Jimenez, J. L., Canagaratna, M. R., Donahue, N. M., Prevot, A. S., Zhang, Q., Kroll, J. H., DeCarlo, P. F., Allan, J. D., Coe, H., Ng, N. L., Aiken, A. C., Docherty, K. S., Ulbrich, I. M., Grieshop, A. P., Robinson, A. L., Duplissy, J., Smith, J. D., Wilson, K. R., Lanz, A. V., Hueglin, C., Sun, Y. L., Tian, J., Laaksonen, A., Raatikainen, T., Rautiainen, J., Vaattovaara, P., Ehn, M., Kulmala, M., Tomlinson, J. M., Collins, D. R., Cubison, M. J., Dunlea, E. J., Huffman, J. A., Onasch, T. B., Alfarra, M. R., Williams, P. I., Bower, K., Kondo, Y., Schneider, J., Drewnick, F., Borrmann, S., Weimer, S., Demerjian, K., Salcedo, D., Cottrell, L., Griffin, R., Takami, A., Miyoshi, T., Hatakeyama, S., Shimono, A., Sun, J. Y., Zhang, Y. M., Dzepina, K., Kimmel, J. R., Sueper, D., Jayne, J. T., Herndon, S. C., Trimborn, A. M., Williams, L. R., Wood, E. C., Middlebrook, A. M., Kolb, C. E., Baltensperger, U., and Worsnop, D. R.: Evolution of Organic Aerosols in the Atmosphere, Science, 326, 1525–1529, doi:10.1126/science.1180353, 2009.

Koo, B., Knipping, E., and Yarwood, G.: 1.5-Dimensional volatility basis set approach for modeling organic aerosol in CAMx and CMAQ, Atmos. Environ., 95, 158–164, doi:10.1016/j.atmosenv.2014.06.031, 2014.

Kuenen, J. J. P., Visschedijk, A. J. H., Jozwicka, M., and Denier van der Gon, H. A. C.: TNO-MACC_II emission inventory; a multi-year (2003–2009) consistent high-resolution European emission inventory for air quality modelling, Atmos. Chem. Phys., 14, 10963–10976, doi:10.5194/acp-14-10963-2014, 2014.

Lane, T. E., Donahue, N. M., and Pandis, S. N.: Simulating secondary organic aerosol formation using the volatility basis-set approach in a chemical transport model, Atmos. Environ., 42, 7439–7451, doi:10.1016/j.atmosenv.2008.06.026, 2008.

Lanz, V. A., Prévôt, A. S. H., Alfarra, M. R., Weimer, S., Mohr, C., DeCarlo, P. F., Gianini, M. F. D., Hueglin, C., Schneider, J., Favez, O., D'Anna, B., George, C., and Baltensperger, U.: Characterization of aerosol chemical composition with aerosol mass spectrometry in Central Europe: an overview, Atmos. Chem. Phys., 10, 10453–10471, doi:10.5194/acp-10-10453-2010, 2010.

Legates, D. R. and McCabe, G. J.: A refined index of model performance: a rejoinder, Int. J. Climatol., 33, 1053–1056, doi:10.1002/joc.3487, 2013.

Murphy, B. N. and Pandis, S. N.: Simulating the Formation of Semivolatile Primary and Secondary Organic Aerosol in a Regional Chemical Transport Model, Environ. Sci. Technol., 43, 4722–4728, doi:10.1021/Es803168a, 2009.

NAEI: UK Emission Mapping Methodology 2009, http://uk-air.defra.gov.uk/assets/documents/reports/cat07/1403100909_UK_Emission_Mapping_Methodology_2011-Issue_1.pdf (last access: 24 May 2016), 2013.

NCAR: A Description of the Advanced Research WRF Version 3, Tech. rep., http://www2.mmm.ucar.edu/wrf/users/docs/arw_v3.pdf (last access: 24 May 2016), 2008.

NCAR: The NCAR Command Language (Version 6.3.0) [Software], UCAR/NCAR/CISL/TDD, Boulder, Colorado, doi:10.5065/D6WD3XH5, 2015.

NCEP: NCEP FNL Operational Model Global Tropospheric Analyses, continuing from July 1999, Research Data Archive at the National Center for Atmospheric Research, Computational and Information Systems Laboratory, Boulder, CO, doi:10.5065/D6M043C6, 2000.

Ng, N. L., Canagaratna, M. R., Zhang, Q., Jimenez, J. L., Tian, J., Ulbrich, I. M., Kroll, J. H., Docherty, K. S., Chhabra, P. S., Bahreini, R., Murphhy, S. M., Seinfeld, J. H., Hildebrandt, L., Donahue, N. M., DeCarlo, P. F., Lanz, V. A., Prévôt, A. S. H., Dinar, E., Rudich, Y., and Worsnop, D. R.: Organic aerosol components observed in Northern Hemispheric datasets from Aerosol Mass Spectrometry, Atmos. Chem. Phys., 10, 4625–4641, doi:10.5194/acp-10-4625-2010, 2010.

Ng, N. L., Canagaratna, M. R., Jimenez, J. L., Zhang, Q., Ulbrich, I. M., and Worsnop, D. R.: Real-Time Methods for Estimating Organic Component Mass Concentrations from Aerosol Mass Spectrometer Data, Environ. Sci. Technol., 45, 910–916, doi:10.1021/es102951k, 2011.

Odum, J. R., Hoffmann, T., Bowman, F., Collins, D., Flagan, R. C., and Seinfeld, J. H.: Gas/Particle Partitioning and Secondary Organic Aerosol Yields, Environ. Sci. Technol., 30, 2580–2585, doi:10.1021/es950943+, 1996.

Paatero, P.: Least squares formulation of robust non-negative factor analysis, Chemometr. Intel. Labor. Syst., 37, 23–35, doi:10.1016/S0169-7439(96)00044-5, 1997.

Paatero, P. and Tapper, U.: Positive matrix factorization: A non-negative factor model with optimal utilization of error estimates of data values, Environmetrics, 5, 111–126, doi:10.1002/env.3170050203, 1994.

Pan, X., Chin, M., Gautam, R., Bian, H., Kim, D., Colarco, P. R., Diehl, T. L., Takemura, T., Pozzoli, L., Tsigaridis, K., Bauer, S., and Bellouin, N.: A multi-model evaluation of aerosols over South Asia: common problems and possible causes, Atmos. Chem. Phys., 15, 5903–5928, doi:10.5194/acp-15-5903-2015, 2015.

Passant, N. R.: Speciation of UK emissions of non-methane volatile organic compounds, Tech. rep., AEA Technology Report ENV-05452002, Culham, Abington, UK, available at: https://uk-air.defra.gov.uk/assets/documents/reports/empire/AEAT_ENV_0545_final_v2.pdf (last access: 24 May 2016), 2002.

Pöschl, U.: Atmospheric aerosols: Composition, transformation, climate and health effects, Angew. Chemie – Int. Edn., 44, 7520–7540, doi:10.1002/anie.200501122, 2005.

Presto, A. A., Miracolo, M. A., Donahue, N. M., and Robinson, A. L.: Secondary Organic Aerosol Formation from High-NO_x Photo-Oxidation of Low Volatility Precursors: n-Alkanes, Environ. Sci. Technol., 44, 2029–2034, doi:10.1021/es903712r, 2010.

Putaud, J. P., Van Dingenen, R., Alastuey, A., Bauer, H., Birmili, W., Cyrys, J., Flentje, H., Fuzzi, S., Gehrig, R., Hansson, H. C., Harrison, R. M., Herrmann, H., Hitzenberger, R., Hüglin, C., Jones, A. M., Kasper-Giebl, A., Kiss, G., Kousa, A., Kuhlbusch, T. A. J., Löschau, G., Maenhaut, W., Molnar, A., Moreno, T., Pekkanen, J., Perrino, C., Pitz, M., Puxbaum, H., Querol, X., Rodriguez, S., Salma, I., Schwarz, J., Smolik, J., Schneider, J., Spindler, G., ten Brink, H., Tursic, J., Viana, M., Wiedensohler, A., and Raes, F.: A European aerosol phenomenology – 3: Physical and chemical characteristics of particulate matter from 60 rural, urban, and kerbside sites across Europe, Atmos. Environ., 44, 1308–1320, doi:10.1016/j.atmosenv.2009.12.011, 2010.

Pye, H. O. T. and Seinfeld, J. H.: A global perspective on aerosol from low-volatility organic compounds, Atmos. Chem. Phys., 10, 4377–4401, doi:10.5194/acp-10-4377-2010, 2010.

R Core Team: R: A Language and Environment for Statistical Computing, R Foundation for Statistical Computing, Vienna, Austria, http://www.R-project.org/ (last access: 24 May 2016), 2014.

Robinson, A. L., Donahue, N. M., Shrivastava, M. K., Weitkamp, E. A., Sage, A. M., Grieshop, A. P., Lane, T. E., Pierce, J. R., and Pandis, S. N.: Rethinking organic aerosols: Semivolatile emissions and photochemical aging, Science, 315, 1259–1262, doi:10.1126/science.1133061, 2007.

Schauer, J. J., Kleeman, M. J., Cass, G. R., and Simoneit, B. R. T.: Measurement of Emissions from Air Pollution Sources. 1. C1 through C29 Organic Compounds from Meat Charbroiling, Environ. Sci. Technology, 33, 1566–1577, doi:10.1021/es980076j, 1999.

Schulz, M., Gauss, M., Benedictow, A., Jonson, J. E., Tsyro, S., Nyiri, A., Simpson, D., Steensen, B. M., Klein, H., Valdebenito, A., Wind, P., Kirkevåg, A., Griesfeller, J., Bartnicki, J., Olivie, D., Grini, A., Iversen, T., Seland, ., Semeena, S. V., Fagerli, H., Aas, W., Hjellbrekke, A., Mareckova, K., Wankmuller, R., Schneider, P., Solberg, S., Svendby, T., Liu, L., Posch, M., Vieno, M., Reis, S., Kryza, M., Werner, M., and Walaszek, K.: Transboundary Acidification, Eutrophication and Ground Level Ozone in Europe in 2011, Tech. rep., Norwegian Meteorological Institute, Oslo, Norway, 1–205, 2013.

Shrivastava, M., Fast, J., Easter, R., Gustafson Jr., W. I., Zaveri, R. A., Jimenez, J. L., Saide, P., and Hodzic, A.: Modeling organic aerosols in a megacity: comparison of simple and complex representations of the volatility basis set approach, Atmos. Chem. Phys., 11, 6639–6662, doi:10.5194/acp-11-6639-2011, 2011.

Shrivastava, M., Easter, R. C., Liu, X., Zelenyuk, A., Singh, B., Zhang, K., Ma, P., Chand, D., Ghan, S., Jimenez, J. L., Zhang, Q., Fast, J., Rasch, P. J., and Tiitta, P.: Global transformation and fate

of SOA: Implications of low-volatility SOA and gas-phase fragmentation reactions, J. Geophys. Res.-Atmos., 120, 4169–4195, doi:10.1002/2014JD022563, 2015.

Shrivastava, M. K., Lane, T. E., Donahue, N. M., Pandis, S. N., and Robinson, A. L.: Effects of gas particle partitioning and aging of primary emissions on urban and regional organic aerosol concentrations, J. Geophys. Res.-Atmos., 113, 1–16, doi:10.1029/2007jd009735, 2008.

Simpson, D., Yttri, K. E., Klimont, Z., Kupiainen, K., Caseiro, A., Gelencser, A., Pio, C., Puxbaum, H., and Legrand, M.: Modeling carbonaceous aerosol over Europe: Analysis of the CARBOSOL and EMEP EC/OC campaigns, J. Geophys. Res.-Atmos., 112, 1–26, doi:10.1029/2006jd008158, 2007.

Simpson, D., Benedictow, A., Berge, H., Bergström, R., Emberson, L. D., Fagerli, H., Flechard, C. R., Hayman, G. D., Gauss, M., Jonson, J. E., Jenkin, M. E., Nyíri, A., Richter, C., Semeena, S. V., Tsyro, S., Tuovinen, J. P., Valdebenito, A., and Wind, P.: The EMEP MSC-W chemical transport model – technical description, Atmos. Chem. Phys., 12, 7825–7865, doi:10.5194/acp-12-7825-2012, 2012.

Spracklen, D. V., Jimenez, J. L., Carslaw, K. S., Worsnop, D. R., Evans, M. J., Mann, G. W., Zhang, Q., Canagaratna, M. R., Allan, J., Coe, H., McFiggans, G., Rap, A., and Forster, P.: Aerosol mass spectrometer constraint on the global secondary organic aerosol budget, Atmos. Chem. Phys., 11, 12109–12136, doi:10.5194/acp-11-12109-2011, 2011.

Tsigaridis, K., Daskalakis, N., Kanakidou, M., Adams, P. J., Artaxo, P., Bahadur, R., Balkanski, Y., Bauer, S. E., Bellouin, N., Benedetti, A., Bergman, T., Berntsen, T. K., Beukes, J. P., Bian, H., Carslaw, K. S., Chin, M., Curci, G., Diehl, T., Easter, R. C., Ghan, S. J., Gong, S. L., Hodzic, A., Hoyle, C. R., Iversen, T., Jathar, S., Jimenez, J. L., Kaiser, J. W., Kirkevåg, A., Koch, D., Kokkola, H., Lee, Y. H., Lin, G., Liu, X., Luo, G., Ma, X., Mann, G. W., Mihalopoulos, N., Morcrette, J.-J., Müller, J.-F., Myhre, G., Myriokefalitakis, S., Ng, N. L., O'Donnell, D., Penner, J. E., Pozzoli, L., Pringle, K. J., Russell, L. M., Schulz, M., Sciare, J., Seland, Ø., Shindell, D. T., Sillman, S., Skeie, R. B., Spracklen, D., Stavrakou, T., Steenrod, S. D., Takemura, T., Tiitta, P., Tilmes, S., Tost, H., van Noije, T., van Zyl, P. G., von Salzen, K., Yu, F., Wang, Z., Wang, Z., Zaveri, R. A., Zhang, H., Zhang, K., Zhang, Q., and Zhang, X.: The AeroCom evaluation and intercomparison of organic aerosol in global models, Atmos. Chem. Phys., 14, 10845–10895, doi:10.5194/acp-14-10845-2014, 2014.

Tsimpidi, A. P., Karydis, V. A., Zavala, M., Lei, W., Molina, L., Ulbrich, I. M., Jimenez, J. L., and Pandis, S. N.: Evaluation of the volatility basis-set approach for the simulation of organic aerosol formation in the Mexico City metropolitan area, Atmos. Chem. Phys., 10, 525–546, doi:10.5194/acp-10-525-2010, 2010.

Tsimpidi, A. P., Karydis, V. A., Pandis, S. N., and Lelieveld, J.: Global combustion sources of organic aerosols: Model comparison with 84 AMS factor analysis data sets, Atmos. Chem. Phys. Discuss., doi:10.5194/acp-2015-989, in review, 2016.

Ulbrich, I. M., Canagaratna, M. R., Zhang, Q., Worsnop, D. R., and Jimenez, J. L.: Interpretation of organic components from Positive Matrix Factorization of aerosol mass spectrometric data, Atmos. Chem. Phys., 9, 2891–2918, doi:10.5194/acp-9-2891-2009, 2009.

USEPA: Integrated Science Assessment for Particulate Matter (Final Report, http://cfpub.epa.gov/ncea/cfm/recordisplay.cfm?deid=216546 (last access: 24 May 2016), 2009.

Vieno, M., Dore, A. J., Stevenson, D. S., Doherty, R., Heal, M. R., Reis, S., Hallsworth, S., Tarrason, L., Wind, P., Fowler, D., Simpson, D., and Sutton, M. A.: Modelling surface ozone during the 2003 heat-wave in the UK, Atmos. Chem. and Phys., 10, 7963–7978, doi:10.5194/acp-10-7963-2010, 2010.

Vieno, M., Heal, M. R., Hallsworth, S., Famulari, D., Doherty, R. M., Dore, A. J., Tang, Y. S., Braban, C. F., Leaver, D., Sutton, M. A., and Reis, S.: The role of long-range transport and domestic emissions in determining atmospheric secondary inorganic particle concentrations across the UK, Atmos. Chem. Phys., 14, 8435–8447, doi:10.5194/acp-14-8435-2014, 2014.

Wickham, H.: ggplot2: Elegant Graphics for Data Analysis, ISBN 978-0-387-98140-6, Springer-Verlag, New York, USA, available at: http://ggplot2.org (last access: 24 May 2016), 2009.

Wiedinmyer, C., Akagi, S. K., Yokelson, R. J., Emmons, L. K., Al-Saadi, J. A., Orlando, J. J., and Soja, A. J.: The Fire INventory from NCAR (FINN): a high resolution global model to estimate the emissions from open burning, Geosci. Model Dev., 4, 625–641, doi:10.5194/gmd-4-625-2011, 2011.

Xu, L., Suresh, S., Guo, H., Weber, R. J., and Ng, N. L.: Aerosol characterization over the southeastern United States using high-resolution aerosol mass spectrometry: spatial and seasonal variation of aerosol composition and sources with a focus on organic nitrates, Atmos. Chem. Phys., 15, 7307–7336, doi:10.5194/acp-15-7307-2015, 2015.

Xu, L., Williams, L. R., Young, D. E., Allan, J. D., Coe, H., Massoli, P., Fortner, E., Chhabra, P., Herndon, S., Brooks, W. A., Jayne, J. T., Worsnop, D. R., Aiken, A. C., Liu, S., Gorkowski, K., Dubey, M. K., Fleming, Z. L., Visser, S., Prévôt, A. S. H., and Ng, N. L.: Wintertime aerosol chemical composition, volatility, and spatial variability in the greater London area, Atmos. Chem. Phys., 16, 1139–1160, doi:10.5194/acp-16-1139-2016, 2016.

Young, D. E., Allan, J. D., Williams, P. I., Green, D. C., Flynn, M. J., Harrison, R. M., Yin, J., Gallagher, M. W., and Coe, H.: Investigating the annual behaviour of submicron secondary inorganic and organic aerosols in London, Atmos. Chem. Phys., 15, 6351–6366, doi:10.5194/acp-15-6351-2015, 2015a.

Young, D. E., Allan, J. D., Williams, P. I., Green, D. C., Harrison, R. M., Yin, J., Flynn, M. J., Gallagher, M. W., and Coe, H.: Investigating a two-component model of solid fuel organic aerosol in London: processes, PM_1 contributions, and seasonality, Atmos. Chem. Phys., 15, 2429–2443, doi:10.5194/acp-15-2429-2015, 2015b.

Zhang, Q. J., Beekmann, M., Drewnick, F., Freutel, F., Schneider, J., Crippa, M., Prevot, A. S. H., Baltensperger, U., Poulain, L., Wiedensohler, A., Sciare, J., Gros, V., Borbon, A., Colomb, A., Michoud, V., Doussin, J., Denier van der Gon, H. A. C., Haeffelin, M., Dupont, J., Siour, G., Petetin, H., Bessagnet, B., Pandis, S. N., Hodzic, A., Sanchez, O., Honoré, C., and Perrussel, O.: Formation of organic aerosol in the Paris region during the MEGAPOLI summer campaign: evaluation of the volatility-basis-set approach within the CHIMERE model, Atmos. Chem. Phys., 13, 5767–5790, doi:10.5194/acp-13-5767-2013, 2013.

Appendix E

Publication

This appendix contains the publication submitted for peer-review which formed the basis for Chapter 4.

Ots, R., Vieno, M., Allan, J. D., Reis, S., Nemitz, E., Young, D. E., Coe, H., Di Marco, C., Detournay, A., Mackenzie, I. A., Green, D. C., and Heal, M. R. (2016). Model simulations of cooking organic aerosol (COA) over the UK using estimates of emissions based on measurements at two sites in London, *Atmos. Chem. Phys. Discuss.*, 1–28, doi: 10.5194/acp-2016-342, accepted for publication in *Atmos. Chem. Phys.*.

Atmos. Chem. Phys. Discuss., doi:10.5194/acp-2016-342, 2016
Manuscript under review for journal Atmos. Chem. Phys.
Published: 6 June 2016

Atmospheric Chemistry and Physics Discussions

Model simulations of cooking organic aerosol (COA) over the UK using estimates of emissions based on measurements at two sites in London

Riinu Ots[1,2], Massimo Vieno[2], James D. Allan[3,4], Stefan Reis[2,5], Eiko Nemitz[2], Dominique E. Young[3,*], Hugh Coe[3], Chiara Di Marco[2], Anais Detournay[2], Ian A. Mackenzie[6], David C. Green[7], and Mathew R. Heal[1]

[1]School of Chemistry, University of Edinburgh, Edinburgh, UK
[2]Natural Environment Research Council, Centre for Ecology & Hydrology, Penicuik, UK
[3]School of Earth, Atmospheric and Environmental Sciences, University of Manchester, Manchester, UK
[4]National Centre for Atmospheric Science, University of Manchester, Manchester, UK
[5]University of Exeter Medical School, European Centre for Environment and Health, Knowledge Spa, Truro, UK
[6]School of GeoSciences, University of Edinburgh, Edinburgh, UK
[7]MRC PHE Centre for Environment and Health, King's College London, London, UK
[*]now at: Department of Environmental Toxicology, University of California, Davis, CA, USA

Correspondence to: M. Heal (M.Heal@ed.ac.uk) and R. Ots (R.Ots@ed.ac.uk)

Abstract.

Cooking organic aerosol (COA) is currently not included in European emission inventories. However, recent positive matrix factorization (PMF) analyses of aerosol mass spectrometer (AMS) measurements have suggested important contributions of COA in several European cities. In this study, emissions of COA were estimated for the UK, based on hourly AMS measurements of COA made at two sites in London (a kerbside site in central London and an urban background site in a residential area close to central London) for the full calendar year of 2012 during the Clean Air for London (ClearfLo) campaign. Iteration of COA emissions estimates and subsequent evaluation and sensitivity experiments were conducted with the EMEP4UK atmospheric chemistry transport modelling system with a horizontal resolution of 5 $\mathrm{km} \times 5\ \mathrm{km}$.

The spatial distribution of these emissions was based on workday population density derived from the 2011 census data. The estimated UK annual COA emission was 7.4 Gg per year, which is an almost 10% addition to the officially reported UK national total anthropogenic emissions of $\mathrm{PM}_{2.5}$ (82 Gg in 2012), corresponding to 320 $\mathrm{mg\,person^{-1}\,day^{-1}}$ on average. Weekday and weekend diurnal variation in COA emissions were also based on the AMS measurements. Modelled concentrations of COA were then independently evaluated against AMS-derived COA measurements from another city and time period (Manchester, Jan–Feb 2007), as well as with COA estimated by a chemical mass balance model of measurements for a two-week period at the Harwell rural site (~80 km west of central London).

The modelled annual average contribution of COA to ambient particulate matter (PM) in central London was between 1–2 $\mu\mathrm{g\,m^{-3}}$, and between 0.5–0.7 $\mu\mathrm{g\,m^{-3}}$ in other major cities in England (Manchester, Birmingham, Leeds). It was also shown that cities smaller than London can have a central hot-spot of population density of smaller area than the computational grid cell, in which case higher localised COA concentrations than modelled here may be expected.

Atmos. Chem. Phys. Discuss., doi:10.5194/acp-2016-342, 2016
Manuscript under review for journal Atmos. Chem. Phys.
Published: 6 June 2016

Atmospheric Chemistry and Physics Discussions

Modelled COA concentrations dropped rapidly outside of major urban areas (annual average of 0.12 $\mu g\,m^{-3}$ for the Harwell location), indicating that although COA can be a notable component in urban air, it does not have a significant effect on PM concentrations on rural areas.

The possibility that the AMS PMF-apportionment measurements overestimate COA concentrations by up to a factor of 2 is discussed. Since COA is a primary emission, any downward adjustments in COA emissions would lead to a proportional linear downward scaling in the absolute magnitudes of COA concentrations simulated in the model.

1 Introduction

Airborne particulate matter (PM) has multiple impacts on atmospheric processes. It affects the transport, transformation and deposition of chemical species and influences radiative forcing (Pöschl, 2005; USEPA, 2009). Ambient surface concentrations of PM in particular contribute to substantial adverse human health effects (Heal et al., 2012; Lim et al., 2012; WHO, 2013; Brauer et al., 2016). The carbonaceous component constitutes a substantial fraction of total particle mass (USEPA, 2009; Putaud et al., 2010; AQEG, 2012), and arises through many diverse primary emission sources and in situ atmospheric processes (Fuzzi et al., 2006; Hallquist et al., 2009; Jimenez et al., 2009). It is necessary to accurately apportion the origin of organic aerosol (OA) in order to devise effective mitigation of ambient PM. This can be facilitated through the integration of measurements and modelling.

Even allowing for the uncertainties in defining and measuring OA components, current atmospheric chemistry transport model (ACTM) simulations tend to underestimate observed amounts of OA (Simpson et al., 2007; Murphy and Pandis, 2009; Hodzic et al., 2010; Aksoyoglu et al., 2011; Jathar et al., 2011; Bergström et al., 2012; Koo et al., 2014; Prank et al., 2016). In some cases, this underestimation has been shown to be due to missing or under-represented emission sources in the underlying emission inventories (Simpson et al., 2007; Denier van der Gon et al., 2015). One such primary source of OA is cooking organic aerosol (COA).

In the US, emissions of OA from meat charbroiling (grilling) or frying have been known for decades to be a significant contributor to ambient air quality (Rogge et al., 1991; Hildemann et al., 1991). Consequently, cooking aerosol is included as a component of particulate matter in the US national emission inventory (USEPA, 2004). In Europe, the impact of cooking emissions on ambient air quality via national emissions has so far been neglected. This might be because of an assumption that there is less meat charbroiling in Europe than in the US. However, using positive matrix factorization (PMF) analyses of aerosol mass spectrometer (AMS) measurements, several recent European studies have apportioned a substantial part of submicron OA to cooking. Allan et al. (2010) estimated that the average contribution of COA to OA in Manchester, UK, was 19% whilst in London, UK, it was 22–30%. For Barcelona, Spain, Mohr et al. (2012) reported a 17% contribution to OA from COA, and measurements at different sites in Paris, France, were interpreted as indicating a 15–20% average contribution from COA (Crippa et al., 2013a, b). Allan et al. (2010) also reported that the COA in London is more likely to be produced from vegetable seed oils used during frying, rather than solely from meat cooking.

Atmos. Chem. Phys. Discuss., doi:10.5194/acp-2016-342, 2016
Manuscript under review for journal Atmos. Chem. Phys.
Published: 6 June 2016

Atmospheric Chemistry and Physics Discussions

Based on the aforementioned PMF apportionment measurements of OA components in Paris, Fountoukis et al. (2016) estimated the emissions of COA to be ~80 $\mathrm{mg\,person^{-1}\,day^{-1}}$ on average. Adding these emissions to their model based on population density enabled their simulations to reproduce measured COA concentrations at two sites during the MEGAPOLI campaign. Fountoukis et al. (2016) then added the same 80 $\mathrm{mg\,person^{-1}\,day^{-1}}$ emission of COA to their model for a European domain, and concluded that, based on this estimate, the contribution of COA emissions from other countries to COA concentrations in Paris was between 0.1–0.2 $\mu\mathrm{g\,m^{-3}}$ of $\mathrm{PM_1}$. Discussion of potential uncertainties in the quantification of COA by PMF of AMS measurements is presented later in this paper.

In this work, AMS-derived measurements of COA for a full calendar year at two sites in London during the 2012 Clean Air for London campaign (ClearfLo; Bohnenstengel et al. (2014); Young et al. (2015)) were combined with gridded UK population density data (Reis et al., 2016) to construct estimates of COA emissions across the UK. The EMEP4UK ACTM (Vieno et al., 2010, 2014, 2016; Ots et al., 2016) was then applied to conduct calibration tests of these novel gridded and temporally-variable emissions of COA, and predictions were compared with a third, independent, dataset of measurements of COA made by AMS in Manchester in Jan–Feb 2007 (Allan et al., 2010).

2 Methods

2.1 Model description

The EMEP4UK model is a regional application of the EMEP MSC-W (European Monitoring and Evaluation Programme Meteorological Sythesizing Centre-West) model. The EMEP MSC-W model is a 3-D Eulerian model that has been used for both scientific studies and to support policy making in Europe. A detailed description of the EMEP MSC-W model, including references to evaluation and application studies is available in Simpson et al. (2012), Schulz et al. (2013), and at www.emep.int. The model used here was based on version v4.5.

The model has 21 vertical levels, extending from the surface to 100 hPa. The lowest vertical layer is ~40 m thick, and the horizontal resolution used in this study is 5 $\mathrm{km} \times 5\ \mathrm{km}$ over a British Isles domain. The model uses one-way nesting from an extended European domain (simulated with 50 $\mathrm{km} \times 50\ \mathrm{km}$ horizontal resolution), but this has no bearing on the COA concentrations presented in this study as COA emissions are not compiled for European countries and in this work were only implemented for the UK. The model was driven by output from the Weather Research and Forecasting (WRF) model (www.wrf-model.org, version 3.1.1) including data assimilation of 6-hourly model meteorological reanalysis from the US National Center for Environmental Prediction (NCEP)/National Center for Atmospheric Research (NCAR) Global Forecast System (GFS) at 1° resolution (NCEP, 2000).

The performance of this version of the EMEP4UK model simulating a standard suite of gas-phase components and secondary inorganic aerosol PM components is reported in Ots et al. (2016) comparing with a full year of measurements in London in 2012.

For the present study, a COA tracer was added into the model with dry and wet deposition properties similar to other fine (i.e. $\mathrm{PM_{2.5}}$) primary OA components (see Simpson et al. (2012) for aerosol specifications in the EMEP MSC-W model). This

Atmos. Chem. Phys. Discuss., doi:10.5194/acp-2016-342, 2016
Manuscript under review for journal Atmos. Chem. Phys.
Published: 6 June 2016

Atmospheric Chemistry and Physics Discussions

COA tracer is non-volatile and does not undergo chemical ageing, but it is included in the total OA budget for the absorptive partitioning of secondary organic aerosol species.

2.2 AMS measurements used in this study

The construction of COA emissions estimates were based on measurements made during the ClearfLo project (Bohnenstengel et al., 2014) at two sites in London, shown in Fig. 1. Marylebone Road is a 'kerbside' site on the edge of a heavily-trafficked urban through-road, whilst the North Kensington site is classified as urban background and is situated in the carpark of a school. The measurements at Marylebone Road were taken with a Q-AMS (Quadrupole AMS; Jayne et al. (2000)) between 11-Jan-2012 and 1-Feb-2013 and were averaged to hourly values, yielding 5996 data points (Detournay et al. (2015); several gaps in the measured data were caused by problems with the instrument computer). The measurements at North Kensington were taken with a cToF-AMS (compact Time of Flight AMS; DeCarlo et al. (2006)) between 11-Jan-2012 and 23-Jan-2013, and with a HR-ToF-AMS between 21-Jul-2012 and 19-Aug-2012 (High-Resolution ToF-AMS), hourly averaging yielded 8035 data points (Young et al., 2015). The annual average (for 2012) concentrations of COA derived from the AMS measurements were 2.2 $\mu g\,m^{-3}$ at Marylebone Road, and 0.8 $\mu g\,m^{-3}$ at North Kensington. Figure S1 shows a satellite image of the Marylebone Road measurement site with food-related commercial establishments (cafes, restaurants, etc.), as known to Google, marked. (The accuracy or comprehensiveness of these establishments marked on Google Maps has not been verified, but are presented to illustrate the number of food outlets in the area.) There is no direct source of cooking emissions close to the Marylebone Road measurement site, so the measured concentrations, although high, are likely to represent an average of the many COA emissions sources in the vicinity.

Positive matrix factorisation (PMF) seeks to reproduce the measured time series of the organic mass spectrum through a linear composition of a (user-selectable) number of factor spectra (representing different OA types or sources) and their mass contribution, taking into account the precision associated with each measurement. Subjectivity is minimized by comparison of concentration time-series with independent measurements and assessment of the robustness of the solution, e.g. through boot-strapping. COA has been identified as a contributor to urban OA measurements because it exhibits a distinct diurnal cycle and the associated factor spectrum is very similar to that of lab-generated cooking oil aerosol (Allan et al., 2010). Nevertheless, there are some inherit uncertainties involved in deriving COA concentrations with AMS measurements. For example, AMS measurements need to be corrected for the fraction of aerosol that is not effectively vaporised due to bounce from the hot surface involved in the AMS's detection mechanism. Whilst this is well characterised for typical, internally-mixed ambient aerosols (e.g. Middlebrook et al. (2012)), it is possible that the COA measured by the AMS is not well mixed with other aerosol components and could therefore be detected at a higher efficiency. If this were the case, AMS measurements may overestimate COA concentrations by up to a factor of 2.

Indeed, a study comparing AMS-PMF derived concentrations of PM components with those estimated based on measurements and a chemical mass balance (CMB) model at the North Kensington site during a 2-week period in the same campaign used in this study concluded that AMS derived COA was on average 1.6 times higher than the CMB derived values, but good correlation was seen (a linear fit of $\mathrm{AMS_{COA}} = 2.24 \times \mathrm{CMB_{COA}} - 0.33$, with $r = 0.89$), Yin et al. (2015)), which is consis-

Atmos. Chem. Phys. Discuss., doi:10.5194/acp-2016-342, 2016
Manuscript under review for journal Atmos. Chem. Phys.
Published: 6 June 2016

Atmospheric Chemistry and Physics Discussions

tent with the AMS collection efficiency (CE) being higher than the usual 0.5. There are also additional sources of uncertainty with PMF, in particular rotational ambiguity, which can cause both over- and underestimates (Allan et al., 2010; Paatero et al., 2002). However, the CMB approach is also not without its uncertainties, in particular that the COA marker(s) used in the CMB may not be fully representative, and because of the need to scale marker concentration to COA concentration.

In summary, the full quantification of COA by AMS (and any other approach) requires further research but it is currently more likely that the AMS overestimates the COA than underestimates it.

2.3 Spatial distribution of COA emissions

Figure 1a shows the residential population density data in the central London area at 1 km × 1 km resolution, overlaid by the EMEP4UK grid cells (5 km × 5 km), and Fig. 1b the equivalent workday population[1] density. These datasets were compiled by Reis et al. (2016) based on the 2011 UK Census, with population data provided on output area level, spatially distributed on a 1 km × 1 km grid for England, Wales and Northern Ireland using the Land Cover Map 2007 land use classes 'urban', 'suburban' and 'urban industrial'.

The North Kensington and Marylebone Road measurement sites are situated in different model grid cells. The Marylebone Road grid cell includes most of the very central part of London, with many popular tourist attractions such as Madam Tussauds, Buckingham Palace, Big Ben and the Houses of Parliament, and the London Eye. Even though there are no gridded data of 'tourist population density', the workday population density data include indication for tourist numbers as many of the jobs (and therefore the workday population density) in this area will be directly related to, or indirectly dependent on, the tourism sector. The total workday population for the grid cell of the Marylebone Road site is more than 3 times higher than for the grid cell for the North Kensington site. The residential population density in the North Kensington grid cell, however, is higher than in the Marylebone Road grid cell. The annual-average measured COA concentration at the Marylebone Road site was 2.8 times higher than at the North Kensington site, very similar to the ratio in gridded workday population density. Therefore, workday population density was chosen as the spatial distribution weighting to apply to COA emissions in the model input.

At present, gridded workday census data are only available for England, Wales, and Northern Ireland, so for Scotland the residential population data had to be used instead. The finer resolution (1 km) information of the COA emissions gridded to population density data was aggregated appropriately to the coarser model resolution during input data preparation.

2.4 Annual total emitted COA

Based on sensitivity tests (Table 1), the annual total COA emissions for the UK applied to the model was set to 7.4 Gg. (The spatial distribution applied to these emissions is explained in the previous section, the temporal variation is explained in the following section.) This is a 9% addition to the UK national total $PM_{2.5}$ emissions for the year 2012 (82 Gg, NAEI (2013)).

[1]The *workday population* is a redistribution of the usually resident population to their place of work, while residents who are not in work remain at their area of residence. The workday population of an area is defined as *"all usual residents aged 16 and above who are in employment and whose workplace is in the area, and all other usual residents of any age who are not in employment but are resident in the area"*; Source: Office for National Statistics, http://www.ons.gov.uk/ons/index.html

Atmos. Chem. Phys. Discuss., doi:10.5194/acp-2016-342, 2016
Manuscript under review for journal Atmos. Chem. Phys.
Published: 6 June 2016

Atmospheric Chemistry and Physics Discussions

This emission corresponds to about 320 $\mathrm{mg\,person^{-1}\,day^{-1}}$ (for a population of 63 million), which is 4 times higher than estimated by Fountoukis et al. (2016) for France. This difference might be explained by differences in cuisines - it is possible that relatively more grilled, fried and, in particular, deep-fried food is consumed in the UK than in France. Furthermore, it is also possible that the difference in the measurement site locations relative to the very centre of either megacity, and the representativeness of the measurement location to model grid average, could increase or decrease the estimate made for the whole country.

2.5 Temporal variation of COA emissions

The average diurnal profiles of measured COA concentrations the Marylebone Road and North Kensington sites are shown in Figs. 2a and 2b. The measured diurnal cycle of COA concentrations at Marylebone Road was taken as a basis for a temporal emission profile. Marylebone Road was chosen because the concentrations are substantially higher than at North Kensington and show a stronger diurnal variation with more pronounced peaks around both the lunchtime (12:00–14:00) and evening (dinnertime, 18:00–21:00) periods. Even though the diurnal COA concentration variation at Marylebone Road is clearly driven by these meal times, it is further influenced by atmospheric processes such as changing boundary layer height and dispersion, potentially introducing a non-linearity between emissions and concentrations. Therefore, the ACTM was used to assess these processes using sensitivity runs with different diurnal emission profiles. As a first test, the diurnal profile of COA emissions was set exactly to the measured profile at Marylebone Road, with separate profiles for weekdays and weekend days (the lunchtime peak is more pronounced on weekdays than on weekends). Further sensitivity runs with modified diurnal emission profiles were conducted with the goal of optimising modelled-measured agreement simultaneously at both the Marylebone Road and North Kensington measurement sites. These sensitivity runs and the final diurnal weekday and weekend diurnal emission profiles selected are explained in detail in the Supplementary Information. The emissions total was applied to all seven days of the week because the measurements showed only very small day-of-the-week trends (Fig. 2c and d) and differed between the two measurement sites. No seasonality (or monthly) variation was assigned to the emission profile under the assumption that cooking is a consistent year-round activity. It is, however, recognised that cooking emissions may also be strongly affected by tourist population density and may thus have some degree of seasonality. For example, the 2012 Summer Olympics took place in London from 25-July to 12-August attracting 680,000 overseas tourists alone (UK Office for National Statistics, 2012).

2.6 Summary of the newly composed COA emissions

- The emissions were spatially gridded to workday population density, not residential population density, as this captured the relative difference between observed annual average COA concentrations between the central, commercially-based (Marylebone Road site) and the residential (North Kensington site) areas.
- The annual total COA emission for the UK was based on a series of sensitivity runs to minimise total bias for both sites. The final amount was 7.4 Gg per year, which is an almost 10% addition to the officially reported total $\mathrm{PM_{2.5}}$ emissions (82 Gg in 2012). This corresponds to about 320 $\mathrm{mg\,person^{-1}\,day^{-1}}$ on average.

Atmos. Chem. Phys. Discuss., doi:10.5194/acp-2016-342, 2016
Manuscript under review for journal Atmos. Chem. Phys.
Published: 6 June 2016

Atmospheric Chemistry and Physics Discussions

– The diurnal profile of COA emissions (i.e. the relative increase of emissions during lunch or dinner) was mainly based on the observations at Marylebone Road (as the concentrations were higher and the emission profile was therefore more pronounced at the very central location). Slightly different diurnal cycles were assigned to weekday and weekend COA emissions, but no day-of-the-week or monthly variations were applied to the emissions.

The annual gridded UK COA emissions used in the model simulations are shown in Fig. 3a, and the resulting annual-average modelled COA surface concentrations (for 2012) are shown in Fig. 3b.

2.7 Model evaluation statistics used in this study

The following numerical metrics were used for model evaluation: FAC2 (Factor of 2) - the proportion of modelled concentrations that are within a factor of 2 of the measured concentrations; NMB - normalised mean bias; NMGE - normalised mean gross error, which is defined as:

$$NMGE = \frac{\frac{1}{n}\sum_{i=1}^{n}|M_i - O_i|}{\overline{O}}, \quad (1)$$

where M_i is the *i*th modelled value, O_i is the corresponding measured value, $\overline{O}$ is the mean measured value, and *n* in the total number of observations; *r* - correlation coefficient; and COE - coefficient of determination, which is defined as:

$$COE = 1.0 - \frac{\sum_{i=1}^{n}|M_i - O_i|}{\sum_{i=1}^{n}|O_i - \overline{O}|}. \quad (2)$$

A COE of 1 indicates perfect agreement between model and measurements. Although the COE does not have a lower bound, a zero or negative COE implies that the model cannot explain any of the variation in the observations (Legates and McCabe, 2013).

3 Results and Discussion

The results section is organised as follows. First, hourly concentrations and average diurnal profiles of measured and modelled COA at the two sites in London are evaluated. Second, an evaluation of daily-averaged measured and modelled COA is presented. These analyses are undertaken for the same sites that were used to estimate the COA emissions. In the third part of the results section, the modelled concentrations are evaluated against a separate, short (two-week) period of measurements from a different location, the centre of the city of Manchester. Finally, modelled concentrations of COA in other major UK cities, as well as in the vicinity of London are discussed.

3.1 Hourly comparison of measured and modelled COA concentrations in London

The average hourly profiles (diurnal cycles) of measured and modelled COA concentrations at the Marylebone Road and North Kensington sites are shown in Fig. 2a and b, respectively. As explained above, the diurnal COA emission profile applied to the model was mainly based on measurements at the Marylebone Road site. Since COA measurements at this site had a notable

Atmos. Chem. Phys. Discuss., doi:10.5194/acp-2016-342, 2016
Manuscript under review for journal Atmos. Chem. Phys.
Published: 6 June 2016

Atmospheric Chemistry and Physics Discussions

lunchtime peak, the modelled lunchtime peak at North Kensington (12:00–14:00, Fig. 2b) is slightly elevated compared with the measurements, but, overall, measured and modelled diurnal cycles are in very good agreement (r = 0.99 for Marylebone Road; r = 0.93 for North Kensington).

Scatterplots of modelled and measured hourly COA concentrations at the Marylebone Road and North Kensington sites, with weekdays and weekends separated, are shown in Fig. 4 (the time series of these hourly data are shown in Figs. S6–S9). The average concentrations for each panel of Fig. 4 are given in Table 2. At the Marylebone Road site, neither the hourly evaluation statistics, nor the mean COA concentrations, show a difference between weekdays and weekends. However, differences in the statistics are observed between weekdays and weekends at the North Kensington site: mean COA concentration for weekdays is 0.7 $\mu g\,m^{-3}$, whereas for weekends it is 1.1 $\mu g\,m^{-3}$. As no day-of-the-week variation was applied to total daily emissions (only to the weekday/weekend diurnal emission profiles), the model can not reproduce this difference (both weekday and weekend mean simulated COA concentrations are 0.9 $\mu g\,m^{-3}$). It is possible in the model to give emissions from each source sector a weekly cycle. This is done for several sectors already. For example, road transport emissions are higher during weekdays, whereas residential heating emissions are higher during the weekends. For cooking emissions, a weekly cycle might be justified for more office dominated areas (like the North Kensington area), but not for the very central commercial and recreational area where the Marylebone Road site is located. It is possible that central London is an exception and that overall, it would be better to assign a weekly cycle to emissions from cooking activities (as it is possible that in every other city than the capital, weekends are busier than weekdays in terms of eating out and therefore a day-of-week factor would be justified). Therefore, more measurements (or alternatively, statistics about the spatial and temporal variability of restaurant customer numbers during different days of the week) should be collected.

Overall, the hourly evaluation statistics are similar for both sites (Fig. 4): FAC2 is 62% (weekdays) and 55% (weekends) for Marylebone Road, and 62% (weekdays) and 65% (weekend) for North Kensington; NMGE is 69% and 60% for Marylebone Road and 64% and 52% for North Kensington; r-values are 0.46 and 0.56 for Marylebone Road and 0.53 and 0.63 for North Kensington. The conclusion is that the diurnal emission profiles derived as model input for COA emissions result in similar model performance for both types of area.

3.2 Evaluation of daily-averaged COA concentrations in London

Time series of daily averaged modelled and measured COA concentrations along with daily evaluation statistics for the two sites in London are shown in Fig. 5. Based on the hourly evaluation in the previous section, some disagreement can be expected at the North Kensington site by not including in the model any difference between weekday and weekend emissions. Despite this, it was shown that the hourly evaluation statistics were similar for both sites. However, North Kensington and Marylebone Road show very different results for the daily evaluation. For the North Kensington site, daily performance is satisfactory (Fig. 5a), with an r-value of 0.56 and a COE of 0.19. The NMGE of 43% could be attributed to the uncertainties in the COA emissions (including the weekdays vs weekends difference), as well as uncertainties in the meteorological driver. For Marylebone Road on the other hand (Fig. 5b), the model does not satisfactorily simulate the measured daily variation of COA concentrations (r = 0.11, COE = -0.22).

Atmos. Chem. Phys. Discuss., doi:10.5194/acp-2016-342, 2016
Manuscript under review for journal Atmos. Chem. Phys.
Published: 6 June 2016

Atmospheric Chemistry and Physics Discussions

Figures 6a–d show polar plots of measured and modelled COA concentrations for the North Kensington and Marylebone Road sites. Wind data are from the the Heathrow Airport meteorological station (Met Office, 2012), about 20 km to the west of central London. Meteorological observations from the airport, rather than more local measurements, are used as the airport measurements are unaffected by large buildings and are likely to be more representative of larger scale wind over Greater London. For comparability, the same wind data are used for both measured and modelled concentrations. Furthermore, the days with missing measurements (Fig. 5, especially important for the Marylebone Road site) are also removed from the modelled concentrations polar plots. However, it should be noted that the datasets used in these plots still differ in size between the two sites (n days = 191 at Marylebone Road and n days = 340 at North Kensington).

It can be seen from Figs. 6a and 6b that at the North Kensington site both measurements and model show higher concentrations when the wind is from the east. This is expected as North Kensington is slightly to the west of central London (Fig. 1) and therefore wind from the east has passed over more local emission sources. However, the polar plots for Marylebone Road show substantial differences between measured and modelled concentrations. The model simulates higher daily COA concentrations at lower wind speeds from all directions (Fig. 6d, see Fig. S10 for scatterplots of these values conditioned by four divisions of wind directions). In contrast, the measurements show a gradient of higher concentrations when winds are southerly and lower concentrations for northerly winds (Fig. 6c, see Fig. S11 for scatterplots of these values conditioned by wind speed quantiles). A detailed map of the Marylebone Road location is shown in Fig. 7. There is a large park (Regent's Park) just to the north of the Marylebone Road measurement site, explaining why lower concentrations are measured from that direction. The model can not of course resolve this 'sub-grid' variation (the model's horizontal resolution is 5 km×5 km, as shown in Fig. 1) and thus misses the effects of the park. Whilst the use of the synoptic wind from Heathrow Airport will represent medium to far-field influences more accurately, the funnelling of the air flow by the street canyon will affect the contribution from very local sources and the degree of ventilation vs. build-up of material emitted from within the canyon. These effects are likely to lead to a more variable concentration at the Marylebone Road roadside site than at the North Kensington background site. Measurements at different locations and more modelling studies (including different models, for example an urban dispersion model) of COA concentrations in London, as well as in other cities would be necessary to draw further conclusions about the variability of COA concentrations in a street canyon situation.

3.3 Comparison with COA measurements in Manchester in 2007

In this section, modelled concentrations (using the emissions based on measurements in London, 2012) are compared with a two-week period of AMS and PMF apportionment measurements in Manchester, Jan–Feb 2007 (taken with a cToF-AMS; Allan et al. (2010)). The Manchester measurement site location, as well as gridded workday population density (1 km × 1 km resolution) overlaid with the modelling grid (5 km × 5 km) is shown in Fig. 8. The model grid cell in which the measurement site is situated includes an area of a few km in width where the workday population density is several times higher than in the rest of the 5 km × 5 km cell (this is very central Manchester around the main train station). Since the measurement site was also located in this high workday population density area it is likely that the measured concentrations represent the highest COA concentrations in Manchester, in contrast, the model simulates an average concentration for the whole grid cell which will

Atmos. Chem. Phys. Discuss., doi:10.5194/acp-2016-342, 2016
Manuscript under review for journal Atmos. Chem. Phys.
Published: 6 June 2016

Atmospheric Chemistry and Physics Discussions

be lower than at the sub-grid measurement hot-spot. It should also be noted that the Manchester measurement site is located 0.5 km from a 'Chinatown', which could have a direct influence on the measured COA concentrations due to its high number of restaurants and deep-drying.

The time series of hourly-averaged measured and modelled concentrations during the 2-week period of measurements in Manchester are shown in Fig. 9a. Average diurnal cycles are shown in Fig. 9b, and a scatterplot of daily averaged concentrations in Fig. 9c. Modelled concentrations are a factor of 2 lower than measurements (NMB = -50%), likely due to the sub-grid modelling issue discussed above. Nevertheless, there is very good measurement-model correlation (r = 0.80 for diurnal profiles, r = 0.63 for hourly-averaged concentrations, r = 0.86 for daily-averaged concentrations). This indicates that the diurnal profile for COA emissions derived based on measurements in London is also suitable for use in other areas. However, the results suggest that because London is a megacity, the high concentrations in the central area can on average be captured by simulations with the 5 km $\times$ 5 km horizontal resolution, whereas for Manchester, a finer set-up (~1-2 km for example) would be needed. Nevertheless, the modelled concentrations are still useful in representing the spatially-averaged concentrations within the whole grid cell. Even allowing for the model resolution, the negative bias between model and measurement suggests that the per capita emissions estimate for COA derived from the London measurements is not an overestimate for COA emissions in Manchester (setting aside the discussion that both London and Manchester AMS measurements maybe be overestimates of COA).

3.4 Maximum modelled COA concentrations in London, Manchester, Leeds, and Birmingham

Some statistics for the range of daily-average COA concentrations at the two London sites are given in Table 3. The modelled and measured mean values match closely, with a bias of -0.1 $\mu g\,m^{-3}$ for the Marylebone Road site, and +0.1 $\mu g\,m^{-3}$ for the North Kensington site. For the Marylebone grid cell, two sets of statistics of modelled concentrations are given: one matched for data availability with measurements (i.e. missing January, most of March, June and July, other odd days), and one for the full calendar year. The influence of the missing periods is small in this case (full year mean is 2.0 $\mu g\,m^{-3}$, measurements-matched mean is 2.1 $\mu g\,m^{-3}$).

The model grid cell encompassing the Marylebone Road site has the highest annual average modelled COA concentration in London, and indeed across the whole of the UK. Therefore, these statistics (both measured and modelled) likely represent the maximum contribution cooking emissions might have on a 5 km $\times$ 5 km area. The annual average COA concentration of 2 $\mu g\,m^{-3}$ in central London is relevant as that constitutes 20% of the WHO $PM_{2.5}$ air quality guideline of 10 $\mu g\,m^{-3}$ for example.

Figure 10 shows the time series of daily-averaged modelled concentrations for 2012 for the other most populous cities in the the UK - Birmingham, Manchester, and Leeds (Glasgow is omitted as the workday population data were not yet available for Scotland). The data shown are for the grid cell over these cities with the largest annual-average COA concentrations. The higher COA concentrations in these cities are also visible in the annual average map of modelled COA surface concentrations in Fig. 11b. Based on the gridded workday population density in Manchester and the results shown in the previous section, it is likely that these simulated 5 km $\times$ 5 km concentrations do not capture the central hot-spots of cities smaller than London, but capture the average of an area wider than the centre itself.

Atmos. Chem. Phys. Discuss., doi:10.5194/acp-2016-342, 2016
Manuscript under review for journal Atmos. Chem. Phys.
Published: 6 June 2016

Atmospheric Chemistry and Physics Discussions

As an annual average in 2012, modelled COA contributed 0.5–0.7 $\mu g\,m^{-3}$ in these cities (data given in Fig. 10). On 36 days of 2012 (90th percentile, denoted Up10 in Fig. 10), modelled COA concentrations are over 0.9 $\mu g\,m^{-3}$ in Leeds and Birmingham, and over 1.3 $\mu g\,m^{-3}$ in Manchester. As a 95th percentile of daily averages for 2012, modelled COA contributed 1.3, 2,2 and 2.9 $\mu g\,m^{-3}$ in Leeds, Birmingham and Manchester, respectively.

3.5 COA concentrations in the vicinity of London

The map of UK modelled surface concentrations of COA presented in Fig. 3 shows that the impact of cooking emissions on an annual average basis is spatially very limited, as COA concentrations drop markedly outside the highly populated urban areas. There are no PMF apportionment measurements of COA concentrations reported outside UK urban areas, but daily-averaged modelled concentrations (for 2012) at Harwell are shown in Fig. 12a for an illustration of anticipated non-urban COA concentrations (Harwell is an EMEP supersite ~80 km west of central London, its exact location is marked on maps in Fig. S8). Harwell was also a measurement site during the ClearfLo project. The modelled time series indicate that the COA concentrations at Harwell are relatively small and episodic. In fact, their characteristic diurnal signature is entirely lost (Fig. 12b) and their time-series becomes very similar to that of other emissions dominated by population density. This is the reason why PMF commonly fails to resolve COA and hydrocarbon-like organic aerosol (HOA, dominated by vehicular emissions) at rural sites.

The modelled COA concentrations for Harwell are similar to the COA concentration derived by Yin et al. (2015) with the chemical mass balance (CMB) method for the same site. For the period 12-Jan-2012 to 8-Feb-2012 Yin et al. (2015) estimate COA of 0.13 $\mu g\,m^{-3}$ (note text in this paper also refers to a COA average value of 0.12 $\mu g\,m^{-3}$); the model here yields a concentration of 0.17 $\mu g\,m^{-3}$ for the same period, 0.12 $\mu g\,m^{-3}$ for the full year average.

Modelled surface concentrations near the Greater London area for the 18 highest days (95th percentile: 0.43 $\mu g\,m^{-3}$ for Harwell) are shown in Fig. S8. Most of the higher concentrations at these location come from London, with the exception of 11-Feb and 12-Feb, when some traces of COA concentrations arrive from northern England. Furthermore, as even the 95th percentile of daily averaged COA concentrations in the vicinity of London sites is rather low, compared with the COA concentrations experienced within the large urban areas, this demonstrates that the impact of cooking emissions is also spatially very limited on a daily basis.

4 Conclusions

In this study, spatially resolved estimates of emissions of cooking organic aerosol (COA) which are currently not included in European emissions inventories were generated for the UK. The magnitude and spatial and diurnal distributions of COA emissions have been derived from determinations of COA concentrations by positive-matrix factorisation (PMF) of aerosol mass spectrometer (AMS) measurements at two sites in London for the full calendar year 2012 (Marylebone Road, a kerbside site in central London; and North Kensington, an urban background site in a residential area close to central London).

Atmos. Chem. Phys. Discuss., doi:10.5194/acp-2016-342, 2016
Manuscript under review for journal Atmos. Chem. Phys.
Published: 6 June 2016

Atmospheric Chemistry and Physics Discussions

An evaluation of daily concentrations in London revealed different results for the two sites. For the North Kensington site, the model captured day-to-day variability throughout the year (r = 0.56, COE = 0.19), whereas for the Marylebone Road site, the model could not simulate observed inter-day variability (r = 0.11, COE = -0.22). Based on polar plots of measured wind directions, the likely source of this disagreement is a sub-(model)-grid effect at the Marylebone Road site and local air flows. Comparing model results with measurements for another time period and location (Manchester, Jan–Feb 2007) suggests that the diurnal profile of COA emissions derived from 2012 measurements at Marylebone Road is suitable for simulating COA concentrations at other central urban areas.

It is shown that in London, annual average COA concentrations are between 1–2 $\mu g\,m^{-3}$ (urban background site to urban central site). Both the measurements and modelled concentrations agree that the 95th percentile of daily averaged COA concentrations at the different locations is 2–4 $\mu g\,m^{-3}$. For three other major cities, Manchester, Leeds and Birmingham, modelled annual average concentrations of COA were between 0.5–0.7 $\mu g\,m^{-3}$, but it should be noted that the model simulates the average concentration of the 5 km $\times$ 5 km grid cells, whereas it was shown for Manchester that cities can exhibit a central hot-spot of smaller scale (1–2 km in dimension). Therefore in some urban centres the contribution might be bigger than is modelled here.

The impact of COA concentrations is spatially very limited as the modelled concentrations drop markedly outside the highly populated urban areas. For example, the simulations estimated an annual average COA concentration of 0.12 $\mu g\,m^{-3}$ for the EMEP supersite Harwell (classified as rural background), which is ~80 km west of central London. This is comparable to estimates of COA concentrations at Harwell derived from a chemical mass balance (CMB) model applied to two weeks of measurements.

It is noted that it is possible that AMS-PMF measurements of COA concentrations might be overestimated by up to a factor of 2 (as was explained in Sect. 2.2). This means that the emission estimate of 7.4 Gg of COA per year (about 320 $mg\,person^{-1}\,day^{-1}$) could be a factor of 2 too high (but since COA is a primary PM emission, modelled COA concentrations scale linearly with changes in COA emission amount in the model). If this were the case then, depending on the degree of overestimation, COA would still an important contributor of PM in very central areas, but possibly less so in wider urban or suburban areas.

In short, the spatially and temporally resolved COA emissions developed here for the UK can contribute to closing the gap between modelled and observed concentrations of carbonaceous aerosol and to total PM mass concentrations in urban areas.

Acknowledgements. The authors acknowledge the UK Department for Environment, Food and Rural Affairs (Defra) and the Devolved Administrations for funding aspects of the development of the EMEP4UK model (AQ0727), for partial support for the aerosol measurements, as well as access to the AURN data, which were obtained from uk-air.defra.gov.uk and are subject to Crown 2014 copyright, Defra, licenced under the Open Government Licence (OGL). Partial support for the EMEP4UK modelling from the European Commission FP7 ECLAIRE project is gratefully acknowledged. This work was supported in part by the UK Natural Environment Research Council (NERC) ClearfLo project [grant ref. NE/H003169/1]. R. Ots was supported by a PhD studentship (University of Edinburgh and NERC-CEH contract 587/NEC03805). D. E. Young was supported by a NERC PhD studentship [ref. NE/I528142/1].

Atmos. Chem. Phys. Discuss., doi:10.5194/acp-2016-342, 2016
Manuscript under review for journal Atmos. Chem. Phys.
Published: 6 June 2016

Atmospheric Chemistry and Physics Discussions

NCAR command language (NCL) was used to produce the maps (NCAR, 2015), and R, openair and ggplot2 for the analysis and all other plots (R Core Team, 2014; Carslaw and Ropkins, 2012; Wickham, 2009).

Atmos. Chem. Phys. Discuss., doi:10.5194/acp-2016-342, 2016
Manuscript under review for journal Atmos. Chem. Phys.
Published: 6 June 2016

Atmospheric Chemistry and Physics Discussions

References

Aksoyoglu, S., Keller, J., Barmpadimos, I., Oderbolz, D., Lanz, V. A., Prévôt, A. S. H., and Baltensperger, U.: Aerosol modelling in Europe with a focus on Switzerland during summer and winter episodes, Atmos. Chem. Phys., 11, 7355–7373, doi:10.5194/acp-11-7355-2011, 2011.

Allan, J. D., Williams, P. I., Morgan, W. T., Martin, C. L., Flynn, M. J., Lee, J., Nemitz, E., Phillips, G. J., Gallagher, M. W., and Coe, H.: Contributions from transport, solid fuel burning and cooking to primary organic aerosols in two UK cities, Atmos. Chem. Phys., 10, 647–668, doi:10.5194/acp-10-647-2010, 2010.

AQEG: Report: Fine Particulate Matter (PM2.5) in the United - Defra, UK, http://uk-air.defra.gov.uk/library/reports?report_id=727, 2012.

Bergström, R., Denier van der Gon, H. A. C., Prévôt, A. S., Yttri, K. E., and Simpson, D.: Modelling of organic aerosols over Europe (2002-2007) using a volatility basis set (VBS) framework: application of different assumptions regarding the formation of secondary organic aerosol, Atmos. Chem. Phys., 12, 8499–8527, doi:10.5194/acp-12-8499-2012, 2012.

Bohnenstengel, S. I., Belcher, S. E., Aiken, A., Allan, J. D., Allen, G., Bacak, A., Bannan, T. J., Barlow, J. F., Beddows, D. C. S., Bloss, W. J., Booth, A. M., Chemel, C., Coceal, O., Di Marco, C. F., Dubey, M. K., Faloon, K. H., Fleming, Z. L., Furger, M., Gietl, J. K., Graves, R. R., Green, D. C., Grimmond, C. S. B., Halios, C. H., Hamilton, J. F., Harrison, R. M., Heal, M. R., Heard, D. E., Helfter, C., Herndon, S. C., Holmes, R. E., Hopkins, J. R., Jones, A. M., Kelly, F. J., Kotthaus, S., Langford, B., Lee, J. D., Leigh, R. J., Lewis, A. C., Lidster, R. T., Lopez-Hilfiker, F. D., McQuaid, J. B., Mohr, C., Monks, P. S., Nemitz, E., Ng, N. L., Percival, C. J., Prévôt, A. S. H., Ricketts, H. M. A., Sokhi, R., Stone, D., Thornton, J. A., Tremper, A. H., Valach, A. C., Visser, S., Whalley, L. K., Williams, L. R., Xu, L., Young, D. E., and Zotter, P.: Meteorology, Air Quality, and Health in London: The ClearfLo Project, Bulletin of the American Meteorological Society, 96, 779–804, doi:10.1175/BAMS-D-12-00245.1, 2014.

Brauer, M., Freedman, G., Frostad, J., van Donkelaar, A., Martin, R. V., Dentener, F., Dingenen, R. v., Estep, K., Amini, H., Apte, J. S., Balakrishnan, K., Barregard, L., Broday, D., Feigin, V., Ghosh, S., Hopke, P. K., Knibbs, L. D., Kokubo, Y., Liu, Y., Ma, S., Morawska, L., Sangrador, J. L. T., Shaddick, G., Anderson, H. R., Vos, T., Forouzanfar, M. H., Burnett, R. T., and Cohen, A.: Ambient Air Pollution Exposure Estimation for the Global Burden of Disease 2013, Environmental Science & Technology, 50, 79–88, doi:10.1021/acs.est.5b03709, 2016.

Carslaw, D. C. and Ropkins, K.: openair — An R package for air quality data analysis, Environmental Modelling & Software, 27–28, 52–61, doi:10.1016/j.envsoft.2011.09.008, 2012.

Crippa, M., Canonaco, F., Slowik, J. G., El Haddad, I., DeCarlo, P. F., Mohr, C., Heringa, M. F., Chirico, R., Marchand, N., Temime-Roussel, B., Abidi, E., Poulain, L., Wiedensohler, A., Baltensperger, U., and Prévôt, A. S. H.: Primary and secondary organic aerosol origin by combined gas-particle phase source apportionment, Atmos. Chem. Phys., 13, 8411–8426, doi:10.5194/acp-13-8411-2013, 2013a.

Crippa, M., DeCarlo, P. F., Slowik, J. G., Mohr, C., Heringa, M. F., Chirico, R., Poulain, L., Freutel, F., Sciare, J., Cozic, J., Di Marco, C. F., Elsasser, M., Nicolas, J. B., Marchand, N., Abidi, E., Wiedensohler, A., Drewnick, F., Schneider, J., Borrmann, S., Nemitz, E., Zimmermann, R., Jaffrezo, J., Prévôt, A. S. H., and Baltensperger, U.: Wintertime aerosol chemical composition and source apportionment of the organic fraction in the metropolitan area of Paris, Atmos. Chem. Phys., 13, 961–981, doi:10.5194/acp-13-961-2013, 2013b.

DeCarlo, P. F., Kimmel, J. R., Trimborn, A., Northway, M. J., Jayne, J. T., Aiken, A. C., Gonin, M., Fuhrer, K., Horvath, T., Docherty, K. S., Worsnop, D. R., and Jimenez, J. L.: Field-Deployable, High-Resolution, Time-of-Flight Aerosol Mass Spectrometer, Analytical Chemistry, 78, 8281–8289, doi:10.1021/ac061249n, 2006.

Atmos. Chem. Phys. Discuss., doi:10.5194/acp-2016-342, 2016
Manuscript under review for journal Atmos. Chem. Phys.
Published: 6 June 2016

Atmospheric Chemistry and Physics Discussions

Denier van der Gon, H. A. C., Bergström, R., Fountoukis, C., Johansson, C., Pandis, S. N., Simpson, D., and Visschedijk, A. J. H.: Particulate emissions from residential wood combustion in Europe – revised estimates and an evaluation, Atmos. Chem. Phys., 15, 6503–6519, doi:10.5194/acp-15-6503-2015, 2015.

Detournay, A., Nemitz, E., Di Marco, C. F., and et al.: A 1-year study of submicron aerosol composition at a kerbside location in London, In Preparation, 2015.

Fountoukis, C., Megaritis, A. G., Skyllakou, K., Charalampidis, P. E., Denier van der Gon, H. A. C., Crippa, M., Prévôt, A. S. H., Fachinger, F., Wiedensohler, A., Pilinis, C., and Pandis, S. N.: Simulating the formation of carbonaceous aerosol in a European Megacity (Paris) during the MEGAPOLI summer and winter campaigns, Atmos. Chem. Phys., 16, 3727–3741, doi:10.5194/acp-16-3727-2016, 2016.

Fuzzi, S., Andreae, M. O., Huebert, B. J., Kulmala, M., Bond, T. C., Boy, M., Doherty, S. J., Guenther, A., Kanakidou, M., Kawamura, K., Kerminen, V., Lohmann, U., Russell, L. M., and Pöschl, U.: Critical assessment of the current state of scientific knowledge, terminology, and research needs concerning the role of organic aerosols in the atmosphere, climate, and global change, Atmos. Chem. Phys., 6, 2017–2038, doi:10.5194/acp-6-2017-2006, 2006.

Hallquist, M., Wenger, J. C., Baltensperger, U., Rudich, Y., Simpson, D., Claeys, M., Dommen, J., Donahue, N. M., George, C., Goldstein, A. H., Hamilton, J. F., Herrmann, H., Hoffmann, T., Iinuma, Y., Jang, M., Jenkin, M. E., Jimenez, J. L., Kiendler-Scharr, A., Maenhaut, W., McFiggans, G., Mentel, T. F., Monod, A., Prévôt, A. S. H., Seinfeld, J. H., Surratt, J. D., Szmigielski, R., and Wildt, J.: The formation, properties and impact of secondary organic aerosol: current and emerging issues, Atmos. Chem. Phys., 9, 5155–5236, doi:10.5194/acp-9-5155-2009, 2009.

Heal, M. R., Kumar, P., and Harrison, R. M.: Particles, air quality, policy and health, Chemical Society Reviews, 41, 6606–6630, doi:10.1039/c2cs35076a, 2012.

Hildemann, L. M., Markowski, G. R., Jones, M. C., and Cass, G. R.: Submicrometer Aerosol Mass Distributions of Emissions from Boilers, Fireplaces, Automobiles, Diesel Trucks, and Meat-Cooking Operations, Aerosol Science and Technology, 14, 138–152, doi:10.1080/02786829108959478, 1991.

Hodzic, A., Jimenez, J. L., Madronich, S., Canagaratna, M. R., DeCarlo, P. F., Kleinman, L., and Fast, J.: Modeling organic aerosols in a megacity: potential contribution of semi-volatile and intermediate volatility primary organic compounds to secondary organic aerosol formation, Atmos. Chem. Phys., 10, 5491–5514, doi:10.5194/acp-10-5491-2010, 2010.

Jathar, S. H., Farina, S. C., Robinson, A. L., and Adams, P. J.: The influence of semi-volatile and reactive primary emissions on the abundance and properties of global organic aerosol, Atmos. Chem. Phys., 11, 7727–7746, doi:10.5194/acp-11-7727-2011, 2011.

Jayne, J. T., Leard, D. C., Zhang, X., Davidovits, P., Smith, K. A., Kolb, C. E., and Worsnop, D. R.: Development of an Aerosol Mass Spectrometer for Size and Composition Analysis of Submicron Particles, Aerosol Science and Technology, 33, 49–70, doi:10.1080/027868200410840, 2000.

Jimenez, J. L., Canagaratna, M. R., Donahue, N. M., Prevot, A. S., Zhang, Q., Kroll, J. H., DeCarlo, P. F., Allan, J. D., Coe, H., Ng, N. L., Aiken, A. C., Docherty, K. S., Ulbrich, I. M., Grieshop, A. P., Robinson, A. L., Duplissy, J., Smith, J. D., Wilson, K. R., Lanz, A. V., Hueglin, C., Sun, Y. L., Tian, J., Laaksonen, A., Raatikainen, T., Rautiainen, J., Vaattovaara, P., Ehn, M., Kulmala, M., Tomlinson, J. M., Collins, D. R., Cubison, M. J., Dunlea, E. J., Huffman, J. A., Onasch, T. B., Alfarra, M. R., Williams, P. I., Bower, K., Kondo, Y., Schneider, J., Drewnick, F., Borrmann, S., Weimer, S., Demerjian, K., Salcedo, D., Cottrell, L., Griffin, R., Takami, A., Miyoshi, T., Hatakeyama, S., Shimono, A., Sun, J. Y., Zhang, Y. M., Dzepina, K., Kimmel, J. R., Sueper, D., Jayne, J. T., Herndon, S. C., Trimborn, A. M., Williams, L. R., Wood, E. C., Middlebrook, A. M., Kolb, C. E., Baltensperger, U., and Worsnop, D. R.: Evolution of Organic Aerosols in the Atmosphere, Science, 326, 1525–1529, doi:DOI 10.1126/science.1180353, 2009.

Atmos. Chem. Phys. Discuss., doi:10.5194/acp-2016-342, 2016
Manuscript under review for journal Atmos. Chem. Phys.
Published: 6 June 2016

Atmospheric Chemistry and Physics Discussions

Koo, B., Knipping, E., and Yarwood, G.: 1.5-Dimensional volatility basis set approach for modeling organic aerosol in CAMx and CMAQ, Atmospheric Environment, 95, 158–164, doi:10.1016/j.atmosenv.2014.06.031, 2014.

Legates, D. R. and McCabe, G. J.: A refined index of model performance: a rejoinder, International Journal of Climatology, 33, 1053–1056, doi:10.1002/joc.3487, 2013.

Lim, S. S., Vos, T., Flaxman, A. D., Danaei, G., Shibuya, K., Adair-Rohani, H., AlMazroa, M. A., Amann, M., Anderson, H. R., Andrews, K. G., Aryee, M., Atkinson, C., Bacchus, L. J., Bahalim, A. N., Balakrishnan, K., Balmes, J., Barker-Collo, S., Baxter, A., Bell, M. L., Blore, J. D., Blyth, F., Bonner, C., Borges, G., Bourne, R., Boussinesq, M., Brauer, M., Brooks, P., Bruce, N. G., Brunekreef, B., Bryan-Hancock, C., Bucello, C., Buchbinder, R., Bull, F., Burnett, R. T., Byers, T. E., Calabria, B., Carapetis, J., Carnahan, E., Chafe, Z., Charlson, F., Chen, H., Chen, J. S., Cheng, A. T., Child, J. C., Cohen, A., Colson, K. E., Cowie, B. C., Darby, S., Darling, S., Davis, A., Degenhardt, L., Dentener, F., Des Jarlais, D. C., Devries, K., Dherani, M., Ding, E. L., Dorsey, E. R., Driscoll, T., Edmond, K., Ali, S. E., Engell, R. E., Erwin, P. J., Fahimi, S., Falder, G., Farzadfar, F., Ferrari, A., Finucane, M. M., Flaxman, S., Fowkes, F. G. R., Freedman, G., Freeman, M. K., Gakidou, E., Ghosh, S., Giovannucci, E., Gmel, G., Graham, K., Grainger, R., Grant, B., Gunnell, D., Gutierrez, H. R., Hall, W., Hoek, H. W., Hogan, A., Hosgood III, H. D., Hoy, D., Hu, H., Hubbell, B. J., Hutchings, S. J., Ibeanusi, S. E., Jacklyn, G. L., Jasrasaria, R., Jonas, J. B., Kan, H., Kanis, J. A., Kassebaum, N., Kawakami, N., Khang, Y., Khatibzadeh, S., Khoo, J., Kok, C., Laden, F., Lalloo, R., Lan, Q., Lathlean, T., Leasher, J. L., Leigh, J., Li, Y., Lin, J. K., Lipshultz, S. E., London, S., Lozano, R., Lu, Y., Mak, J., Malekzadeh, R., Mallinger, L., Marcenes, W., March, L., Marks, R., Martin, R., McGale, P., McGrath, J., Mehta, S., Memish, Z. A., Mensah, G. A., Merriman, T. R., Micha, R., Michaud, C., Mishra, V., Hanafiah, K. M., Mokdad, A. A., Morawska, L., Mozaffarian, D., Murphy, T., Naghavi, M., Neal, B., Nelson, P. K., Nolla, J. M., Norman, R., Olives, C., Omer, S. B., Orchard, J., Osborne, R., Ostro, B., Page, A., Pandey, K. D., Parry, C. D., Passmore, E., Patra, J., Pearce, N., Pelizzari, P. M., Petzold, M., Phillips, M. R., Pope, D., Pope III, C. A., Powles, J., Rao, M., Razavi, H., Rehfuess, E. A., Rehm, J. T., Ritz, B., Rivara, F. P., Roberts, T., Robinson, C., Rodriguez-Portales, J. A., Romieu, I., Room, R., Rosenfeld, L. C., Roy, A., Rushton, L., Salomon, J. A., Sampson, U., Sanchez-Riera, L., Sanman, E., Sapkota, A., Seedat, S., Shi, P., Shield, K., Shivakoti, R., Singh, G. M., Sleet, D. A., Smith, E., Smith, K. R., Stapelberg, N. J., Steenland, K., Stöckl, H., Stovner, L. J., Straif, K., Straney, L., Thurston, G. D., Tran, J. H., Van Dingenen, R., van Donkelaar, A., Veerman, J. L., Vijayakumar, L., Weintraub, R., Weissman, M. M., White, R. A., Whiteford, H., Wiersma, S. T., Wilkinson, J. D., Williams, H. C., Williams, W., Wilson, N., Woolf, A. D., Yip, P., Zielinski, J. M., Lopez, A. D., Murray, C. J., and Ezzati, M.: A comparative risk assessment of burden of disease and injury attributable to 67 risk factors and risk factor clusters in 21 regions, 1990–2010: a systematic analysis for the Global Burden of Disease Study 2010, The Lancet, 380, 2224–2260, doi:10.1016/S0140-6736(12)61766-8, 2012.

Met Office: Met Office Integrated Data Archive System (MIDAS) Land and Marine Surface Stations Data (1853-current), Tech. rep., NCAS British Atmospheric Data Centre, http://catalogue.ceda.ac.uk/uuid/220a65615218d5c9cc9e4785a3234bd0, 2012.

Middlebrook, A. M., Bahreini, R., Jimenez, J. L., and Canagaratna, M. R.: Evaluation of Composition-Dependent Collection Efficiencies for the Aerodyne Aerosol Mass Spectrometer using Field Data, Aerosol Science and Technology, 46, 258–271, doi:10.1080/02786826.2011.620041, 2012.

Mohr, C., DeCarlo, P. F., Heringa, M. F., Chirico, R., Slowik, J. G., Richter, R., Reche, C., Alastuey, A., Querol, X., Seco, R., Peñuelas, J., Jiménez, J. L., Crippa, M., Zimmermann, R., Baltensperger, U., and Prévôt, A. S. H.: Identification and quantification of organic aerosol from cooking and other sources in Barcelona using aerosol mass spectrometer data, Atmos. Chem. Phys., 12, 1649–1665, doi:10.5194/acp-12-1649-2012, 2012.

Murphy, B. N. and Pandis, S. N.: Simulating the Formation of Semivolatile Primary and Secondary Organic Aerosol in a Regional Chemical Transport Model, Environmental Science & Technology, 43, 4722–4728, doi:10.1021/Es803168a, 2009.

Atmos. Chem. Phys. Discuss., doi:10.5194/acp-2016-342, 2016
Manuscript under review for journal Atmos. Chem. Phys.
Published: 6 June 2016

Atmospheric Chemistry and Physics Discussions

NAEI: UK Emission Mapping Methodology 2009, http://uk-air.defra.gov.uk/assets/documents/reports/cat07/1403100909_UK_Emission_Mapping_Methodology_2011-Issue_1.pdf, 2013.

NCAR: The NCAR Command Language (Version 6.3.0) [Software], Boulder, Colorado: UCAR/NCAR/CISL/TDD, doi:10.5065/D6WD3XH5, 2015.

NCEP: NCEP FNL Operational Model Global Tropospheric Analyses, continuing from July 1999, Research Data Archive at the National Center for Atmospheric Research, Computational and Information Systems Laboratory, Boulder CO, 2000.

Ots, R., Young, D. E., Vieno, M., Xu, L., Dunmore, R. E., Allan, J. D., Coe, H., Williams, L. R., Herndon, S. C., Ng, N. L., Hamilton, J. F., Bergström, R., Di Marco, C., Nemitz, E., Mackenzie, I. A., Kuenen, J. J. P., Green, D. C., Reis, S., and Heal, M. R.: Simulating secondary organic aerosol from missing diesel-related intermediate-volatility organic compound emissions during the Clean Air for London (ClearfLo) campaign, Atmospheric Chemistry and Physics Discussions, pp. 1–36, doi:10.5194/acp-2015-920, 2016.

Paatero, P., Hopke, P. K., Song, X., and Ramadan, Z.: Understanding and controlling rotations in factor analytic models, Chemometrics and Intelligent Laboratory Systems, 60, 253–264, doi:10.1016/S0169-7439(01)00200-3, 2002.

Pöschl, U.: Atmospheric aerosols: Composition, transformation, climate and health effects, Angewandte Chemie-International Edition, 44, 7520–7540, doi:DOI 10.1002/anie.200501122, 2005.

Prank, M., Sofiev, M., Tsyro, S., Hendriks, C., Semeena, V. S., Vazhappilly Francis, X., Butler, T., Denier van der Gon, H., Friedrich, R., Hendricks, J., Kong, X., Lawrence, M., Righi, M., Samaras, Z., Sausen, R., Kukkonen, J., and Sokhi, R.: Evaluation of the performance of four chemical transport models in predicting the aerosol chemical composition in Europe in 2005, Atmospheric Chemistry and Physics Discussions, pp. 1–42, doi:10.5194/acp-2015-1028, 2016.

Putaud, J. P., Van Dingenen, R., Alastuey, A., Bauer, H., Birmili, W., Cyrys, J., Flentje, H., Fuzzi, S., Gehrig, R., Hansson, H. C., Harrison, R. M., Herrmann, H., Hitzenberger, R., Hüglin, C., Jones, A. M., Kasper-Giebl, A., Kiss, G., Kousa, A., Kuhlbusch, T. A. J., Löschau, G., Maenhaut, W., Molnar, A., Moreno, T., Pekkanen, J., Perrino, C., Pitz, M., Puxbaum, H., Querol, X., Rodriguez, S., Salma, I., Schwarz, J., Smolik, J., Schneider, J., Spindler, G., ten Brink, H., Tursic, J., Viana, M., Wiedensohler, A., and Raes, F.: A European aerosol phenomenology – 3: Physical and chemical characteristics of particulate matter from 60 rural, urban, and kerbside sites across Europe, Atmospheric Environment, 44, 1308–1320, doi:10.1016/j.atmosenv.2009.12.011, 2010.

R Core Team: R: A Language and Environment for Statistical Computing, R Foundation for Statistical Computing, Vienna, Austria, http://www.R-project.org/, 2014.

Reis, S., Steinle, S., Carnell, E. J., Leaver, D., Vieno, M., Beck, R., and Dragosits, U.: UK gridded population based on Census 2011 and Land Cover Map 2007, NERC Environmental Information Data Centre, doi:10.5285/61f10c74-8c2c-4637-a274-5fa9b2e5ce44, 2016.

Rogge, W. F., Hildemann, L. M., Mazurek, M. A., Cass, G. R., and Simoneit, B. R. T.: Sources of fine organic aerosol. 1. Charbroilers and meat cooking operations, Environmental Science & Technology, 25, 1112–1125, doi:10.1021/es00018a015, 1991.

Schulz, M., Gauss, M., Benedictow, A., Jonson, J. E., Tsyro, S., Nyiri, A., Simpson, D., Steensen, B. M., Klein, H., Valdebenito, A., Wind, P., Kirkevåg, A., Griesfeller, J., Bartnicki, J., Olivie, D., Grini, A., Iversen, T., Seland, ., Semeena, S. V., Fagerli, H., Aas, W., Hjellbrekke, A., Mareckova, K., Wankmuller, R., Schneider, P., Solberg, S., Svendby, T., Liu, L., Posch, M., Vieno, M., Reis, S., Kryza, M., Werner, M., and Walaszek, K.: Transboundary Acidification, Eutrophication and Ground Level Ozone in Europe in 2011, Tech. rep., Norwegian Meteorological Institute, 2013.

Simpson, D., Yttri, K. E., Klimont, Z., Kupiainen, K., Caseiro, A., Gelencser, A., Pio, C., Puxbaum, H., and Legrand, M.: Modeling carbonaceous aerosol over Europe: Analysis of the CARBOSOL and EMEP EC/OC campaigns, Journal of Geophysical Research-Atmospheres, 112, doi:10.1029/2006jd008158, 2007.

Atmos. Chem. Phys. Discuss., doi:10.5194/acp-2016-342, 2016
Manuscript under review for journal Atmos. Chem. Phys.
Published: 6 June 2016

Atmospheric Chemistry and Physics Discussions

Simpson, D., Benedictow, A., Berge, H., Bergström, R., Emberson, L. D., Fagerli, H., Flechard, C. R., Hayman, G. D., Gauss, M., Jonson, J. E., Jenkin, M. E., Nyíri, A., Richter, C., Semeena, S. V., Tsyro, S., Tuovinen, J. P., Valdebenito, A., and Wind, P.: The EMEP MSC-W chemical transport model - technical description, Atmos. Chem. Phys., 12, 7825–7865, doi:10.5194/acp-12-7825-2012, 2012.

UK Office for National Statistics: Overseas Travel and Tourism - Monthly Release, August 2012, Tech. rep., http://webarchive.nationalarchives.gov.uk/20160105160709/http://www.ons.gov.uk/ons/rel/ott/overseas-travel-and-tourism---monthly-release/august-2012/index.html, 2012.

USEPA: 2002 National Emission Inventory (NEI) Preparation Plan, Tech. rep., USEPA, ftp://ftp.epa.gov/EmisInventory/2002finalnei/general_information/2002neiplan_081004final.pdf, 2004.

USEPA: Integrated Science Assessment for Particulate Matter (Final Report), http://cfpub.epa.gov/ncea/cfm/recordisplay.cfm?deid=216546, 2009.

Vieno, M., Dore, A. J., Stevenson, D. S., Doherty, R., Heal, M. R., Reis, S., Hallsworth, S., Tarrason, L., Wind, P., Fowler, D., Simpson, D., and Sutton, M. A.: Modelling surface ozone during the 2003 heat-wave in the UK, Atmos. Chem. and Phys., 10, 7963–7978, doi:DOI 10.5194/acp-10-7963-2010, 2010.

Vieno, M., Heal, M. R., Hallsworth, S., Famulari, D., Doherty, R. M., Dore, A. J., Tang, Y. S., Braban, C. F., Leaver, D., Sutton, M. A., and Reis, S.: The role of long-range transport and domestic emissions in determining atmospheric secondary inorganic particle concentrations across the UK, Atmos. Chem. Phys., 14, 8435–8447, doi:10.5194/acp-14-8435-2014, 2014.

Vieno, M., Heal, M. R., Williams, M. L., Carnell, E. J., Nemitz, E., Stedman, J. R., and Reis, S.: The sensitivities of emissions reductions for the mitigation of UK PM2.5, Atmos. Chem. Phys., 16, 265–276, doi:10.5194/acp-16-265-2016, 2016.

WHO: Review of evidence on health aspects of air pollution – REVIHAAP Project, Tech. rep., World Health Organisation, Copenhagen, Denmark, 2013.

Wickham, H.: ggplot2: elegant graphics for data analysis, Springer New York, 2009.

Yin, J., Cumberland, S. A., Harrison, R. M., Allan, J., Young, D. E., Williams, P. I., and Coe, H.: Receptor modelling of fine particles in southern England using CMB including comparison with AMS-PMF factors, Atmos. Chem. Phys., 15, 2139–2158, doi:10.5194/acp-15-2139-2015, 2015.

Young, D. E., Allan, J. D., Williams, P. I., Green, D. C., Flynn, M. J., Harrison, R. M., Yin, J., Gallagher, M. W., and Coe, H.: Investigating the annual behaviour of submicron secondary inorganic and organic aerosols in London, Atmos. Chem. Phys., 15, 6351–6366, doi:10.5194/acp-15-6351-2015, 2015.

Atmos. Chem. Phys. Discuss., doi:10.5194/acp-2016-342, 2016
Manuscript under review for journal Atmos. Chem. Phys.
Published: 6 June 2016

Atmospheric Chemistry and Physics Discussions

Table 1. Results of sensitivity tests for setting the annual total COA emission for the UK (gridded to workday population density). Model normalised mean biases of COA concentrations at the London Marylebone Road and North Kensington sites are shown for total UK emissions of 2 Gg, 8 Gg, and 7.4 Gg. A total emission of 7.4 Gg was chosen and is used in the rest of the simulations presented in this work.

Site	Measured	Modelled (NMB)		
		2 Gg	8 Gg	7.4 Gg
North Kensington	0.8 $\mu g\,m^{-3}$	-70%	+18%	+8%
Marylebone Road	2.2 $\mu g\,m^{-3}$	-75%	-2%	-4%

Table 2. Measured and modelled mean concentrations of COA for approximately one year at two sites in London for weekdays (Monday–Friday) and weekends (Saturday–Sunday). Values in brackets are the 95% confidence interval of the mean. The number of (hourly) data points used for calculating each mean are given in Fig. 4.

	Marylebone Road		North Kensington	
	Meas.	Mod.	Meas.	Mod.
Weekdays [$\mu g\,m^{-3}$]	2.2 (2.1–2.3)	2.1 (2.0–2.2)	0.7 (0.7–0.7)	0.9 (0.9–1.0)
Weekend [$\mu g\,m^{-3}$]	2.1 (2.0–2.3)	2.2 (2.1–2.3)	1.1 (1.0–1.2)	0.9 (0.9–1.0)

Table 3. Statistics for measured and modelled daily averaged COA concentrations at the two sites in London (site abbreviation as follows: MARY - Marylebone Road, NKEN - North Kensington). Up10 is the 90th percentile (upper 10% of the values), and Up5 is the 95th percentile (upper 5% of the values). The time-series of these values are shown in Fig. 5. Values in the "Modelled" line are for model values matched for data availability with the measurements. As Marylebone Road exhibits a few longer periods with missing measurements, modelled stats for the full year are also presented (red line in Fig. 5a). All units in $\mu g\,m^{-3}$.

		Mean	Median	Up10	Up5	Max.
MARY	Meas.	2.2	2.1	3.5	4.1	5.9
	Mod.	2.1	1.8	3.2	3.9	10.0
	Mod. (full year)	2.0	1.8	3.1	3.7	10.0
NKEN	Meas.	0.8	0.6	1.7	2.0	4.1
	Mod.	0.9	0.7	1.4	2.0	6.8

Atmos. Chem. Phys. Discuss., doi:10.5194/acp-2016-342, 2016
Manuscript under review for journal Atmos. Chem. Phys.
Published: 6 June 2016

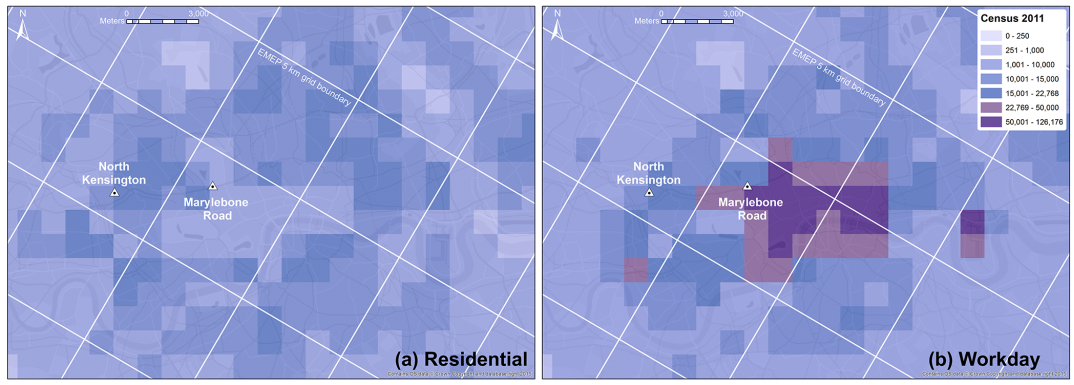

Figure 1. Residential (a) and workday (b) population density in central London at 1 km × 1 km resolution. The residential population maps are based on Reis et al. (2016). While the same methodology is applied to derive workday population maps, they are not yet published due to delays in the prevision of workday population census data for Scotland. Also shown are the measurement sites, and the EMEP4UK 5 km × 5 km grid used in this study (white lines). Underlying map contains Ordinance Survey (OS) data © Crown Copyright 2015.

Atmos. Chem. Phys. Discuss., doi:10.5194/acp-2016-342, 2016
Manuscript under review for journal Atmos. Chem. Phys.
Published: 6 June 2016

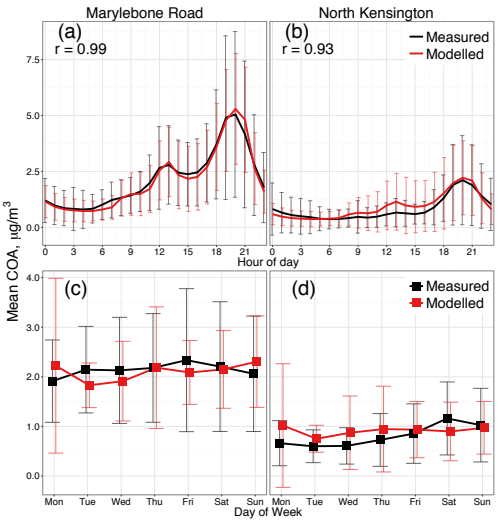

Figure 2. Average temporal profiles of COA concentrations at the two sites in central London in 2012: (a) diurnal profile at the Marylebone Road site, (b) diurnal profile at the North Kensington site, (c) day-of-week profile at the Marylebone Road site, (d) day-of-week profile at the North Kensington site. The timestamp of panels (a) and (b) is at the beginning of the hour. Also shown are standard deviations for each mean value.

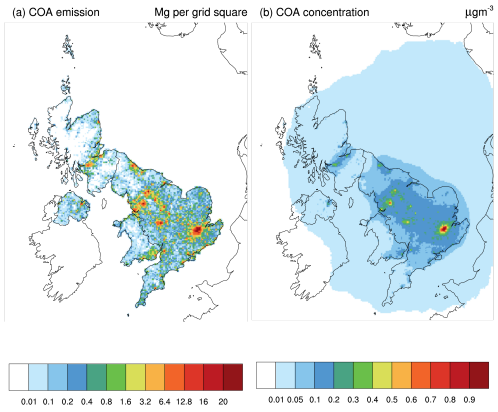

Figure 3. (a) Gridded COA emissions used in the model for the year 2012 (Mg per 5 km × 5 km grid cell, note the nonlinear scale), (b) annual average concentrations ($\mu g\,m^{-3}$).

Atmos. Chem. Phys. Discuss., doi:10.5194/acp-2016-342, 2016
Manuscript under review for journal Atmos. Chem. Phys.
Published: 6 June 2016

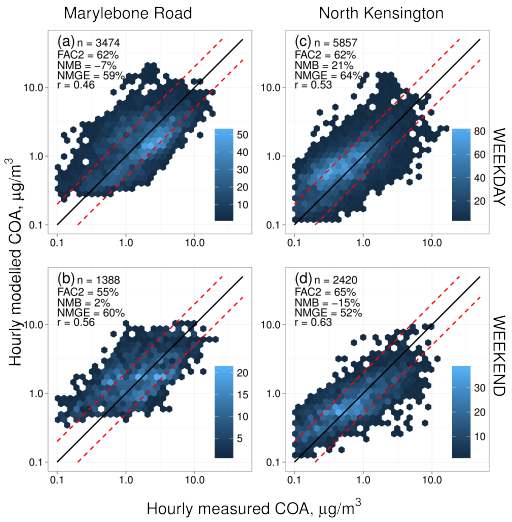

Figure 4. Data density scatterplots of measured versus modelled hourly COA concentrations for approximately one year at two sites in London: (a) Marylebone Road on weekdays, (b) Marylebone Road on weekends, (c) North Kensington on weekdays, (d) North Kensington on weekends. The colour scales indicate number of instances in a hexagonal (concentrations) bin. The straight lines are the 2:1, 1:1, and 1:2 lines. Note that on this Fig. the NMB for Marylebone Road for weekdays is -7%, but calculating the same statistic based on the numbers in Table 2 gives a NMB of -5%. This small discrepancy is caused by the rounding of concentrations for Table 2.

Atmos. Chem. Phys. Discuss., doi:10.5194/acp-2016-342, 2016
Manuscript under review for journal Atmos. Chem. Phys.
Published: 6 June 2016

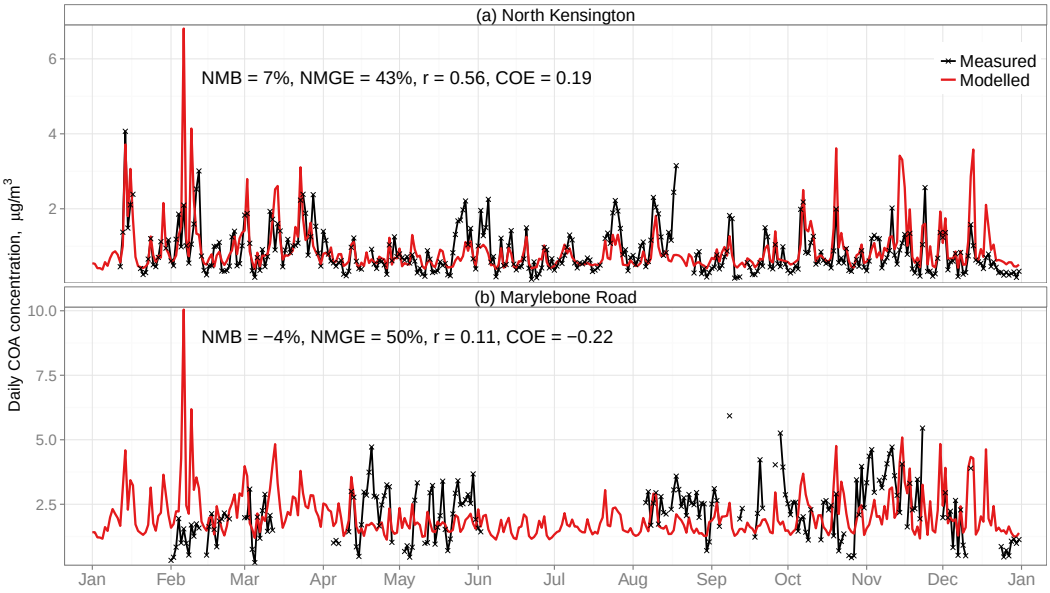

Figure 5. Time series of measured and modelled daily averaged COA concentrations at the (a) North Kensington, and (b) Marylebone Road measurement sites, year 2012.

Atmos. Chem. Phys. Discuss., doi:10.5194/acp-2016-342, 2016
Manuscript under review for journal Atmos. Chem. Phys.
Published: 6 June 2016

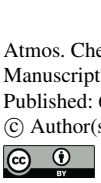

Atmospheric Chemistry and Physics Discussions

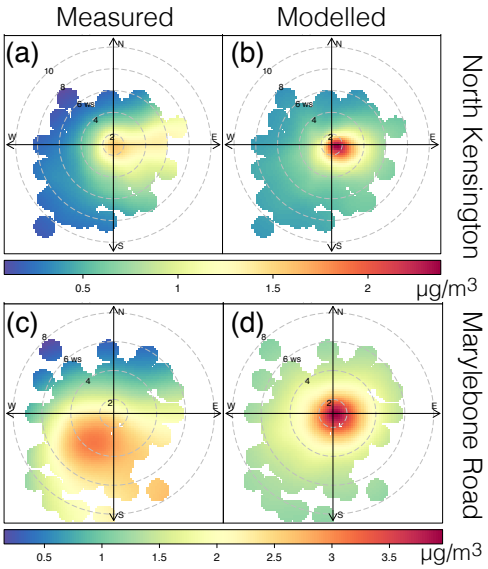

Figure 6. Polar plots of daily-average COA concentrations for wind speed (ws, $\mathrm{m\,s^{-1}}$) and direction measured at the Heathrow Airport meteorological station (Met Office, 2012). (a) measured and (b) modelled concentrations at the North Kensington site. (c) measured and (d) modelled concentrations at the Marylebone Road site.

Figure 7. Location of the Marylebone Road measurement site, arrows indicate the West and South directions from the site. The measurement station is on the southern pavement of the street. Map from © OpenStreetMap contributors.

Atmos. Chem. Phys. Discuss., doi:10.5194/acp-2016-342, 2016
Manuscript under review for journal Atmos. Chem. Phys.
Published: 6 June 2016

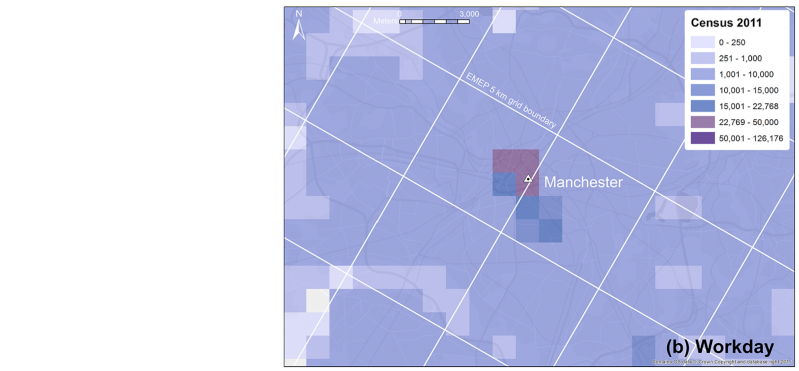

Figure 8. Workday population density in Manchester at 1 km × 1 km resolution in the OSGB36 (Ordinance Survey Great Britain 1936) projection. Also shown is the measurement site, and the EMEP4UK 5 km × 5 km grid used in this study (white lines). Underlying map from © OpenStreetMap contributors.

Atmos. Chem. Phys. Discuss., doi:10.5194/acp-2016-342, 2016
Manuscript under review for journal Atmos. Chem. Phys.
Published: 6 June 2016

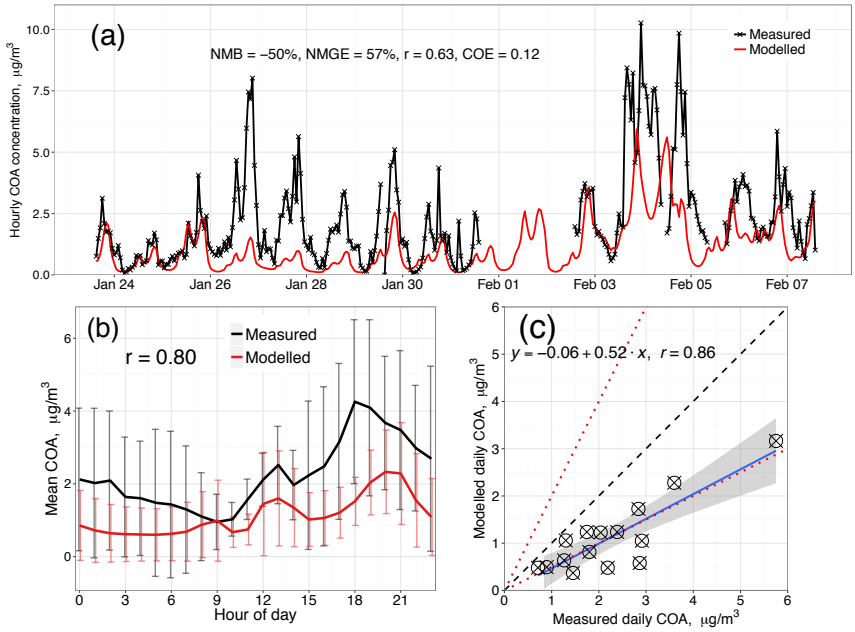

Figure 9. Comparison of modelled COA concentrations with an independent dataset of AMS measurements in Manchester, 2007. (a) Time series of measured and modelled hourly averaged COA concentrations. (b) Average diurnal profiles of measured and modelled COA (the timestamp is at the beginning of the hour, also shown are standard deviations for each mean value). (c) Scatterplots of daily-averaged modelled versus measured concentrations (the dotted and dashed lines are the 2:1, 1:1, and 1:2 lines, the blue line is the linear fit, the shading is the 95% confidence interval of the fit).

Atmos. Chem. Phys. Discuss., doi:10.5194/acp-2016-342, 2016
Manuscript under review for journal Atmos. Chem. Phys.
Published: 6 June 2016

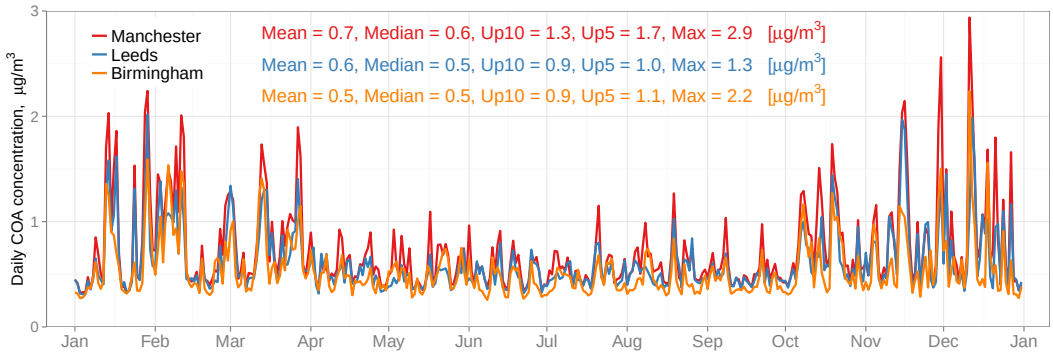

Figure 10. Time series of modelled daily-averaged COA concentrations for Manchester, Leeds, and Birmingham, year 2012. Up10 is the 90th percentile (upper 10% of the values), and Up5 is the 95th percentile (upper 5% of the values). The locations of these cities are shown in Fig. 11.

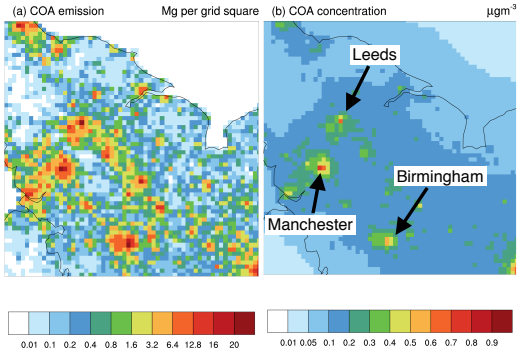

Figure 11. As Fig. 3, but zoomed in on northern England to show three other major cities with large estimated COA emissions: Manchester, Leeds, and Birmingham. (a) total COA emissions for the year 2012 (Mg per 5 km × 5 km grid cell, note the nonlinear scale), (b) annual average concentrations ($\mu g\, m^{-3}$).

Atmos. Chem. Phys. Discuss., doi:10.5194/acp-2016-342, 2016
Manuscript under review for journal Atmos. Chem. Phys.
Published: 6 June 2016

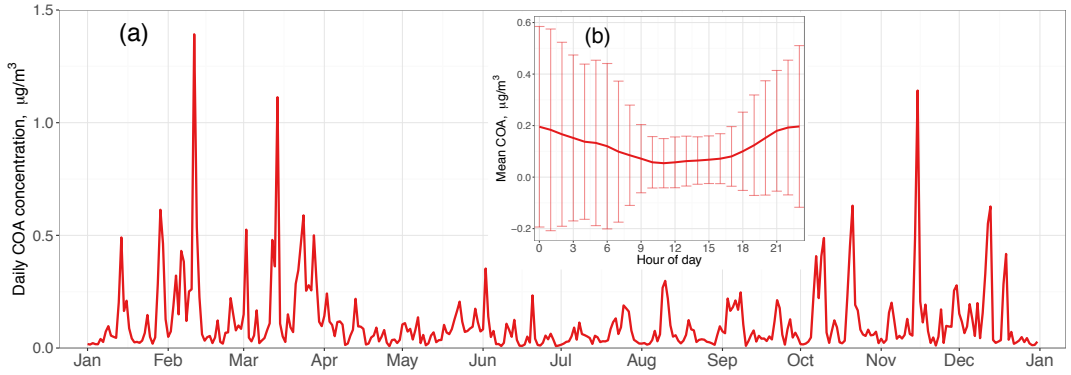

Figure 12. Modelled COA concentrations for the Harwell EMEP supersite location (a rural background site ~80 km from central London), year 2012. (a) Time series of modelled daily averaged COA concentrations. (b) Average diurnal profiles (the timestamp is at the beginning of the hour, also shown are standard deviations for each mean value).